

Processing of gas in cosmological filaments around Virgo cluster

G. Castignani^{1,2,*}, F. Combes^{3,4}, P. Jablonka^{2,5}, R. A. Finn⁶, G. Rudnick⁷, B. Vulcani⁸, V. Desai⁹, D. Zaritsky¹⁰, and P. Salomé³

¹ Dipartimento di Fisica e Astronomia, Alma Mater Studiorum Università di Bologna, Via Gobetti 93/2, I-40129 Bologna, Italy

² Laboratoire d'astrophysique, École Polytechnique Fédérale de Lausanne, Observatoire de Sauverny, 1290 Versoix, Switzerland

³ Observatoire de Paris, PSL university, Sorbonne Université, CNRS, LERMA, F-75014, Paris, France

⁴ Collège de France, 11 Place Marcelin Berthelot, 75231 Paris, France

⁵ GEPI, Observatoire de Paris, Université PSL, CNRS, Place Jules Janssen, F-92190 Meudon, France

⁶ Department of Physics & Astronomy, Siena College, 515 Loudon Road, Loudonville, NY 12211, USA

⁷ The University of Kansas, Department of Physics and Astronomy, Malott Room 1082, 1251 Wescoe Hall Drive, Lawrence, KS, 66045, USA

⁸ INAF- Osservatorio astronomico di Padova, Vicolo Osservatorio 5, I-35122 Padova, Italy

⁹ Spitzer Science Center, California Institute of Technology, MS 220-6, Pasadena, CA 91125, USA

¹⁰ Steward Observatory, University of Arizona, 933 North Cherry Avenue, Tucson, AZ 85721-0065, USA

Received: December 16, 2020

ABSTRACT

It is now well established that galaxies have different morphology, gas content and star formation rate in dense environments like galaxy clusters. The impact of environmental density extends to several virial radii, and galaxies appear to be pre-processed in filaments and groups, before falling into the cluster. Our goal is to quantify this pre-processing, in terms of gas content, and star formation rate, as a function of density in cosmic filaments. We have observed the two first CO transitions in 163 galaxies with the IRAM-30m telescope, and added 82 more measurements from the literature, for a sample of 245 galaxies in the filaments around Virgo. We gathered HI-21cm measurements from the literature, and observed 69 galaxies with the Nançay telescope, to complete our sample. We compare our filament galaxies with comparable samples from the Virgo cluster and with the isolated galaxies of the AMIGA sample. We find a clear progression from field galaxies to filament and cluster ones for decreasing star formation rate, increasing fraction of galaxies in the quenching phase, increasing proportion of early-type galaxies and decreasing gas content. Galaxies in the quenching phase, defined as having star formation rate below one third of the main sequence rate, are only between 0-20% in the isolated sample, according to local galaxy density, while they are 20-60% in the filaments and 30-80% in the Virgo cluster. Processes that lead to star formation quenching are already at play in filaments. They depend mostly on the local galaxy density, while the distance to filament spine is a secondary parameter. While the HI to stellar mass ratio decreases with local density by an order of magnitude in the filaments, and two orders of magnitude in the Virgo cluster with respect to the field, the decrease is much less for the H₂ to stellar mass ratio. As the environmental density increases, the gas depletion time decreases, since the gas content decreases faster than the star formation rate. This suggests that gas depletion significantly precedes star formation quenching.

Key words. Galaxies: clusters: general; Galaxies: star formation; Molecular data; ISM: general.

1. Introduction

There is strong observational evidence that dense local environments can have a large impact on the evolutionary path of galaxies. Following the pioneering work by Dressler (1980), numerous studies have shown that dense Mpc-scale environments regulate the star formation activity (Butcher & Oemler 1984; Peng et al. 2010) and gas content (Chung et al. 2009; Vollmer et al. 2012). Galaxy clusters are also the sites where the most dramatic morphological transformations of galaxies are observed, which are ultimately driven by galaxy-galaxy interactions within the complex cosmic web and give rise to the so called morphology *versus* density relation in the cores of clusters (Postman & Geller 1984; Dressler et al. 1997; Goto et al. 2003).

Environmental processes can remove gas through tidal heating and stripping that occurs in gravitational interactions and mergers between galaxies (Merritt 1983; Moore et al. 1998),

ram-pressure stripping due to a passage through the hot intracluster gas (Gunn & Gott 1972; Roediger & Hensler 2005), or the suppression of the gas accretion from the cosmic web, a process called starvation (Larson et al. 1980; Balogh et al. 2000). All these processes occur in clusters and in some cases dramatically, for example in the spectacular ram-pressure stripping reported by Jáchym et al. (2014, 2019). Statistically, the HI deficiency in clusters has now been firmly established (e.g., Chung et al. 2009), and molecular gas is also known to be depleted in dense environments (Casoli et al. 1998; Lavezzi & Dickey 1998; Vollmer et al. 2008; Scott et al. 2013). Boselli et al. (2014a,b) also reported tentative evidence of correlation between HI and H₂ deficiencies for cluster galaxies.

There is also ample evidence that galaxy star formation rates are suppressed at distances up to ~ 5 virial radii (r_{200}) from the cluster center (e.g., Lewis et al. 2002; Gómez et al. 2003; Vulcani et al. 2010; Finn et al. 2010; Haines et al. 2015). It is now clear that both field and group galaxies are being pre-processed before they fall into the cluster itself (e.g., Zabludoff & Mulchaey 1998;

* e-mail: gianluca.castignani@unibo.it; full tables will be available electronically at CDS

Poggianti et al. 1999; Cortese et al. 2006; Rudnick et al. 2017; Hou et al. 2014).

Large galaxy redshift surveys have revealed that galaxies are distributed in a complex network of matter with a large dynamic range of local density, called the cosmic web or filamentary structures (Kitaura et al. 2009; Darvish et al. 2014, 2017; Alpaslan et al. 2016; Chen et al. 2016, 2017; Malavasi et al. 2017; Kuutma et al. 2017; Kraljic et al. 2018; Laigle et al. 2018; Sarron et al. 2019; Luber et al. 2019; Salerno et al. 2019). To determine the effect of environment on galaxy evolution, it is necessary to understand how galaxies are altered as they move through the cosmic web and enter the densest regions of clusters.

Hydrodynamic simulations of the cluster infall regions predict that the density of gas in filaments is able to enhance the ram pressure up to a factor of ~ 100 with respect to the pressure in the lower density regions (Bahé et al. 2013). According to the authors this means that freshly infalling galaxies with stellar masses $\log(M_*/M_\odot) < 9.5$ near a massive cluster can be stripped of their cold gas even well outside the virial radius. For more massive galaxies or at larger distances from the cluster, the ram pressure in filaments is still sufficient to strip off the hot gas that will replenish the dense star-forming gas, although it will likely not affect directly the densest cold gas. The latter will then be consumed on a timescale of ~ 2.3 Gyr (Bigiel et al. 2011).

In this work we observationally quantify the amount of pre-processing of cold gas of galaxies in cosmic filaments and investigate galaxy properties as a function of the environment. To this aim we report a multi-wavelength study of a stellar mass complete sample of 245 galaxies observed in cold gas, both atomic (HI) and molecular (CO). These sources live in cosmic filaments surrounding Virgo, the benchmark cluster in the local Universe. Virgo has a distance of ~ 17 Mpc (Mei et al. 2007) and a virial radius of ~ 6 deg in projection. Due to the complex structure of Virgo, several estimates around ~ 2 Mpc have been reported in the literature for its virial radius: 1.55 Mpc (McLaughlin et al. 1999), 1.72 Mpc (Hoffman et al. 1980), and 2.2 Mpc (Fouqué et al. 2001).

The paper is structured as follows. In Sect. 2 we characterize the filamentary structures around Virgo. In Sect. 3 we describe our sample and present our cold gas observations. In Sect. 4 we derive gas properties such as H₂ and HI gas masses. In Sect. 5 we introduce the comparison samples of field and Virgo cluster galaxies. In Sect. 6 we provide a description of the environment of our sample of filament galaxies. In Sect. 7 we describe our results. In Sect. 8 we summarize the results and draw the conclusions. In the Appendices A, B, C, and D we report supplementary material including diagnostic plots, spectra, and tables.

Throughout this paper, we assume a Hubble constant of $H_0 = 100 h^{-1} \text{ km s}^{-1} \text{ Mpc}^{-1}$, where $h = 0.74$ (Tully et al. 2008). See however Planck Collaboration (2020); Riess et al. (2019). Stellar masses and star formation rates adopted in this work rely on the Kroupa & Weidner (2003) initial mass function.

2. The cosmic web around Virgo

We have characterized in detail the filamentary network surrounding Virgo. A release of the catalog of galaxies surrounding Virgo, of the associated filaments, and their properties will be done in a forthcoming paper (Castignani et al., in prep.). In the following we give an overview of our analysis.

2.1. The sample of galaxies around Virgo

Following early work by de Vaucouleurs (1953, 1956) who noted an excess of nearby galaxies in the vicinity of the North Galactic pole, several studies attempted to provide a detailed characterization of the complex cosmic web around Virgo, which is indeed embedded in the Laniakea supercluster, including the local group (Bahcall & Joss 1976; Tully 1982; Tully et al. 2014, 2016). Simulations also contributed to these efforts, with the aim to reproduce in detail the cosmic flow in the local Universe (Libenskind et al. 2018, 2020).

In this work we follow instead the recent approach by Kim et al. (2016), who identified the spines of several cosmological filaments around Virgo. Similarly to Kim et al. (2016) we built a complete sample of galaxies around Virgo, which have been selected within the following J2000 coordinate ranges of $100 \text{ deg} < \text{R.A.} < 280 \text{ deg}$ and $-35 \text{ deg} < \text{Dec.} < 75 \text{ deg}$, around Virgo cluster, whose center is at (R.A. ; Dec.) = (187.70; 12.34) deg. We further limited ourselves to sources with heliocentric velocities $V_H < 3300 \text{ km s}^{-1}$. The catalog was primarily built by merging the NASA Sloan Atlas (NSA)¹ and HyperLeda² (Makarov et al. 2014) catalogs. Our selection yields 10,305 galaxies, all with unique NED counterparts, in the cosmic web around Virgo.

2.2. Distances

To characterize in 3D the cosmic web around Virgo we have then followed the method described in Mould et al. (2000). We have first derived the correction of the observed heliocentric velocities of the galaxies to the centroid of the Local Group. Then we have included an additional correction that takes into account the infall towards the Virgo attractor. With this procedure heliocentric radial velocities V_H have been converted into cosmic radial velocities V_{cosmic} .

We have then searched by name for redshift independent distances within the Steer et al. (2017) catalog. Redshift-independent distances have been also homogenized to $H_0 = 74 \text{ km s}^{-1} \text{ Mpc}^{-1}$ used in this work. Our search yielded redshift independent distances for 2,763 sources out of the 10,305 galaxies (27%) around Virgo. Limiting ourselves to our sample of 245 filament galaxies, that will be described in Sect. 3 in more detail, we have found redshift independent distances for 181 (74%). This higher fraction for our sample compared to that of the full catalog can be explained by the fact that our filament galaxies are overall massive, while the cosmic web and filaments in particular tend to be largely populated by less massive systems, including dwarfs (Kim et al. 2016).

For these 2,763 sources we have replaced the model dependent V_{cosmic} velocities with those inferred via redshift independent distances. As further outlined below, we verified that this replacement does not introduce any bias for our environmental analysis and, on the contrary, leads to a robust characterization of the cosmic web around Virgo. Note also that, since our sources are all at redshift $z \approx 0$ in good approximation, recession velocities V_{cosmic} have been translated into distances via the Hubble law as V_{cosmic}/H_0 .

In Fig. 1 (left) we report the resulting distance distribution for the 245 filament galaxies in our sample (Sect. 3), where redshift independent distances are highlighted. Our filament sources have a median distance of ~ 29 Mpc, and are thus behind Virgo

¹ <http://www.nsatlas.org/>

² <http://leda.univ-lyon1.fr/>

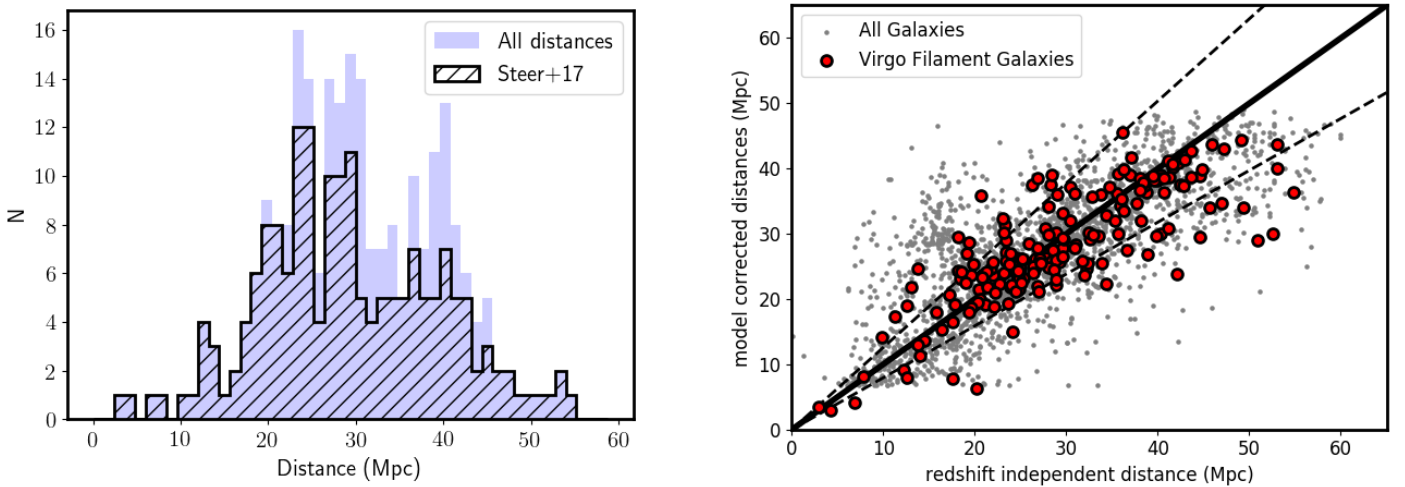


Fig. 1: **Left:** distribution of distances for the 245 sources of our sample. Redshift independent distances (Steer et al. 2017) are reported in foreground (dashed histogram), while in the background (blue filled histogram) we report all adopted distances, including those model-corrected. **Right:** scatter plot with model-corrected distances (y-axis) vs. redshift independent distances (x-axis). Red points refer to our sample of 245 filament galaxies, gray points refer to galaxies in the field of Virgo at distances in the range $\sim(0\text{--}60)$ Mpc. The solid black line shows the one-to-one relation, while the dashed lines correspond to an $\text{rms} = 0.1$ dex.

cluster (see also Kim et al. 2016). When considering the sub-sample of 181 sources with redshift independent distances and the full sample of 245 sources, separately, we obtain median distances of $(28.0^{+12.3}_{-8.4})$ Mpc and $(29.3^{+11.3}_{-8.5})$ Mpc, respectively. The two median values are thus in perfect agreement with each other, within the reported uncertainties.³

In Fig. 1 (right) we report a comparison between model corrected distances (D_{model} , y-axis) and redshift independent distances ($D_{z\text{-independent}}$, x-axis). Remarkably, the comparison yields a negligible bias and a limited rms scatter of ~ 0.1 dex, i.e. of quality competitive with that found in recent studies of the local Universe (Leroy et al. 2019). For the full catalog of sources around Virgo and the 181 filament galaxies in our sample with redshift independent distances, the mean logarithmic difference is indeed found to be $\log(D_{\text{model}}/D_{z\text{-independent}}) = 0.004 \pm 0.15$ and -0.015 ± 0.10 , respectively. Here the reported uncertainty is the rms dispersion around the mean.

As seen in Fig. 1 sources with redshift-independent distances $\gtrsim 40$ Mpc tend to deviate from the one-to-one line, being larger than the corresponding model corrected distances. This shift is likely due to the fact that at recession velocities of $\gtrsim 3,000$ km s $^{-1}$ galaxy start to be dominated by the Hubble flow. We refer to Leroy et al. (2019) for a similar discussion. However, we checked that for this sub-sample of distant sources the mean logarithmic difference of $\log(D_{\text{model}}/D_{z\text{-independent}}) = -0.08 \pm 0.08$ is still limited and within the 1σ dispersion, for both the full catalog of sources around Virgo and the sub-sample of 181 filament sources.

2.3. Filament Spines

All galaxies around Virgo have been mapped into the 3D Cartesian super Galactic (SGX, SGY, SGZ) coordinate system (Tully

et al. 2008). This can be appreciated in Fig. 2, where the sources in the cosmic web around Virgo are shown and color coded in gray scale according to their distance V_{cosmic}/H_0 . Our sample of 245 filament galaxies observed both in CO and HI is highlighted with different colors, according to the associated filament. Similarly to Kim et al. (2016) the following filamentary structures in the Northern hemisphere were considered: VirgoIII filament, NGC 5353/4 filament, W-M sheet, as well as the Leo Cloud, with the Leo Minor, LeoII A, and LeoII B filaments. We additionally considered the nearby Ursa Major Cloud (Tully 1982; Tully & Fisher 1988). Part of our 245 sources also belong to additional structures that were targeted, after visual selection, for our observations: VirgoIII Filament Extension, Virgo Northern Filament, Filament 3 and its companion Filament 3b. All these filaments are reported in Fig. 2, in addition to Canes Venatici filament, Virgo Southern Extension, and Crater Filament, which have not been considered in this work.

Following Kim et al. (2016) the spines of the filaments, which are shown in Fig. 2 in projection, were determined via fitting the locations of galaxies with a third order polynomial curve, in super Galactic coordinates. In Fig. A.1 we report the filament spines in the Cartesian (SGX, SGY, SGZ) coordinate system, together with the corresponding filament galaxies.

2.4. Environmental parameters

We aim to fully characterize the environment of the 245 sources in our sample. Therefore, we estimated several environmental properties as outlined in the following. Quantities were computed in 3D within the (SGX, SGY, SGZ) Cartesian frame or in 2D, by projection onto the (SGX, SGZ) plane. Several estimators have been used for the local density: the 5th-nearest neighbor density, both in 2D and in 3D; the modified 10-th nearest neighbor density in 3D (Cowan & Ivezić 2008). We refer to Muldrew et al. (2012) for a review.

³ Hereafter in this work we report the 1σ confidence interval as uncertainty to the median value, unless otherwise stated.

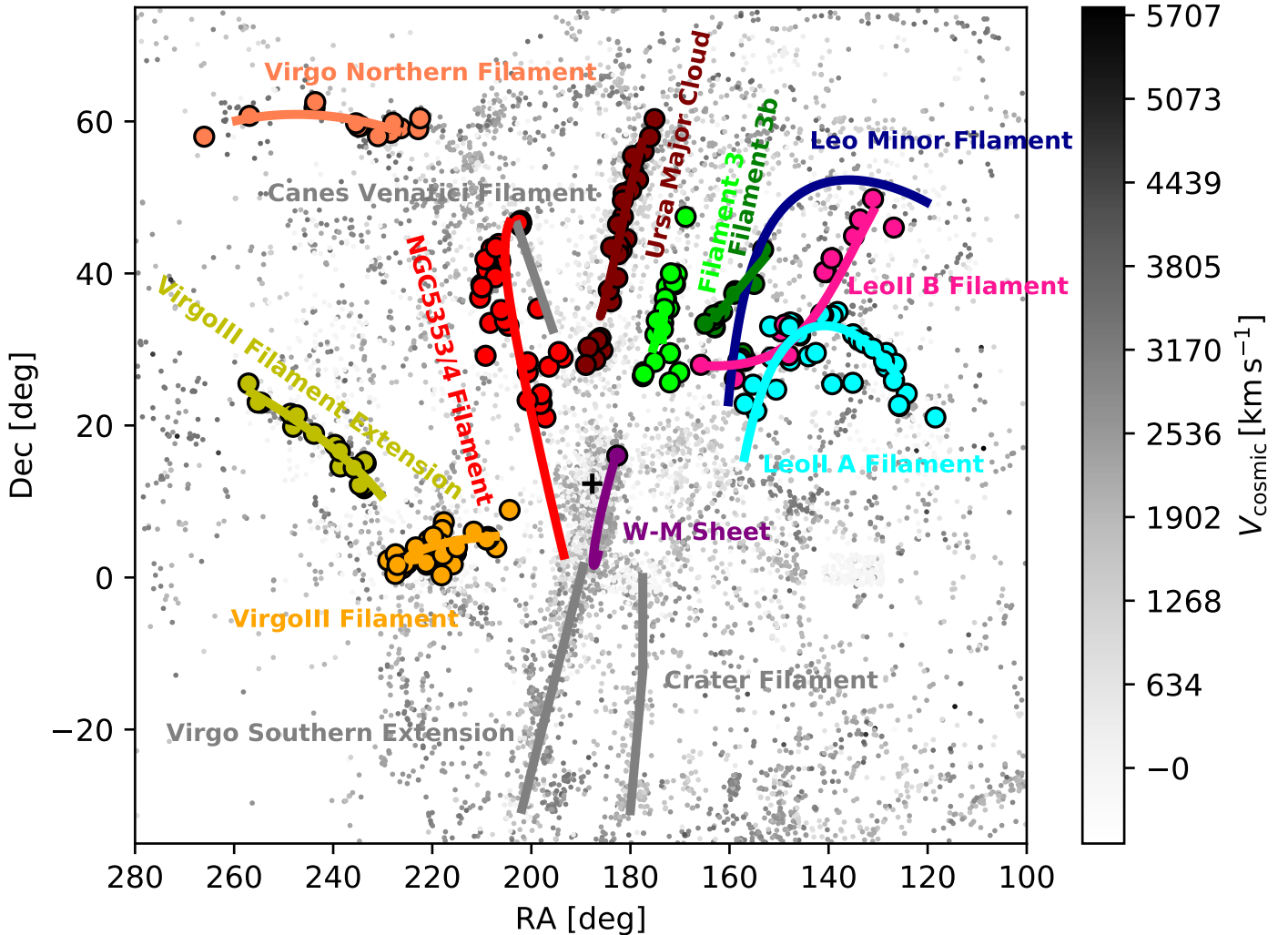


Fig. 2: Cosmic web up to ~ 12 virial radii from Virgo cluster, whose coordinates are (R.A. ; Dec.) = (187.70; 12.34) deg (J2000) and ($\text{SGX}; \text{SGY}; \text{SGZ}$) = (-2.26; 9.90; -0.42) h^{-1} Mpc, as denoted by the central cross. Gray points show galaxies color coded according to their distance. Big colored points show filament galaxies in our sample with CO and HI observations, while the curves are the locations of the filament spines. Different colors refer to different filaments.

For each galaxy we also estimated, in the Super Galactic Coordinate frame, the minimum separation from its corresponding filament spine (d_{fil}) and from Virgo cluster center (d_{cluster}), both in 3D and in projection (2D). We verified that the standard 5th-nearest neighbor density and 3D quantities (i.e., local densities and distances) provide a good description of the environment of our sources. We then use them throughout this work. Indeed, when comparing different density estimators and 2D vs. 3D quantities we did not find any significant difference. We refer to the forthcoming catalog paper (Castignani et al. in prep.) for further details about the comparison. The fact that our results are somehow independent of 2D vs. 3D quantities suggests that line of sight uncertainties (~ 0.1 dex) do not significantly impact our environmental analysis. In Table B.1 we report the environmental properties for our sample.

3. Our sample of filament galaxies

3.1. Sample selection

To characterize the effects of the filament environment on the galaxy gas content, we selected 245 galaxies belonging to the highest contrast and longest filaments around Virgo. They extend up to several virial radii from the cluster center and span up to ~ 30 Mpc in length (e.g., Kim et al. 2016).

Our goal is to make the first substantial exploration of molecular gas in the filamentary environment. Our sample is supported by a wealth of existing data which enable robust estimates of the stellar mass, stellar population, and the star formation rate (SFR) for our galaxies: SDSS ugriz imaging, optical spectroscopy, and far infrared fluxes (WISE, IRAS).

The initial selection of the filament galaxies was done on the basis of their recession velocities and positions in the sky, by requiring proximity to the filamentary structures. We also restricted to the stellar mass range between $\sim 10^9 M_\odot$ and $\sim 10^{11} M_\odot$. Below this range, the low expected metallicity could prevent us from detecting CO, while at higher masses than this

range we expect intrinsic quenching processes to play a more important role.

3.2. Galaxy Properties

Properties of our sample of filament galaxies are listed in Table B.2. They include galaxy coordinates and recession velocities, morphologies, sizes, inclinations, position angles, stellar masses, and star formation rates, both absolute and relative to the main sequence (MS).

3.2.1. Morphology

Figure 3 shows the distribution in morphology, taken from HyperLeda, of our sample of filament galaxies. It can be noted that the barred galaxy fraction is about 2/3 as usual for spirals, except for Sb types, which could be a statistical fluke. Note also that the classification is coming from optical images, while bars are better seen in the infrared (Eskridge et al. 2000). Hereafter we denote the de Vaucouleurs morphological parameter as T , while early type galaxies ($T < 0$) will be also often distinguished from late type galaxies ($T \geq 0$).

A number of studies have suggested a link between the cessation (quenching) of star formation and the presence of bars (e.g., James & Percival 2016; Fraser-McKelvie et al. 2020). Indeed bars favor gas inflows, while subsequent bar-induced shocks may inject substantial turbulent energy into galactic disk to stabilize the molecular gas against collapse (Khoperskov et al. 2018). As further outlined in the following sections, we have investigated in this work both star formation and gas content of our sample of filament galaxies, but we have not found any statistical significant difference between barred and non-barred galaxies. We suspect that the absence of correlations is due to the limited statistics of our sample, which comprises 41 and 31 galaxies classified as SB and SAB, respectively. Therefore, in the following sections, we will not distinguish between the two classes.

3.2.2. Stellar masses and star formation rates

We looked for the sources of our sample within the recent Leroy et al. (2019) catalog of local sources. The catalog is based on a multi-wavelength dataset including WISE in infrared and GALEX in ultraviolet and provides accurate stellar masses and SFRs of local sources up to distances ~ 50 Mpc.

We have found stellar masses for 235 sources out of 245 in Leroy et al. (2019). For the remaining 10 sources, stellar masses have been taken from the NASA Sloan Atlas, calibrated to $h = 0.74$. Out of 245 sources in our sample, 231 have M_\star estimates from both Leroy et al. (2019) and the NASA Sloan Atlas. The median logarithmic difference between the two estimates is $-0.05^{+0.18}_{-0.17}$. The comparison thus yields a good agreement, with a negligible bias and a limited 1σ scatter.

Estimates of the SFR by Leroy et al. (2019) have been found for a subsample of 234 sources. For the remaining 11 galaxies we have gathered the SFRs from the literature, as follows. For six sources, namely NGC 4144, PGC 023706, PGC 031387, PGC 049002, PGC 1925809, and PGC 2151881, we have taken the SFRs estimated by Chang et al. (2015), based on both SDSS and WISE photometry, quite similarly to Leroy et al. (2019). For NGC 2592, NGC 4214, and NGC 4244 the SFRs have instead taken from the DustPedia archive⁴, which provides the SFRs

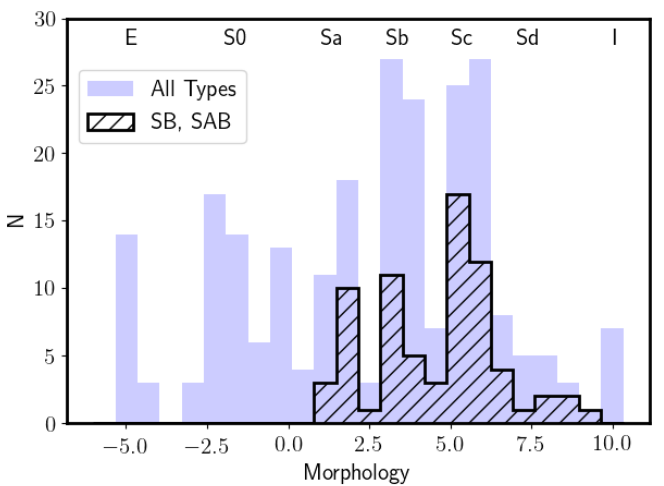


Fig. 3: Hubble type distribution (de Vaucouleurs classification) for the sources in our sample.

estimated by fitting multi-wavelength spectral energy distributions with CIGALE (Burgarella et al. 2005; Noll et al. 2009; Boquien et al. 2019). NGC 2793 is a ring galaxy and we have the $\text{SFR} \sim 0.2 M_\odot/\text{yr}$ estimated by Mayya & Romano (2002) via H_α imaging. Last, for PGC 049386 (i.e., CGCG 219-021) we have not found any estimate from the literature and we have thus converted its $22 \mu\text{m}$ W4 WISE emission into the SFR using the Calzetti et al. (2007) relation. We refer also to Table B.2, where stellar masses and SFRs of all sources are reported.

For 132 sources out of 245, SFR estimates have been found from both Leroy et al. (2019) and Chang et al. (2015). The median logarithmic difference between the two estimates is $0.48^{+0.93}_{-0.59}$ dex. Our comparison thus suggests that Leroy et al. (2019) SFRs are, on average, higher than those estimated by Chang et al. (2015), although the reported 1σ scatter is not negligible.

3.3. Observations

We have observed in CO the majority of our filament galaxies, and for the rest we gathered CO fluxes from the literature. Archival HI masses are also available for many sources, while we have observed the missing ones with the Nançay telescope, as described below. We have also gathered detailed $\text{H}\alpha$ maps using wide-field imagers, to reveal the status and spatial distribution of the hot gas, which will be described in forthcoming papers.

3.3.1. IRAM-30m CO observations

For 82 sources out of the 245 in our sample, CO observations were found in the literature. In case of multiple observations we gave preference to the ones with higher SNR, generally more recent. Note that Ursa Major Cloud is nearby and the corresponding cold gas observations come all from the literature.

The remaining 163 sources in our sample (i.e., 67%) were observed by us at the IRAM-30m telescope at Pico Veleta, Granada, Spain, during October and December 2016, then March and July 2017. For each source we observed both CO(1→0) and CO(2→1), simultaneously.

⁴ <http://dustpedia.astro.noa.gr/>

The full width half power (FWHP) beam size is 23 arcsec and 12 arcsec at the CO(1→0) and CO(2→1) frequencies of 115 GHz and 230 GHz, respectively. Our targets have recession velocities between 1000 and 3000 km s⁻¹, and can be considered at $z \approx 0$.

The SIS receivers (EMIR) were used for observations in the wobbler-switching mode, with reference positions offset by ±120 arcsec in azimuth. The main-beam efficiency of IRAM-30m is $\eta_{\text{mb}} = B_{\text{eff}}/F_{\text{eff}} = T_{\text{A}}^*/T_{\text{mb}} = 0.83$ and 0.64 at 115 GHz and 230 GHz, respectively. B_{eff} and F_{eff} are the main beam and forward efficiencies, respectively, while T_{A}^* and T_{mb} denote the antenna temperature and the brightness temperature, respectively. The system temperatures ranged between 150 K and 400 K at 2.6 mm and between 200 K and 800 K at 1.3 mm. The pointing was regularly checked every 2 h on a nearby planet or a bright continuum source, and the focus was reviewed after each sunrise, and at the beginning of each run. The on-source time typically ranged from 0.3 h to 2 h, according to the SNR already reached on a target and the weather. Two backends were used simultaneously, the autocorrelator WILMA, and the Fourier transform spectrometer FTS. The T_{mb} root mean square (rms) noise level in 2 h integration was $\sigma_{\text{mb}} \approx 1.4$ mK with a spectrometer resolution of 20 km s⁻¹ for 115 GHz and $\sigma_{\text{mb}} \approx 1.8$ mK for 230 GHz. These can be lower in very good weather. The upper limits reported in next sections for the velocity integrated CO fluxes are computed at 3σ at a resolution of 300 km s⁻¹ and assuming a standard IRAM-30m T_{mb} -to-flux conversion of 5 Jy K⁻¹.

Seven additional sources were observed with the IRAM-30m since at the time of our observations they were considered as filament galaxies on the basis of their recession velocities and positions in the projected space. However, following accurate environmental analysis, we have conservatively removed them *a posteriori* from our main sample, as described in the following. UGC 7039, UGC 7143, PGC 38859 fall in the field of the W-M sheet, which span Y-axis super Galactic coordinates SGY~(16 – 25) h⁻¹ Mpc (Kim et al. 2016). However, our environmental analysis, described in Sect. 2, finds that the sources have SGY~29, 28, and 27 h⁻¹ Mpc, respectively. Given the location of Virgo in the sky, SGY coordinates can be considered as a distance proxy, at least at first order. IC 777 falls in the field of the nearby Ursa Major Cloud (Tully 1982; Tully & Fisher 1988), that spans the range SGY~(2 – 16) h⁻¹ Mpc, but it is located well behind it, since the source has SGY~41 h⁻¹ Mpc. Similarly, NGC 5089 (SGY~34 h⁻¹ Mpc) and NGC 5240 (SGY~31 h⁻¹ Mpc) are both located in the field of the NGC 5353/4 filament, but are at much higher distance than the filament, since it spans SGY~(22 – 27) h⁻¹ Mpc (Kim et al. 2016). These results suggest that all the six sources are located behind the main filamentary structure of reference. The seventh source is PGC 214137, or equivalently, UGC 08656 NOTES01. It has been erroneously targeted at the place of its more massive companion UGC 08656 during our IRAM-30m observations. We conservatively decided not to consider any of the two sources for our main sample of 245.

In Table B.3 we report the results of our IRAM-30m observations for the 163 sources of our main sample. At the bottom of the Table we also report the results for the 7 sources that have been removed *a posteriori* from the main sample. Upper limits at 3σ are also reported, together with secure and tentative (SNR≤3) detections, which are distinguished in the Table.

By considering CO(1→0) or CO(2→1) out of the 163 sources in our sample we have securely detected 137 galaxies (i.e., 84%), for 5 sources (UGC 05020, PGC 035472, IC 4263,

UGC 09556, and UGC 10968) we have found tentative detections in CO, while for 21 galaxies we set 3σ upper limits. In Fig. C.1 we report the IRAM-30m spectra and the Gaussian fits for the CO lines for all 148 sources, including six out of the seven sources considered separately, with tentative or secure detections.

In Fig. D.1 we report the FWHM distribution for the sources detected with our IRAM-30m campaign. It shows that the large majority of FWHM are below 300 km/s, and therefore this value used for upper limits is very conservative. In Table B.4 we summarize the molecular gas properties for the subsample of 82 sources with CO observations from the literature.

3.3.2. Nançay HI observations

New HI observations of 69 galaxies in the filamentary structures around Virgo were obtained using the Nançay decimetric radio telescope and 1024-channel autocorrelator spectrometer between January and December 2017. The Nançay telescope is a meridian transit-type instrument with an effective collecting area of ~7000 m². At 21 cm, the FWHP beam size is 3.6' (East-West) × 23' (North-South) within the range of declinations spanned by of our sources. The FWHP beam size changes only slightly with the source declination (Fouqué et al. 1990). Observations were obtained through position switching, with an OFF at (14-20) arcmin East, and alternating 2 min ON and 2 min OFF. Tracking was limited to about one hour per source per day. For most of the sources, one track was sufficient, in some cases, we repeated the track, due to technical problems. The system temperature was typically 35 K. With an efficiency of 0.8 Jy/K, evaluated at the declination of our sources, we obtained an rms of 2 mJy at a velocity resolution of 13 km s⁻¹ for all spectra. The total available bandwidth being nearly 10,000 km/s, we observed all sources with a common tuning, given their recession velocity range (1000–2500) km s⁻¹.

The spectra were first calibrated and reduced using the NAPS reduction package available at the Nançay site. The spectra were then exported into fits files, analysed, and fitted using the GILDAS-CLASS software. Peak and integrated fluxes, velocity widths, and recession velocities were derived from the Gaussian fits. The corresponding results are reported in Table B.5.

Among the 69 sources observed in HI at Nançay, 58 are part of our sample of 245 filament galaxies. The HI results for the remaining 11 are reported separately at the bottom of the Table. While having been observed by us in HI at Nançay, these sources have not been observed in CO with our IRAM-30m campaign. We checked that they do not have CO observations from the literature either. Therefore, we preferred not to include them in our main sample of filament galaxies. In Fig. C.2 we report the HI spectra, and the Gaussian fits of the HI lines, for all 48 sources out of the 69 observed at Nançay with secure (46) or tentative (2) HI detections. For the remaining 21 sources we set 3σ upper limits at 300 km s⁻¹ resolution, similarly to what we have for the upper limits in CO (Sect. 3.3.1).

4. Molecular and atomic gas

4.1. H₂ gas masses

Molecular gas masses have been estimated using a Galactic conversion factor $\alpha_{\text{CO}} = 4.3 M_{\odot} (\text{K km s}^{-1} \text{ pc}^2)^{-1}$, equivalently, $X_{\text{CO}} = N_{\text{H}_2}/I_{\text{CO}} = 2.0 \times 10^{20} \text{ cm}^{-2} (\text{K km s}^{-1})^{-1}$ (e.g., Dickman et al. 1986; Strong et al. 1988), where N_{H_2} is the H₂ column density (in units of cm⁻²) and I_{CO} the velocity integrated CO line

intensity, in units of K km s^{-1} . The molecular gas mass was then determined (e.g., Bolatto et al. 2013, for a review) as follows:

$$\frac{M_{\text{H}_2}}{M_{\odot}} = 1.05 \times 10^4 \frac{X_{\text{CO}}}{2.0 \times 10^{20} \text{ cm}^{-2} (\text{K km s}^{-1})^{-1}} \frac{S_{\text{CO}(1 \rightarrow 0)} \Delta v}{\text{Jy km s}^{-1}} \left(\frac{D}{\text{Mpc}} \right)^2 \quad (1)$$

or, equivalently, as:

$$\frac{M_{\text{H}_2}}{M_{\odot}} = \frac{\alpha_{\text{CO}}}{M_{\odot} (\text{K km s}^{-1} \text{ pc}^2)^{-1}} \frac{L'_{\text{CO}(1 \rightarrow 0)}}{\text{K km s}^{-1} \text{ pc}^2}. \quad (2)$$

Here $S_{\text{CO}(1 \rightarrow 0)} \Delta v$ and $L'_{\text{CO}(1 \rightarrow 0)}$ are the velocity integrated CO($1 \rightarrow 0$) flux and luminosity, respectively, while D is the distance of the source considered. The $L'_{\text{CO}(J \rightarrow J-1)}$ luminosity for the generic CO($J \rightarrow J-1$) transition can be also expressed as:

$$\frac{L'_{\text{CO}(J \rightarrow J-1)}}{\text{K km s}^{-1} \text{ pc}^2} = 3.25 \times 10^7 \frac{S_{\text{CO}(J \rightarrow J-1)} \Delta v}{\text{Jy km s}^{-1}} \left(\frac{\nu_{\text{CO}(J \rightarrow J-1)}}{\text{GHz}} \right)^{-2} \left(\frac{D}{\text{Mpc}} \right)^2, \quad (3)$$

where Eq. 3 by Solomon & Vanden Bout (2005) has been used, in the limit $z \ll 1$, that is valid for nearby sources such as those considered in this work. The frequency $\nu_{\text{CO}(J \rightarrow J-1)}$ is that associated with the CO($J \rightarrow J-1$) transition. In this work we use the $S_{\text{CO}(1 \rightarrow 0)}$ flux to estimate H₂ molecular gas mass, via Eqs. (1, 2). In the cases where the $S_{\text{CO}(1 \rightarrow 0)}$ flux was at low SNR < 3 (tentative detections) or not available we have used higher-J transitions via $M_{\text{H}_2} = \alpha_{\text{CO}} L'_{\text{CO}(J \rightarrow J-1)} / r_{J1}$.

Here $r_{J1} = L'_{\text{CO}(J \rightarrow J-1)} / L'_{\text{CO}(1 \rightarrow 0)}$ is the excitation ratio. We have assumed the following fiducial excitation ratios, typical of star-forming galaxies, namely, $r_{21} = 0.8$ (Bothwell et al. 2013; Daddi et al. 2015; Freundlich et al. 2019) and $r_{31} = 0.5$ (Bothwell et al. 2013; Carilli & Walter 2013). Note that we have used the CO($3 \rightarrow 2$) transition only for NGC3265, to set an upper limit to its H₂ gas mass, using JCMT observations by Wilson et al. (2012). From the same authors we have found CO($3 \rightarrow 2$) observations also for NGC4559. However, for this source we have used the CO($1 \rightarrow 0$) flux by Sage (1993) to estimate M_{H_2} . We refer to Table B.4 for details. In the cases where only 3σ upper limits to M_{H_2} were available we used the most stringent one between those estimated via CO($2 \rightarrow 1$) and CO($1 \rightarrow 0$).

4.2. Aperture corrections

Equations (1, 2) relate the M_{H_2} molecular gas mass to the total CO emission. However, since the sources in our sample are extended and nearby their extension may be larger than the beam size Θ , which is equal, for our IRAM-30m observations, to 21 arcsec and 10.5 arcsec in the case of CO($1 \rightarrow 0$) and CO($2 \rightarrow 1$), respectively. Therefore, following Lisenfeld et al. (2011), when estimating the M_{H_2} mass, we have multiplied the observed CO flux by the inverse of the filling factor, f_{ap} , which we estimate as follows:

$$f_{\text{ap}} = \frac{2}{\pi r_e^2} \int_0^\infty dx \int_0^\infty dy \exp \left\{ -\ln(2) \left[\left(\frac{2x}{\Theta} \right)^2 + \left(\frac{2y \cos i}{\Theta} \right)^2 \right] \right\} \exp \left(-\frac{\sqrt{x^2 + y^2}}{r_e} \right), \quad (4)$$

where i is the inclination angle between the line of sight and the polar axis of the galaxy. The above equation also relies on the additional assumption that the CO line intensity has an exponential radial profile $I_{\text{CO}}(r) \propto \exp(-r/r_e)$ (Nishiyama et al. 2001; Regan

et al. 2001; Leroy et al. 2008), where r_e is the CO scale length, which previous studies found to be well correlated with the optical exponential scale length (e.g., Regan et al. 2001; Leroy et al. 2008; Saintonge et al. 2012). Consistently with previous studies (Leroy et al. 2008; Lisenfeld et al. 2011; Boselli et al. 2014a) we assumed $r_e \simeq 0.1 D_{25}$, where D_{25} is the optical 25 mag arcsec⁻² isophotal diameter.

4.2.1. Datasets from the literature

According to the CO aperture correction described above we have revised the CO fluxes from the literature, to have the most homogeneous dataset possible. To this aim, we have applied the same extrapolation as in Eq. (4) to the CO fluxes coming from single dish and central pointing observations (Braine et al. 1993; Welch & Sage 2003; Combes et al. 2007; Young et al. 2011; Vila-Vilaro et al. 2015; O'Sullivan et al. 2015, 2018). According to the different telescopes used by these studies, we have adopted the corresponding FWHP beam size Θ .

CO fluxes reported by Lisenfeld et al. (2011) were corrected for the aperture as in Eq. 4. Therefore, we did not apply any additional correction. Similarly, Boselli et al. (2014a) used an aperture correction very similar to that used by Lisenfeld et al. (2011), with an additional non-negligible disk width in their formalism. However, a detailed comparison between their 3D extrapolated fluxes and those extrapolated via a 2D modeling, e.g., as in Eq. 4, leads to negligible statistical differences at a few percent level, both in the mean values and in the rms dispersion (see Table 7 of Boselli et al. 2014a). Therefore, when considering their CO fluxes we safely adopted their extrapolation.

Observations by Sage (1993); Young et al. (1995); Wilson et al. (2012) took into account the extension of the sources when estimating CO fluxes by means of multiple pointings, when needed. Similarly, Alatalo et al. (2013) showed that their interferometric maps were able to recover on average more flux than the IRAM-30m, for the same targets (see their Table 3). Therefore, we preferred not to apply any aperture correction, limiting to the CO fluxes from these studies.

In Table B.4 we summarize the molecular properties for the sources with CO observations from the literature. We also report the excitation ratio, the aperture correction adopted, as well as the corresponding reference and telescope.

4.2.2. Aperture correction distribution

In Fig. 4 we report the aperture correction distribution for both CO($1 \rightarrow 0$) and CO($2 \rightarrow 1$) observations. The Figure shows similar distributions for the extrapolation, when considering the sources observed with our IRAM-30m campaign and the full sample of 245 filament galaxies, thus including also (extrapolated) CO fluxes from the literature. For the full sample of 245 sources, the aperture corrections span the ranges of $1/f_{\text{ap}} \sim 1 - 10$ and $\sim 1 - 20$ for CO($1 \rightarrow 0$) and CO($2 \rightarrow 1$), with only a few exceptions with higher corrections. For our IRAM-30m observations we have median aperture corrections $1/f_{\text{ap}} = 2.1_{-0.6}^{+1.2}$ and $1/f_{\text{ap}} = 4.0_{-1.7}^{+3.5}$, respectively. They are thus of the order of unity, consistently with those previously found in previous studies (e.g., Lisenfeld et al. 2011; Boselli et al. 2014a). Note that the highest aperture corrections $1/f_{\text{ap}} \gtrsim 10$ for CO($1 \rightarrow 0$) and $\gtrsim 25$ for CO($2 \rightarrow 1$) are found only in a few cases, when CO observations from the literature are considered. The higher aperture corrections estimated for CO($2 \rightarrow 1$) are mainly due to the smaller FWHP than for CO($1 \rightarrow 0$) since the FWHP scales with the in-

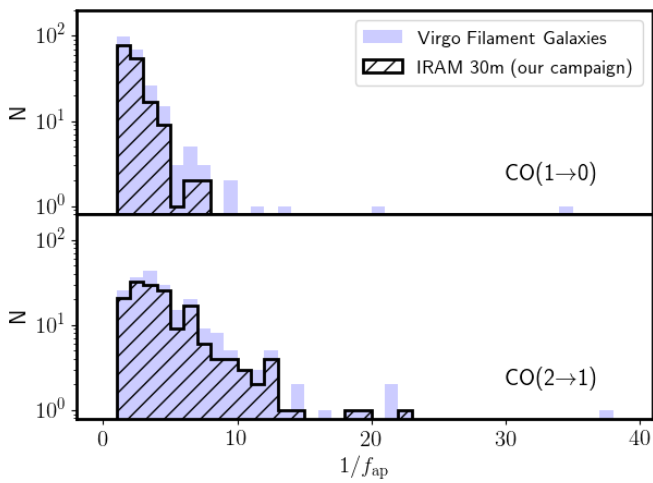


Fig. 4: Distribution for the CO aperture correction for the filament sources in our sample (blue filled histogram). The subsample of sources from our IRAM-30m campaign is highlighted (dashed histogram).

verse of the observed frequency. The smaller $1/f_{ap}$ observed for CO($1\rightarrow 0$) also adds another piece of evidence in favor of its use, against higher-J transitions, when estimating H₂ masses.

4.2.3. Multiple IRAM-30m pointings

Among the 163 sources targeted with our IRAM-30m campaign, four sources, namely NGC 5985, NGC 5350, NGC 5290, and UGC 09837, have been observed at their center, and also with one or two symmetric pointings off-center, along the galaxy extension. This is illustrated in Fig. 5, where the spiral morphologies of the four galaxies are shown, together with IRAM-30m spectra at the different pointings. The three NGC galaxies are almost perfectly face-on, while UGC 09837 is more edge-on. These four filament galaxies are also among those of our sample with the largest extension in the projected sky and are therefore good test cases to evaluate the amount of CO coming from the center and the arms with ongoing star formation. However, because of their large extension, note that these four sources have high aperture corrections, as further outlined below, so they are not representative of the mean population, for which lower corrections are needed. The results of our observations are summarized in Table 1.

Our results show that the observed CO emission of our targets, considering both central and off-center pointings, ranges between ~ 2.3 - 3.1 and between ~ 1.6 - 4.4 times that observed at the galaxy center, for CO($1\rightarrow 0$) and CO($2\rightarrow 1$), respectively. Note also that these ratios are lower limits to the actual aperture correction, since our off-center pointings do not cover uniformly the whole galaxy disc. This can be appreciated directly from the galaxy images in Fig. 5, where the IRAM-30m CO($2\rightarrow 1$) beams are also reported. Indeed, for these sources we have estimated larger corrections ranging between $1/f_{ap} \simeq 3.4 - 6.3$ and $\simeq 7.7 - 20.5$ for CO($1\rightarrow 0$) and CO($2\rightarrow 1$), respectively (see Table B.3).

Furthermore, from the CO results reported for these four sources in Table 1, we see that the bulk of the CO emission

ID (1)	CO(J→J-1) (2)	$S_{CO(J\rightarrow J-1)}\Delta v$ (Jy km s ⁻¹) (3)	FWHM (km s ⁻¹) (4)
NGC 5985			
center	1→0	15.10 ± 2.77	226 ± 61
	2→1	6.72 ± 2.53	83 ± 43
North	1→0	19.04 ± 1.64	81 ± 9
	2→1	16.56 ± 3.61	66 ± 21
South	1→0	12.86 ± 1.54	89 ± 12
	2→1	6.24 ± 2.44	58 ± 23
NGC 5350			
center	1→0	48.04 ± 1.95	258 ± 12
	2→1	71.41 ± 3.11	220 ± 11
North	1→0	35.29 ± 2.10	221 ± 17
	2→1	18.22 ± 2.73	124 ± 22
South	1→0	33.39 ± 2.19	178 ± 15
	2→1	22.85 ± 2.66	148 ± 18
NGC 5290			
center	1→0	99.00 ± 2.25	248 ± 6
	2→1	126.23 ± 3.09	242 ± 7
West	1→0	70.30 ± 2.71	190 ± 9
	2→1	61.03 ± 3.66	160 ± 12
East	1→0	59.10 ± 2.49	212 ± 11
	2→1	55.36 ± 3.80	193 ± 17
UGC 09837			
center	1→0	2.53 ± 0.61	73 ± 21
	2→1	1.77 ± 0.74	30 ± 16
West	1→0	< 4.29	—
	2→1	5.42 ± 1.77	85 ± 28

Table 1: CO results for the four filament galaxies with multiple IRAM-30m pointings. Column description: (1) target ID and pointing; (2) CO($J\rightarrow J-1$) transition; (3) observed velocity integrated CO($J\rightarrow J-1$) flux, not aperture corrected; (4) FWHM of the CO($J\rightarrow J-1$) line. For the CO($1\rightarrow 0$) emission of UGC 09837 a 3σ upper limit at 300 km s⁻¹ resolution is reported.

generally comes from the central regions of the galaxies, consistently with the declining disc profile adopted for the CO flux extrapolation. This consistency is also seen in velocity: our observations show that the galaxy centers have a larger velocity dispersion than the outskirts, in fact the closer to the center, the steeper the profile (e.g., Salomé et al. 2015). NGC 5985 may be an exception, since off-center pointings are associated with a large amount of CO, comparable to that observed from the center, but still with lower FWHM. This may be due to the fact that off-center pointings specifically targeted clumpy star forming regions in the spiral arms, as it is tentatively suggested by visual inspection of the galaxy (Fig. 5).

4.3. Excitation Ratios

Excitation ratios r_{21} , or their upper limits, have been estimated for 147 out of 245 sources (i.e., 60%). They are all detected in CO($1\rightarrow 0$) and have detections (141) or upper limits (6) in CO($2\rightarrow 1$). We set 3σ upper limits to the latter six sources, namely, NGC 3245, NGC 5346, PGC 028169, UGC 08318, UGC 09556, and UGC 09661. For NGC 4151, NGC 4414, and NGC 4559 the CO fluxes reported in Table B.4 imply low values

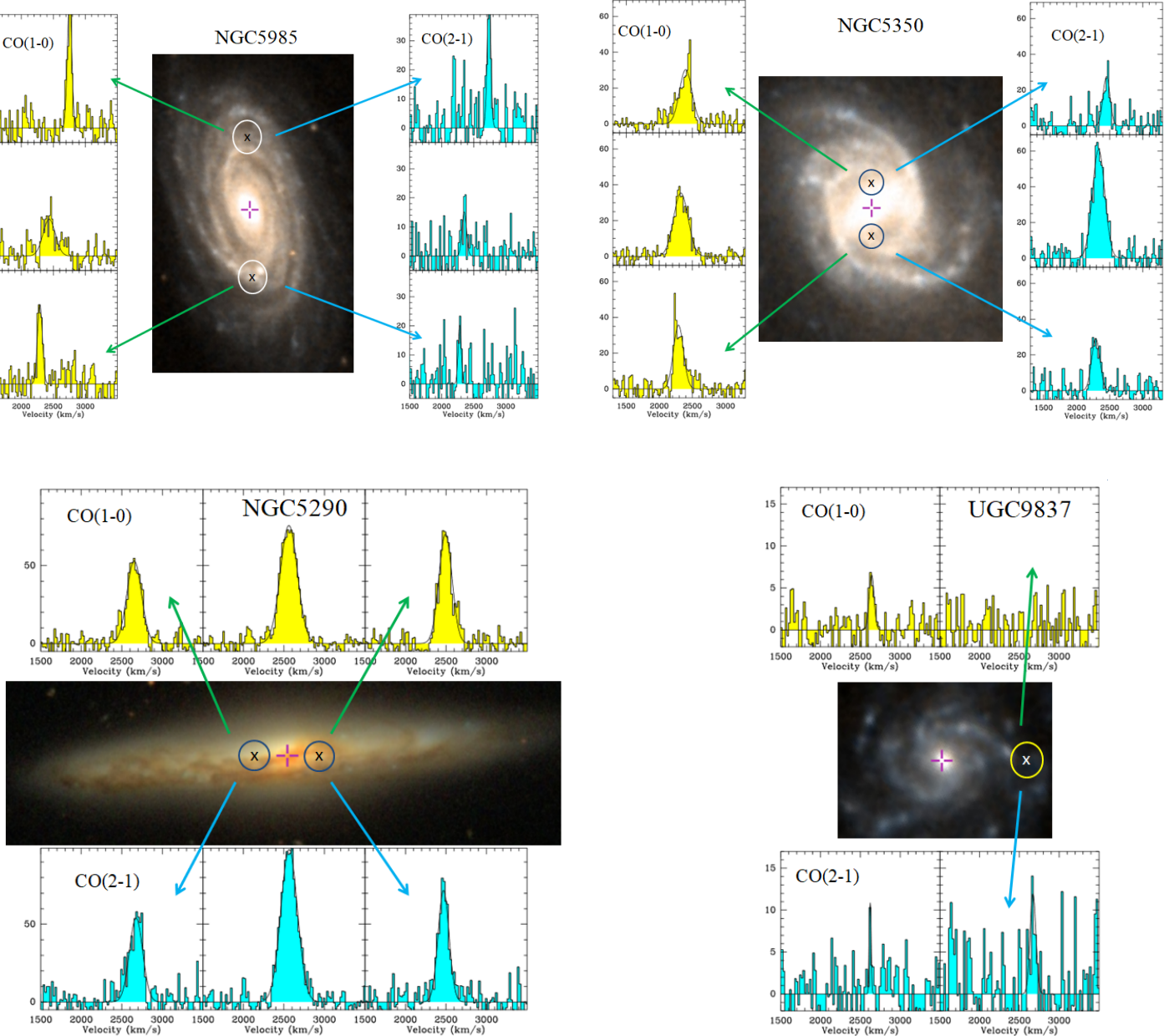


Fig. 5: Optical images and IRAM-30m spectra of the four sources in our sample with multiple pointings. In the images, North is up, East is left, while the crosses in magenta (+) and black/white (x) correspond to the central and offset pointings, respectively. The circles correspond to the CO($2 \rightarrow 1$) beams of $10.5''$ each, with the exception of NGC 5985, for which the CO($1 \rightarrow 0$) beams of $21''$ each are instead reported. The reported spectra are baseline-subtracted, the x- and y-axes show the relative velocity and T_{mb} (in mK), respectively. The solid lines in the spectra are the Gaussian fits to the CO($1 \rightarrow 0$) and CO($2 \rightarrow 1$) lines.

of $r_{21} \simeq 0.01 - 0.02$. Such low values are ultimately due to the fact that, at a fixed galaxy, CO fluxes are associated with observations done with different telescopes and observational strategies. The corresponding excitation ratios are thus very uncertain and we conservatively preferred *a posteriori* not to report any r_{21} for the three galaxies.

In Fig. 6 we report the excitation ratio r_{21} as a function of galaxy morphology for the 147 sources. The associated median value is $r_{21} = 0.53^{+0.37}_{-0.19}$. It is formally lower than that of $r_{21} \sim 0.8$ assumed for our sources. Note that excitation ratio estimates are also very uncertain, which is confirmed by the large reported

uncertainties and the wide range of values within $r_{21} \sim 0.1 - 3$ that are found for our sources.

The scatter plot reported in Fig. 6, along with the running mean, show an increase of the excitation from late-type ($T \geq 0$) to early-type ($T < 0$) galaxies. A good correlation is found with the Spearman test between r_{21} and morphology (p-value = 1.93×10^{-3}). Early type galaxies are in fact more concentrated and have denser gas reservoirs than late type galaxies.

As illustrated by the color bar in the Figure, there is also a tentative dependence of r_{21} as a function of the star formation activity. Indeed, the sub-sample of 5 sources with the highest sSFR = $\text{SFR}/M_{\star} > 3.5 \times 10^{-10} M_{\odot}/\text{yr}$ tend to populate the region

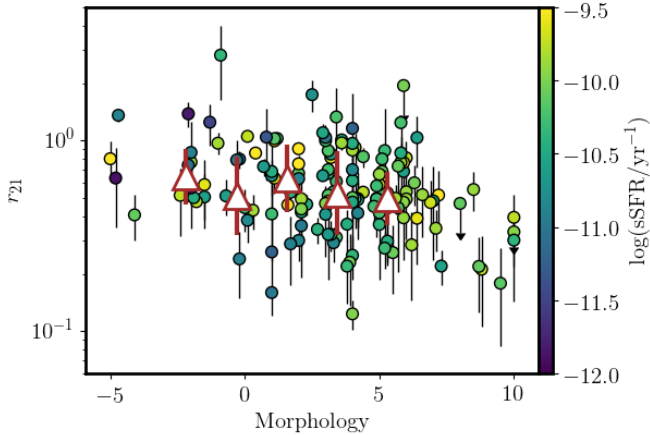


Fig. 6: Excitation ratio (r_{21}) vs. morphological type for the filament galaxies in our sample. Points are color coded according to the sSFR, as illustrated in the color bar (right). Triangles correspond to the binned running median, while the error bars are the rms uncertainties.

in the plot associated with highest excitations, with a median of $r_{21} = 0.86$, hence close to $r_{21} \sim 1$. This result is consistent with the fact that fully or highly excited gas is commonly found in systems with strong ongoing star-formation activity, as for example it is the case for highly star-forming (ultra) luminous infrared galaxies (Bothwell et al. 2013; Daddi et al. 2015). On the other hand no clear trend was found when plotting r_{21} against the stellar mass, distance to Virgo, distance to the filament spine, and local density.

4.4. HI gas Masses

Our observations at Nançay targeted 58 out of the 245 in our sample of filament galaxies, as described in Sect. 3.3.2. We have complemented them by looking for HI observations from the literature for the remaining 187. HI properties are summarized in Table B.5. At variance with the CO fluxes, no flux extrapolation was needed for the HI fluxes from our campaign at Nançay. This is due to the large FWHP beam size of $3.6' \times 23'$ (East-West) $\times 23'$ (North-South) of the Nançay telescope (see Sect. 3.3.2). It is safely larger than the size $D_{25} \leq 4.1$ arcmin of the sample galaxies that we observed at Nançay, while our filament sources have overall a median diameter of $D_{25} = (1.67^{+1.30}_{-0.76})$ arcmin, as reported in Table B.2.

Gas masses were then homogeneously estimated for all sources in our sample using the following formula:

$$M_{\text{HI}} = 2.36 \times 10^5 \frac{S_{\text{HI}} \Delta v}{\text{Jy km s}^{-1}} \left(\frac{D}{\text{Mpc}} \right)^2 M_{\odot}, \quad (5)$$

where $S_{\text{HI}} \Delta v$ is the velocity integrated HI flux, D is the distance of the source considered. We refer to Wild (1952); Roberts (1962) for further details.

We have also estimated the correction to M_{HI} due to self-absorption of HI, which affects the densest regions in the galaxy disc. The correction is expected to be stronger for

edge-on galaxies and is estimated as the multiplicative factor $\kappa = (a/b)^{0.12}$ (Giovanelli et al. 1994; Springob et al. 2005; Ciccone et al. 2017), where a and b are the optical major and minor axes of our galaxies, taken from HyperLeda. We have verified that the correction due to HI self-absorption is negligible. It is not greater than 28% for the 245 sources in our sample, while on average it is at the level of a few percent, given the median value of $\kappa = 1.07^{+0.09}_{-0.05}$.

In Table B.6 we summarize the cold gas (both H₂ and HI) properties of our sample.

5. Comparison Samples

5.1. Virgo cluster members

There is a rich ensemble of data available for the galaxies inside the Virgo cluster. For our comparison we have thus considered the sample of Virgo cluster members from Boselli et al. (2014a), requiring both CO and HI observations. HI observations are reported in Boselli et al. (2014a) and have been taken from the literature, mostly from the HI survey ALFALFA (Giovanelli et al. 2005; Haynes et al. 2011). We have then updated the HI dataset by using exclusively the most recent release of the ALFALFA survey by Haynes et al. (2018). CO(1→0) have been obtained with several radio telescopes (e.g., Kitt Peak, IRAM-30m, FCRAO, SEST, Onsala, and BELL) and are also reported in Boselli et al. (2014a). For the sake of homogeneity we have converted CO(1→0) and HI fluxes into gas masses, as described in Sect. 4. In particular, we have adopted a Galactic conversion factor $\alpha_{\text{CO}} = 4.3 M_{\odot} (\text{K km s}^{-1} \text{ pc}^2)^{-1}$. We have also used the CO fluxes as reported by Boselli et al. (2014a). In the case of single-beam observations, the authors adopted a 3D aperture correction, very similar to that used for our observations of filament galaxies (see also Sect. 4.2).

To enable a homogeneous comparison in terms of stellar masses, $\log(M_{\star}/M_{\odot}) \gtrsim 9$, and SFRs we have then cross-matched the sample of Virgo sources with the Leroy et al. (2019) catalog, similarly to what has been done for the filament galaxies (see Sect. 3.2.2). This selection yields 109 galaxies. Consistently with Boselli et al. (2014a) we have assumed a distance of 23 Mpc for galaxies within the Virgo B cloud, and of 17 Mpc for all other Virgo cluster members.

Since our full catalog covers the Virgo cluster (see Fig. 2), analogously to what we have done for our sample of filament galaxies, we have assigned morphological classifications from HyperLeda and local densities to all Virgo galaxies considered for our comparison.

5.2. The field: AMIGA isolated galaxies

The comparison of our sample of filament galaxies with field sources is also essential to understand the effect of the filamentary structures on galaxy evolution. To this aim we have considered the multi-wavelength Analysis of the interstellar Medium in Isolated GAlaxies (AMIGA) survey.⁵ It comprises a sample of $\sim 1,000$ galaxies in the local Universe peaking at distances of ~ 70 Mpc (Verdes-Montenegro et al. 2005). They have been primarily selected to be in isolation, by inspection of their local environment.

This sample thus contains pure field galaxies and is optimal for our comparison, since it has minimum contamination from

⁵ <http://amiga.iaa.es>

field galaxies belonging to poor or moderately rich groups. The AMIGA sample has also a wealth of ancillary data, which allow us to perform a homogeneous comparison with respect to our filament galaxies.

5.2.1. Stellar mass, SFR, and gas masses

We assigned stellar mass and SFR estimates to AMIGA sources using the Leroy et al. (2019) catalog, to have a homogeneous comparison with our sample of filament galaxies and Virgo cluster members. Among the full sample of AMIGA galaxies, we then selected those with cold gas observations, both in HI and CO. This selection yields 200 sources within AMIGA.

HI observations of AMIGA sources were done with Arecibo, Effelsberg, Green Bank, and Nançay radio telescopes (Jones et al. 2018). CO(1→0) observations are instead reported in Lisenfeld et al. (2011) and have been done mostly with IRAM 30m and FCRAO telescopes or, alternatively, they have been gathered from the literature by the authors. To convert the CO fluxes into gas masses, we have followed the procedure described in Sect. 4. In particular we have adopted a Galactic conversion factor $\alpha_{\text{CO}} = 4.3 M_{\odot} (\text{K km s}^{-1} \text{ pc}^2)^{-1}$. Note also that Lisenfeld et al. (2011) used the same CO aperture correction as the one adopted in this work (Eq. 4).

For both AMIGA and Virgo cluster galaxies, in case of non-detection, 3σ upper limits to gas masses have been derived at a resolution of 300 km/s for both CO and HI, assuming an full width at half maximum (FWHM) of 300 km/s, as has been done for our sources of filament galaxies.

5.2.2. Local densities

Among the 200 AMIGA sources, 45 (23%) are in our full sample of galaxies around Virgo (Fig. 2). We have thus assigned to these sources local density estimates, computed as described in Sect. 2.4. For the remaining 155 galaxies we have assigned n_5 local densities using projected densities estimated by Verley et al. (2007a) by means of the k -th nearest neighbor, typically with $k = 5$. These densities are estimated in projection, however we have converted them into 3D-densities, assuming statistically spherical symmetry around AMIGA sources and using the list of neighbors reported by Verley et al. (2007b). For the sake of homogeneity local densities for the 155 AMIGA sources have been then increased by a factor of 4.3, which takes into account the mean logarithmic offset of 0.63 ± 0.74 that is found for the densities of the AMIGA sources that belong also to our catalog of sources around Virgo.

Finally, seven out of the 200 AMIGA sources, namely PGC 022100, UGC 04659, PGC 02731, NGC 5016, NGC 5375, UGC 09556, and NGC 6012, are also in our sample of filament galaxies and we have removed them from our comparison. Our selection thus yields a sample of 193 AMIGA sources, all with local density estimates.

6. Environment

6.1. Environmental parameters

In this section we investigate the clustering properties of our sample of filament galaxies around Virgo. To this aim, in Fig. 7 we report the local densities n_5 , estimated using the 5th-nearest neighbor, for the 245 sources in our sample. Local densities are

exponential scale length			
$d_{0,\text{fil}}$	2.29 ± 0.55	h^{-1}	Mpc
$d_{0,\text{cluster}}$	9.69 ± 3.14	h^{-1}	Mpc
central density			
$n(d_{\text{fil}} \ll d_{0,\text{fil}}, \langle d_{\text{cluster}} \rangle)$	$2.94^{+1.86}_{-1.38}$	h^3	Mpc $^{-3}$
$n(\langle d_{\text{fil}} \rangle, d_{\text{cluster}} \ll d_{0,\text{cluster}})$	$5.56^{+2.10}_{-1.75}$	h^3	Mpc $^{-3}$
large scale density (field)			
$n(d_{\text{fil}} \gg d_{0,\text{fil}}, \langle d_{\text{cluster}} \rangle)$	~ 0.08	h^3	Mpc $^{-3}$
$n(\langle d_{\text{fil}} \rangle, d_{\text{cluster}} \gg d_{0,\text{cluster}})$	~ 0.07	h^3	Mpc $^{-3}$

Table 2: Density profile parameters.

plotted against the distances to the filament spines d_{fil} (left) and to the Virgo cluster d_{cluster} (right). The reported densities and distances are estimated in the 3D Super Galactic Coordinate frame. We refer to Sect. 2.4 for details.

Note that in this work we refer to our filament galaxies with no distinction. However, as seen in Fig. 7 the sources span a broad range of distances from the spine, up to $d_{\text{fil}} \sim 20 h^{-1}$ Mpc for a few sources, where the filamentary structures are less dense and more similar to the field in terms of their local environment. We also consider all filamentary structures altogether, but we stress that they have different properties in terms of their structure (e.g., filament, cloud, sheet), as well as richness, thickness, and length (e.g., Kim et al. 2016).

6.1.1. Filament profiles and scale lengths

We have fitted with an exponential model the local densities of our 245 filament galaxies altogether, as a function of their position relative to the filament spine and Virgo cluster, as follows. We assume that the density along filaments depends on two parameters, the distances d_{fil} and d_{cluster} . We also assume that these two dependencies are separable. We have used exponential functions to fit the data points. According to this simple model, the 3D local density n_5 can be expressed as follows:

$$n_5(d_{\text{fil}}, d_{\text{cluster}}) = \Phi_{\text{fil}}(d_{\text{fil}}) \times \Phi_{\text{cluster}}(d_{\text{cluster}}), \quad (6)$$

where

$$\Phi_i(d_i) = a_i \exp(-d_i/d_{0,i}) + b_i. \quad (7)$$

The suffix $i = \text{fil}, \text{cluster}$ corresponds to filaments or Virgo cluster, respectively.

In the left and right panels of Fig. 7 we report the best fit curves evaluated at the median distances $\langle d_{\text{cluster}} \rangle$ and $\langle d_{\text{fil}} \rangle$, respectively. With 6 best fit parameters and 245 data points we have a degree of freedom $\text{dof} = 238$. The best fit to the 245 data points yields a $\chi^2/\text{dof} = 2730/238 = 11.5$. The reduced χ^2 is thus higher than unity, which reflects the large scatter in the data points. In Table 2 we report the best fit exponential scale lengths as well as the central and large scale densities that result from our fit.

A typical filament thickness $d_{0,\text{fil}} = (2.29 \pm 0.55) h^{-1}$ Mpc is inferred from our fit, which is within the range of values found in the literature. Our estimate is in fact lower than that of $(5.1 \pm 0.1) h^{-1}$ Mpc found in Bonjean et al. (2020) by fitting an

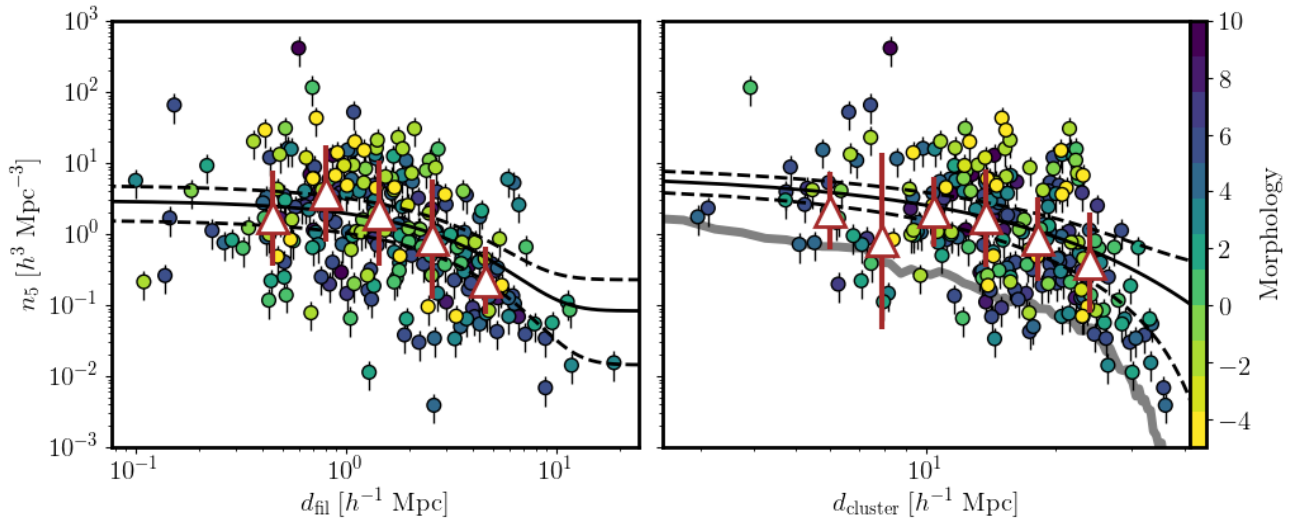


Fig. 7: Density profile for filament sources in our sample as function of the distance from the filament spine (left) and from the Virgo cluster center (right). The solid lines show the best fit to the data performed with the exponential model described in the text and estimated at the median distances $\langle d_{\text{cluster}} \rangle$ (left) and $\langle d_{\text{fil}} \rangle$ (right). Dashed lines denote the $\pm 1\sigma$ uncertainties to the fit. Triangles show the running median, their error bars are the rms uncertainty. In the right panel the gray solid line shows the average field density estimated in concentric shells with Virgo.

exponential profile to cosmological filaments at $0.1 < z < 0.3$, but higher than both $\sim (0.2 - 0.9) h^{-1}$ Mpc found by Lee et al. (2020) by fitting the individual profiles of some major filaments around Virgo and the values of $\sim (0.7 - 1.0) h^{-1}$ Mpc recently found in hydrodynamic simulations (Kuchner et al. 2020; Rost et al. 2020b). These different values for the filament thickness, which is of the order of $\sim 1.0 h^{-1}$ Mpc, are not surprising. Indeed the specific smoothing scale associated with different studies may have an impact on structural properties of the recovered filaments (e.g., Kuutma et al. 2020; Kraljic et al. 2018, for a discussion).

The local density declines less rapidly as a function of the distance to the cluster (Fig. 7, right), with a typical scale $d_{0,\text{cluster}} = (9.69 \pm 3.14) h^{-1}$ Mpc. This is consistent with the fact that we are indeed probing filaments over several virial radii between $\sim (2 - 36) h^{-1}$ Mpc, in 3D, but also in projection on the (SGX, SGZ) plane. This last aspect also shows that the extension of the considered filaments is, on average, mostly along the projected sky, which minimizes the impact of line of sight uncertainties on our analysis.

6.1.2. Central and large scale densities

As reported in Table 2, our fit also yields central densities between $\sim (3 - 6) h^3 \text{ Mpc}^{-3}$, more than an order of magnitude higher than those $\sim 0.1 h^3 \text{ Mpc}^{-3}$ found at large distances from both cluster center and the filament spines, that nicely resemble those typical of our comparison field sample (i.e., AMIGA, see Sect. 7.2.4). A similar density contrast of about an order of magnitude up to $d_{\text{cluster}} \sim 30 h^{-1}$ Mpc is also found in Fig. 7 (right) by comparing the best fit to the local density n_5 with the average field value (gray solid line) estimated in shells centered on Virgo.

6.2. Groups within filaments

We further characterize the environmental properties of our sample of filament galaxies using the group catalog of Kourkchi & Tully (2017). This catalog has a recession velocity cut at $3,500 \text{ km s}^{-1}$, safely higher than that used for our sample. We found indeed all sources in our sample, except two (i.e., UGC 6455, KUG 1128+358). The vast majority of our sources, $\sim 72\%$ (77/245), is distributed in 81 groups, that have at least two members. We report the group mass vs. richness scatter plot for these groups in Fig. 8. The two quantities are nicely correlated.

About $\sim 12\%$ (30/245) of our sources belong to two rich groups, which encompass more than 40 members with masses $\gtrsim 10^{13} M_\odot$. In practice, a total of 12 and 18 of our filament galaxies belong to the well-known NGC 5846 and NGC 5353/4 groups, with a total of 84 and 61 members, respectively. They are the end points (i.e., knots) of the rich VirgoIII and NGC 5353/4 filaments.

Fig. 8 also indicates that the number of sources in our CO sample increases as a function of group richness. The correlation is robust as quantified by the low p-value = 1.87×10^{-11} of the Spearman test. Therefore our galaxies sample in a fairly unbiased way the group galaxy populations.

We are thus homogeneously characterizing the filamentary structures around Virgo, from the poorest to the richest groups. We refer to Table B.1, where group properties for our sample, taken by Kourkchi & Tully (2017) are reported.

6.3. Galaxy alignments with filaments

For our environmental analysis we also measured the orientation $\theta_{\text{alignment}}$ between the major axis of the source and the direction

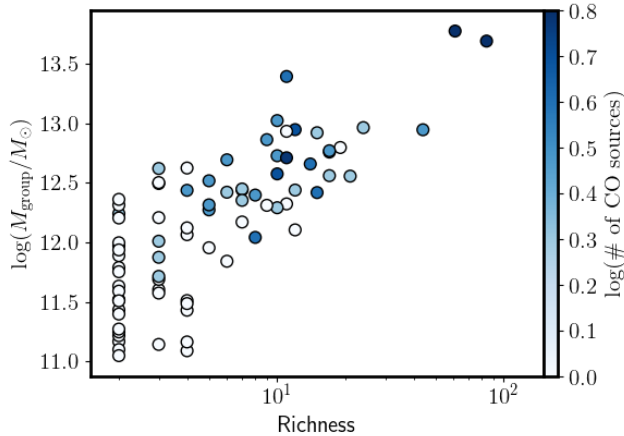


Fig. 8: Group mass vs. richness for the 81 groups in filaments with at least two galaxies (Kourkchi & Tully 2017). Points are color coded according to the number of group members that are part of our sample of filament galaxies.

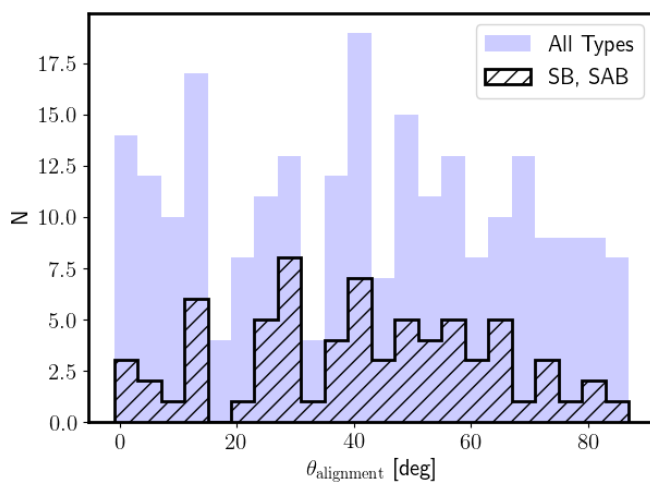


Fig. 9: Distribution of the projected orientation $\theta_{\text{alignment}}$ of the galaxy major axis with respect to the filament spine for the sources in our sample.

of the filament spine, estimated locally. The values of $\theta_{\text{alignment}}$ are also reported in Table B.1, for each galaxy.

In Fig. 9 we show the distribution of $\theta_{\text{alignment}}$ for our sources, where barred galaxies (SB, SAB) are highlighted. Interestingly, our sources quite homogeneously span all possible alignments, which implies that there is no preferred direction with respect to the filament spine. This applies also when barred galaxies are considered separately, for which the position angle is better determined. Similarly, no clear trend has been found when cross-correlating $\theta_{\text{alignment}}$ with i) local densities, ii) distances from the filament spine, and iii) galaxy morphology, separately.

Interestingly, the absence of correlation of $\theta_{\text{alignment}}$ with respect to the galaxy morphology is at odd with some previous

studies based on both cosmological simulations and wide field surveys (Tempel et al. 2013; Tempel & Libeskind 2013; Hirv et al. 2017; Codis et al. 2018; Chen et al. 2019; Welker et al. 2020). They show indeed that the spin axis or major axis of low-mass galaxies is preferentially aligned with their local environment or the nearest filament, while higher mass galaxies more likely display an orthogonal orientation. However, this effect is found to be small in all these studies. The absence of any correlation for our sample could therefore be explained by our small sample size, which is particularly true if we limit ourselves to the more massive early galaxies. Uncertainties in the position angles and filament directions, as well as the fact that $\theta_{\text{alignment}}$ are estimated in projection could contribute to weaken any possible correlation. Similarly to what found for our sample, we also note that Krolewski et al. (2019) recently found no evidence for alignment between galaxy spins and filament directions for nearby galaxies within the MANGA survey.

7. Results

In the following we focus on galaxies with HI and CO observations, placing them in the general cosmic context presented above.

7.1. Galaxy properties

We start by investigating the distribution of the galaxy morphologies, stellar masses and star formation rates in connection with their large scale structure environment as traced by the field (isolation), filaments, and cluster.

Figure 10 presents the distribution of the different samples in the star-formation rate vs. stellar mass diagram, with our sample of filament galaxies in the central panel, the AMIGA sources on the left panel, and the Virgo cluster galaxies on the right. The position of the MS as derived by Leroy et al. (2019) and the associated scatter are also displayed. For the three sample, galaxies are homogeneously covering the same stellar mass range $\log(M_*/M_\odot) \sim 9 - 11$.

7.1.1. Morphology

The bulk of the galaxy population in the three samples under investigation is composed of late type galaxies (LTGs, $T \geq 0$). Indeed the fraction of early type galaxies (ETGs, $T < 0$) is only about $\sim 27\%$ for both filament (65/245) and Virgo cluster (30/109) galaxies, while it drops significantly to $\sim 8\%$ (i.e., 16/193) for the AMIGA sources. Since AMIGA sources were primarily selected to be in isolation, ETGs in isolation are possibly associated with *rare* fossil groups (Ponman et al. 1994; Jones et al. 2003). In these groups the central ellipticals are isolated (e.g., as a result of previous mergers), thus in the final phase of their mass assembly (e.g., Barnes 1989; Zepf & Whitmore 1993; Khosroshahi et al. 2006).

7.1.2. Main sequence and morphology

We further investigate the location of galaxies with respect to the MS, distinguishing between LTGs and ETGs. For AMIGA, filaments, and Virgo, the bulk of the galaxy populations lies on the MS and is essentially composed of LTGs, as mentioned above.

The fraction of both ETGs and LTGs that are located below the MS, i.e., with $\text{SFR} < 1/3 \text{SFR}_{\text{MS}}$, increases as one moves from the field (AMIGA) to filaments. For the LTGs, only

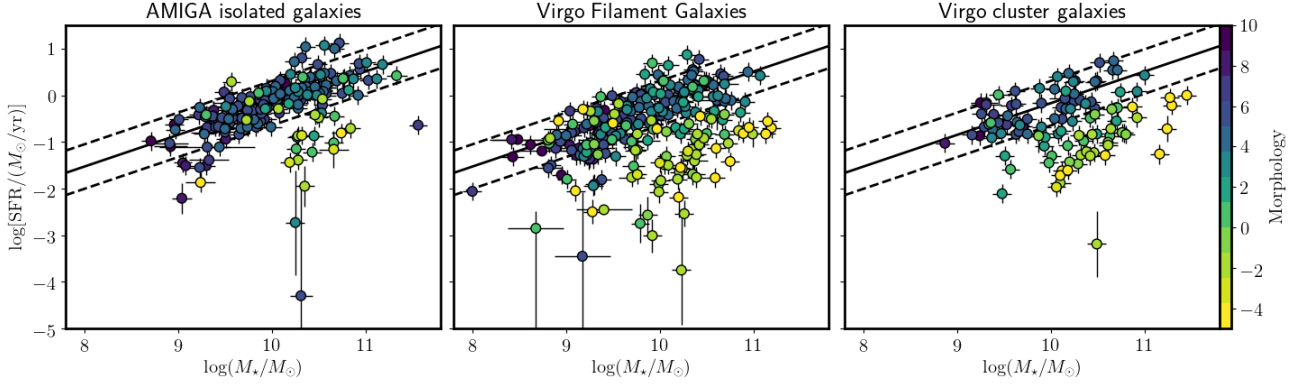


Fig. 10: SFR vs. stellar mass scatter plots for the Virgo filament sources in our sample (center), AMIGA isolated galaxies (left), and Virgo cluster galaxies (right). Sources are color-coded according to their morphological de Vaucouleurs classification, as shown in the color bar. The solid dashed line show the local MS relation by Leroy et al. (2019), while the dashed lines correspond to $\pm \log(3) = \pm 0.48$ dex uncertainty.

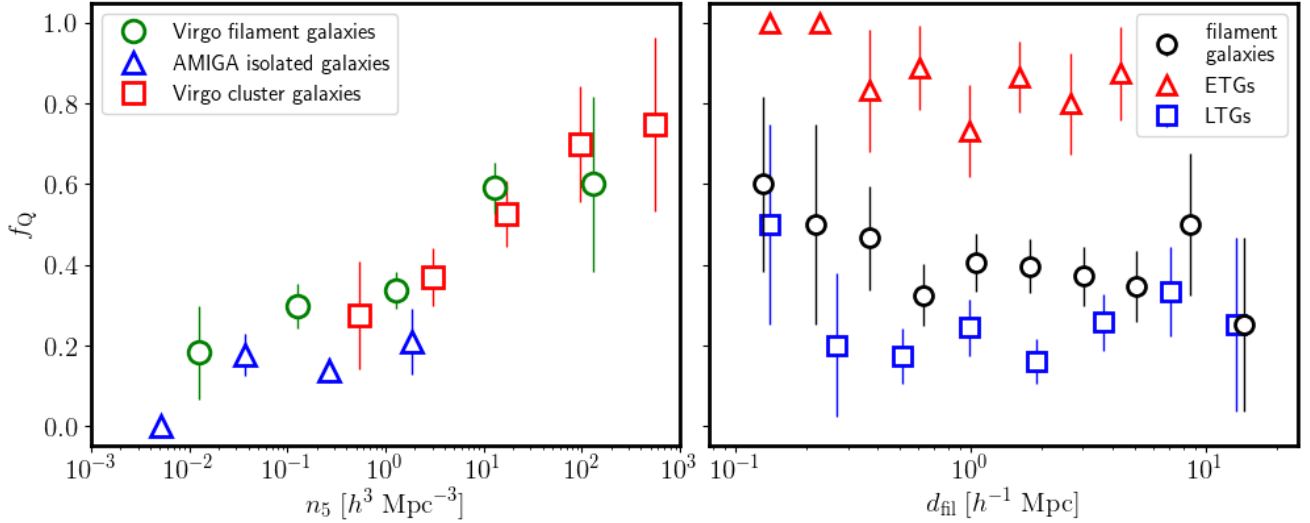


Fig. 11: Quenching fraction f_Q vs. local density (left) and distance to the filament (right).

$11\% \pm 2\%^6$ of the AMIGA sample is below the MS, compared to $23\% \pm 3\%$ ($41/180$) in the filaments, and $25\% \pm 5\%$ ($20/79$) in the Virgo cluster. Conversely, the fraction of ETGs below the MS is $69\% \pm 12\%$ ($11/16$) for AMIGA sources, $83\% \pm 5\%$ ($54/65$) for filament galaxies, and 100% ($30/30$) for the Virgo cluster galaxies. This shows that galaxy star formation activity is more effectively suppressed in filaments than the field, but less strongly than in Virgo cluster. Therefore the processes that lead to star formation quenching are already at play in filaments for LTGs and even more effectively for ETGs.

7.1.3. Fraction of galaxies with suppressed star formation as a function of their environment

We now quantify the impact of filamentary structures on the star formation activity of galaxies by defining explicitly the quenching fraction f_Q as that of sources with suppressed star formation, i.e., $SFR < 1/3 SFR_{MS}$. These are sources well below the MS and with low levels of ongoing star formation (specific star formation rate, $sSFR < 9 \times 10^{-11} \text{ yr}^{-1}$). Figure 11 displays f_Q as a function of the environment, that we parameterize using the local density n_5 (left) and distance to the filament (right). The AMIGA and Virgo galaxies are associated with the lowest ($n_5 = (0.19^{+0.41}) h^3 \text{ Mpc}^{-3}$) and highest ($n_5 = (6.29^{+27.47}) h^3 \text{ Mpc}^{-3}$) densities, respectively. Filament galaxies are found at intermediate densities, with a median of $n_5 = (1.12^{+5.64}) h^3 \text{ Mpc}^{-3}$. They also span a broader range of n_5 with an overlap in density with

⁶ Hereafter, rms uncertainties in the fractions are estimated using binomial statistics (see e.g., Castignani et al. 2014).

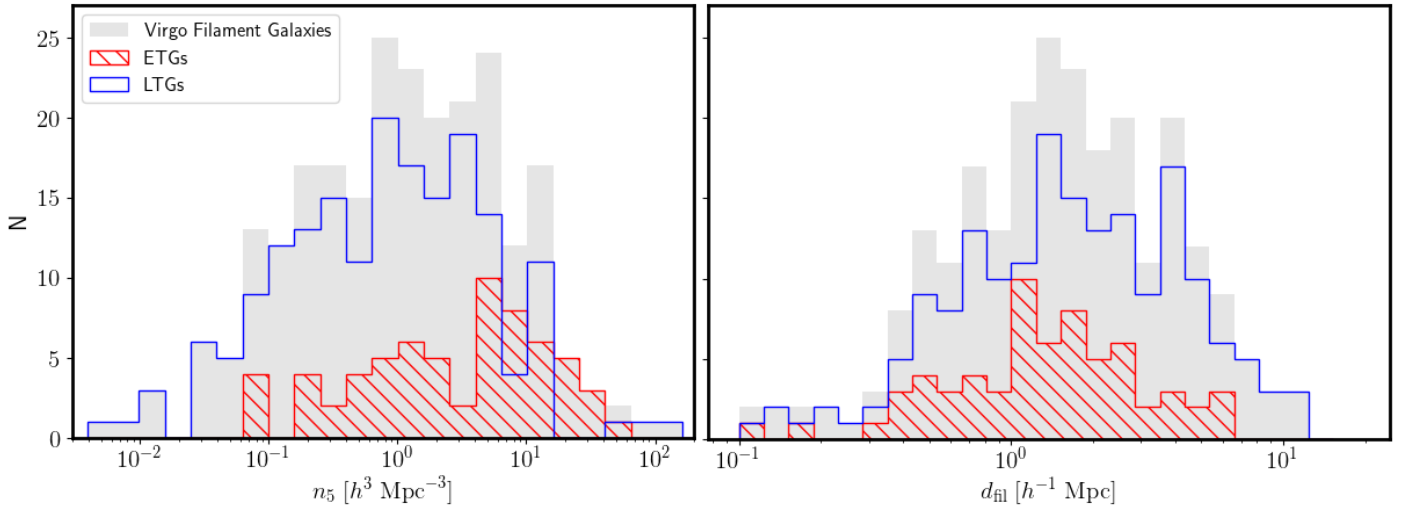


Fig. 12: Distribution in local density and distance to the filament spine for our sample of filament galaxies (gray) as well as for the subsamples of ETGs and LTGs.

field and cluster galaxies at the low and high end of the distribution, respectively, similarly to what has been found for example in simulations (Cautun et al. 2014).

The left panel of Fig. 11 reveals a monotonic increase of the quenching fraction from the lowest to the highest densities for field, filament, and cluster galaxies. The AMIGA sources, which are found at the lowest densities $n_5 \lesssim 1 h^3 \text{ Mpc}^{-3}$, exhibit the lowest values $f_Q \lesssim 0.2$. On the other extreme, the Virgo cluster shows an increasing fraction ranging from $f_Q \sim 0.3$ to $f_Q \sim 0.8$ at the highest density regions with $n_5 \sim 10^3 h^3 \text{ Mpc}^{-3}$. For the filaments specifically, the quenching fraction increases from $f_Q \sim 0.2$ to 0.6 within the broad range of densities that they cover, i.e., $n_5 \sim (10^{-2} \text{ to } 10^2) h^3 \text{ Mpc}^{-3}$. At comparable densities, filaments have similar f_Q values as the field and the Virgo cluster. A similar behaviour of increasing f_Q with local density is observed also when we limit ourselves to massive galaxies with stellar masses above $10^{10} M_\odot$. For galaxies with M_\star below this value, the quenching ratio is lower, $f_Q \lesssim 0.4$, for the three cosmic environments and at low to moderate local densities below $10 h^3 \text{ Mpc}^{-3}$, while at higher densities non-negligible shot noise for the counts prevents us to draw firm conclusions.

Considering the filament galaxies altogether, we find $f_Q = (39 \pm 3)\%$, i.e., 95/245. This value is fairly consistent with the quiescent fraction $\sim 50\%$ found by Bonjean et al. (2020) for higher redshift $0.1 < z < 0.3$ cosmological filaments. Interestingly, this may indicate that the average star formation properties of filament galaxies have not dramatically evolved over the last ~ 2 Gyr.

The right panel of Fig. 11 shows the variation of f_Q with the distance to the filament spine. The fraction of filament galaxies with suppressed star formation declines from $f_Q \sim 0.6$ in the central regions down to $f_Q \sim 0.2$ at $d_{\text{fil}} \lesssim 1 h^{-1} \text{ Mpc}$. This suggests that filaments do not start affecting the star formation until galaxies are within $\sim 1 h^{-1} \text{ Mpc}$. This radius at which the quenching starts is fairly consistent with that of $(3.0 \pm 1.1) h^{-1} \text{ Mpc}$ found by Bonjean et al. (2020) in filaments at higher redshifts $0.1 < z < 0.3$ and with the average filament thickness $d_{0,\text{fil}} \sim 2 h^{-1} \text{ Mpc}$ for the density profile reported in Sect. 6.

The f_Q of ETGs and LTGs is dramatically different at all distances from the filament spine. In the central regions ($d_{\text{fil}} \lesssim 0.2 h^{-1} \text{ Mpc}$), half of the LTGs have suppressed star formation ($f_Q \sim 0.5$), and this fraction declines with the distance to the filament increases. In contrast, nearly all the ETGs show suppressed star formation, regardless of the separation. At larger distances, both LTGs and ETGs see their f_Q decreasing but the ETGs stay at much higher values than LTGs ($f_Q \sim 0.8$ vs 0.2).

Figure 11 thus suggests that the suppression of star formation in filaments is strongly regulated by the local density, at a level that is intermediate between the field and Virgo cluster. The distance to the filament spine appears as a secondary parameter, but the onset of the passive population in filaments emerges once the separation $\sim 1 h^{-1} \text{ Mpc}$ is reached. At the lookback time of Virgo, nearly all ETGs have already seen their star formation activity impacted, while LTGs are still sensitive to their position relative to the filament spine. The next section clarifies further the inter-relation between local density and distance to the filament spines.

7.1.4. Local densities and distances to the filaments

In Fig. 12 we show the distribution of our filament galaxies as a function of local density (left panel) and distance to the filament spine (right panel). The distribution of ETGs and LTGs are shown with the hatched red and blue histograms, respectively, while the filled gray histogram shows the combined populations. As shown in the left panel of Fig. 12, LTGs are spread over a wide range of local densities and distances to the filaments, with a moderate median density of $n_5 = (0.9^{+4.4}_{-0.7}) h^3 \text{ Mpc}^{-3}$. ETGs are preferentially found in regions of higher local densities, with a median value of $n_5 = (4.1^{+10.8}_{-3.6}) h^3 \text{ Mpc}^{-3}$. While the ETGs also span a wide range in local densities (a factor of 1000 in density), they do not populate the lowest density regions. The right panel of Fig. 12 shows that ETGs are also preferentially located closer to the filament spines than LTGs; the median distance for ETGs is $\langle d_{\text{fil}} \rangle = (1.4^{+1.3}_{-0.8}) h^{-1} \text{ Mpc}$, whereas the median distance for LTGs is $\langle d_{\text{fil}} \rangle = (1.7^{+2.6}_{-1.1}) h^{-1} \text{ Mpc}$. The Mann–Whitney–Wilcoxon test indicates that the difference in

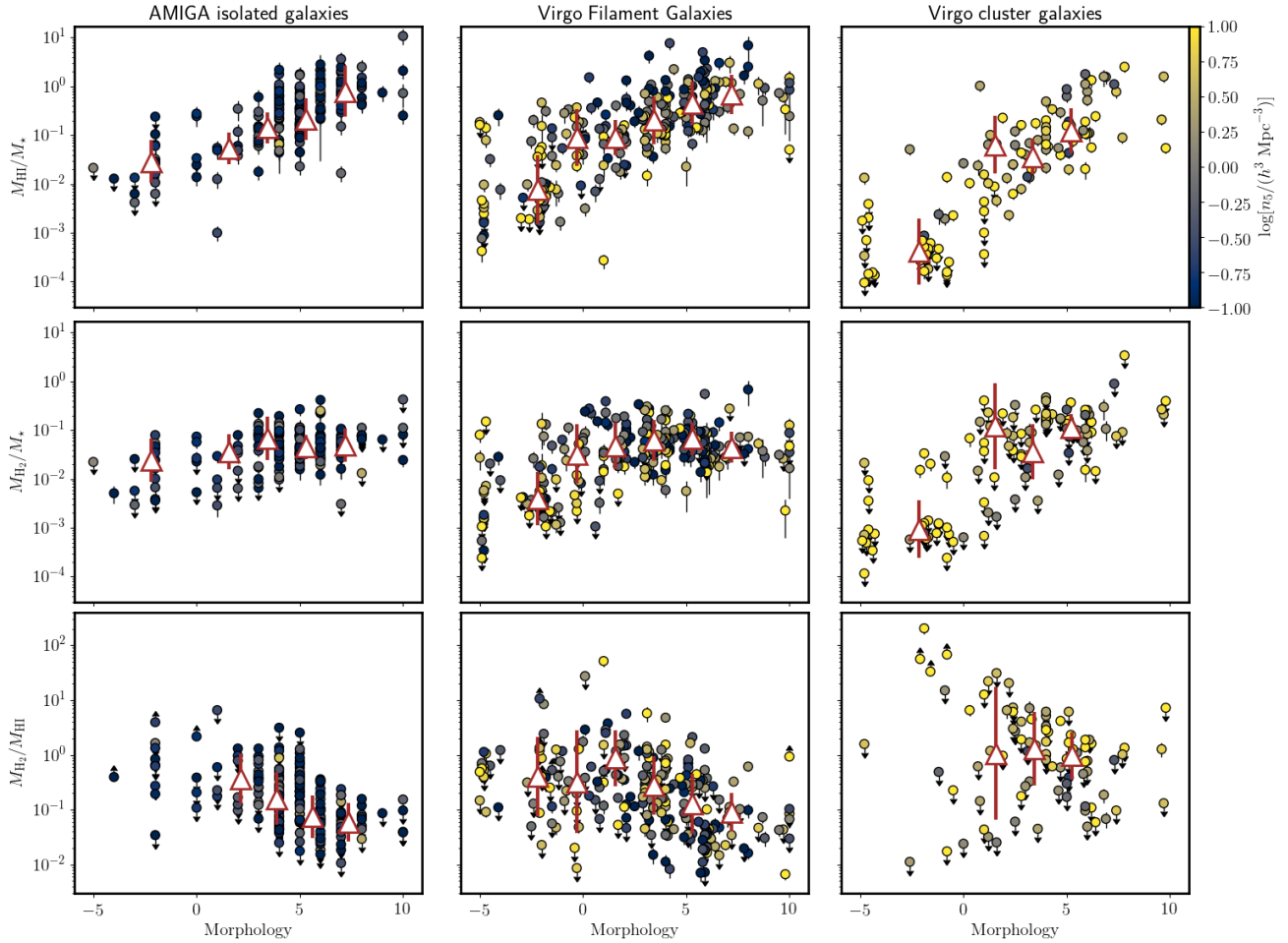


Fig. 13: From top to bottom: M_{HI}/M_{\star} , M_{H_2}/M_{\star} , and $M_{\text{H}_2}/M_{\text{HI}}$ as a function of morphology for Virgo filament galaxies (center), AMIGA isolated galaxies (left) and Virgo cluster galaxies (right). The triangles show the running median values, with the associated rms uncertainties. Points are color-coded according to the local density n_5 .

the median values between the two morphological classes is statistically significant for both local densities (p -values 5.61×10^{-6}) and distances d_{fil} (p -value = 3.89×10^{-2}).

We thus observe a segregation of massive galaxies in the densest central regions of filaments in the local Universe, possibly as a result of previous mergers of lower mass sources. This segregation is in agreement with similar findings, that have been found at higher redshifts for a number of spectroscopic surveys (Tempel & Libeskind 2013; Malavasi et al. 2017; Laigle et al. 2018; Kraljic et al. 2018; Welker et al. 2020; Kuutma et al. 2020). Our finding is also consistent with the result of Rost et al. (2020a), who compared three catalogs of cosmological filaments identified in the Sloan Digital Sky Survey and found that the overdensity profile of red galaxies is systematically higher than that of blue galaxies. Fig. 7 shows that there is a wide range of local densities at fixed distance from the filament spines, except for the largest distances for which densities are only low. So while distances and densities are correlated, we show in the sections that follow (e.g., Sects 7.2.4, 7.2.5) that local density seems to be a stronger driver of morphological evolution than distance from the filament.

7.2. Atomic and molecular gas

We now investigate the general properties of the gas reservoirs of filament galaxies, in comparison with those of AMIGA and Virgo cluster galaxies.

7.2.1. Relation between gas fraction and morphology

Fig. 13 presents the M_{HI}/M_{\star} ratio as a function of galaxy morphology for the three samples considered, as well as the molecular gas to stellar mass ratio, M_{H_2}/M_{\star} , and the $M_{\text{H}_2}/M_{\text{HI}}$ ratio. Both M_{HI}/M_{\star} and M_{H_2}/M_{\star} ratios clearly increase from ETGs to LTGs. The slope of this function is increasingly steeper when passing from isolation to the cluster core, as the consequence of the fact that while late galaxies have very similar gas fractions in all cosmic structures, early type galaxies are more strongly gas-depleted in very dense ones such as clusters. This observed trend of gas fraction with morphology is stronger for M_{HI}/M_{\star} than for M_{H_2}/M_{\star} , again driven by the ETGs being increasingly gas poor with increasing density of the environment.

The median gas to stellar mass ratios for ETGs decrease in the three environments as follows:

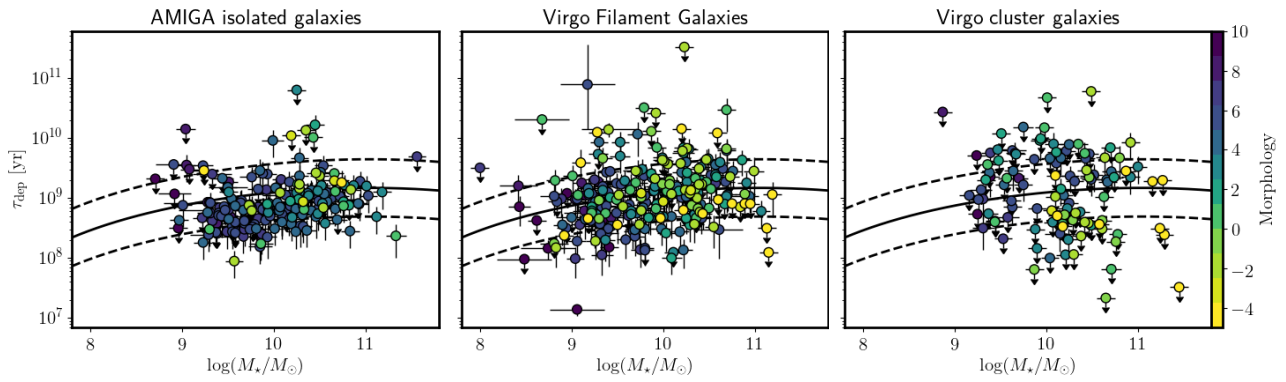


Fig. 14: Depletion time vs. stellar mass. Different panel refer to Virgo filament galaxies (center), AMIGA isolated galaxies (left), and Virgo cluster galaxies (right). Solid and dashed lines correspond to the local prescription and model uncertainties by Tacconi et al. (2018) for MS galaxies, calibrated using a Galactic conversion factor $\alpha_{\text{CO}} = 4.3 M_\odot (\text{K km s}^{-1} \text{ pc}^2)^{-1}$.

– ETGs –	AMIGA	Filaments	Virgo
$M_{\text{HI}}/M_\star =$	$0.02^{+0.04}_{-0.01}$	$0.01^{+0.15}_{-0.01}$	$0.0005^{+0.0018}_{-0.0003}$
$M_{\text{H}_2}/M_\star =$	$0.02^{+0.03}_{-0.02}$	$0.004^{+0.025}_{-0.003}$	$0.0009^{+0.0117}_{-0.0003}$

For LTGs the median ratios are higher than ETGs and fairly similar between the three different environments, within the dispersions:

– LTGs –	AMIGA	Filaments	Virgo
$M_{\text{HI}}/M_\star =$	$0.34^{+0.71}_{-0.25}$	$0.30^{+0.85}_{-0.21}$	$0.08^{+0.51}_{-0.07}$
$M_{\text{H}_2}/M_\star =$	$0.05^{+0.05}_{-0.02}$	$0.05^{+0.09}_{-0.03}$	$0.11^{+0.15}_{-0.09}$

The scatter around the median values increases as we move from the poorest to the richest environments, with an increased fraction of upper limits in HI and/or H₂. This result is consistent with Bok et al. (2020), who found that the scatter in the gas content is significantly higher for galaxies in pairs than for isolated AMIGA galaxies.

7.2.2. Relation between H₂ to HI mass ratio and morphology

The bottom row of Figure 13 shows the molecular to atomic mass ratio of $M_{\text{H}_2}/M_{\text{HI}}$ as a function of galaxy morphology, where sources with upper limits both in H₂ and HI have been conservatively excluded. The ratios of $M_{\text{H}_2}/M_{\text{HI}}$ are essentially $\lesssim 1$ regardless of the considered environment of the galaxy: isolation, in filament, or in Virgo cluster.

Both the isolated AMIGA and filament galaxies show a decrease in $M_{\text{H}_2}/M_{\text{HI}}$ with increasing T type. This is mostly driven by the rapid increase of the HI mass in galaxies moving towards late-type morphology, steeper than for M_{H_2} . This correlation was also discussed by Obreschkow & Rawlings (2009) as the result of the increased importance of the bulge component towards earlier types along the Hubble sequence. Massive galaxies are less

dense due to their larger disk sizes. Therefore their M_{H_2}/M_\star fraction is lower.

The scatter seen in each of M_{H_2} and M_{HI} taken independently, is increased for the ratio $M_{\text{H}_2}/M_{\text{HI}}$, as we move from the field to the filaments, to cluster galaxies, likely as the result of the variety of ways galaxies can be depleted in gas, and the level at which this happened.

	AMIGA	Filaments	Virgo
$M_{\text{H}_2}/M_{\text{HI}} =$	$0.16^{+0.42}_{-0.11}$	$0.24^{+0.84}_{-0.19}$	$1.10^{+5.33}_{-0.99}$

The last value for Virgo is essentially an upper limit. The ratios are fairly in agreement, within the large scatter, with the value of $M_{\text{H}_2}/M_{\text{HI}} \sim 0.5$ for field galaxies, as found in previous studies (e.g., Saintonge et al. 2011). For further clarification we refer to the Appendix D, where diagnostic plots between gas content, stellar mass, and star formation are reported.

7.2.3. Relation between depletion timescale and stellar mass

Figure 14 presents the depletion timescale, $\tau_{\text{dep}} = M_{\text{H}_2}/\text{SFR}$, i.e., the time over which the galaxy molecular gas reservoir will be consumed by star formation, as a function of stellar mass. On average, in isolation and in filaments, more massive galaxies tend to have longer depletion timescales than less massive ones. This relation is mainly driven by the LTGs for which the H₂ reservoir is augmented by a factor of $\sim \times 1000$, between $\log(M_*/M_\odot) \approx 9 - 11$.

The solid line in Fig. 14 shows the prescription of depletion time versus stellar mass from Tacconi et al. (2018), and the dashed lines show the uncertainty in the relation. Noticeably, the AMIGA galaxies (left panel) are shifted to low τ_{dep} with respect to the local prescription, most likely as a consequence of their large fraction of late type galaxies, while the filament (middle panel) and cluster (right panel) galaxies scatter around this standard relation. The scatter increases steadily with environmental density, from the field, to the filaments, to Virgo, to a point where the relation between τ_{dep} and M_\star breaks down for Virgo galaxies. As can be seen further in the Appendix D, the number of galaxies with upper limits in H₂ and non-negligible SFR, often

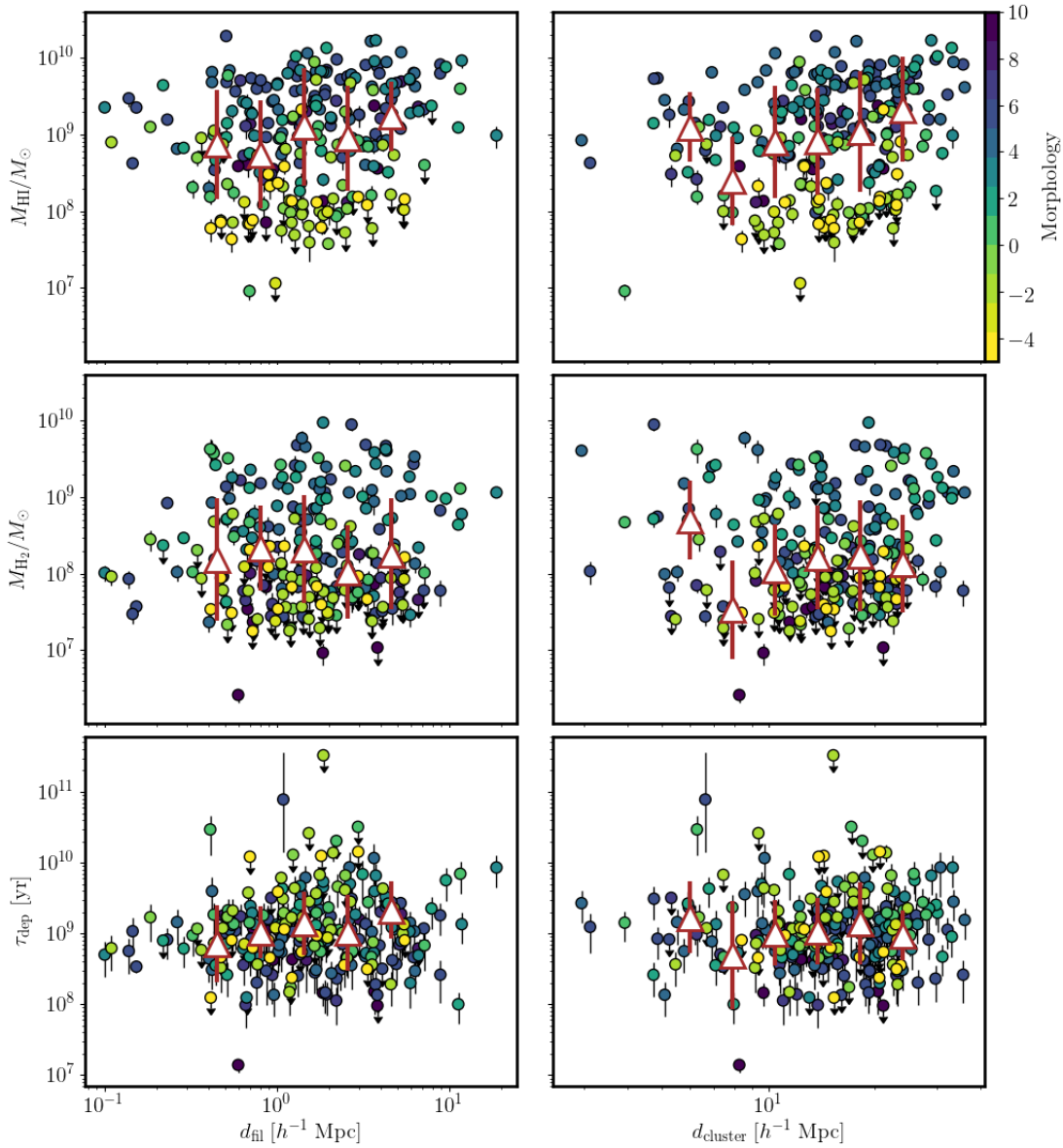


Fig. 15: M_{HI} , M_{H_2} , and depletion time plotted against the distance from the filament spine and the distance to the Virgo cluster for our sample of filament galaxies. Triangles correspond to the binned running median, while the error bars are the rms uncertainties.

at the level of the MS, increases at stellar masses $\gtrsim 10^{9.5} M_{\odot}$. This suggests that gas depletion precedes star formation quenching for these sources, the majority of which are ETGs. In the Virgo cluster, this effect is also observed in LTGs.

7.2.4. Relation between gas masses and environmental parameters

In Fig. 15, we show the HI and H₂ gas masses and the gas depletion timescale as a function of distance to the filament (left column) and distance to Virgo (right column) for the 245 filament galaxies in our sample. The HI gas mass increases with increasing distance to the filaments ($p\text{-value} = 7.88 \times 10^{-4}$) and to the cluster core ($p\text{-value}=1.56 \times 10^{-4}$).⁷

⁷ The p-values reported in Sects 7.2.4 and 7.2.5 are those of the Spearman test. The reported correlations are found at lower significance when

In contrast, the M_{H_2} gas mass shows no trend with distance to either the filaments or Virgo. Finally, the depletion time τ_{dep} shows no correlation with distance from the Virgo cluster, but a tentative increase with increasing distance from the filament spine is observed, by means of the increasing τ_{dep} running median with d_{fil} in Fig. 15.

In Fig 16, we show the gas masses, molecular-to-atomic gas ratio, and depletion time as a function of local density. In addition, we show the filament sample (center column) in comparison with the AMIGA (left column) and Virgo cluster galaxies (right column). For the filament galaxies, we see that the HI content decreases with increasing density ($p\text{-value} = 5.25 \times 10^{-5}$). The H₂ mass decreases with local density as well, but less strongly ($p\text{-value}=0.017$) than M_{HI} . For both HI and H₂ masses,

LTGs and ETGs are considered separately. This is because of the poorer statistics of the two individual sub-samples.

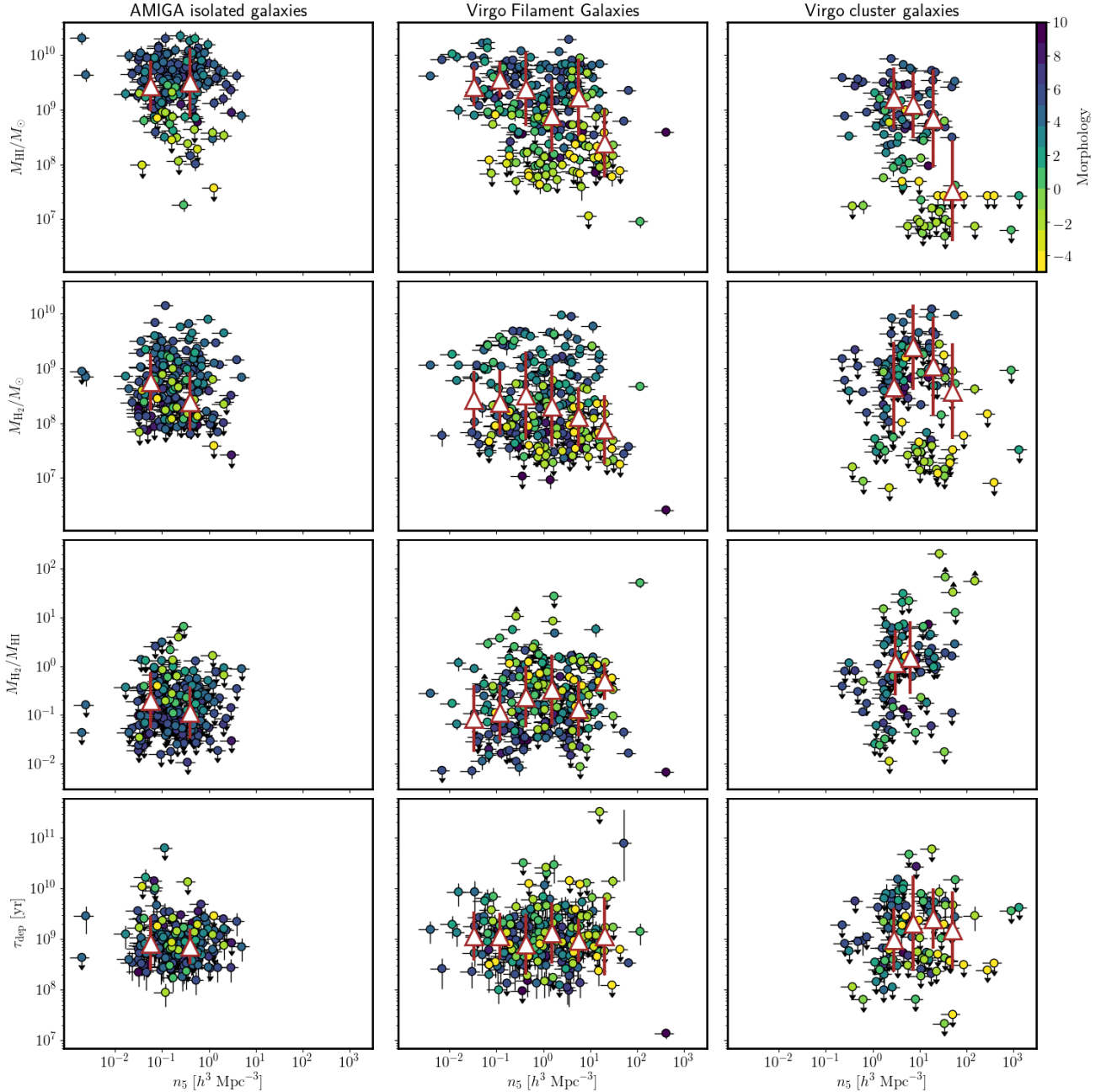


Fig. 16: From top to bottom: M_{HI} , M_{H_2} , $M_{\text{H}_2}/M_{\text{HI}}$, and τ_{dep} plotted against local densities for Virgo filament galaxies (center), AMIGA isolated galaxies (left) and Virgo cluster galaxies (right). Triangles correspond to the binned running median, while the error bars are the rms uncertainties.

the decrease is also more clear above a threshold density of $\sim 0.1 h^3 \text{ Mpc}^{-3}$, characteristic of the field. The decrease becomes extreme at the highest densities $\geq 10 h^3 \text{ Mpc}^{-3}$ in filaments and in Virgo cluster, where the fraction of sources with only gas mass upper limits significantly increases.

The color coding in Fig 16 reflects morphology. As seen in the top row, ETGs in all environments have the lowest HI masses, on average about an order of magnitude lower than LTGs. In filaments, the early-type and late-type filament galaxies have indeed a median HI mass of $M_{\text{HI}} = (1.38^{+6.71}_{-0.73})10^8 M_{\odot}$ and $M_{\text{HI}} = (1.89^{+4.34}_{-1.49})10^9 M_{\odot}$, respectively. Moreover, moving

from the status of an isolated system to a cluster member, the HI content of the ETGs drops dramatically. Inspection of the upper range of HI masses shows that the fraction of galaxies with the highest values of $M_{\text{HI}} \geq 10^{10} M_{\odot}$ (these are all LTGs) depends on the global environment, steadily decreasing from the AMIGA sample of isolated galaxies, filaments, to Virgo cluster. This suggests that these late type galaxies do experience a certain degree of HI processing already in filaments.

Early and late-type galaxies also distinguish themselves in terms of molecular gas, as seen in the second row of Figure 16. For example, in filaments, ETGs never reach M_{H_2} val-

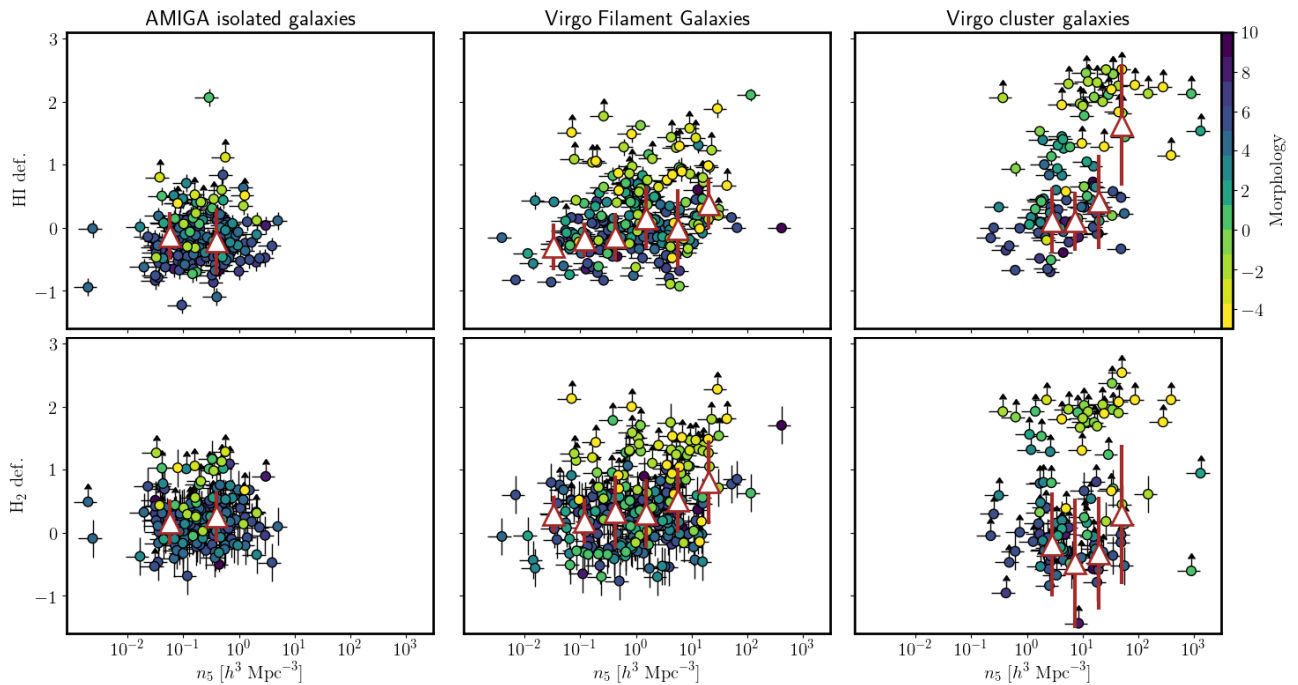


Fig. 17: HI deficiency (top row) and H_2 deficiency (bottom row) plotted against local densities for Virgo filament galaxies (center), AMIGA isolated galaxies (left), and Virgo cluster galaxies (right). Triangles correspond to the binned running median, while the error bars are the rms uncertainties.

ues as high as LTGs and have a low median value of $M_{H_2} = (0.08^{+0.13}_{-0.05}) 10^9 M_\odot$. However, the median does not tell the full story, as a large number of the LTGs have as low a reservoir of molecular gas as the ETGs, and this is true in all three environments. In the filaments, these LTGs with low molecular reservoir ($M_{H_2} \lesssim 10^8 M_\odot$) have, on average, normal HI content, with a median value of $M_{HI} = (0.94^{+1.80}_{-0.69}) 10^9 M_\odot$. They thus belong to the subsample of LTGs with low M_{H_2}/M_{HI} already seen in Fig 13 and a relatively high median morphological index of $T = 6.0^{+2.6}_{-2.8}$. They are essentially only seen in moderately dense regions in filaments ($n_5 = (0.77^{+4.26}_{-0.65}) h^3 \text{ Mpc}^{-3}$).

The third and fourth rows of Fig. 16 show the ratio of molecular-to-atomic gas masses and the depletion time, respectively. As M_{HI} depends more strongly than M_{H_2} on the local density, the M_{H_2}/M_{HI} ratio in filaments increases with increasing local density. The dispersion in the ratio also increases significantly as the environmental density increases. However, the mean value of M_{H_2}/M_{HI} does not vary much from isolation to the cluster core.

The dichotomy between the two broad classes of galaxy morphologies is not seen in the depletion time scales: both ETGs and LTGs, in filaments, scatter around the median value of $\tau_{\text{dep}} = (1.08^{+2.05}_{-0.72}) \text{ Gyr}$. At the highest local densities $\gtrsim 10 h^3 \text{ Mpc}^{-3}$ in filaments and Virgo cluster, the depletion times are strongly suppressed, with about $\sim 40\%$ and $\sim 70\%$ of the sources, respectively, having only upper limits in M_{H_2} and τ_{dep} . This suggests a rapid environment-driven exhaustion of the H_2 reservoirs in these dense regions.

Taken together, the results from Fig. 15 and Fig. 16 show that a galaxy's gas content varies with location within the cosmic web (isolation, filament, cluster). While the local density plays a stronger role than the distance to the filament spines or to cluster

core, it appears to be a secondary factor, contributing to amplify the gas depletion. The impact of the filaments is clear, with the rise of the fraction of ETGs and the removal of HI gas for even the most gaseous systems, preparing for the galaxy population that is commonly witnessed in clusters.

The HI gas is essentially distributed in the galaxy outer regions, hence is easily stripped, while the dense and molecular gas is shielded in the inner parts of galaxies. As a consequence, H_2 is therefore less impacted by the environment, except for the densest regions in filaments and in Virgo cluster. The clear emergence of ETGs in filaments environments, with increasingly low gas content and low depletion times is a striking feature of Fig. 16, as we move from the field, filaments, to Virgo. It raises the question of the timescale and relative contribution of the different physical mechanisms that can play a role: gas exhaustion during mergers and consecutive change in morphologies or lack of gas supply (e.g., starvation). In particular, for ETGs in filaments that show low gas masses, the HI stripping likely cuts off the supply of cold gas. This then favors the suppression of the star formation and quenching, possibly via starvation/strangulation in group environments (Kawata & Mulchaey 2008). Part of the cluster members can have experienced - *in situ* - the same transformations as in the filaments, but a fraction of the infalling population have certainly been pre-processed in the filaments before they reach the cluster core.

7.2.5. Gas deficiency

The HI-deficiency parameter (HI-def.) is defined as the logarithmic difference between the observed HI mass of a galaxy and the average HI mass of a reference sample of isolated galaxies with the same morphological type and size. In the following, we

HI-def.	All galaxies	LTGs	ETGs
AMIGA	(5.7 ± 1.7)% 11/193	(3.4 ± 1.4)% 6/177	(31.2 ± 11.6)% 5/16
Filaments	(23.3 ± 2.7)% 57/245	(11.7 ± 2.4)% 21/180	(55.4 ± 6.2)% 36/65
Virgo Cluster	(47.7 ± 4.8)% 52/109	(30.4 ± 5.2)% 24/79	(93.3 ± 4.6)% 28/30
H₂-def.	All galaxies	LTGs	ETGs
AMIGA	(18.7 ± 2.8)% 36/193	(15.3 ± 2.7)% 27/177	(56.2 ± 12.4)% 9/16
Filaments	(41.6 ± 3.1)% 102/245	(26.7 ± 3.3)% 48/180	(83.1 ± 4.1)% 54/65
Virgo Cluster	(37.6 ± 4.6)% 41/109	(19.0 ± 4.4)% 15/79	(86.7 ± 6.2)% 26/30
HI-def. & H₂-def.	All galaxies	LTGs	ETGs
AMIGA	(4.1 ± 1.4)% 8/193	(2.3 ± 1.1)% 4/177	(25.0 ± 10.8)% 4/16
Filaments	(15.5 ± 2.3)% 38/245	(2.2 ± 1.1)% 4/180	(52.3 ± 6.2)% 34/65
Virgo Cluster	(24.8 ± 4.1)% 27/109	(3.8 ± 2.2)% 3/79	(80.0 ± 7.3)% 24/30

Table 3: Fractions of deficient galaxies in HI (top), H₂ (center), and simultaneously both in HI and H₂ (bottom).

use the definition of HI-def. by Boselli & Gavazzi (2009), calibrated to $h = 0.74$, that was updated from the original parameter defined by Haynes & Giovanelli (1984). Similarly, we have used the definition of the H₂-deficiency parameter (H₂-def.) by Boselli et al. (2014b), as a function of the stellar mass, assuming $\alpha_{\text{CO}} = 4.3 M_{\odot} (\text{K km s}^{-1} \text{ pc}^2)^{-1}$. Galaxies with HI-def.> 0.5 considered as deficient in HI. Galaxies with H₂-def.> 0.5 are considered as as deficient in H₂.

Figure 17 presents the relation between HI-def. and H₂-def. and the local density for the isolated, filament, and cluster galaxies. In both the filament and cluster environments, both the number of HI and H₂-deficient galaxies and the median deficiency parameters increase with increasing local density. In addition, the number of both HI and H₂-deficient galaxies at a fixed local density increases going from isolated, to filament, to cluster environments. On average, AMIGA galaxies have a normal gas content, with median HI-def., H₂-def.< 0.5, while the average values steadily increase with density in the filaments and reach the highest values $\gtrsim 2$ in the Virgo cluster.

For Virgo filament galaxies the HI-def. and H₂-def. correlate well ($p\text{-value} \approx (5 - 8) \times 10^{-5}$) with the local density. This correlation is driven by the rise of the number of gas deficient galaxies in denser environments, mainly composed of ETGs. Table 3 reports the fractions of gas deficient galaxies. There is a strong dichotomy in the gas deficiencies between LTGs and ETGs, sim-

ilarly to what has been discussed in Sect. 7.2.4. ETGs are the majority of the gas deficient galaxies in any cosmic environment. They represent indeed $\sim 90\%$ of the sources that are gas deficient simultaneously both in HI and H₂.

HI-def. rises with decreasing distances to the filament ($p\text{-value} = 1.59 \times 10^{-3}$) and to the Virgo cluster core ($p\text{-value} = 7.65 \times 10^{-4}$), unlike for H₂-def. which is insensitive to these parameters. This echoes what has been found for the HI and H₂ gas masses in Fig. 15. No similar study exists on the H₂ content of galaxies in filaments.

As to HI, Lee et al. (2020) have not detected the same correlation between distance and HI deficiency as highlighted here, but our results on HI-def. are in agreement with those of Crone Odekon et al. (2018) on the ALFALFA HI survey, who found that HI-def. of their sample galaxies decreasing with distance from the filament spine, and suggest that galaxies are cut off from their supply of cold gas.

8. Summary and conclusions

We have presented the first large observational effort to gather the gas status, in both molecular and atomic gas phases, of large scale structures linked to a central galaxy cluster. This comprehensive study aims at evaluating the impact of cosmological filaments in the processing the cold gas reservoirs of galaxies, as

they move within the cosmic web and before they fall into the cluster itself. To this end, we have built a homogeneous sample of 245 galaxies with stellar masses $\log(M_\star/M_\odot) \sim 9 - 11$; they are located in major filaments surrounding Virgo. Stellar masses and star formation rate (SFR) estimates have been gathered from the literature. H₂ and HI masses have been estimated thanks to our CO and HI campaigns at the IRAM-30m and Nançay telescopes, respectively, or taken from previous published observations.

Environmental parameters such as alignments with respect to the filament spines, local densities, distances from the filament spines and from Virgo cluster have been calculated, following an accurate 3D characterization of the cosmic web around Virgo. We have compared the properties of these filament galaxies with those of two samples of galaxies with similar size: i) isolated field galaxies (AMIGA) and ii) galaxies belonging to the Virgo cluster itself. Stellar and gas masses, SFRs, depletion times, quiescent fractions, and environmental properties have been considered for all three samples, with a homogeneous treatment of the data.

8.1. Summary of the results

- The filamentary structures around Virgo contain a large number of groups, from poor to rich ones. As such, they exhibit a broad range of local densities. They are fairly well described by exponentially decaying profiles (Sect. 6).
- The bulk of our filament galaxy sample with CO and HI observations is primarily composed of spiral galaxies, like the AMIGA and the Virgo cluster samples. The large majority of these LTGs fall on the MS of star forming galaxies. ETGs appear in significant numbers in the filaments, with the majority in the quenching phase, while they are hardly present in isolation. (Sects. 7.1.1, 7.1.2).
- The fraction of galaxies with suppressed star formation (f_Q), well below the MS, monotonically increases from the field, to the filaments, and to the Virgo cluster. At comparable local density, filaments have similar quenching fractions as the field and Virgo cluster (Sect. 7.1.3).
- The f_Q fraction significantly differs between ETGs and LTGs. It stays high, $f_Q \gtrsim 80\%$, at all distances from the filament spine. For LTGs it reaches $f_Q \sim 50\%$, close to the filament spines, but is otherwise of the order of $\sim 25\%$ (Sect. 7.1.3).
- Not only ETGs tend to populate the densest regions within filaments, but they are also preferentially located closer to the filament spines than LTGs (Sect. 7.1.4).
- The atomic and molecular gas fractions, M_{HI}/M_\star and M_{H_2}/M_\star , increase from early-type to late type morphologies, with a slope which steepens when passing from isolation, filaments, to Virgo. This is the consequence of the fact that while late galaxies have very similar gas fractions in all cosmic structures, early type galaxies are more strongly gas-depleted in very dense regions such as clusters. This effect is stronger for HI than for H₂ (Sects. 7.2.1, 7.2.2).
- In isolation and in filaments the average depletion timescale increases with stellar mass, as a consequence of massive galaxies having larger H₂ gas reservoirs. The scatter in the relation between depletion timescale and galaxy stellar mass increases steadily with density, from the field to the filaments

to Virgo, up to a point where the relation between τ_{dep} and M_\star breaks down (Sect. 7.2.3).

- Both H₂ and HI gas mass of the galaxies in filaments decreases with increasing local densities, the latter more steeply than the former. The HI mass also increases with increasing distances from the filament spine (d_{fil}) and Virgo cluster (d_{cluster}). The average depletion time tentatively increases with d_{fil} . In contrast, the galaxy H₂ mass shows no clear trend as a function of the distances (Sect. 7.2.4).
- The number of galaxies, LTGs, with very large HI reservoirs ($M_{\text{HI}} \gtrsim 10^{10} M_\odot$) steadily decreases with the global cosmic structure in which galaxies reside, i.e., in isolation, in filaments, or in the Virgo cluster. Filament ETGs have average HI and H₂ reservoirs $\sim 10^8 M_\odot$ and never reach the highest values found for LTGs, in all three considered environments (Sect. 7.2.4).
- The average HI-def. and H₂-def. parameters increase with local densities. The HI-deficiency is also anti-correlated with distances d_{fil} and d_{cluster} . The fraction of gas deficient galaxies, in majority ETGs, as well as gas the average deficiency parameters, both in HI and in H₂, significantly increase from the field, filaments, to Virgo clusters (Sect. 7.2.5).

8.2. Conclusions

Our survey highlights the importance of the cosmic filaments in modifying galaxy properties. Our study reveals indeed that the specific environment in which galaxies are located (field, filaments, cluster) act as primary driver of galaxy transformations. Cosmic web local densities, distances to the filament spines, and to the cluster center, in this order, are secondary parameters, but still significant dependencies of galaxy properties on these environmental parameters are found. Much of the gas deficiencies and changes in the morphological composition of the galaxy population, that are classically attributed to galaxy clusters, are already in place in these medium density environments that are the filaments. Part of the cluster galaxy properties can therefore be acquired in the clusters themselves, the rest being the consequence of the infall of the filament galaxies onto the cluster cores.

As to the physical processes at play, mergers, stripping, tidal interactions, and starvation are the most commonly invoked mechanisms. Overall, going from the field, filaments, to Virgo cluster we have observed the emergence of ETGs in particular, but also LTGs, with increasing levels of gas deficiency, both in HI and H₂. Indeed, a large fraction 121/245 (i.e., $49\% \pm 6\%$) of filament galaxies are deficient either in HI or H₂, or both. As these gas deficient sources are observed preferentially in dense regions within filaments, in groups, their gas reservoirs have likely experienced strong environment-driven pre-processing.

The HI envelopes of HI gas deficient galaxies in filaments have been likely stripped, possibly via tidal interactions or ram pressure. For HI, our proposed scenario is in agreement with Džudžar et al. (2020), who investigated environmental processing in late type-dominated groups using high-resolution HI observations. The authors further discussed the possibility that groups with the highest levels of processing are transitioning towards Hickson compact or fossil groups, that are environments similar to those associated with the isolated ellipticals in our AMIGA comparison sample. Filament galaxies around Virgo that are HI deficient and live in the highest density regions within filaments may be experiencing a similar transition.

Our scenario is also in line with previous studies (e.g., on the HIPASS survey, Denes et al. 2014; Reynolds et al. 2020), who find that HI sources living in denser environments show, on average, asymmetries and higher HI-def. than those in less dense environments. However, Reynolds et al. (2020) also find groups and clusters that are not HI poor, confirming the large dispersion between HI-def. and local density that we report in the present study.

While the densest regions in the filaments are able to effectively remove or deplete the HI envelope of galaxies via stripping, cosmic induced starvation in HI is a less likely mechanism. Indeed filaments are quite rich in hot gas and baryons, as shown by both simulations and observations (Eckert et al. 2015; Martizzi et al. 2019; Libenskind et al. 2020; Tanimura et al. 2020). Gas accretion from filaments (Bournaud et al. 2005), ultimately feeding star formation, or hydrodynamical interactions with the intergalactic medium (Watts et al. 2020) could also be responsible for gas asymmetries, that we may ultimately observe in terms of different levels of gas deficiencies.

Concerning H₂, starvation by lack of cold gas supply feeding star formation may explain the low molecular content associated with a fraction of our filament galaxies, in particular those LTGs in filaments with low H₂ gas reservoirs, that live in fact in relatively low density environments $\sim 0.8 h^3 \text{ Mpc}^{-3}$. Starvation (e.g., strangulation in groups) or H₂ exhaustion induced by past mergers are possible scenarios to explain the H₂ gas deficiencies observed in the large fraction ($\sim 84\%$) of filament ETGs, which in fact preferentially live in denser regions than LTGs. While ram pressure or tidal stripping in H₂ is still a viable mechanism to explain the H₂ gas deficiencies, it may be a less likely mechanism. Cold gas reservoirs are in fact less extended than the HI envelopes and are associated with higher gas densities. H₂ is thus more difficult to strip than HI. H₂ stripping would require higher densities and infall velocities more typical of galaxies in clusters than in filaments (e.g., Jáchym et al. 2014, 2019). Higher angular resolution observations in CO would provide the needed insights on the physical processes responsible for the processing of the cold gas reservoirs in filament galaxies.

Acknowledgements. GC acknowledges financial support from the Swiss National Science Foundation (SNSF) and fruitful discussion with Amelie Saintonge concerning the CO aperture correction. The authors acknowledge Mindy Townsend, Dara Norman, and Kim Conger for helpful discussion. GHR acknowledges funding support from NSF AST-1716690. BV acknowledges financial contribution from the grant PRIN MIUR 2017 n.20173ML3WW_001 (PI Cimatti) and from the INAF main-stream funding program (PI Vulcani). RAF gratefully acknowledges support from NSF grants AST-0847430 and AST-1716657. This work is based on observations carried out with the Nançay decimetric radio telescope and the IRAM 30m telescope. IRAM is supported by INSU/CNRS (France), MPG (Germany) and IGN (Spain). The authors thank the hospitality of International Space Science Institute (ISSI) in Bern (Switzerland) and of the Lorentz Center in Leiden (Netherlands). Regular group meetings in these institutes allowed the authors to make substantial progress on the project and finalize the present work. We acknowledge the usage of the NASA Sloan Atlas, HyperLeda, NASA/IPAC Extragalactic, and DustPedia databases.

References

- Alatalo, K., Davis, T. A., Bureau, M. et al. 2013, MNRAS, 432, 1796
 Alpaslan, M., Grootes, M., Marcum, P. M. et al. 2016, MNRAS, 457, 2287
 Bahcall, J. N. & Joss, P. C., 1976, ApJ, 203, 23
 Bahé, Y. M., McCarthy, I. G., Balogh, M. L. et al. 2013, MNRAS, 430, 3017
 Barnes, J. E. 1989, Nature, 338, 123
 Balogh, M. L., Navarro, J. F., & Morris, S. L., 2000, ApJ, 540, 113
 Bigiel, F., Leroy, A., Walter, F. et al. 2008, AJ, 136, 2846
 Bigiel, F., Leroy, A. K., Walter, F. et al. 2011, ApJ, 730, 13
 Bok, J., Skelton, R. E., Cluver, M. E. et al. 2020, MNRAS, 499, 3193
 Bolatto, A. T. et al. 2013, ARA&A, 51, 207
 Bonjean, V., Aghanim, N., Douspis, M. et al. 2020, A&A, 638, 75
 Boquien, M., Burgarella, D., Roehlly, Y. et al. 2019, A&A, 622, 103
 Boselli, A. & Gavazzi, G. 2009, A&A, 508, 201
 Boselli, A., Cortese, L., & Boquien, M., 2014a, A&A, 564, 65
 Boselli, A., Cortese, L., Boquien, M. et al. 2014b, A&A, 564, 67
 Bothwell, M. S., Smail, I., Chapman, S. C., et al. 2013, MNRAS, 429, 3047
 Bournaud, F., Combes, F., Jog, C. J. et al. 2005, A&A, 438, 507
 Braine, J., Combes, F., Casoli, F. et al. 1993, A&AS, 97, 887
 Burgarella, D., Buat, V., & Iglesias-Páramo, J., 2005, MNRAS, 360, 1411
 Butcher, H. & Oemler, A. 1984, ApJ, 285, 426
 Calzetti, D., Kennicutt, R. C., Engelbracht, C. W. et al. 2007, ApJ, 666, 870
 Carilli, C. L., & Walter, F. 2013, ARA&A, 51, 105
 Casoli, F., Sauty, S., Gerin, M., et al. 1998, A&A, 331, 451
 Castignani, G., Chiaberge, M., Celotti, A. et al. 2014, ApJ, 792, 114
 Castignani, G., Combes, F., Salomé, P. et al. 2020, A&A, 635, 32
 Cautun, M., van de Weygaert, R., Jones, B. J. T. et al. 2014, MNRAS, 441, 2923
 Chang, Y.-Y., van der Wel, A., da Cunha, E. et al. 2015, ApJS, 219, 8
 Chen, Y.-C., Ho, S., Brinkmann, J., et al. 2016, MNRAS, 461, 3896
 Chen, Y.-C., Ho, S., Mandelbaum, R. et al. 2017, MNRAS, 466, 1880
 Chen, Y.-C., Ho, S., Blazek, B. et al. 2019, MNRAS, 485, 2492
 Chung, A., van Gorkom, J. H., Kenney, J. D. P. et al. 2009, AJ, 138, 1741
 Cicone, C., Bothwell, M., Wagg, J. et al. 2017, A&A, 604, 53
 Codis, S., Jindal, A., Chisari, N. E. et al. 2018, MNRAS, 481, 4
 Combes, F., Young, L. M., Bureau, M. et al. 2007, MNRAS, 377, 1795
 Cortese, L., Gavazzi, G., Boselli, A. et al. 2006 A&A 453, 847
 Cowan, N. B. & Ivezić, Ž. 2008, ApJ, 674, 13
 Crone Odekon, M., Hallenbeck, G., Haynes, M. P. et al. 2018, ApJ, 852, 142
 Daddi, E., Dannerbauer, H., Liu, D. et al. 2015, A&A, 577, 46
 Darvish, B., Sobral, D., Mobasher, B. et al. 2014, ApJ, 796, 51
 Darvish, B., Mobasher, B., Martin, D. C. et al. 2017, ApJ, 837, 16
 Dénes, H., Kilborn, V. A., Koribalski, B. S. et al. 2014, MNRAS, 444, 667
 De Looze, I., Lamperti, I., Saintonge, A. et al. 2020, MNRAS in press
 de Vaucouleurs, G. 1953, AJ, 58, 30
 de Vaucouleurs, G. 1956, VA, 2, 1584
 de Vaucouleurs, G., de Vaucouleurs, A., Corwin, H. G. Jr. et al. 1991, Third Reference Catalogue of Bright Galaxies
 Dickman, R. L., Snell, R. L., & Schloerb, F. P. 1986, ApJ, 309, 326
 Dressler, A., 1980, ApJ 236, 351
 Dressler, A., Oemler, A. Jr., Couch, W. J. et al. 1997, ApJ, 490, 577
 Džudžar, R., Kilborn, V., Sweet, S. M. et al. 2020, arXiv:2011.01438, MNRAS in press
 Eckert, D., Jauzac, M., Shan, H. et al. 2015, Nature, 528, 105
 Eskridge, P. B., Frogel, J. A., Pogge, R. W. et al. 2000, AJ, 119, 536
 Finn, R. A., Desai, V., Rudnick, G. et al. 2010, ApJ, 720, 87
 Fouqué, P., Bottinelli, L., Durand, N. et al. 1990, A&AS, 86, 473
 Fouqué, P., Solanes, J. M., Sanchis, T. et al. 2001, A&A, 375, 770
 Fraser-McKelvie, A., Merrifield, M., Aragón-Salamanca, A. et al. 2020, MNRAS, 499, 111
 Freundlich, J., Combes, F., Tacconi, L. J. et al. 2019, A&A, 622, 105
 Giovanelli, R., Haynes, M. P., Salzer, J. J. et al. 1994, AJ, 107, 2036
 Giovanelli, R., Haynes, M., Kent, B., et al. 2005, AJ, 130, 2598
 Gómez, P. L., Nichol, R. C., Miller, C. J. et al. 2003, ApJ, 584, 210
 Goto, T., Yamauchi, C., Fujita, Y. et al. 2003, MNRAS, 346, 601
 Grossi, M., di Serego Alighieri, S., Giovanardi, C. et al. 2009, A&A, 498, 407
 Gunn, J. E. & Gott, J. R. III, 1972, ApJ, 176, 1
 Haines, C. P., Pereira, M. J., Smith, G. P. et al. 2015, ApJ, 806, 101
 Haynes, M., & Giovanelli, R. 1984, AJ, 89, 758
 Haynes, M., Giovanelli, R., Martin, A. et al. 2011, AJ, 142, 170
 Haynes, M., Giovanelli, R., Kent, B. R. et al. 2018, ApJ, 861, 49
 Hirv, A., Pelt, J., Saar, E. et al. 2017, A&A, 599, 31
 Hoffman, G. L., Olson, D. W., & Salpeter, E. E. 1980, ApJ, 242, 861
 Hou, A., Parker, L. C., & Harris, W. E., 2014, MNRAS, 442, 406
 Huchtmeier, W. K. & Richter, O.-G. 1989, A General Catalog of HI Observations of Galaxies, 1989, New York: Springer-Verlag
 Jáchym, P., Combes, F., Cortese, L. et al. 2014, ApJ, 792, 11
 Jáchym, P., Kenney, J. D. P., Sun, M. et al. 2019
 James, P. A., & Percival, S. M. 2016, MNRAS, 457, 917
 Jones, L. R., Ponman, T. J., Horton, A., et al. 2003, MNRAS, 343, 627
 Jones, M. G., Espada, D., Verdes-Montenegro, L. et al. 2018, A&A, 609, 17
 Kawata, D. & Mulchaey, J. S. 2008, ApJ, 672, 103
 Khoperskov, S., Haywood, M., Di Matteo, P. et al. 2018, A&A, 609, 60
 Khosroshahi, H. G., Ponman, T. J., Jones, L. R. et al. 2006, MNRAS, 372, 68.
 Kim, S., Rey, S.-C., Bureau, M. et al. 2016, ApJ, 833, 207
 Kitaura, F., Jasche, J., Li, C. et al. 2009, MNRAS, 400, 183
 Kourkchi, E., & Tully, R. B. 2017, ApJ, 843, 16
 Kraljic, K., Arnouts, S., Pichon, C. et al. 2018, MNRAS, 474, 54
 Krolewski, A., Ho, S., Chen, Y.-C. et al. 2019 ApJ, 876, 52
 Kroupa, P., & Weidner, C. 2003, ApJ, 598, 1076
 Kuchner, U., Aragón-Salamanca, A., Pearce, F. R., et al. 2020, MNRAS, 494, 5473
 Kuutma, T., Tamm, A., & Tempel, E. 2017, A&A, 600, 6

- Kuutma, T., Poudel, A., Einasto M. et al. 2020, A&A, 639, 71
 Laigle, C., Pichon, C., Arnouts, S. et al. 2018, MNRAS, 474, 5437
 Larson, R., Tinsley, B., & Caldwell, N., 1980, ApJ, 237, 692
 Lavezzzi, T. E., & Dickey, J. M., 1998, AJ, 115, 405
 Lee, Y., Kim, S., Rey, S.-C. et al. 2020, arXiv:2011.11169
 Leroy, A. K., Walter, F., Brinks, E., et al. 2008, AJ, 136, 2782
 Leroy A. K., Walter F., Sandstrom K. et al. 2013, AJ, 146, 19
 Leroy, A. K., Sandstrom, K. M., Lang, D. et al. 2019, ApJS, 244, 24
 Lewis I., Balogh, M., De Propris, R. et al. 2002, MNRAS, 334, 673
 Libeskind, N. I., van de Weygaert, R., Cautun, M. et al. 2018, MNRAS, 473, 1195
 Libeskind, N. I., Carlesi, E., & Grand, R. J. J. 2020, MNRAS, 498, 2968
 Lisenfeld, U., Espada, D., Verdes-Montenegro, L. et al. 2011, A&A, 534, 102
 Luber, N., van Gorkom, J. H., Hess, K. M. et al. 2019, AJ, 157, 254
 Lucero, D. M. & Young, L. M. 2013, AJ, 145, 56
 Mayya, Y. D. & Romano, R. 2002, ASSL, 274, 155
 Malavasi, N., Arnouts, S., Vibert, D. et al. 2017, MNRAS, 465, 3817
 Makarov, D., Prugniel, P., Terekhova, N. et al. 2014, A&A, 570, 13
 Martizzi, D., Vogelsberger, M., Artale, M. C. et al. 2019, MNRAS, 486, 3766
 McLaughlin, D. E. 1999, ApJL, 512, 9
 Mei, S., Blakeslee, J. P., Côté, P. et al. 2007, ApJ, 655, 144
 Merritt, D., 1983, ApJ 264, 24
 Moore B., Lake G., & Katz N., 1998 ApJ 495, 139
 Mould, J. R., Huchra, J. P., Freedman, W. L., et al. 2000, ApJ, 529, 786
 Muldrew, S. I., Croton, D. J. et al. 2012, MNRAS, 419, 2670
 Nishiyama, K., Nakai, N., & Kuno, N. 2001, PASJ, 53, 757
 Noll, S., Burgarella, D., Giovannoli, E. et al. 2009, A&A, 507, 1793
 Obreschkow, D. & Rawlings, S. 2009, MNRAS, 394, 1857
 O'Neil, K., 2004, AJ, 128, 2080
 O'Sullivan, E., Combes, F.; Salomé, P. et al. 2018, A&A, 618, 126
 O'Sullivan, E., Combes, F., Hamer, S. et al. 2015, A&A, 573, 111
 Peng, Y.-j.; Lilly, S. J.; Kováč, K. et al. 2010, ApJ, 721, 193
 Planck Collaboration results VI; Planck Collaboration: Aghanim, N., Akrami, Y., Ashdown, M. et al. 2020, A&A, 641, 6
 Ponman, T. J., Allan, D. J., Jones, L. R., et al. 1994, Nature, 369, 462
 Poggianti, B. M., Smail, I., Dressler, A. et al. 1999, ApJ, 518, 576
 Popping, A. & Braun, R. 2011, A&A, 528, 28
 Postman, M. & Geller, M. J. 1984, ApJ, 281, 95
 Regan, M. W., Thornley, M. D., Helfer, T. T., et al. 2001, ApJ, 561, 218
 Reynolds, T. N., Westmeier, T., & Staveley-Smith, L. 2020, MNRAS, 499, 3233
 Riess, A. G., Casertano, S., Yuan, W. et al. 2019, ApJ, 876, 85
 Roberts, M. S. 1962, AJ 67, 437
 Roediger, E., & Hensler G., 2005, A&A, 433, 875
 Rost, A., Stasyszyn, F., Pereyra, L. et al. 2020a, MNRAS, 493, 1936
 Rost, A., Kuchner, U., Welker, C. et al. 2020b, arXiv:2012.02850
 Rudnick, G., Jablonka, P., Moustakas, J. et al. 2017, ApJ, 850, 181
 Saintonge, A., Kauffmann, G., Kramer, C. et al. 2011, MNRAS, 415, 32
 Saintonge, A., Tacconi, L. J., Fabello, S. et al. 2012, ApJ, 758, 73
 Sage, L. J. 1993, A&A, 272, 123
 Salerno, J. M., Martínez, H. J., & Muriel, H. 2019, MNRAS, 484, 2
 Salomé, Q., Salomé, P., & Combes, F., 2015, A&A, 574, 34
 Sarron, F., Adami, C., Durret, F. et al. 2019, A&A, 632, 49
 Schneider, S. E., Thuan, T. X., Magri, C. et al. 1990, ApJS, 72, 245
 Schneider, S. E., Thuan, T. X., Mangum, J. G. et al. 1992, ApJS, 81, 5
 Schruba A., Leroy A. K., Walter F. et al. 2011, AJ, 142, 37
 Scott, T. C., Usero A., Brinks E. et al. 2013, MNRAS 429, 221
 Serra, P., Oosterloo, T., Morganti, R. et al. 2012, MNRAS, 422, 1835
 Solomon, P. M. & Vanden Bout, P. A., 2005, ARA&A, 43, 677
 Springob, C. M., Haynes, M. P., Giovanelli, R. et al. 2005, ApJSS, 160, 149
 Steer, I., Madore, B. F., Mazzarella, J. M. et al. 2017, AJ, 153, 37
 Stewart, I. M., Blyth, S.-L., & de Blok, W. J. G. 2014, A&A, 567, 61
 Strong, A., Bloemen, J., Dame, T. et al. 1988, ApJ 207, 1
 Tacconi, L. J., Genzel, R., Saintonge, A., et al. 2018, ApJ, 853, 179
 Tang, Y.-W., Kuo, C.-Y., Lim, J. et al. 2008, ApJ, 679, 1094
 Tanimura, N., Aghanim, A., Kolodziga, et al. 2020, A&A, 643, 2
 Tempel, E. & Libeskind, N. I. 2013, ApJL, 775, 42
 Tempel, E., Stoica, R. S. & Saar, E. 2013, MNRAS, 428, 1827
 Theureau, G., Bottinelli, L., Coudreau-Durand, N. et al. 1998, A&AS, 130, 333
 Tully, R. B. 1982, ApJ, 257, 389
 Tully, R. B., Shaya, E. J., Karachentsev, I. D., et al. 2008, ApJ, 676, 184
 Tully, R. B., Courtois, H., Hoffman, Y. et al. 2014, Nature, 513, 71
 Tully, R. B., Courtois, H. M., & Sorce, J. G. 2016, AJ, 152, 50
 Tully, B. & Fisher, J. R., Catalog of Nearby Galaxies, pp. 224. ISBN 0521352991. Cambridge, UK: Cambridge University Press, April 1988
 Verdes-Montenegro, L. , Sulentic, J., Lisenfeld, U. et al. 2005, A&A, 436, 443
 Verley, S., Leon, S., Verdes-Montenegro, L. et al. 2007a, A&A, 472, 121
 Verley, S., Odewahn, S. C., Verdes-Montenegro, L. et al. 2007, A&A, 470, 505
 Vila-Vilaro, B., Cepa, J., & Zabludoff, A. 2015, ApJS, 218, 28
 Vogt, N. P., Haynes, M. P., Herter, T. et al. 2004, AJ, 127, 3273
 Vollmer, B., Braine, J., Pappalardo, C. et al. 2008, A&A, 491, 455
 Vollmer, B., Wong, O. I., Braine, J., et al. 2012, A&A, 543, 33
 Vulcani, B., Poggianti, B. M., Finn, R. A. et al. 2010, ApJ, 710, 1
 Watts, A. B., Power, C., Catinella, B. et al. 2020, MNRAS, 499, 5205
 Welch, G. A. & Sage, L. J. 2003, ApJ, 584, 260
 Welker, C., Bland-Hawthorn, J., Van de Sande, J. et al. 2020, MNRAS, 491, 2864
 Wild, J.P. 1952 ApJ 115, 206
 Wilson, C. D., Warren, B. E., Israel, F. P. et al. 2012, MNRAS, 424, 3050
 Young, J. S., Xie, S., Tacconi, L. et al. 1995, ApJS, 98, 219
 Young, L. M., Bureau, M., Davis, T. A., 2011, MNRAS, 414, 940
 Zabludoff A. I., & Mulchaey J. S., 1998, ApJ, 496, 39
 Zepf, S. E. & Whitmore, B. C. 1993, ApJ, 418, 72

Appendix A: Virgo Filaments

In this Section we provide a 3D visual representation of the filaments around Virgo, in Super Galactic coordinates.

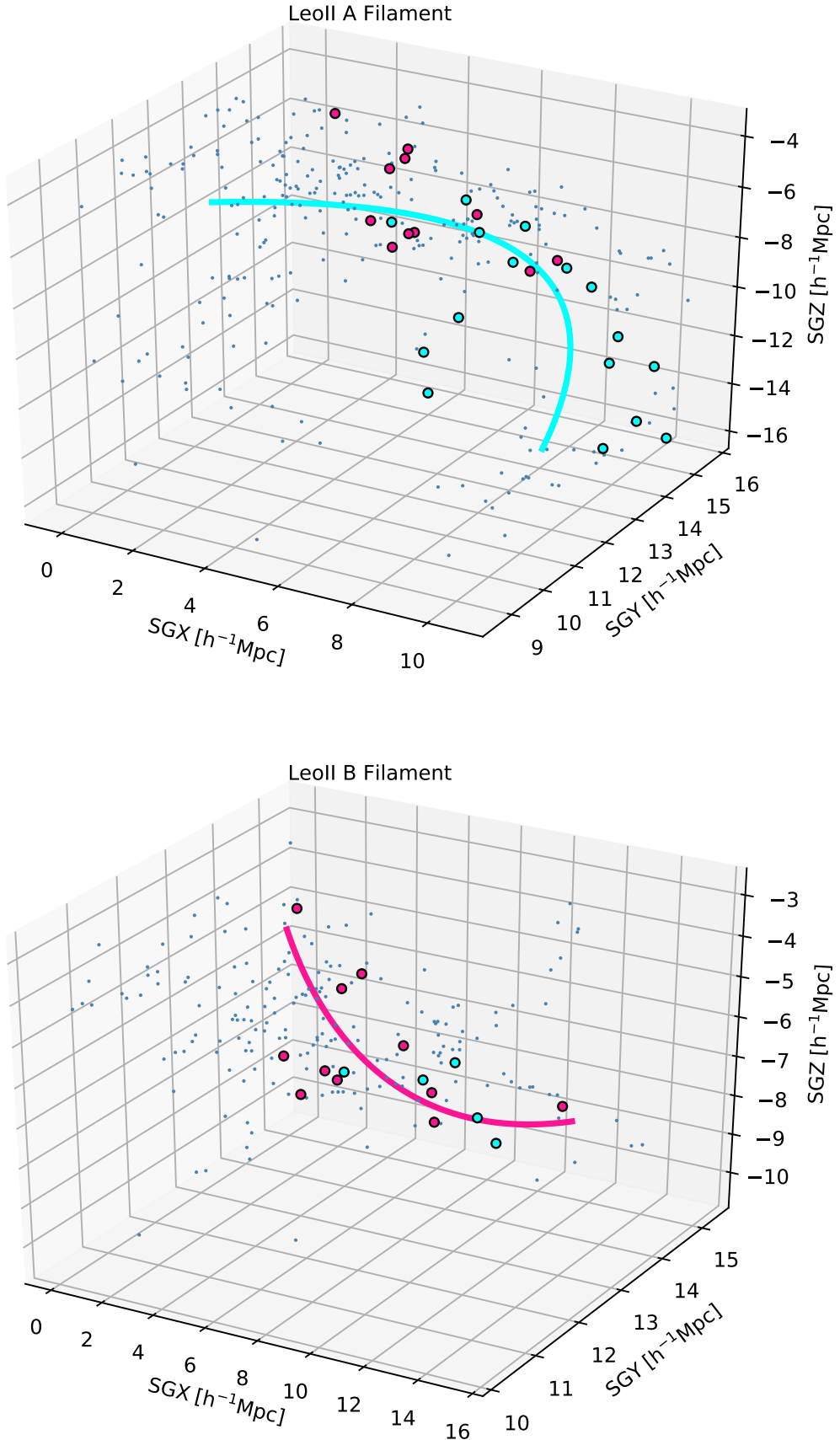


Fig. A.1: Super Galactic coordinates 3D scatter plots for galaxies around filaments. Each plot corresponds to a given filament. The color code is the same as in Fig. 2. The solid lines show the filament spines. Big dots correspond to filament galaxies belonging to our sample of 245, while small dots are galaxies around filaments which are not part of our sample.

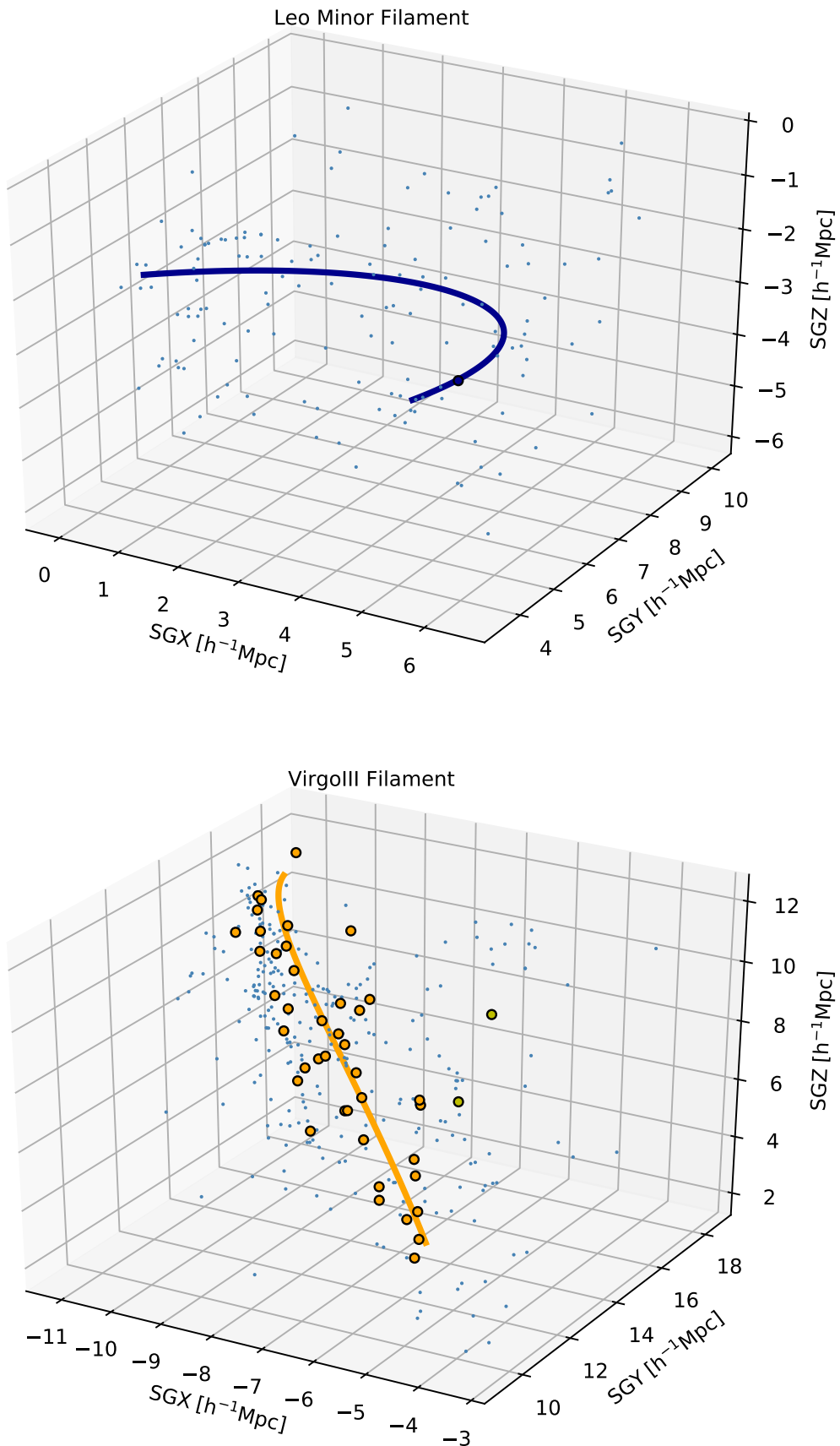


Fig. A.1: Continued.

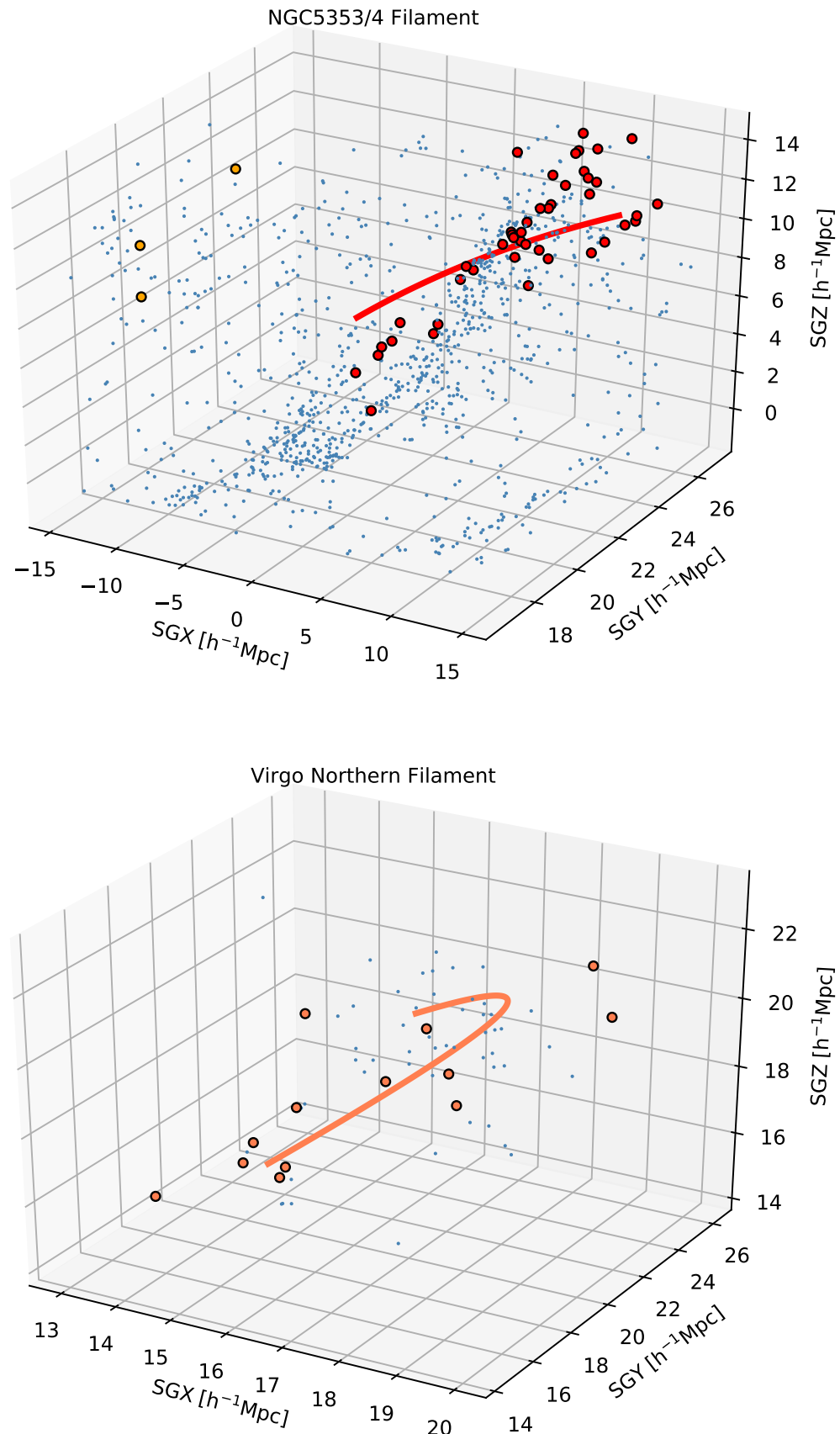


Fig. A.1: Continued.

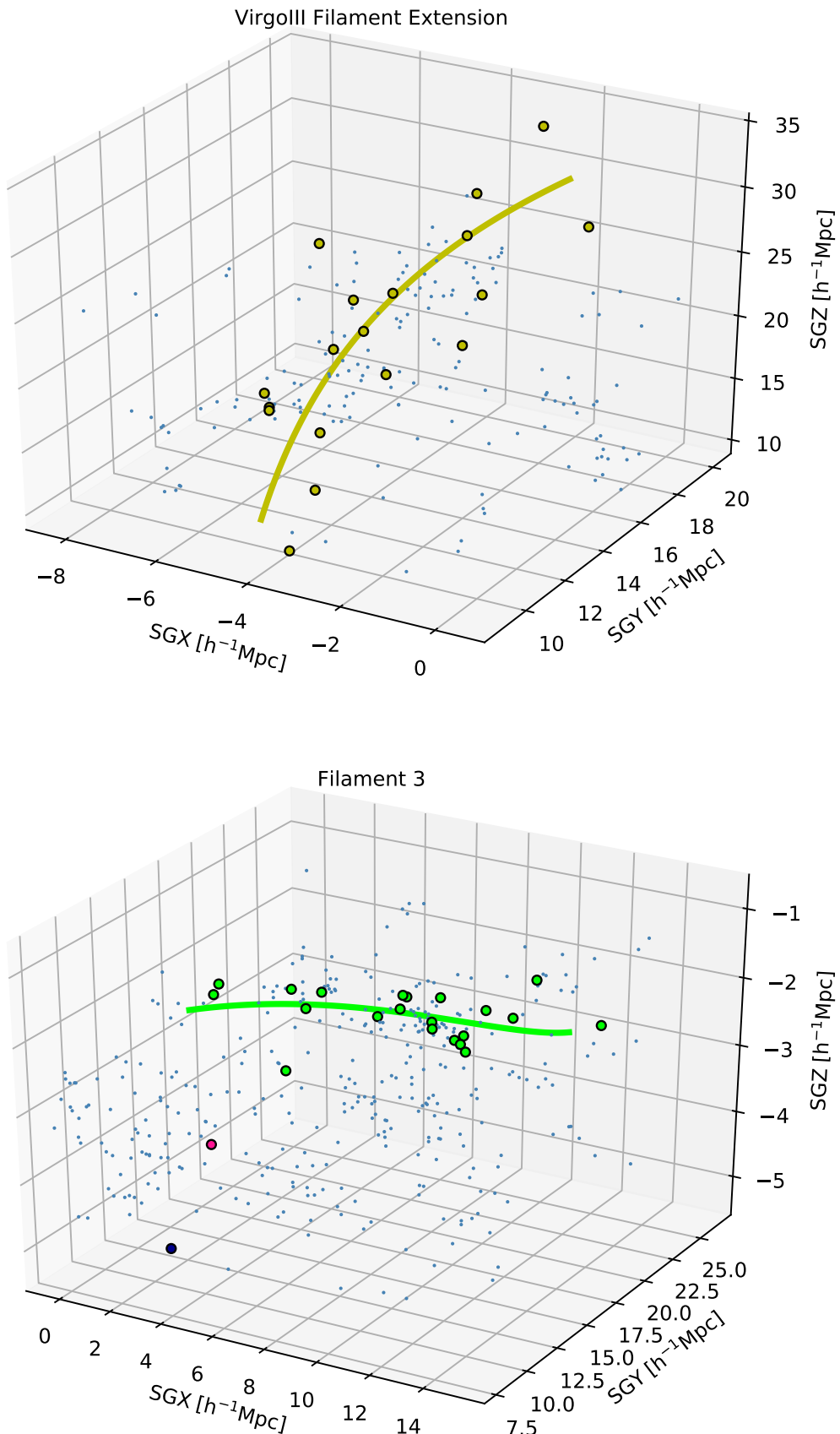


Fig. A.1: Continued.

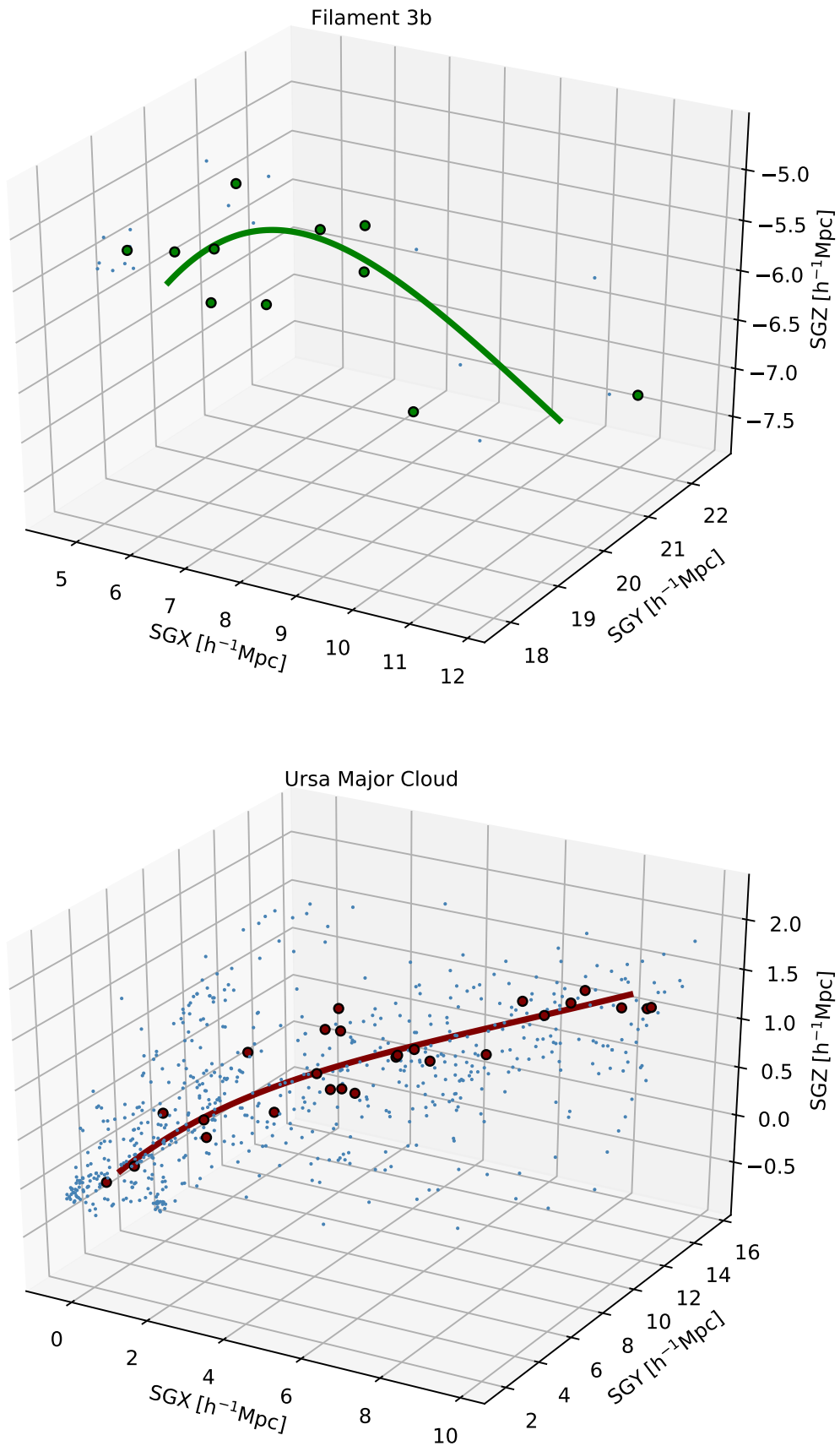


Fig. A.1: Continued.

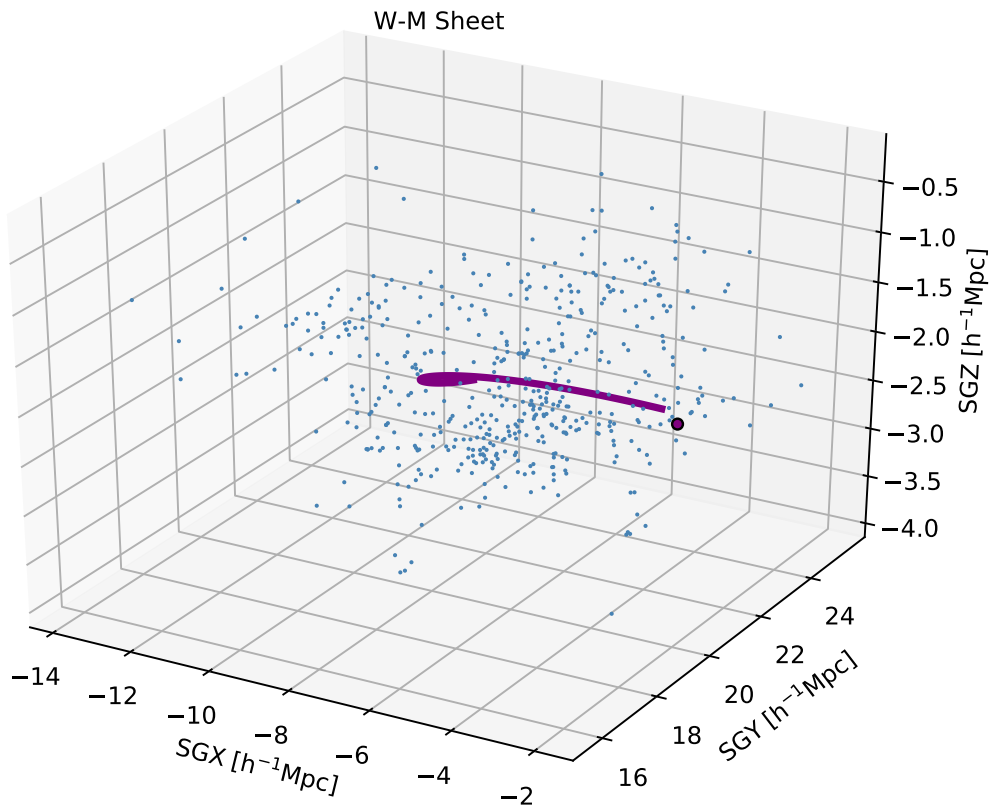


Fig. A.1: Continued.

Appendix B: Properties of Virgo filament galaxies

In this Section we provide several Tables with the properties of our sample of filament galaxies.

Galaxy	R.A.	Dec.	SG (X;Y;Z)	Filament	d_{fil}	d_{cluster}	$\theta_{\text{alignment}}$	Group	Richness	$\log(\frac{M_{\text{group}}}{M_{\odot}})$	$\log(\frac{n_{2D}}{h^2 \text{ Mpc}^{-2}})$	$\log(\frac{n_{3D}}{h^3 \text{ Mpc}^{-3}})$	
(1)	(hh:mm:ss.s)	(dd:mm:ss.s)	(h^{-1} Mpc)	(5)	(h^{-1} Mpc)	(h^{-1} Mpc)	(deg)	ID	(Mpc)	(10)	(11)	(12)	(13)
	(2)	(3)	(4)		(6)	(7)	(8)						
PGC022100	07:53:45.27	+21:02:57.90	(9.48;10.63;-17.29)	LeoII A	3.64 (3D) 3.04 (2D)	20.57 (3D) 20.55 (2D)	13	22100	1	11.46	$0.68^{+0.16}_{-0.26}$ (n_5)	$-0.52^{+0.16}_{-0.26}$ (n_5) $-0.46^{+0.11}_{-0.15}$ (n_{10})	
IC2256	08:16:54.45	+24:10:35.76	(10.93;14.76;-18.61)	LeoII A	5.14 (3D) 4.69 (2D)	23.00 (3D) 22.48 (2D)	38	23214	1	11.16	$0.50^{+0.16}_{-0.26}$ (n_5)	$-0.52^{+0.16}_{-0.26}$ (n_5) $-0.67^{+0.11}_{-0.15}$ (n_{10})	
NGC2577	08:22:43.45	+22:33:11.10	(10.14;15.20;-19.00)	LeoII A	5.47 (3D) 4.83 (2D)	22.96 (3D) 22.34 (2D)	59	23498	7	12.35	$-0.18^{+0.16}_{-0.26}$ (n_5)	$-0.78^{+0.16}_{-0.26}$ (n_5) $-0.84^{+0.11}_{-0.15}$ (n_{10})	
UGC04375	08:23:11.28	+22:39:52.92	(11.50;17.27;-21.46)	LeoII A	8.86 (3D) 7.56 (2D)	26.20 (3D) 25.15 (2D)	47	23498	7	12.35	$-0.72^{+0.16}_{-0.26}$ (n_5)	$-1.47^{+0.16}_{-0.26}$ (n_5) $-1.48^{+0.11}_{-0.15}$ (n_{10})	
IC2361	08:25:44.49	+27:52:28.20	(10.07;13.56;-14.78)	LeoII A	1.38 (3D) 1.04 (2D)	19.29 (3D) 18.94 (2D)	32	23646	1	11.39	$0.67^{+0.16}_{-0.26}$ (n_5)	$0.12^{+0.16}_{-0.26}$ (n_5) $0.03^{+0.11}_{-0.15}$ (n_{10})	
UGC04395	08:25:47.59	+28:07:04.80	(12.76;17.08;-18.52)	LeoII A	7.12 (3D) 5.57 (2D)	24.60 (3D) 23.53 (2D)	73	23643	1	10.97	$-0.61^{+0.16}_{-0.26}$ (n_5)	$-1.41^{+0.16}_{-0.26}$ (n_5) $-1.29^{+0.11}_{-0.15}$ (n_{10})	
NGC2592	08:27:08.05	+25:58:13.10	(10.15;14.52;-16.34)	LeoII A	2.96 (3D) 2.29 (2D)	20.71 (3D) 20.19 (2D)	1	23701	10	12.29	$0.65^{+0.16}_{-0.26}$ (n_5)	$0.56^{+0.16}_{-0.26}$ (n_5) $0.48^{+0.11}_{-0.15}$ (n_{10})	
NGC2594	08:27:17.16	+25:52:43.70	(10.60;15.22;-17.14)	LeoII A	4.12 (3D) 3.21 (2D)	21.77 (3D) 21.10 (2D)	26	23701	10	12.29	$0.44^{+0.16}_{-0.26}$ (n_5)	$-0.12^{+0.16}_{-0.26}$ (n_5) $-0.23^{+0.11}_{-0.15}$ (n_{10})	
PGC023706	08:27:18.07	+46:02:03.10	(15.77;15.18;-10.13)	LeoII B	3.83 (3D) 3.51 (2D)	21.16 (3D) 20.49 (2D)	57	23660	4	11.51	$-0.05^{+0.16}_{-0.26}$ (n_5)	$-0.45^{+0.16}_{-0.26}$ (n_5) $-0.78^{+0.11}_{-0.15}$ (n_{10})	
NGC2604	08:33:23.13	+29:32:19.68	(10.34;14.33;-14.26)	LeoII A	1.91 (3D) 1.34 (2D)	19.25 (3D) 18.73 (2D)	2	23998	4	11.49	$1.13^{+0.16}_{-0.26}$ (n_5)	$0.12^{+0.16}_{-0.26}$ (n_5) $0.05^{+0.11}_{-0.15}$ (n_{10})	
PGC024012	08:33:42.55	+27:42:43.92	(10.47;15.24;-15.75)	LeoII A	3.26 (3D) 1.97 (2D)	20.64 (3D) 19.94 (2D)	10	24012	1	11.22	$0.36^{+0.16}_{-0.26}$ (n_5)	$-0.03^{+0.16}_{-0.26}$ (n_5) $-0.11^{+0.11}_{-0.15}$ (n_{10})	
NGC2608	08:35:17.04	+28:28:30.72	(7.54;10.91;-10.97)	LeoII A	3.29 (3D) 1.58 (2D)	14.44 (3D) 14.41 (2D)	5	24111	2	11.97	$-0.57^{+0.16}_{-0.26}$ (n_5)	$-1.47^{+0.16}_{-0.26}$ (n_5) $-1.36^{+0.11}_{-0.15}$ (n_{10})	
UGC04551	08:44:05.92	+49:47:37.90	(13.44;13.36;-6.98)	LeoII B	0.68 (3D) 0.62 (2D)	17.37 (3D) 17.02 (2D)	39	24528	2	11.94	$-0.12^{+0.16}_{-0.26}$ (n_5)	$-1.11^{+0.16}_{-0.26}$ (n_5) $-1.05^{+0.11}_{-0.15}$ (n_{10})	
UGC04559	08:44:07.68	+30:07:08.76	(13.45;20.15;-18.37)	LeoII A	9.56 (3D) 5.92 (2D)	25.97 (3D) 23.86 (2D)	5	24530	1	11.75	$-0.08^{+0.16}_{-0.26}$ (n_5)	$-1.25^{+0.16}_{-0.26}$ (n_5) $-1.29^{+0.11}_{-0.15}$ (n_{10})	
PGC1925809	08:51:32.06	+30:58:03.72	(9.91;15.44;-13.12)	LeoII A	2.21 (3D) 1.10 (2D)	18.45 (3D) 17.59 (2D)	81	24884	3	11.87	$0.30^{+0.16}_{-0.26}$ (n_5)	$0.07^{+0.16}_{-0.26}$ (n_5) $-0.10^{+0.11}_{-0.15}$ (n_{10})	
NGC2679	08:51:32.94	+30:51:55.30	(9.34;14.60;-12.44)	LeoII A	1.06 (3D) 0.44 (2D)	17.36 (3D) 16.71 (2D)	67	24884	3	11.87	$0.49^{+0.16}_{-0.26}$ (n_5)	$-0.22^{+0.16}_{-0.26}$ (n_5) $-0.42^{+0.11}_{-0.15}$ (n_{10})	
UGC04659	08:54:40.53	+47:06:17.60	(16.89;18.67;-10.01)	LeoII B	6.60 (3D) 4.29 (2D)	23.15 (3D) 21.42 (2D)	43	25012	1	11.09	$-0.33^{+0.16}_{-0.26}$ (n_5)	$-1.16^{+0.16}_{-0.26}$ (n_5) $-1.17^{+0.11}_{-0.15}$ (n_{10})	
PGC025063	08:55:33.19	+31:12:41.76	(9.79;15.67;-12.88)	LeoII A	2.29 (3D) 1.07 (2D)	18.27 (3D) 17.34 (2D)	11	25063	1	11.29	$0.33^{+0.16}_{-0.26}$ (n_5)	$-0.18^{+0.16}_{-0.26}$ (n_5) $-0.08^{+0.11}_{-0.15}$ (n_{10})	
NGC2712	08:59:30.47	+44:54:50.00	(13.60;16.15;-9.01)	LeoII B	2.85 (3D) 1.45 (2D)	19.10 (3D) 18.04 (2D)	30	25248	2	12.00	$0.79^{+0.16}_{-0.26}$ (n_5)	$-0.07^{+0.16}_{-0.26}$ (n_5) $-0.18^{+0.11}_{-0.15}$ (n_{10})	
PGC025273	09:00:13.32	+31:59:54.24	(9.23;15.01;-11.73)	LeoII A	1.20 (3D) 0.45 (2D)	16.92 (3D) 16.13 (2D)	76	25273	2	11.27	$0.97^{+0.16}_{-0.26}$ (n_5)	$0.21^{+0.16}_{-0.26}$ (n_5) $0.08^{+0.11}_{-0.15}$ (n_{10})	
UGC04722	09:00:23.54	+25:36:40.60	(6.19;12.33;-11.02)	LeoII A	3.00 (3D) 2.29 (2D)	13.78 (3D) 13.56 (2D)	42	25292	1	11.10	$-0.06^{+0.16}_{-0.26}$ (n_5)	$-0.96^{+0.16}_{-0.26}$ (n_5) $-1.04^{+0.11}_{-0.15}$ (n_{10})	
NGC2780	09:12:44.40	+34:55:31.80	(17.53;28.86;-19.29)	LeoII A	18.79 (3D) 10.49 (2D)	33.28 (3D) 27.35 (2D)	84	25955	4	12.06	$-1.91^{+0.16}_{-0.26}$ (n_5)	$-1.81^{+0.16}_{-0.26}$ (n_5) $-1.81^{+0.11}_{-0.15}$ (n_{10})	
NGC2793	09:16:47.28	+34:25:47.64	(8.62;14.82;-9.74)	LeoII A	0.70 (3D) 0.52 (2D)	15.15 (3D) 14.33 (2D)	2	26189	2	11.22	$0.32^{+0.16}_{-0.26}$ (n_5)	$0.06^{+0.16}_{-0.26}$ (n_5) $-0.03^{+0.11}_{-0.15}$ (n_{10})	

UGC04902	09:17:05.28	+25:25:45.00	(5.85;13.81;-11.00)	LeoII A	2.56 (3D) 2.48 (2D)	13.90 (3D) 13.34 (2D)	71	26218	1	11.27	-0.08 ^{+0.16} _{-0.26} (n ₅) -0.67 ^{+0.11} _{-0.15} (n ₁₀)	-0.58 ^{+0.16} _{-0.26} (n ₅) -0.73 ^{+0.11} _{-0.15} (n ₁₀)
NGC2798	09:17:22.79	+41:59:59.00	(9.20;12.95;-6.94)	LeoII B	1.74 (3D) 1.42 (2D)	13.54 (3D) 13.19 (2D)	14	26232	3	12.01	0.21 ^{+0.16} _{-0.26} (n ₅) -0.62 ^{+0.16} _{-0.26} (n ₅)	-0.73 ^{+0.11} _{-0.15} (n ₁₀)
NGC2799	09:17:31.03	+41:59:38.70	(10.90;15.36;-8.23)	LeoII B	1.48 (3D) 0.12 (2D)	16.25 (3D) 15.31 (2D)	27	26232	3	12.01	1.03 ^{+0.16} _{-0.26} (n ₅) -0.74 ^{+0.16} _{-0.26} (n ₅)	0.61 ^{+0.11} _{-0.15} (n ₁₀)
NGC2844	09:21:48.01	+40:09:04.50	(15.62;23.68;-12.95)	LeoII B	11.59 (3D) 5.88 (2D)	25.83 (3D) 21.84 (2D)	40	26501	3	11.57	0.15 ^{+0.16} _{-0.26} (n ₅) -1.07 ^{+0.16} _{-0.26} (n ₅)	-1.07 ^{+0.11} _{-0.15} (n ₁₀)
NGC2852	09:23:14.59	+40:09:49.70	(10.93;16.71;-9.04)	LeoII B	2.95 (3D) 0.87 (2D)	17.18 (3D) 15.76 (2D)	2	26571	3	11.71	0.45 ^{+0.16} _{-0.20} (n ₅) -0.43 ^{+0.16} _{-0.26} (n ₅)	-0.38 ^{+0.11} _{-0.15} (n ₁₀)
NGC2853	09:23:17.33	+40:12:00.20	(10.54;16.11;-8.70)	LeoII B	2.25 (3D) 0.49 (2D)	16.47 (3D) 15.25 (2D)	56	26571	3	11.71	0.58 ^{+0.16} _{-0.26} (n ₅) -0.07 ^{+0.16} _{-0.26} (n ₅)	0.07 ^{+0.11} _{-0.15} (n ₁₀)
NGC2859	09:24:18.53	+34:30:48.60	(7.68;13.92;-8.64)	LeoII B	0.34 (3D) 0.34 (2D)	13.52 (3D) 12.91 (2D)	55	26649	7	12.44	0.71 ^{+0.16} _{-0.26} (n ₅) -0.12 ^{+0.16} _{-0.26} (n ₅)	-0.12 ^{+0.11} _{-0.15} (n ₁₀)
UGC05015	09:25:48.00	+34:16:37.50	(7.99;14.75;-9.10)	LeoII A	0.49 (3D) 0.38 (2D)	14.29 (3D) 13.44 (2D)	58	26649	7	12.44	0.68 ^{+0.16} _{-0.26} (n ₅) 0.09 ^{+0.11} _{-0.15} (n ₁₀)	0.22 ^{+0.16} _{-0.26} (n ₅)
UGC05020	09:26:01.48	+34:39:12.24	(10.14;18.51;-11.30)	LeoII A	4.67 (3D) 1.72 (2D)	18.62 (3D) 16.50 (2D)	8	26649	7	12.44	0.55 ^{+0.16} _{-0.26} (n ₅) -0.81 ^{+0.11} _{-0.15} (n ₁₀)	-0.72 ^{+0.16} _{-0.26} (n ₅)
NGC2893	09:30:16.96	+29:32:24.00	(6.96;15.70;-10.43)	LeoII A	1.79 (3D) 1.26 (2D)	14.79 (3D) 13.61 (2D)	2	26979	1	11.52	0.05 ^{+0.16} _{-0.26} (n ₅) -0.44 ^{+0.11} _{-0.15} (n ₁₀)	-0.51 ^{+0.16} _{-0.26} (n ₅)
PGC027311	09:36:07.52	+29:06:42.90	(6.25;15.09;-9.68)	LeoII A	1.41 (3D) 1.27 (2D)	13.61 (3D) 12.58 (2D)	86	27311	1	11.03	0.37 ^{+0.16} _{-0.26} (n ₅) -0.17 ^{+0.11} _{-0.15} (n ₁₀)	-0.15 ^{+0.16} _{-0.26} (n ₅)
NGC2964	09:42:54.23	+31:50:50.60	(5.37;12.27;-7.04)	LeoII B	1.65 (3D) 0.45 (2D)	10.38 (3D) 10.11 (2D)	21	27777	8	12.40	1.01 ^{+0.16} _{-0.26} (n ₅) 0.13 ^{+0.11} _{-0.15} (n ₁₀)	0.58 ^{+0.16} _{-0.26} (n ₅)
NGC2968	09:43:12.01	+31:55:43.30	(3.61;8.26;-4.71)	Leo Minor	3.53 (3D) 2.91 (2D)	7.47 (3D) 7.28 (2D)	78	27777	8	12.40	0.25 ^{+0.16} _{-0.26} (n ₅) -0.64 ^{+0.11} _{-0.15} (n ₁₀)	-0.41 ^{+0.16} _{-0.26} (n ₅)
NGC2970	09:43:31.05	+31:58:37.20	(7.11;16.24;-9.24)	LeoII A	1.81 (3D) 0.37 (2D)	14.35 (3D) 12.87 (2D)	30	27777	8	12.40	0.33 ^{+0.16} _{-0.26} (n ₅) -0.38 ^{+0.11} _{-0.15} (n ₁₀)	-0.31 ^{+0.16} _{-0.26} (n ₅)
PGC028169	09:48:04.69	+32:52:57.00	(6.59;15.06;-8.09)	LeoII A	0.68 (3D) 0.21 (2D)	12.80 (3D) 11.72 (2D)	50	28357	8	12.04	1.20 ^{+0.16} _{-0.26} (n ₅) 0.71 ^{+0.11} _{-0.15} (n ₁₀)	0.84 ^{+0.16} _{-0.26} (n ₅)
NGC3003	09:48:35.46	+33:25:17.30	(5.63;12.65;-6.69)	LeoII B	1.50 (3D) 0.89 (2D)	10.45 (3D) 10.08 (2D)	39	28357	8	12.04	0.91 ^{+0.16} _{-0.26} (n ₅) 0.14 ^{+0.11} _{-0.15} (n ₁₀)	0.34 ^{+0.16} _{-0.26} (n ₅)
NGC3026	09:50:55.39	+28:33:03.96	(5.34;15.05;-8.72)	LeoII A	1.23 (3D) 0.97 (2D)	12.38 (3D) 11.26 (2D)	41	28351	1	11.21	0.59 ^{+0.16} _{-0.26} (n ₅) 0.10 ^{+0.11} _{-0.15} (n ₁₀)	0.06 ^{+0.16} _{-0.26} (n ₅)
NGC3021	09:50:57.15	+33:33:13.10	(7.13;16.21;-8.38)	LeoII A	1.77 (3D) 0.30 (2D)	13.84 (3D) 12.31 (2D)	6	28357	8	12.04	0.63 ^{+0.16} _{-0.26} (n ₅) -0.01 ^{+0.11} _{-0.15} (n ₁₀)	0.14 ^{+0.16} _{-0.26} (n ₅)
UGC05287	09:51:28.09	+32:56:35.00	(8.38;19.58;-10.23)	LeoII A	5.22 (3D) 0.73 (2D)	17.42 (3D) 14.47 (2D)	68	28357	8	12.04	-0.57 ^{+0.16} _{-0.26} (n ₅) -1.36 ^{+0.11} _{-0.15} (n ₁₀)	-1.37 ^{+0.16} _{-0.26} (n ₅)
NGC3032	09:52:08.15	+29:14:10.40	(4.85;13.37;-7.56)	LeoII B	0.55 (3D) 0.27 (2D)	10.66 (3D) 10.08 (2D)	27	28424	3	11.69	1.07 ^{+0.16} _{-0.26} (n ₅) 0.14 ^{+0.11} _{-0.15} (n ₁₀)	0.20 ^{+0.16} _{-0.26} (n ₅)
UGC05326	09:55:24.50	+33:15:46.00	(5.98;14.21;-7.13)	LeoII B	0.73 (3D) 0.66 (2D)	11.47 (3D) 10.63 (2D)	14	28758	2	11.10	1.32 ^{+0.16} _{-0.26} (n ₅) 0.54 ^{+0.11} _{-0.15} (n ₁₀)	0.56 ^{+0.16} _{-0.26} (n ₅)
NGC3067	09:58:21.08	+32:22:11.60	(4.84;12.21;-6.11)	LeoII B	1.81 (3D) 0.89 (2D)	9.39 (3D) 9.10 (2D)	3	28805	1	11.86	0.24 ^{+0.16} _{-0.26} (n ₅) -0.20 ^{+0.11} _{-0.15} (n ₁₀)	-0.02 ^{+0.16} _{-0.26} (n ₅)
NGC3098	10:02:16.69	+24:42:39.90	(3.62;14.22;-8.14)	LeoII A	1.12 (3D) 1.02 (2D)	10.64 (3D) 9.72 (2D)	55	29067	1	11.75	0.58 ^{+0.16} _{-0.26} (n ₅) 0.04 ^{+0.11} _{-0.15} (n ₁₀)	0.04 ^{+0.16} _{-0.26} (n ₅)
PGC029347	10:06:18.11	+28:56:40.40	(4.80;15.24;-7.71)	LeoII A	1.18 (3D) 0.36 (2D)	11.47 (3D) 10.15 (2D)	23	29347	1	11.09	0.80 ^{+0.16} _{-0.26} (n ₅) 0.06 ^{+0.11} _{-0.15} (n ₁₀)	0.03 ^{+0.16} _{-0.26} (n ₅)

NGC3118	10:07:11.54	+33:01:38.60	(6.51;17.07;-7.79)	LeoII A	2.70 (3D) 0.51 (2D)	13.52 (3D) 11.46 (2D)	74	29415	2	11.05	$1.41^{+0.16}_{-0.26}$ (n_5) $-0.48^{+0.11}_{-0.15}$ (n_{10})	$-0.52^{+0.16}_{-0.26}$ (n_5) $-0.72^{+0.11}_{-0.15}$ (n_{10})
IC0598	10:12:48.57	+43:08:43.90	(11.63;21.53;-6.90)	3b	1.09 (3D) 0.80 (2D)	19.24 (3D) 15.33 (2D)	52	29745	2	11.79	$-0.07^{+0.16}_{-0.26}$ (n_5) $-0.72^{+0.11}_{-0.15}$ (n_{10})	$-0.70^{+0.16}_{-0.26}$ (n_5) $-0.86^{+0.11}_{-0.15}$ (n_{10})
NGC3193	10:18:24.90	+21:53:38.30	(3.05;18.66;-9.87)	LeoII A	5.51 (3D) 3.15 (2D)	13.94 (3D) 10.85 (2D)	44	30083	19	12.79	$0.00^{+0.16}_{-0.26}$ (n_5) $-0.86^{+0.11}_{-0.15}$ (n_{10})	$-0.72^{+0.16}_{-0.26}$ (n_5) $-0.96^{+0.11}_{-0.15}$ (n_{10})
UGC05577	10:20:03.64	+38:36:56.00	(8.84;20.04;-6.93)	3b	1.32 (3D) 0.42 (2D)	16.39 (3D) 12.88 (2D)	35	30206	1	11.41	$-0.25^{+0.16}_{-0.26}$ (n_5) $-0.96^{+0.11}_{-0.15}$ (n_{10})	$-0.92^{+0.16}_{-0.26}$ (n_5) $-0.63^{+0.11}_{-0.15}$ (n_{10})
UGC05588	10:20:57.13	+25:21:53.40	(3.46;16.06;-7.73)	LeoII A	2.40 (3D) 0.93 (2D)	11.14 (3D) 9.29 (2D)	78	30263	2	11.17	$0.72^{+0.16}_{-0.26}$ (n_5) $-0.13^{+0.11}_{-0.15}$ (n_{10})	$-0.08^{+0.16}_{-0.26}$ (n_5) $-0.13^{+0.11}_{-0.15}$ (n_{10})
NGC3245A	10:27:01.13	+28:38:21.60	(4.04;15.84;-6.69)	LeoII B	2.05 (3D) 0.20 (2D)	10.70 (3D) 8.89 (2D)	40	30744	10	12.57	$1.61^{+0.16}_{-0.26}$ (n_5) $-0.02^{+0.11}_{-0.15}$ (n_{10})	$-0.12^{+0.16}_{-0.26}$ (n_5) $-0.02^{+0.11}_{-0.15}$ (n_{10})
NGC3245	10:27:18.39	+28:30:26.80	(3.58;14.20;-6.00)	LeoII B	0.47 (3D) 0.07 (2D)	9.16 (3D) 8.08 (2D)	76	30744	10	12.57	$1.26^{+0.16}_{-0.26}$ (n_5) $0.41^{+0.11}_{-0.15}$ (n_{10})	$0.63^{+0.16}_{-0.26}$ (n_5) $0.41^{+0.11}_{-0.15}$ (n_{10})
NGC3248	10:27:45.44	+22:50:49.90	(2.47;15.78;-7.53)	LeoII A	2.49 (3D) 1.02 (2D)	10.38 (3D) 8.55 (2D)	15	30776	2	11.63	$1.55^{+0.16}_{-0.26}$ (n_5) $0.32^{+0.11}_{-0.15}$ (n_{10})	$0.29^{+0.16}_{-0.26}$ (n_5) $0.29^{+0.11}_{-0.15}$ (n_{10})
NGC3254	10:29:19.94	+29:29:30.60	(6.04;22.88;-9.25)	3b	3.51 (3D) 3.23 (2D)	17.76 (3D) 12.12 (2D)	83	30744	10	12.57	$-0.55^{+0.16}_{-0.26}$ (n_5) $-1.32^{+0.11}_{-0.15}$ (n_{10})	$-1.30^{+0.16}_{-0.26}$ (n_5) $-1.30^{+0.11}_{-0.15}$ (n_{10})
NGC3265	10:31:06.77	+28:47:48.00	(3.63;14.63;-5.91)	LeoII B	0.91 (3D) 0.16 (2D)	9.35 (3D) 8.06 (2D)	27	30744	10	12.57	$1.28^{+0.16}_{-0.26}$ (n_5) $0.45^{+0.11}_{-0.15}$ (n_{10})	$1.15^{+0.16}_{-0.26}$ (n_5) $0.45^{+0.11}_{-0.15}$ (n_{10})
NGC3277	10:32:55.45	+28:30:42.20	(4.06;16.99;-6.79)	LeoII A	3.14 (3D) 0.96 (2D)	11.45 (3D) 8.98 (2D)	71	30744	10	12.57	$2.05^{+0.16}_{-0.26}$ (n_5) $-0.01^{+0.16}_{-0.26}$ (n_5)	$-0.01^{+0.16}_{-0.26}$ (n_5) $-0.01^{+0.11}_{-0.15}$ (n_{10})
PGC031357	10:35:22.72	+37:40:18.00	(7.00;18.09;-5.45)	3b	0.95 (3D) 0.93 (2D)	13.36 (3D) 10.55 (2D)	74	31428	2	12.24	$0.05^{+0.16}_{-0.26}$ (n_5) $-0.59^{+0.11}_{-0.15}$ (n_{10})	$-0.54^{+0.16}_{-0.26}$ (n_5) $-0.54^{+0.11}_{-0.15}$ (n_{10})
PGC031387	10:35:42.04	+26:07:33.00	(2.98;15.46;-6.36)	LeoII B	1.85 (3D) 0.65 (2D)	9.68 (3D) 7.92 (2D)	89	31387	1	11.02	$0.99^{+0.16}_{-0.26}$ (n_5) $0.19^{+0.11}_{-0.15}$ (n_{10})	$0.15^{+0.16}_{-0.26}$ (n_5) $0.19^{+0.11}_{-0.15}$ (n_{10})
NGC3294	10:36:16.25	+37:19:28.90	(7.18;18.95;-5.72)	3b	1.27 (3D) 1.25 (2D)	14.12 (3D) 10.83 (2D)	2	31428	2	12.24	$-0.01^{+0.16}_{-0.26}$ (n_5) $-0.77^{+0.11}_{-0.15}$ (n_{10})	$-0.79^{+0.16}_{-0.26}$ (n_5) $-0.77^{+0.11}_{-0.15}$ (n_{10})
UGC05870	10:45:59.38	+34:57:53.60	(6.78;21.38;-6.19)	3b	0.11 (3D) 0.10 (2D)	15.71 (3D) 10.72 (2D)	2	32134	1	11.49	$0.02^{+0.16}_{-0.26}$ (n_5) $-0.67^{+0.16}_{-0.26}$ (n_5)	$-0.67^{+0.16}_{-0.26}$ (n_5) $-0.67^{+0.11}_{-0.15}$ (n_{10})
NGC3381	10:48:24.82	+34:42:41.10	(5.56;18.07;-5.11)	3b	0.64 (3D) 0.60 (2D)	12.25 (3D) 9.12 (2D)	43	32302	1	11.38	$0.96^{+0.16}_{-0.26}$ (n_5) $0.53^{+0.11}_{-0.15}$ (n_{10})	$0.60^{+0.16}_{-0.26}$ (n_5) $0.60^{+0.11}_{-0.15}$ (n_{10})
NGC3424	10:51:46.33	+32:54:02.70	(5.21;19.30;-5.54)	3b	0.67 (3D) 0.66 (2D)	13.06 (3D) 9.06 (2D)	13	32614	12	12.44	$1.56^{+0.16}_{-0.26}$ (n_5) $0.22^{+0.11}_{-0.15}$ (n_{10})	$0.34^{+0.16}_{-0.26}$ (n_5) $0.34^{+0.11}_{-0.15}$ (n_{10})
NGC3430	10:52:11.40	+32:57:01.60	(5.37;19.90;-5.67)	3b	0.51 (3D) 0.51 (2D)	13.63 (3D) 9.27 (2D)	85	32614	12	12.44	$0.98^{+0.16}_{-0.26}$ (n_5) $-0.02^{+0.16}_{-0.26}$ (n_5)	$0.54^{+0.16}_{-0.26}$ (n_5) $-0.02^{+0.11}_{-0.15}$ (n_{10})
UGC05990	10:52:38.34	+34:28:59.30	(6.42;21.80;-5.88)	3b	0.51 (3D) 0.20 (2D)	15.72 (3D) 10.27 (2D)	63	32652	1	11.15	$0.14^{+0.16}_{-0.26}$ (n_5) $-0.63^{+0.11}_{-0.15}$ (n_{10})	$-0.61^{+0.16}_{-0.26}$ (n_5) $-0.61^{+0.11}_{-0.15}$ (n_{10})
NGC3442	10:53:08.11	+33:54:37.30	(6.05;21.29;-5.81)	3b	0.29 (3D) 0.21 (2D)	15.10 (3D) 9.91 (2D)	68	32679	1	11.37	$0.44^{+0.16}_{-0.26}$ (n_5) $-0.27^{+0.11}_{-0.15}$ (n_{10})	$-0.09^{+0.16}_{-0.26}$ (n_5) $-0.27^{+0.11}_{-0.15}$ (n_{10})
UGC06070	10:59:46.28	+33:23:30.60	(5.34;20.39;-5.17)	3b	0.66 (3D) 0.65 (2D)	13.80 (3D) 8.97 (2D)	80	33118	2	11.40	$1.40^{+0.16}_{-0.26}$ (n_5) $0.02^{+0.11}_{-0.15}$ (n_{10})	$0.54^{+0.16}_{-0.26}$ (n_5) $0.54^{+0.11}_{-0.15}$ (n_{10})
NGC3504	11:03:11.21	+27:58:21.00	(2.31;13.95;-3.99)	LeoII B	0.44 (3D) 0.33 (2D)	7.08 (3D) 5.80 (2D)	60	33371	3	12.21	$0.19^{+0.16}_{-0.26}$ (n_5) $-0.59^{+0.11}_{-0.15}$ (n_{10})	$-0.66^{+0.16}_{-0.26}$ (n_5) $-0.66^{+0.11}_{-0.15}$ (n_{10})
NGC3595	11:15:25.55	+47:26:49.30	(10.78;22.52;-1.87)	3	5.37 (3D) 5.32 (2D)	18.21 (3D) 13.13 (2D)	10	34325	1	12.05	$0.88^{+0.16}_{-0.26}$ (n_5) $-0.11^{+0.11}_{-0.15}$ (n_{10})	$-0.07^{+0.16}_{-0.26}$ (n_5) $-0.07^{+0.11}_{-0.15}$ (n_{10})
NGC3629	11:20:31.81	+26:57:48.10	(2.85;24.27;-5.54)	3	3.82 (3D) 3.82 (2D)	16.09 (3D) 7.24 (2D)	50	34719	1	11.28	$-0.08^{+0.16}_{-0.26}$ (n_5) $-0.88^{+0.11}_{-0.15}$ (n_{10})	$-0.78^{+0.16}_{-0.26}$ (n_5) $-0.78^{+0.11}_{-0.15}$ (n_{10})

NGC3648	11:22:31.49	+39:52:37.00	(7.16;21.70;-2.68)	3	1.86 (3D) 1.83 (2D)	15.27 (3D) 9.69 (2D)	86	34908	5	11.95	$1.62_{-0.26}^{+0.16}$ (n_5) $1.14_{-0.15}^{+0.11}$ (n_{10})	$1.20_{-0.26}^{+0.16}$ (n_5) $1.14_{-0.15}^{+0.11}$ (n_{10})
NGC3658	11:23:58.49	+38:33:46.90	(6.84;22.43;-2.89)	3	1.41 (3D) 1.37 (2D)	15.69 (3D) 9.43 (2D)	54	35064	15	12.92	$1.91_{-0.26}^{+0.16}$ (n_5) $1.01_{-0.15}^{+0.11}$ (n_{10})	$1.32_{-0.26}^{+0.16}$ (n_5) $1.01_{-0.15}^{+0.11}$ (n_{10})
NGC3665	11:24:43.40	+38:45:43.90	(4.97;16.18;-2.02)	3	1.27 (3D) 1.19 (2D)	9.71 (3D) 7.41 (2D)	37	35064	15	12.92	$0.45_{-0.26}^{+0.16}$ (n_5) $-0.58_{-0.15}^{+0.11}$ (n_{10})	$-0.58_{-0.26}^{+0.16}$ (n_5) $-0.58_{-0.15}^{+0.11}$ (n_{10})
UGC06455	11:27:21.91	+40:00:47.00	(7.23;22.28;-2.38)	3	1.86 (3D) 1.84 (2D)	15.72 (3D) 9.69 (2D)	84	—	—	—	$1.29_{-0.26}^{+0.16}$ (n_5) $0.76_{-0.15}^{+0.11}$ (n_{10})	$0.82_{-0.26}^{+0.16}$ (n_5) $0.76_{-0.15}^{+0.11}$ (n_{10})
NGC3687	11:28:00.60	+29:30:39.80	(2.77;18.93;-3.44)	3	2.07 (3D) 2.04 (2D)	10.78 (3D) 5.88 (2D)	3	35285	1	11.97	$0.71_{-0.26}^{+0.16}$ (n_5) $0.10_{-0.15}^{+0.11}$ (n_{10})	$0.74_{-0.26}^{+0.16}$ (n_5) $0.10_{-0.15}^{+0.11}$ (n_{10})
NGC3689	11:28:10.99	+25:39:40.00	(2.50;30.07;-6.28)	3	4.29 (3D) 4.28 (2D)	21.55 (3D) 7.55 (2D)	67	35294	1	12.32	$0.31_{-0.26}^{+0.16}$ (n_5) $-0.77_{-0.15}^{+0.11}$ (n_{10})	$-0.39_{-0.26}^{+0.16}$ (n_5) $-0.77_{-0.15}^{+0.11}$ (n_{10})
NGC3694	11:28:54.12	+35:24:50.40	(6.23;25.63;-3.48)	3	0.47 (3D) 0.45 (2D)	18.14 (3D) 9.03 (2D)	48	35352	2	11.75	$0.89_{-0.26}^{+0.16}$ (n_5) $-0.26_{-0.15}^{+0.11}$ (n_{10})	$-0.32_{-0.26}^{+0.16}$ (n_5) $-0.26_{-0.15}^{+0.11}$ (n_{10})
PGC035472	11:30:33.37	+38:14:26.60	(6.23;21.61;-2.37)	3	1.01 (3D) 1.00 (2D)	14.60 (3D) 8.72 (2D)	10	35472	1	11.02	$0.90_{-0.26}^{+0.16}$ (n_5) $0.60_{-0.15}^{+0.11}$ (n_{10})	$0.68_{-0.26}^{+0.16}$ (n_5) $0.60_{-0.15}^{+0.11}$ (n_{10})
PGC035503	11:31:07.42	+35:35:23.10	(5.19;21.41;-2.72)	3	0.15 (3D) 0.12 (2D)	13.91 (3D) 7.80 (2D)	43	—	—	—	$0.81_{-0.26}^{+0.16}$ (n_5) $0.01_{-0.15}^{+0.11}$ (n_{10})	$0.23_{-0.26}^{+0.16}$ (n_5) $0.01_{-0.15}^{+0.11}$ (n_{10})
PGC035508	11:31:09.55	+36:36:02.50	(5.74;22.11;-2.65)	3	0.40 (3D) 0.37 (2D)	14.77 (3D) 8.31 (2D)	5	35508	2	11.25	$1.04_{-0.26}^{+0.16}$ (n_5) $0.39_{-0.15}^{+0.11}$ (n_{10})	$0.44_{-0.26}^{+0.16}$ (n_5) $0.39_{-0.15}^{+0.11}$ (n_{10})
UGC06517	11:32:02.39	+36:41:52.70	(6.95;26.75;-3.10)	3	1.03 (3D) 1.03 (2D)	19.39 (3D) 9.60 (2D)	55	35569	1	11.46	$1.10_{-0.26}^{+0.16}$ (n_5) $-0.14_{-0.15}^{+0.11}$ (n_{10})	$0.03_{-0.26}^{+0.16}$ (n_5) $-0.14_{-0.15}^{+0.11}$ (n_{10})
UGC06526	11:32:39.50	+35:19:42.10	(3.06;12.97;-1.61)	3	0.84 (3D) 0.77 (2D)	6.26 (3D) 5.45 (2D)	90	35621	1	11.35	$-0.02_{-0.26}^{+0.16}$ (n_5) $-0.66_{-0.15}^{+0.11}$ (n_{10})	$-0.70_{-0.26}^{+0.16}$ (n_5) $-0.66_{-0.15}^{+0.11}$ (n_{10})
PGC035688	11:33:30.15	+33:30:27.80	(5.64;27.69;-3.71)	3	0.43 (3D) 0.43 (2D)	19.75 (3D) 8.57 (2D)	13	35754	6	11.84	$1.49_{-0.26}^{+0.16}$ (n_5) $0.94_{-0.15}^{+0.11}$ (n_{10})	$1.08_{-0.26}^{+0.16}$ (n_5) $0.94_{-0.15}^{+0.11}$ (n_{10})
UGC06545	11:33:44.00	+32:38:00.90	(5.32;28.14;-3.92)	3	0.80 (3D) 0.79 (2D)	20.06 (3D) 8.35 (2D)	28	35707	1	11.74	$1.25_{-0.26}^{+0.16}$ (n_5) $0.41_{-0.15}^{+0.11}$ (n_{10})	$0.57_{-0.26}^{+0.16}$ (n_5) $0.41_{-0.15}^{+0.11}$ (n_{10})
UGC06610	11:38:44.09	+33:48:20.90	(4.85;24.19;-2.75)	3	0.86 (3D) 0.84 (2D)	16.14 (3D) 7.49 (2D)	28	36079	1	10.95	$0.41_{-0.26}^{+0.16}$ (n_5) $-0.38_{-0.15}^{+0.11}$ (n_{10})	$-0.40_{-0.26}^{+0.16}$ (n_5) $-0.38_{-0.15}^{+0.11}$ (n_{10})
NGC3786	11:39:42.50	+31:54:32.90	(5.45;32.49;-4.00)	3	0.52 (3D) 0.51 (2D)	24.14 (3D) 8.50 (2D)	88	36160	3	12.62	$-0.30_{-0.26}^{+0.16}$ (n_5) $-0.84_{-0.15}^{+0.11}$ (n_{10})	$-0.86_{-0.26}^{+0.16}$ (n_5) $-0.84_{-0.15}^{+0.11}$ (n_{10})
NGC3788	11:39:44.65	+31:55:52.30	(6.45;38.44;-4.72)	3	1.29 (3D) 1.28 (2D)	30.15 (3D) 9.72 (2D)	22	36160	3	12.62	$-1.89_{-0.26}^{+0.16}$ (n_5) $-1.95_{-0.15}^{+0.11}$ (n_{10})	$-1.94_{-0.26}^{+0.16}$ (n_5) $-1.95_{-0.15}^{+0.11}$ (n_{10})
UGC06637	11:40:24.87	+28:22:26.30	(3.52;32.50;-4.70)	3	2.46 (3D) 2.45 (2D)	23.72 (3D) 7.19 (2D)	89	36211	1	11.22	$-0.27_{-0.26}^{+0.16}$ (n_5) $-1.02_{-0.15}^{+0.11}$ (n_{10})	$-1.02_{-0.26}^{+0.16}$ (n_5) $-1.02_{-0.15}^{+0.11}$ (n_{10})
NGC3796	11:40:31.00	+60:17:56.00	(9.44;13.26;1.35)	Ursa Major	0.98 (3D) 0.70 (2D)	12.30 (3D) 11.83 (2D)	40	36215	2	11.51	$1.41_{-0.26}^{+0.16}$ (n_5) $0.82_{-0.15}^{+0.11}$ (n_{10})	$0.97_{-0.26}^{+0.16}$ (n_5) $0.82_{-0.15}^{+0.11}$ (n_{10})
NGC3838	11:44:13.00	+57:56:53.00	(9.21;14.13;1.25)	Ursa Major	0.52 (3D) 0.48 (2D)	12.34 (3D) 11.59 (2D)	26	36505	12	12.10	$1.74_{-0.26}^{+0.16}$ (n_5) $0.96_{-0.15}^{+0.11}$ (n_{10})	$1.49_{-0.26}^{+0.16}$ (n_5) $0.96_{-0.15}^{+0.11}$ (n_{10})
NGC3900	11:49:09.46	+27:01:19.30	(1.59;21.81;-2.64)	3	3.61 (3D) 3.54 (2D)	12.72 (3D) 4.45 (2D)	14	36914	5	12.27	$1.22_{-0.26}^{+0.16}$ (n_5) $-0.52_{-0.15}^{+0.11}$ (n_{10})	$0.60_{-0.26}^{+0.16}$ (n_5) $-0.52_{-0.15}^{+0.11}$ (n_{10})
NGC3898	11:49:15.00	+56:05:03.00	(8.49;14.07;1.20)	Ursa Major	0.22 (3D) 0.16 (2D)	11.65 (3D) 10.87 (2D)	60	36921	7	12.17	$1.38_{-0.26}^{+0.16}$ (n_5) $0.85_{-0.15}^{+0.11}$ (n_{10})	$0.96_{-0.26}^{+0.16}$ (n_5) $0.85_{-0.15}^{+0.11}$ (n_{10})
UGC06791	11:49:23.61	+26:44:29.70	(1.64;24.14;-2.95)	3	4.00 (3D) 3.95 (2D)	14.99 (3D) 4.66 (2D)	14	36914	5	12.27	$0.63_{-0.26}^{+0.16}$ (n_5) $-1.02_{-0.15}^{+0.11}$ (n_{10})	$-1.04_{-0.26}^{+0.16}$ (n_5) $-1.02_{-0.15}^{+0.11}$ (n_{10})
NGC3912	11:50:04.46	+26:28:45.30	(1.08;17.18;-2.08)	3	2.73 (3D) 2.54 (2D)	8.18 (3D) 3.73 (2D)	11	36914	5	12.27	$-0.15_{-0.26}^{+0.16}$ (n_5) $-0.86_{-0.15}^{+0.11}$ (n_{10})	$-0.83_{-0.26}^{+0.16}$ (n_5) $-0.86_{-0.15}^{+0.11}$ (n_{10})

NGC3953	11:53:48.00	+52:19:36.00	(6.03;11.66;0.78)	Ursa Major	1.40 (3D) 0.70 (2D)	8.56 (3D) 8.38 (2D)	27	37617	24	12.96	$1.47_{-0.20}^{+0.16}$ (n_5) $0.88_{-0.15}^{+0.11}$ (n_{10})	$1.06_{-0.26}^{+0.16}$ (n_5) $1.20_{-0.15}^{+0.16}$ (n_5) $1.12_{-0.15}^{+0.11}$ (n_{10})
NGC3982	11:56:28.00	+55:07:30.00	(7.55;13.17;1.27)	Ursa Major	0.55 (3D) 0.17 (2D)	10.49 (3D) 9.96 (2D)	37	37642	17	12.56	$1.53_{-0.26}^{+0.16}$ (n_5)	$1.21_{-0.26}^{+0.16}$ (n_5) $1.17_{-0.15}^{+0.11}$ (n_{10})
NGC3992	11:57:35.00	+53:22:28.00	(6.95;13.01;1.11)	Ursa Major	0.53 (3D) 0.14 (2D)	9.85 (3D) 9.34 (2D)	87	37617	24	12.96	$1.50_{-0.26}^{+0.16}$ (n_5)	$1.21_{-0.26}^{+0.16}$ (n_5) $1.17_{-0.15}^{+0.11}$ (n_{10})
NGC3998	11:57:56.00	+55:27:12.00	(7.79;13.46;1.38)	Ursa Major	0.36 (3D) 0.19 (2D)	10.82 (3D) 10.21 (2D)	29	37642	17	12.56	$1.72_{-0.26}^{+0.16}$ (n_5)	$1.30_{-0.26}^{+0.16}$ (n_5) $1.07_{-0.15}^{+0.11}$ (n_{10})
NGC4026	11:59:25.00	+50:57:42.00	(5.07;10.50;0.76)	Ursa Major	1.77 (3D) 1.21 (2D)	7.45 (3D) 7.42 (2D)	12	38795	17	12.77	$1.93_{-0.20}^{+0.16}$ (n_5)	$1.36_{-0.26}^{+0.16}$ (n_5) $1.20_{-0.15}^{+0.11}$ (n_{10})
NGC4051	12:03:09.00	+44:31:52.00	(3.45;9.73;0.37)	Ursa Major	1.02 (3D) 0.84 (2D)	5.77 (3D) 5.76 (2D)	25	38440	14	12.66	$1.33_{-0.26}^{+0.16}$ (n_5)	$1.19_{-0.26}^{+0.16}$ (n_5) $0.84_{-0.15}^{+0.11}$ (n_{10})
NGC4088	12:05:34.00	+50:32:20.00	(4.53;9.70;0.84)	Ursa Major	1.93 (3D) 1.53 (2D)	6.91 (3D) 6.91 (2D)	61	38795	17	12.77	$1.31_{-0.26}^{+0.16}$ (n_5)	$1.04_{-0.26}^{+0.16}$ (n_5) $0.86_{-0.15}^{+0.11}$ (n_{10})
NGC4096	12:06:01.00	+47:28:42.00	(3.40;8.37;0.56)	Ursa Major	1.63 (3D) 1.49 (2D)	5.95 (3D) 5.75 (2D)	37	39600	21	12.55	$1.32_{-0.26}^{+0.16}$ (n_5)	$0.72_{-0.26}^{+0.16}$ (n_5) $0.68_{-0.15}^{+0.11}$ (n_{10})
NGC4100	12:06:08.00	+49:34:57.00	(6.12;13.68;1.11)	Ursa Major	0.42 (3D) 0.20 (2D)	9.32 (3D) 8.52 (2D)	0	38795	17	12.77	$1.38_{-0.26}^{+0.16}$ (n_5)	$0.52_{-0.26}^{+0.16}$ (n_5) $0.30_{-0.15}^{+0.11}$ (n_{10})
NGC4111	12:07:03.00	+43:03:56.00	(3.12;9.68;0.39)	Ursa Major	0.77 (3D) 0.66 (2D)	5.45 (3D) 5.45 (2D)	13	38440	14	12.66	$1.36_{-0.26}^{+0.16}$ (n_5)	$0.62_{-0.26}^{+0.16}$ (n_5) $0.60_{-0.15}^{+0.11}$ (n_{10})
NGC4138	12:09:29.00	+43:41:07.00	(3.80;11.48;0.60)	Ursa Major	0.18 (3D) 0.14 (2D)	6.35 (3D) 6.15 (2D)	16	38440	14	12.66	$1.55_{-0.26}^{+0.16}$ (n_5)	$0.61_{-0.26}^{+0.16}$ (n_5) $0.47_{-0.15}^{+0.11}$ (n_{10})
NGC4143	12:09:36.00	+42:32:03.00	(3.85;12.41;0.56)	Ursa Major	0.48 (3D) 0.35 (2D)	6.68 (3D) 6.19 (2D)	22	38440	14	12.66	$1.43_{-0.26}^{+0.16}$ (n_5)	$1.12_{-0.26}^{+0.16}$ (n_5) $0.68_{-0.15}^{+0.11}$ (n_{10})
NGC4144	12:09:58.00	+46:27:25.00	(1.81;4.72;0.34)	Ursa Major	1.09 (3D) 1.06 (2D)	6.62 (3D) 4.14 (2D)	54	39600	21	12.55	$1.66_{-0.26}^{+0.16}$ (n_5)	$1.72_{-0.26}^{+0.16}$ (n_5) $1.44_{-0.15}^{+0.11}$ (n_{10})
NGC4151	12:10:32.00	+39:24:20.00	(2.05;8.08;0.24)	Ursa Major	0.51 (3D) 0.49 (2D)	4.72 (3D) 4.36 (2D)	68	38739	9	12.31	$1.41_{-0.26}^{+0.16}$ (n_5)	$0.48_{-0.26}^{+0.16}$ (n_5) $0.37_{-0.15}^{+0.11}$ (n_{10})
NGC4152	12:10:37.50	+16:01:58.50	(-3.01;21.59;-2.26)	W-M Sheet	0.42 (3D) 0.42 (2D)	11.86 (3D) 1.99 (2D)	20	38890	11	12.93	$0.75_{-0.26}^{+0.16}$ (n_5)	$-0.04_{-0.26}^{+0.16}$ (n_5) $-0.01_{-0.15}^{+0.11}$ (n_{10})
UGC07271	12:15:33.00	+43:26:02.00	(2.83;8.86;0.62)	Ursa Major	0.93 (3D) 0.80 (2D)	5.30 (3D) 5.20 (2D)	3	39211	1	10.60	$1.16_{-0.26}^{+0.16}$ (n_5)	$0.64_{-0.26}^{+0.16}$ (n_5) $0.62_{-0.15}^{+0.11}$ (n_{10})
NGC4214	12:15:39.00	+36:19:36.00	(0.40;2.08;0.06)	Ursa Major	0.60 (3D) 0.11 (2D)	8.27 (3D) 2.71 (2D)	18	39225	4	11.09	$3.34_{-0.26}^{+0.16}$ (n_5)	$2.62_{-0.26}^{+0.16}$ (n_5) $2.04_{-0.15}^{+0.11}$ (n_{10})
NGC4244	12:17:29.00	+37:48:25.00	(0.67;3.08;0.13)	Ursa Major	0.15 (3D) 0.15 (2D)	7.44 (3D) 2.98 (2D)	69	39422	4	11.16	$2.22_{-0.26}^{+0.16}$ (n_5)	$1.82_{-0.26}^{+0.16}$ (n_5) $1.77_{-0.15}^{+0.11}$ (n_{10})
NGC4314	12:22:31.00	+29:53:45.00	(0.56;7.24;0.12)	Ursa Major	0.69 (3D) 0.67 (2D)	3.92 (3D) 2.87 (2D)	15	40692	44	12.94	$2.18_{-0.26}^{+0.16}$ (n_5)	$2.06_{-0.26}^{+0.16}$ (n_5) $1.44_{-0.15}^{+0.11}$ (n_{10})
NGC4359	12:24:11.00	+31:31:18.00	(1.39;13.55;0.43)	Ursa Major	2.99 (3D) 2.19 (2D)	5.23 (3D) 3.75 (2D)	58	40330	1	11.25	$1.10_{-0.26}^{+0.16}$ (n_5)	$0.42_{-0.26}^{+0.16}$ (n_5) $0.42_{-0.15}^{+0.11}$ (n_{10})
NGC4414	12:26:27.00	+31:13:24.00	(1.23;12.96;0.50)	Ursa Major	2.71 (3D) 2.06 (2D)	4.74 (3D) 3.61 (2D)	3	40692	44	12.94	$0.94_{-0.26}^{+0.16}$ (n_5)	$0.60_{-0.26}^{+0.16}$ (n_5) $0.48_{-0.15}^{+0.11}$ (n_{10})
NGC4448	12:28:15.00	+28:37:13.00	(0.74;14.91;0.47)	Ursa Major	4.42 (3D) 3.03 (2D)	5.91 (3D) 3.13 (2D)	49	40692	44	12.94	$1.76_{-0.26}^{+0.16}$ (n_5)	$0.33_{-0.26}^{+0.16}$ (n_5) $0.17_{-0.15}^{+0.11}$ (n_{10})
NGC4525	12:33:51.00	+30:16:38.00	(0.68;9.58;0.58)	Ursa Major	1.36 (3D) 1.25 (2D)	3.12 (3D) 3.11 (2D)	70	41755	1	11.29	$2.00_{-0.26}^{+0.16}$ (n_5)	$0.37_{-0.26}^{+0.16}$ (n_5) $0.34_{-0.15}^{+0.11}$ (n_{10})
NGC4559	12:35:57.00	+27:57:35.00	(0.17;5.77;0.33)	Ursa Major	0.71 (3D) 0.69 (2D)	4.85 (3D) 2.55 (2D)	11	42002	1	11.78	$2.16_{-0.26}^{+0.16}$ (n_5)	$0.94_{-0.26}^{+0.16}$ (n_5) $0.96_{-0.15}^{+0.11}$ (n_{10})

NGC4793	12:54:40.62	+28:56:19.20	(0.58;20.75;2.72)	NGC5353/4	6.21 (3D) 3.92 (2D)	11.65 (3D) 4.23 (2D)	38	43939	2	12.36	-0.04 ^{+0.16} _{-0.26} (n ₅) -0.86 ^{+0.11} _{-0.15} (n ₁₀)	-0.87 ^{+0.16} _{-0.26} (n ₅) -0.10 ^{+0.11} _{-0.15} (n ₁₀)
UGC08076	12:57:49.94	+29:39:15.10	(1.04;27.90;4.07)	NGC5353/4	3.74 (3D) 2.88 (2D)	18.85 (3D) 5.57 (2D)	76	44370	1	11.45	0.83 ^{+0.16} _{-0.26} (n ₅)	0.55 ^{+0.16} _{-0.26} (n ₅) -0.67 ^{+0.11} _{-0.15} (n ₁₀)
NGC4961	13:05:47.57	+27:44:02.90	(-0.08;29.16;4.91)	NGC5353/4	3.94 (3D) 1.70 (2D)	20.11 (3D) 5.75 (2D)	90	45311	2	11.59	0.18 ^{+0.16} _{-0.26} (n ₅)	-0.69 ^{+0.16} _{-0.26} (n ₅) -0.43 ^{+0.11} _{-0.15} (n ₁₀)
IC0851	13:08:34.27	+21:02:59.90	(-3.92;32.42;4.97)	NGC5353/4	6.33 (3D) 1.01 (2D)	23.21 (3D) 5.63 (2D)	46	45552	1	11.46	-0.28 ^{+0.16} _{-0.26} (n ₅)	-0.98 ^{+0.16} _{-0.26} (n ₅) -1.09 ^{+0.11} _{-0.15} (n ₁₀)
NGC5012	13:11:37.04	+22:54:55.80	(-2.45;26.84;4.64)	NGC5353/4	1.31 (3D) 0.88 (2D)	17.68 (3D) 5.06 (2D)	6	45795	3	12.49	0.49 ^{+0.16} _{-0.20} (n ₅)	-0.50 ^{+0.16} _{-0.26} (n ₅) -0.71 ^{+0.11} _{-0.15} (n ₁₀)
NGC5016	13:12:06.68	+24:05:42.00	(-2.09;29.31;5.25)	NGC5353/4	3.56 (3D) 0.74 (2D)	20.23 (3D) 5.67 (2D)	41	45836	1	12.03	0.53 ^{+0.16} _{-0.26} (n ₅)	-0.34 ^{+0.16} _{-0.26} (n ₅) -0.43 ^{+0.11} _{-0.15} (n ₁₀)
UGC08290	13:12:41.78	+22:49:47.20	(-2.77;29.54;5.22)	NGC5353/4	3.67 (3D) 0.52 (2D)	20.44 (3D) 5.66 (2D)	26	45795	3	12.49	0.53 ^{+0.16} _{-0.26} (n ₅)	-0.34 ^{+0.16} _{-0.26} (n ₅) -0.42 ^{+0.11} _{-0.15} (n ₁₀)
UGC08318	13:14:30.59	+35:23:12.60	(3.40;27.27;6.30)	NGC5353/4	2.57 (3D) 1.77 (2D)	19.47 (3D) 8.78 (2D)	68	46041	3	11.14	0.50 ^{+0.16} _{-0.26} (n ₅)	-0.58 ^{+0.16} _{-0.26} (n ₅) -0.83 ^{+0.11} _{-0.15} (n ₁₀)
NGC5116	13:22:55.61	+26:58:50.60	(-0.94;31.42;7.33)	NGC5353/4	5.92 (3D) 1.02 (2D)	22.91 (3D) 7.86 (2D)	24	46744	1	12.07	-0.37 ^{+0.16} _{-0.26} (n ₅)	-0.90 ^{+0.16} _{-0.26} (n ₅) -1.17 ^{+0.11} _{-0.15} (n ₁₀)
NGC5117	13:22:56.47	+28:18:59.10	(-0.18;27.86;6.63)	NGC5353/4	2.34 (3D) 0.12 (2D)	19.40 (3D) 7.34 (2D)	41	46746	1	11.31	0.50 ^{+0.16} _{-0.26} (n ₅)	-0.42 ^{+0.16} _{-0.26} (n ₅) -0.57 ^{+0.11} _{-0.15} (n ₁₀)
UGC08409	13:23:00.86	+23:18:22.90	(-2.93;30.90;6.83)	NGC5353/4	5.27 (3D) 1.55 (2D)	22.23 (3D) 7.27 (2D)	64	46753	1	11.35	-0.21 ^{+0.16} _{-0.26} (n ₅)	-0.90 ^{+0.16} _{-0.26} (n ₅) -0.94 ^{+0.11} _{-0.15} (n ₁₀)
NGC5169	13:28:10.05	+46:40:19.70	(9.44;28.51;9.18)	NGC5353/4	1.69 (3D) 0.68 (2D)	23.99 (3D) 15.13 (2D)	53	47441	11	12.71	1.22 ^{+0.16} _{-0.26} (n ₅)	0.06 ^{+0.16} _{-0.26} (n ₅) -0.20 ^{+0.11} _{-0.15} (n ₁₀)
NGC5173	13:28:25.27	+46:35:29.90	(8.53;25.89;8.35)	NGC5353/4	1.39 (3D) 1.23 (2D)	21.19 (3D) 13.90 (2D)	62	47441	11	12.71	1.49 ^{+0.16} _{-0.26} (n ₅)	0.65 ^{+0.16} _{-0.26} (n ₅) 0.54 ^{+0.11} _{-0.15} (n ₁₀)
IC4263	13:28:33.19	+46:55:37.80	(9.26;27.55;8.93)	NGC5353/4	0.94 (3D) 0.74 (2D)	23.06 (3D) 14.83 (2D)	55	47441	11	12.71	1.22 ^{+0.16} _{-0.26} (n ₅)	0.58 ^{+0.16} _{-0.26} (n ₅) 0.25 ^{+0.11} _{-0.15} (n ₁₀)
PGC047274	13:28:33.65	+46:29:59.70	(8.66;26.44;8.53)	NGC5353/4	1.07 (3D) 1.05 (2D)	21.75 (3D) 14.12 (2D)	27	47441	11	12.71	1.18 ^{+0.16} _{-0.26} (n ₅)	1.18 ^{+0.16} _{-0.26} (n ₅) 0.71 ^{+0.11} _{-0.15} (n ₁₀)
PGC047295	13:28:49.76	+46:15:44.60	(8.82;27.33;8.81)	NGC5353/4	0.83 (3D) 0.75 (2D)	22.62 (3D) 14.42 (2D)	32	47441	11	12.71	1.12 ^{+0.16} _{-0.26} (n ₅)	0.77 ^{+0.16} _{-0.26} (n ₅) 0.39 ^{+0.11} _{-0.15} (n ₁₀)
NGC5198	13:30:11.40	+46:40:14.80	(9.15;27.68;9.10)	NGC5353/4	0.89 (3D) 0.54 (2D)	23.18 (3D) 14.86 (2D)	38	47441	11	12.71	1.24 ^{+0.16} _{-0.26} (n ₅)	0.83 ^{+0.16} _{-0.26} (n ₅) 0.35 ^{+0.11} _{-0.15} (n ₁₀)
NGC5248	13:37:32.02	+08:53:06.60	(-3.21;8.54;2.03)	VirgoIII	4.32 (3D) 2.68 (2D)	2.95 (3D) 2.62 (2D)	27	48130	11	12.32	1.23 ^{+0.16} _{-0.26} (n ₅)	0.24 ^{+0.16} _{-0.26} (n ₅) 0.22 ^{+0.11} _{-0.15} (n ₁₀)
UGC08630	13:38:24.87	+33:07:03.70	(1.70;24.41;7.69)	NGC5353/4	1.01 (3D) 0.17 (2D)	17.09 (3D) 9.02 (2D)	81	48206	1	11.31	0.44 ^{+0.16} _{-0.26} (n ₅)	-0.84 ^{+0.16} _{-0.26} (n ₅) -0.81 ^{+0.11} _{-0.15} (n ₁₀)
UGC08662	13:41:17.25	+33:46:21.40	(1.71;21.35;7.01)	NGC5353/4	4.08 (3D) 0.48 (2D)	14.22 (3D) 8.42 (2D)	60	48441	1	10.86	-0.44 ^{+0.16} _{-0.26} (n ₅)	-1.16 ^{+0.16} _{-0.26} (n ₅) -1.16 ^{+0.11} _{-0.15} (n ₁₀)
UGC08693	13:44:28.40	+35:11:31.90	(3.13;29.81;10.28)	NGC5353/4	4.79 (3D) 2.07 (2D)	23.24 (3D) 11.98 (2D)	19	48690	1	11.45	-0.20 ^{+0.16} _{-0.26} (n ₅)	-0.88 ^{+0.16} _{-0.26} (n ₅) -0.85 ^{+0.11} _{-0.15} (n ₁₀)
NGC5289	13:45:08.71	+41:30:12.20	(6.14;27.37;10.00)	NGC5353/4	1.68 (3D) 0.93 (2D)	22.01 (3D) 13.38 (2D)	79	48767	9	12.86	1.49 ^{+0.16} _{-0.26} (n ₅)	1.10 ^{+0.16} _{-0.26} (n ₅) 0.77 ^{+0.11} _{-0.15} (n ₁₀)
NGC5290	13:45:19.18	+41:42:45.30	(5.52;24.20;8.87)	NGC5353/4	1.47 (3D) 0.32 (2D)	18.75 (3D) 12.12 (2D)	89	48767	9	12.86	0.68 ^{+0.16} _{-0.26} (n ₅)	0.14 ^{+0.16} _{-0.26} (n ₅) 0.22 ^{+0.11} _{-0.15} (n ₁₀)
NGC5297	13:46:23.67	+43:52:20.40	(5.53;20.45;7.71)	NGC5353/4	5.26 (3D) 1.36 (2D)	15.43 (3D) 11.26 (2D)	41	48815	6	12.42	0.08 ^{+0.16} _{-0.26} (n ₅)	-0.48 ^{+0.16} _{-0.26} (n ₅) -0.49 ^{+0.11} _{-0.15} (n ₁₀)

NGC5300	13:48:16.04	+03:57:03.10	(-6.22;12.65;3.48)	VirgoIII	0.89 (3D) 0.64 (2D)	6.20 (3D) 5.56 (2D)	54	48959	1	11.52	$0.70_{-0.26}^{+0.16}$ (n_5) $0.04_{-0.15}^{+0.11}$ (n_{10})	$0.16_{-0.26}^{+0.16}$ (n_5) $0.04_{-0.15}^{+0.11}$ (n_{10})
UGC08733	13:48:38.99	+43:24:44.20	(5.41;20.73;7.96)	NGC5353/4	4.93 (3D) 1.11 (2D)	15.69 (3D) 11.36 (2D)	1	48815	6	12.42	$0.29_{-0.26}^{+0.16}$ (n_5) $-0.39_{-0.15}^{+0.11}$ (n_{10})	$-0.42_{-0.26}^{+0.16}$ (n_5) $-0.39_{-0.15}^{+0.11}$ (n_{10})
PGC049002	13:48:45.16	+41:42:35.30	(6.28;27.60;10.48)	NGC5353/4	2.06 (3D) 1.36 (2D)	22.48 (3D) 13.84 (2D)	5	48767	9	12.86	$0.85_{-0.26}^{+0.16}$ (n_5) $0.54_{-0.15}^{+0.11}$ (n_{10})	$0.86_{-0.26}^{+0.16}$ (n_5) $0.54_{-0.15}^{+0.11}$ (n_{10})
NGC5311	13:48:56.08	+39:59:06.40	(5.39;27.79;10.44)	NGC5353/4	2.49 (3D) 1.54 (2D)	22.29 (3D) 13.28 (2D)	79	49356	61	13.77	$1.53_{-0.26}^{+0.16}$ (n_5) $0.75_{-0.15}^{+0.11}$ (n_{10})	$1.04_{-0.26}^{+0.16}$ (n_5) $0.75_{-0.15}^{+0.11}$ (n_{10})
UGC08736	13:49:04.55	+39:29:51.60	(4.63;25.08;9.40)	NGC5353/4	0.87 (3D) 0.71 (2D)	19.35 (3D) 11.99 (2D)	12	49356	61	13.77	$1.48_{-0.26}^{+0.16}$ (n_5) $0.49_{-0.15}^{+0.11}$ (n_{10})	$0.54_{-0.26}^{+0.16}$ (n_5) $0.49_{-0.15}^{+0.11}$ (n_{10})
NGC5313	13:49:44.34	+39:59:05.20	(5.76;29.71;11.25)	NGC5353/4	4.28 (3D) 2.48 (2D)	24.35 (3D) 14.15 (2D)	49	49356	61	13.77	$0.89_{-0.26}^{+0.16}$ (n_5) $-0.56_{-0.15}^{+0.11}$ (n_{10})	$-0.39_{-0.26}^{+0.16}$ (n_5) $-0.56_{-0.15}^{+0.11}$ (n_{10})
NGC5320	13:50:20.38	+41:21:58.40	(5.41;24.54;9.44)	NGC5353/4	1.24 (3D) 0.55 (2D)	19.25 (3D) 12.49 (2D)	13	49356	61	13.77	$1.07_{-0.26}^{+0.16}$ (n_5) $0.55_{-0.15}^{+0.11}$ (n_{10})	$0.61_{-0.26}^{+0.16}$ (n_5) $0.55_{-0.15}^{+0.11}$ (n_{10})
IC4336	13:50:43.37	+39:42:24.40	(4.95;26.29;10.03)	NGC5353/4	1.38 (3D) 1.22 (2D)	20.73 (3D) 12.70 (2D)	30	49356	61	13.77	$1.75_{-0.26}^{+0.16}$ (n_5) $0.78_{-0.15}^{+0.11}$ (n_{10})	$1.12_{-0.26}^{+0.16}$ (n_5) $0.78_{-0.15}^{+0.11}$ (n_{10})
NGC5326	13:50:50.70	+39:34:29.50	(3.40;18.32;7.00)	NGC5353/4	7.18 (3D) 1.14 (2D)	12.57 (3D) 9.33 (2D)	56	49356	61	13.77	$0.70_{-0.26}^{+0.16}$ (n_5) $-0.44_{-0.15}^{+0.11}$ (n_{10})	$-0.18_{-0.26}^{+0.16}$ (n_5) $-0.44_{-0.15}^{+0.11}$ (n_{10})
PGC049191	13:51:25.37	+40:12:47.70	(5.15;26.03;10.04)	NGC5353/4	1.22 (3D) 1.17 (2D)	20.61 (3D) 12.82 (2D)	3	49356	61	13.77	$1.59_{-0.26}^{+0.16}$ (n_5) $0.79_{-0.15}^{+0.11}$ (n_{10})	$1.18_{-0.26}^{+0.16}$ (n_5) $0.79_{-0.15}^{+0.11}$ (n_{10})
NGC5336	13:52:09.79	+43:14:34.60	(6.23;24.23;9.61)	NGC5353/4	1.66 (3D) 0.56 (2D)	19.45 (3D) 13.14 (2D)	81	49250	2	11.52	$1.65_{-0.26}^{+0.16}$ (n_5) $0.44_{-0.15}^{+0.11}$ (n_{10})	$0.73_{-0.26}^{+0.16}$ (n_5) $0.44_{-0.15}^{+0.11}$ (n_{10})
NGC5337	13:52:23.03	+39:41:14.10	(6.29;33.57;13.03)	NGC5353/4	7.89 (3D) 4.32 (2D)	28.54 (3D) 15.93 (2D)	45	49356	61	13.77	$-0.53_{-0.26}^{+0.16}$ (n_5) $-1.31_{-0.15}^{+0.11}$ (n_{10})	$-1.26_{-0.26}^{+0.16}$ (n_5) $-1.31_{-0.15}^{+0.11}$ (n_{10})
PGC2151881	13:52:24.87	+39:33:27.40	(5.13;27.76;10.77)	NGC5353/4	2.74 (3D) 1.91 (2D)	22.34 (3D) 13.41 (2D)	47	49356	61	13.77	$1.54_{-0.26}^{+0.16}$ (n_5) $0.83_{-0.15}^{+0.11}$ (n_{10})	$1.20_{-0.26}^{+0.16}$ (n_5) $0.83_{-0.15}^{+0.11}$ (n_{10})
NGC5346	13:53:01.89	+39:34:50.80	(4.79;25.87;10.10)	NGC5353/4	1.35 (3D) 1.33 (2D)	20.38 (3D) 12.66 (2D)	25	49356	61	13.77	$1.41_{-0.26}^{+0.16}$ (n_5) $0.71_{-0.15}^{+0.11}$ (n_{10})	$0.69_{-0.26}^{+0.16}$ (n_5) $0.71_{-0.15}^{+0.11}$ (n_{10})
NGC5347	13:53:17.83	+33:29:27.00	(1.00;14.30;5.38)	NGC5353/4	11.28 (3D) 1.75 (2D)	7.97 (3D) 6.65 (2D)	72	49342	1	11.99	$-0.27_{-0.26}^{+0.16}$ (n_5) $-0.90_{-0.15}^{+0.11}$ (n_{10})	$-0.95_{-0.26}^{+0.16}$ (n_5) $-0.90_{-0.15}^{+0.11}$ (n_{10})
NGC5350	13:53:21.60	+40:21:50.00	(3.93;19.60;7.71)	NGC5353/4	5.88 (3D) 0.72 (2D)	14.09 (3D) 10.22 (2D)	24	49356	61	13.77	$1.15_{-0.26}^{+0.16}$ (n_5) $-0.10_{-0.15}^{+0.11}$ (n_{10})	$0.77_{-0.26}^{+0.16}$ (n_5) $-0.10_{-0.15}^{+0.11}$ (n_{10})
NGC5353	13:53:26.69	+40:16:58.90	(4.55;22.89;9.01)	NGC5353/4	2.67 (3D) 0.52 (2D)	17.44 (3D) 11.63 (2D)	36	49356	61	13.77	$1.41_{-0.26}^{+0.16}$ (n_5) $0.72_{-0.15}^{+0.11}$ (n_{10})	$0.94_{-0.26}^{+0.16}$ (n_5) $0.72_{-0.15}^{+0.11}$ (n_{10})
NGC5355	13:53:45.56	+40:20:19.20	(4.81;24.08;9.51)	NGC5353/4	1.69 (3D) 0.79 (2D)	18.70 (3D) 12.19 (2D)	23	49356	61	13.77	$1.43_{-0.26}^{+0.16}$ (n_5) $0.59_{-0.15}^{+0.11}$ (n_{10})	$0.62_{-0.26}^{+0.16}$ (n_5) $0.59_{-0.15}^{+0.11}$ (n_{10})
PGC049386	13:53:59.49	+39:42:56.00	(5.05;26.91;10.61)	NGC5353/4	2.12 (3D) 1.75 (2D)	21.55 (3D) 13.23 (2D)	68	49356	61	13.77	$1.70_{-0.26}^{+0.16}$ (n_5) $0.82_{-0.15}^{+0.11}$ (n_{10})	$1.48_{-0.26}^{+0.16}$ (n_5) $0.82_{-0.15}^{+0.11}$ (n_{10})
NGC5358	13:54:00.41	+40:16:38.30	(4.98;25.11;9.94)	NGC5353/4	1.24 (3D) 1.13 (2D)	19.78 (3D) 12.64 (2D)	48	49356	61	13.77	$1.68_{-0.26}^{+0.16}$ (n_5) $0.60_{-0.15}^{+0.11}$ (n_{10})	$0.92_{-0.26}^{+0.16}$ (n_5) $0.60_{-0.15}^{+0.11}$ (n_{10})
NGC5348	13:54:11.27	+05:13:38.80	(-5.54;11.71;3.63)	VirgoIII	0.26 (3D) 0.09 (2D)	5.51 (3D) 5.20 (2D)	83	49547	17	12.76	$0.76_{-0.26}^{+0.16}$ (n_5) $-0.20_{-0.15}^{+0.11}$ (n_{10})	$-0.12_{-0.26}^{+0.16}$ (n_5) $-0.20_{-0.15}^{+0.11}$ (n_{10})
NGC5362	13:54:53.30	+41:18:48.70	(4.12;18.86;7.58)	NGC5353/4	6.64 (3D) 0.95 (2D)	13.61 (3D) 10.23 (2D)	77	49356	61	13.77	$0.78_{-0.26}^{+0.16}$ (n_5) $-0.19_{-0.15}^{+0.11}$ (n_{10})	$0.41_{-0.26}^{+0.16}$ (n_5) $-0.19_{-0.15}^{+0.11}$ (n_{10})
NGC5356	13:54:58.46	+05:20:01.40	(-7.56;16.01;5.03)	VirgoIII	3.66 (3D) 1.51 (2D)	9.75 (3D) 7.59 (2D)	83	49547	17	12.76	$0.87_{-0.26}^{+0.16}$ (n_5) $-0.38_{-0.15}^{+0.11}$ (n_{10})	$0.03_{-0.26}^{+0.16}$ (n_5) $-0.38_{-0.15}^{+0.11}$ (n_{10})
NGC5360	13:55:38.75	+04:59:06.20	(-6.80;14.14;4.48)	VirgoIII	1.99 (3D) 0.89 (2D)	7.91 (3D) 6.67 (2D)	33	49547	17	12.76	$0.58_{-0.26}^{+0.16}$ (n_5) $-0.28_{-0.15}^{+0.11}$ (n_{10})	$-0.11_{-0.26}^{+0.16}$ (n_5) $-0.28_{-0.15}^{+0.11}$ (n_{10})

NGC5371	13:55:39.94	+40:27:42.30	(3.87;19.18;7.73)	NGC5353/4	6.29 (3D) 0.67 (2D)	13.79 (3D) 10.19 (2D)	4	49356	61	13.77	$1.27_{-0.20}^{+0.16}$ (n_5) $-0.10_{-0.15}^{+0.11}$ (n_{10})	$0.72_{-0.26}^{+0.16}$ (n_5) $-0.10_{-0.15}^{+0.11}$ (n_{10})
NGC5363	13:56:07.21	+05:15:17.20	(-5.93;12.46;3.98)	VirgoIII	0.41 (3D) 0.18 (2D)	6.27 (3D) 5.72 (2D)	40	49547	17	12.76	$0.83_{-0.26}^{+0.16}$ (n_5) $0.03_{-0.15}^{+0.11}$ (n_{10})	$0.23_{-0.26}^{+0.16}$ (n_5) $0.03_{-0.15}^{+0.11}$ (n_{10})
NGC5364	13:56:12.00	+05:00:52.10	(-5.29;11.00;3.51)	VirgoIII	0.96 (3D) 0.25 (2D)	5.08 (3D) 4.96 (2D)	47	49547	17	12.76	$0.69_{-0.26}^{+0.16}$ (n_5) $-0.28_{-0.15}^{+0.11}$ (n_{10})	$-0.14_{-0.26}^{+0.16}$ (n_5) $-0.28_{-0.15}^{+0.11}$ (n_{10})
NGC5375	13:56:56.00	+29:09:51.70	(-0.34;28.15;10.73)	NGC5353/4	4.65 (3D) 3.77 (2D)	21.47 (3D) 11.31 (2D)	14	49604	4	12.12	$-0.35_{-0.26}^{+0.16}$ (n_5) $-1.11_{-0.15}^{+0.11}$ (n_{10})	$-1.12_{-0.26}^{+0.16}$ (n_5) $-1.11_{-0.15}^{+0.11}$ (n_{10})
NGC5383	13:57:04.97	+41:50:46.50	(5.52;24.12;9.93)	NGC5353/4	1.85 (3D) 0.99 (2D)	19.24 (3D) 12.95 (2D)	86	49356	61	13.77	$1.52_{-0.20}^{+0.16}$ (n_5) $0.33_{-0.15}^{+0.11}$ (n_{10})	$0.39_{-0.26}^{+0.16}$ (n_5) $0.33_{-0.15}^{+0.11}$ (n_{10})
NGC5403	13:59:50.75	+38:10:57.20	(4.39;27.98;11.58)	NGC5353/4	3.69 (3D) 2.89 (2D)	22.70 (3D) 13.72 (2D)	41	49820	4	12.44	$0.71_{-0.26}^{+0.16}$ (n_5) $-0.18_{-0.15}^{+0.11}$ (n_{10})	$-0.27_{-0.26}^{+0.16}$ (n_5) $-0.18_{-0.15}^{+0.11}$ (n_{10})
PGC049824	13:59:57.09	+38:12:03.30	(4.37;27.83;11.54)	NGC5353/4	3.57 (3D) 2.85 (2D)	22.55 (3D) 13.67 (2D)	46	49820	4	12.44	$0.74_{-0.26}^{+0.16}$ (n_5) $-0.15_{-0.15}^{+0.11}$ (n_{10})	$-0.12_{-0.26}^{+0.16}$ (n_5) $-0.15_{-0.15}^{+0.11}$ (n_{10})
PGC049852	14:00:25.00	+38:31:13.00	(4.37;26.74;11.15)	NGC5353/4	2.70 (3D) 2.47 (2D)	21.48 (3D) 13.33 (2D)	29	49820	4	12.44	$0.33_{-0.26}^{+0.16}$ (n_5) $-0.05_{-0.15}^{+0.11}$ (n_{10})	$0.04_{-0.26}^{+0.16}$ (n_5) $-0.05_{-0.15}^{+0.11}$ (n_{10})
PGC049927	14:01:24.02	+36:48:00.30	(3.72;28.64;11.95)	NGC5353/4	4.58 (3D) 3.45 (2D)	23.24 (3D) 13.74 (2D)	66	49927	1	11.51	$0.36_{-0.26}^{+0.16}$ (n_5) $-0.51_{-0.15}^{+0.11}$ (n_{10})	$-0.34_{-0.26}^{+0.16}$ (n_5) $-0.51_{-0.15}^{+0.11}$ (n_{10})
NGC5470	14:06:31.91	+06:01:46.90	(-7.22;15.25;5.75)	VirgoIII	2.65 (3D) 0.88 (2D)	9.55 (3D) 7.91 (2D)	37	50317	1	11.32	$0.45_{-0.26}^{+0.16}$ (n_5) $-0.03_{-0.15}^{+0.11}$ (n_{10})	$0.04_{-0.26}^{+0.16}$ (n_5) $-0.03_{-0.15}^{+0.11}$ (n_{10})
NGC5560	14:20:04.49	+03:59:32.90	(-6.26;11.60;5.20)	VirgoIII	0.74 (3D) 0.13 (2D)	7.10 (3D) 6.90 (2D)	14	51233	12	12.95	$0.80_{-0.26}^{+0.16}$ (n_5) $-0.19_{-0.15}^{+0.11}$ (n_{10})	$-0.15_{-0.26}^{+0.16}$ (n_5) $-0.19_{-0.15}^{+0.11}$ (n_{10})
NGC5566	14:20:19.89	+03:56:01.50	(-6.07;11.21;5.04)	VirgoIII	1.08 (3D) 0.24 (2D)	6.79 (3D) 6.66 (2D)	60	51233	12	12.95	$0.58_{-0.26}^{+0.16}$ (n_5) $-0.18_{-0.15}^{+0.11}$ (n_{10})	$-0.02_{-0.26}^{+0.16}$ (n_5) $-0.18_{-0.15}^{+0.11}$ (n_{10})
NGC5574	14:20:55.97	+03:14:16.80	(-8.20;14.67;6.64)	VirgoIII	1.97 (3D) 1.18 (2D)	10.38 (3D) 9.22 (2D)	41	51233	12	12.95	$0.82_{-0.26}^{+0.16}$ (n_5) $0.38_{-0.15}^{+0.11}$ (n_{10})	$0.41_{-0.26}^{+0.16}$ (n_5) $0.38_{-0.15}^{+0.11}$ (n_{10})
NGC5576	14:21:03.68	+03:16:15.60	(-7.13;12.78;5.79)	VirgoIII	0.55 (3D) 0.52 (2D)	8.40 (3D) 7.89 (2D)	7	51233	12	12.95	$0.59_{-0.26}^{+0.16}$ (n_5) $-0.22_{-0.15}^{+0.11}$ (n_{10})	$-0.08_{-0.26}^{+0.16}$ (n_5) $-0.22_{-0.15}^{+0.11}$ (n_{10})
NGC5577	14:21:13.11	+03:26:08.80	(-7.74;13.96;6.34)	VirgoIII	1.38 (3D) 0.84 (2D)	9.60 (3D) 8.70 (2D)	39	51233	12	12.95	$0.73_{-0.26}^{+0.16}$ (n_5) $0.11_{-0.15}^{+0.11}$ (n_{10})	$0.17_{-0.26}^{+0.16}$ (n_5) $0.11_{-0.15}^{+0.11}$ (n_{10})
UGC09215	14:23:27.12	+01:43:34.70	(-8.88;14.81;6.88)	VirgoIII	2.21 (3D) 1.62 (2D)	11.01 (3D) 9.85 (2D)	59	51400	1	11.21	$1.05_{-0.26}^{+0.16}$ (n_5) $0.43_{-0.15}^{+0.11}$ (n_{10})	$0.51_{-0.26}^{+0.16}$ (n_5) $0.43_{-0.15}^{+0.11}$ (n_{10})
NGC5636	14:29:39.02	+03:15:58.70	(-9.11;15.91;8.03)	VirgoIII	2.41 (3D) 1.54 (2D)	12.42 (3D) 10.87 (2D)	56	51787	15	12.42	$1.15_{-0.26}^{+0.16}$ (n_5) $0.89_{-0.15}^{+0.11}$ (n_{10})	$0.90_{-0.26}^{+0.16}$ (n_5) $0.89_{-0.15}^{+0.11}$ (n_{10})
NGC5638	14:29:40.38	+03:13:59.90	(-8.47;14.76;7.45)	VirgoIII	1.70 (3D) 1.01 (2D)	11.14 (3D) 10.02 (2D)	50	51787	15	12.42	$1.31_{-0.26}^{+0.16}$ (n_5) $0.65_{-0.15}^{+0.11}$ (n_{10})	$0.66_{-0.26}^{+0.16}$ (n_5) $0.65_{-0.15}^{+0.11}$ (n_{10})
IC1022	14:30:01.84	+03:46:22.30	(-12.86;22.92;11.63)	VirgoIII	5.95 (3D) 2.01 (2D)	20.66 (3D) 16.04 (2D)	66	51787	15	12.42	$-0.32_{-0.26}^{+0.16}$ (n_5) $-1.14_{-0.15}^{+0.11}$ (n_{10})	$-1.16_{-0.26}^{+0.16}$ (n_5) $-1.14_{-0.15}^{+0.11}$ (n_{10})
NGC5645	14:30:39.35	+07:16:30.30	(-5.52;11.50;5.92)	VirgoIII	1.36 (3D) 1.02 (2D)	7.30 (3D) 7.13 (2D)	12	51846	2	11.52	$0.63_{-0.26}^{+0.16}$ (n_5) $-0.07_{-0.15}^{+0.11}$ (n_{10})	$-0.06_{-0.26}^{+0.16}$ (n_5) $-0.07_{-0.15}^{+0.11}$ (n_{10})
IC1024	14:31:27.20	+03:00:32.70	(-7.47;12.84;6.62)	VirgoIII	0.43 (3D) 0.43 (2D)	9.23 (3D) 8.75 (2D)	70	51787	15	12.42	$0.80_{-0.26}^{+0.16}$ (n_5) $-0.00_{-0.15}^{+0.11}$ (n_{10})	$-0.00_{-0.26}^{+0.16}$ (n_5) $-0.00_{-0.15}^{+0.11}$ (n_{10})
NGC5661	14:31:57.39	+06:15:01.50	(-14.19;28.09;14.66)	VirgoIII	11.81 (3D) 4.86 (2D)	26.47 (3D) 19.22 (2D)	75	51921	3	11.60	$-1.08_{-0.26}^{+0.16}$ (n_5) $-1.89_{-0.15}^{+0.11}$ (n_{10})	$-1.85_{-0.26}^{+0.16}$ (n_5) $-1.89_{-0.15}^{+0.11}$ (n_{10})
NGC5658	14:32:28.51	+00:17:38.40	(-8.69;13.31;6.91)	VirgoIII	1.37 (3D) 1.35 (2D)	10.33 (3D) 9.74 (2D)	13	51957	1	11.26	$0.93_{-0.26}^{+0.16}$ (n_5) $0.24_{-0.15}^{+0.11}$ (n_{10})	$0.29_{-0.26}^{+0.16}$ (n_5) $0.24_{-0.15}^{+0.11}$ (n_{10})
NGC5668	14:33:24.34	+04:27:01.60	(-8.53;15.50;8.20)	VirgoIII	1.94 (3D) 1.02 (2D)	12.04 (3D) 10.66 (2D)	2	52018	4	11.43	$1.37_{-0.26}^{+0.16}$ (n_5) $0.71_{-0.15}^{+0.11}$ (n_{10})	$0.78_{-0.26}^{+0.16}$ (n_5) $0.71_{-0.15}^{+0.11}$ (n_{10})

NGC5692	14:38:18.11	+03:24:37.20	(-8.40;14.38;8.04)	VirgoIII	1.06 (3D) 0.62 (2D)	11.37 (3D) 10.45 (2D)	70	52317	2	11.43	$1.49_{-0.26}^{+0.16}$ (n_5) $0.71_{-0.15}^{+0.16}$ (n_{10})
NGC5701	14:39:11.08	+05:21:48.50	(-8.28;15.40;8.72)	VirgoIII	1.65 (3D) 0.78 (2D)	12.24 (3D) 10.94 (2D)	73	52365	7	12.45	$1.43_{-0.26}^{+0.16}$ (n_5) $0.64_{-0.15}^{+0.16}$ (n_{10})
NGC5725	14:40:58.32	+02:11:11.60	(-8.33;13.42;7.73)	VirgoIII	0.64 (3D) 0.63 (2D)	10.75 (3D) 10.15 (2D)	72	52665	10	13.02	$1.19_{-0.26}^{+0.16}$ (n_5) $0.43_{-0.15}^{+0.16}$ (n_{10})
IC1048	14:42:58.00	+04:53:22.10	(-9.35;16.84;9.93)	VirgoIII	1.70 (3D) 1.49 (2D)	14.34 (3D) 12.55 (2D)	76	52365	7	12.45	$0.99_{-0.26}^{+0.16}$ (n_5) $-0.26_{-0.15}^{+0.16}$ (n_{10})
NGC5740	14:44:24.45	+01:40:47.20	(-10.22;15.97;9.55)	VirgoIII	1.37 (3D) 1.29 (2D)	14.13 (3D) 12.76 (2D)	88	52665	10	13.02	$0.86_{-0.26}^{+0.16}$ (n_5) $0.36_{-0.15}^{+0.16}$ (n_{10})
NGC5746	14:44:55.92	+01:57:18.00	(-10.45;16.48;9.92)	VirgoIII	1.16 (3D) 1.14 (2D)	14.73 (3D) 13.18 (2D)	82	52665	10	13.02	$0.94_{-0.26}^{+0.16}$ (n_5) $0.18_{-0.15}^{+0.16}$ (n_{10})
UGC09556	14:49:46.09	+60:23:54.70	(20.25;29.72;18.82)	Virgo N	8.88 (3D) 3.01 (2D)	35.64 (3D) 29.61 (2D)	54	52952	1	11.12	$-1.33_{-0.26}^{+0.16}$ (n_5) $-2.19_{-0.15}^{+0.16}$ (n_{10})
NGC5777	14:51:17.85	+58:58:40.60	(16.14;25.05;16.00)	Virgo N	3.75 (3D) 1.08 (2D)	28.95 (3D) 24.66 (2D)	72	53043	2	12.20	$-0.01_{-0.26}^{+0.16}$ (n_5) $-1.08_{-0.15}^{+0.16}$ (n_{10})
IC1066	14:53:02.80	+03:17:46.00	(-10.88;17.70;11.65)	VirgoIII	0.72 (3D) 0.61 (2D)	16.75 (3D) 14.82 (2D)	28	53247	6	12.69	$1.33_{-0.26}^{+0.16}$ (n_5) $-0.20_{-0.15}^{+0.16}$ (n_{10})
IC1067	14:53:05.25	+03:19:54.40	(-8.33;13.57;8.93)	VirgoIII	0.10 (3D) 0.05 (2D)	11.73 (3D) 11.14 (2D)	21	53247	6	12.69	$1.80_{-0.26}^{+0.16}$ (n_5) $0.74_{-0.15}^{+0.16}$ (n_{10})
NGC5770	14:53:15.02	+03:57:35.00	(-6.87;11.50;7.58)	VirgoIII	1.53 (3D) 0.70 (2D)	9.36 (3D) 9.23 (2D)	12	53247	6	12.69	$0.71_{-0.26}^{+0.16}$ (n_5) $0.01_{-0.15}^{+0.16}$ (n_{10})
NGC5806	15:00:00.40	+01:53:28.70	(-8.80;13.20;9.36)	VirgoIII	0.70 (3D) 0.36 (2D)	12.21 (3D) 11.76 (2D)	63	53932	84	13.69	$1.64_{-0.26}^{+0.16}$ (n_5) $0.81_{-0.15}^{+0.16}$ (n_{10})
NGC5813	15:01:11.23	+01:42:07.10	(-10.52;15.59;11.19)	VirgoIII	0.41 (3D) 0.36 (2D)	15.34 (3D) 14.25 (2D)	60	53932	84	13.69	$1.35_{-0.26}^{+0.16}$ (n_5) $1.21_{-0.15}^{+0.16}$ (n_{10})
UGC09661	15:02:03.51	+01:50:28.60	(-6.97;10.36;7.50)	VirgoIII	2.56 (3D) 0.79 (2D)	9.22 (3D) 9.21 (2D)	40	53932	84	13.69	$0.69_{-0.26}^{+0.16}$ (n_5) $0.10_{-0.15}^{+0.16}$ (n_{10})
NGC5831	15:04:07.00	+01:13:11.70	(-9.81;14.11;10.45)	VirgoIII	0.70 (3D) 0.43 (2D)	13.88 (3D) 13.23 (2D)	3	53932	84	13.69	$1.39_{-0.26}^{+0.16}$ (n_5) $0.84_{-0.15}^{+0.16}$ (n_{10})
NGC5838	15:05:26.26	+02:05:57.60	(-9.45;14.04;10.53)	VirgoIII	0.65 (3D) 0.41 (2D)	13.73 (3D) 13.09 (2D)	86	53932	84	13.69	$1.80_{-0.26}^{+0.16}$ (n_5) $0.94_{-0.15}^{+0.16}$ (n_{10})
NGC5839	15:05:27.49	+01:38:05.30	(-8.43;12.29;9.23)	VirgoIII	1.40 (3D) 0.57 (2D)	11.69 (3D) 11.45 (2D)	3	53932	84	13.69	$1.57_{-0.26}^{+0.16}$ (n_5) $1.10_{-0.15}^{+0.16}$ (n_{10})
PGC2586382	15:05:35.73	+59:05:37.60	(14.23;21.41;14.81)	Virgo N	0.32 (3D) 0.27 (2D)	25.23 (3D) 22.45 (2D)	6	2586382	1	11.40	$0.65_{-0.26}^{+0.16}$ (n_5) $-0.45_{-0.15}^{+0.16}$ (n_{10})
NGC5845	15:06:00.81	+01:38:01.70	(-10.26;14.92;11.27)	VirgoIII	0.72 (3D) 0.57 (2D)	15.02 (3D) 14.15 (2D)	88	53932	84	13.69	$1.75_{-0.26}^{+0.16}$ (n_5) $1.29_{-0.15}^{+0.16}$ (n_{10})
NGC5846	15:06:29.28	+01:36:20.20	(-8.95;12.99;9.85)	VirgoIII	1.10 (3D) 0.54 (2D)	12.64 (3D) 12.25 (2D)	71	53932	84	13.69	$1.69_{-0.26}^{+0.16}$ (n_5) $1.19_{-0.15}^{+0.16}$ (n_{10})
NGC5854	15:07:47.70	+02:34:07.10	(-7.59;11.43;8.77)	VirgoIII	1.99 (3D) 0.85 (2D)	10.73 (3D) 10.62 (2D)	48	53932	84	13.69	$0.58_{-0.26}^{+0.16}$ (n_5) $0.03_{-0.15}^{+0.16}$ (n_{10})
PGC054037	15:08:05.85	+01:39:05.50	(-9.87;14.28;11.01)	VirgoIII	0.87 (3D) 0.59 (2D)	14.41 (3D) 13.73 (2D)	48	53932	84	13.69	$1.27_{-0.26}^{+0.16}$ (n_5) $1.02_{-0.15}^{+0.16}$ (n_{10})
NGC5864	15:09:33.55	+03:03:10.00	(-8.80;13.44;10.50)	VirgoIII	1.08 (3D) 0.77 (2D)	13.20 (3D) 12.72 (2D)	48	53932	84	13.69	$0.84_{-0.26}^{+0.16}$ (n_5) $0.91_{-0.15}^{+0.16}$ (n_{10})
NGC5869	15:09:49.44	+00:28:12.10	(-10.22;13.98;11.00)	VirgoIII	1.22 (3D) 0.79 (2D)	14.50 (3D) 13.91 (2D)	49	53932	84	13.69	$1.35_{-0.26}^{+0.16}$ (n_5) $0.71_{-0.15}^{+0.16}$ (n_{10})

NGC5894	15:11:40.98	+59:48:32.20	(14.37;20.74;14.80)	Virgo N	0.61 (3D) 0.36 (2D)	25.01 (3D) 22.54 (2D)	54	54234	1	12.42	$0.82_{-0.26}^{+0.16}$ (n_5) $-0.19_{-0.15}^{+0.11}$ (n_{10})	$0.40_{-0.26}^{+0.16}$ (n_5) $-0.19_{-0.15}^{+0.11}$ (n_{10})
PGC054346	15:13:29.18	+58:30:33.70	(13.69;20.75;14.99)	Virgo N	0.56 (3D) 0.31 (2D)	24.69 (3D) 22.18 (2D)	16	54346	1	11.47	$0.50_{-0.26}^{+0.16}$ (n_5) $-0.31_{-0.15}^{+0.11}$ (n_{10})	$-0.10_{-0.26}^{+0.16}$ (n_5) $-0.31_{-0.15}^{+0.11}$ (n_{10})
PGC054452	15:15:34.61	+02:14:53.80	(-10.01;14.48;12.03)	VirgoIII	1.54 (3D) 1.31 (2D)	15.36 (3D) 14.66 (2D)	52	54452	1	11.45	$0.93_{-0.26}^{+0.16}$ (n_5) $0.62_{-0.15}^{+0.11}$ (n_{10})	$0.81_{-0.26}^{+0.16}$ (n_5) $0.62_{-0.15}^{+0.11}$ (n_{10})
UGC09837	15:23:51.67	+58:03:10.60	(14.37;21.66;16.58)	Virgo N	0.76 (3D) 0.72 (2D)	26.53 (3D) 23.78 (2D)	43	54976	1	11.37	$0.29_{-0.26}^{+0.16}$ (n_5) $-0.61_{-0.15}^{+0.11}$ (n_{10})	$-0.60_{-0.26}^{+0.16}$ (n_5) $-0.61_{-0.15}^{+0.11}$ (n_{10})
NGC5951	15:33:43.06	+15:00:26.20	(-5.11;13.95;13.18)	VirgoIII Ext.	0.57 (3D) 0.42 (2D)	14.47 (3D) 13.89 (2D)	53	55480	5	12.31	$0.68_{-0.26}^{+0.16}$ (n_5) $-0.16_{-0.15}^{+0.11}$ (n_{10})	$0.38_{-0.26}^{+0.16}$ (n_5) $-0.16_{-0.15}^{+0.11}$ (n_{10})
NGC5953	15:34:32.38	+15:11:37.60	(-4.34;11.98;11.40)	VirgoIII Ext.	1.05 (3D) 1.02 (2D)	12.17 (3D) 11.99 (2D)	10	55480	5	12.31	$-0.35_{-0.26}^{+0.16}$ (n_5) $-1.20_{-0.15}^{+0.11}$ (n_{10})	$-1.19_{-0.26}^{+0.16}$ (n_5) $-1.20_{-0.15}^{+0.11}$ (n_{10})
NGC5954	15:34:35.02	+15:12:00.30	(-6.10;16.84;16.03)	VirgoIII Ext.	2.05 (3D) 0.95 (2D)	18.26 (3D) 16.89 (2D)	40	55480	5	12.31	$0.45_{-0.26}^{+0.16}$ (n_5) $-0.32_{-0.15}^{+0.11}$ (n_{10})	$-0.30_{-0.26}^{+0.16}$ (n_5) $-0.32_{-0.15}^{+0.11}$ (n_{10})
NGC5956	15:34:58.54	+11:45:01.00	(-6.70;14.72;14.24)	VirgoIII Ext.	1.39 (3D) 1.27 (2D)	16.05 (3D) 15.31 (2D)	28	55665	5	12.52	$0.78_{-0.26}^{+0.16}$ (n_5) $0.16_{-0.15}^{+0.11}$ (n_{10})	$0.26_{-0.26}^{+0.16}$ (n_5) $0.16_{-0.15}^{+0.11}$ (n_{10})
NGC5957	15:35:23.21	+12:02:51.40	(-6.39;14.27;13.84)	VirgoIII Ext.	1.00 (3D) 0.92 (2D)	15.47 (3D) 14.84 (2D)	35	55665	5	12.52	$1.07_{-0.26}^{+0.16}$ (n_5) $0.26_{-0.15}^{+0.11}$ (n_{10})	$0.57_{-0.26}^{+0.16}$ (n_5) $0.26_{-0.15}^{+0.11}$ (n_{10})
NGC5981	15:37:53.45	+59:23:30.30	(18.43;25.40;20.82)	Virgo N	4.32 (3D) 1.13 (2D)	33.46 (3D) 29.65 (2D)	56	55674	11	13.39	$-0.65_{-0.26}^{+0.16}$ (n_5) $-1.31_{-0.15}^{+0.11}$ (n_{10})	$-1.27_{-0.26}^{+0.16}$ (n_5) $-1.31_{-0.15}^{+0.11}$ (n_{10})
NGC5970	15:38:29.97	+12:11:11.80	(-6.27;14.01;13.96)	VirgoIII Ext.	0.80 (3D) 0.79 (2D)	15.48 (3D) 14.92 (2D)	30	55665	5	12.52	$1.19_{-0.26}^{+0.16}$ (n_5) $0.19_{-0.15}^{+0.11}$ (n_{10})	$0.27_{-0.26}^{+0.16}$ (n_5) $0.19_{-0.15}^{+0.11}$ (n_{10})
NGC5982	15:38:39.83	+59:21:21.00	(13.07;18.00;14.81)	Virgo N	3.34 (3D) 0.92 (2D)	23.08 (3D) 21.61 (2D)	43	55674	11	13.39	$-0.24_{-0.26}^{+0.16}$ (n_5) $-1.18_{-0.15}^{+0.11}$ (n_{10})	$-1.16_{-0.26}^{+0.16}$ (n_5) $-1.18_{-0.15}^{+0.11}$ (n_{10})
NGC5985	15:39:37.09	+59:19:55.00	(14.29;19.65;16.26)	Virgo N	1.80 (3D) 0.61 (2D)	25.44 (3D) 23.50 (2D)	55	55674	11	13.39	$0.05_{-0.26}^{+0.16}$ (n_5) $-0.49_{-0.15}^{+0.11}$ (n_{10})	$-0.40_{-0.26}^{+0.16}$ (n_5) $-0.49_{-0.15}^{+0.11}$ (n_{10})
NGC5989	15:41:32.80	+59:45:18.80	(16.03;21.57;17.98)	Virgo N	0.23 (3D) 0.22 (2D)	28.45 (3D) 25.95 (2D)	49	55674	11	13.39	$0.76_{-0.26}^{+0.16}$ (n_5) $-0.07_{-0.15}^{+0.11}$ (n_{10})	$0.05_{-0.26}^{+0.16}$ (n_5) $-0.07_{-0.15}^{+0.11}$ (n_{10})
UGC09991	15:43:23.97	+14:26:08.90	(-7.73;19.78;20.38)	VirgoIII Ext.	4.61 (3D) 2.95 (2D)	23.67 (3D) 21.51 (2D)	8	55867	1	11.36	$-0.08_{-0.26}^{+0.16}$ (n_5) $-0.95_{-0.15}^{+0.11}$ (n_{10})	$-0.62_{-0.26}^{+0.16}$ (n_5) $-0.95_{-0.15}^{+0.11}$ (n_{10})
NGC6012	15:54:13.94	+14:36:04.50	(-3.64;9.17;10.38)	VirgoIII Ext.	2.53 (3D) 1.72 (2D)	10.91 (3D) 10.88 (2D)	67	56334	2	11.89	$0.26_{-0.26}^{+0.16}$ (n_5) $-0.59_{-0.15}^{+0.11}$ (n_{10})	$-0.30_{-0.26}^{+0.16}$ (n_5) $-0.59_{-0.15}^{+0.11}$ (n_{10})
UGC10086	15:54:41.25	+16:37:01.90	(-5.90;17.41;19.57)	VirgoIII Ext.	1.69 (3D) 0.95 (2D)	21.65 (3D) 20.31 (2D)	64	56352	1	11.34	$-0.23_{-0.26}^{+0.16}$ (n_5) $-0.78_{-0.15}^{+0.11}$ (n_{10})	$-0.67_{-0.26}^{+0.16}$ (n_5) $-0.78_{-0.15}^{+0.11}$ (n_{10})
IC1151	15:58:32.34	+17:26:29.30	(-5.17;16.27;18.80)	VirgoIII Ext.	0.51 (3D) 0.07 (2D)	20.46 (3D) 19.44 (2D)	29	56537	1	11.62	$0.19_{-0.26}^{+0.16}$ (n_5) $-0.50_{-0.15}^{+0.11}$ (n_{10})	$-0.39_{-0.26}^{+0.16}$ (n_5) $-0.50_{-0.15}^{+0.11}$ (n_{10})
IC1210	16:14:30.15	+62:32:12.10	(19.86;21.93;21.05)	Virgo N	1.94 (3D) 1.53 (2D)	33.09 (3D) 30.82 (2D)	81	57589	1	11.80	$-0.33_{-0.26}^{+0.16}$ (n_5) $-1.32_{-0.15}^{+0.11}$ (n_{10})	$-1.19_{-0.26}^{+0.16}$ (n_5) $-1.32_{-0.15}^{+0.11}$ (n_{10})
PGC057611	16:15:02.83	+61:46:55.40	(17.69;20.00;19.37)	Virgo N	1.36 (3D) 0.44 (2D)	29.86 (3D) 28.10 (2D)	38	57611	1	11.61	$-0.03_{-0.26}^{+0.16}$ (n_5) $-0.83_{-0.15}^{+0.11}$ (n_{10})	$-0.73_{-0.26}^{+0.16}$ (n_5) $-0.83_{-0.15}^{+0.11}$ (n_{10})
UGC10297	16:15:28.82	+18:54:17.50	(-4.65;16.56;21.91)	VirgoIII Ext.	0.14 (3D) 0.11 (2D)	23.42 (3D) 22.45 (2D)	62	57627	1	11.37	$0.59_{-0.26}^{+0.16}$ (n_5) $-0.57_{-0.15}^{+0.11}$ (n_{10})	$-0.58_{-0.26}^{+0.16}$ (n_5) $-0.57_{-0.15}^{+0.11}$ (n_{10})
UGC10413	16:29:27.13	+21:20:11.70	(-3.88;19.03;27.86)	VirgoIII Ext.	2.22 (3D) 0.91 (2D)	29.75 (3D) 28.32 (2D)	74	58336	1	11.34	$-0.85_{-0.26}^{+0.16}$ (n_5) $-1.49_{-0.15}^{+0.11}$ (n_{10})	$-1.52_{-0.26}^{+0.16}$ (n_5) $-1.49_{-0.15}^{+0.11}$ (n_{10})
NGC6181	16:32:20.96	+19:49:35.60	(-3.33;13.19;20.05)	VirgoIII Ext.	3.27 (3D) 1.76 (2D)	20.76 (3D) 20.50 (2D)	64	58470	4	12.62	$-0.24_{-0.26}^{+0.16}$ (n_5) $-0.80_{-0.15}^{+0.11}$ (n_{10})	$-0.65_{-0.26}^{+0.16}$ (n_5) $-0.80_{-0.15}^{+0.11}$ (n_{10})
NGC6186	16:34:25.48	+21:32:27.20	(-3.39;17.39;26.52)	VirgoIII Ext.	0.43 (3D) 0.07 (2D)	27.98 (3D) 26.96 (2D)	6	58523	2	12.31	$0.24_{-0.26}^{+0.16}$ (n_5) $-1.04_{-0.15}^{+0.11}$ (n_{10})	$-0.93_{-0.26}^{+0.16}$ (n_5) $-1.04_{-0.15}^{+0.11}$ (n_{10})

NGC6267	16:58:08.66	+22:59:06.40	(-2.29;18.56;34.52)	VirgoIII Ext.	2.62 (3D) 1.90 (2D)	35.99 (3D) 34.93 (2D)	35	59426	10	12.73	-1.61 ^{+0.16} _{-0.26} (n ₅) -2.35 ^{+0.11} _{-0.15} (n ₁₀)	-2.41 ^{+0.16} _{-0.26} (n ₅) -2.35 ^{+0.11} _{-0.15} (n ₁₀)
NGC6276	17:00:45.09	+23:02:38.40	(-1.64;14.00;26.65)	VirgoIII Ext.	3.38 (3D) 1.59 (2D)	27.38 (3D) 27.07 (2D)	71	59426	10	12.73	0.16 ^{+0.16} _{-0.26} (n ₅) -0.25 ^{+0.11} _{-0.15} (n ₁₀)	-0.19 ^{+0.16} _{-0.26} (n ₅) -0.25 ^{+0.11} _{-0.15} (n ₁₀)
NGC6278	17:00:50.33	+23:00:39.70	(-1.51;12.71;24.23)	VirgoIII Ext.	4.78 (3D) 2.43 (2D)	24.82 (3D) 24.66 (2D)	64	59426	10	12.73	-0.22 ^{+0.16} _{-0.26} (n ₅) -1.06 ^{+0.11} _{-0.15} (n ₁₀)	-1.08 ^{+0.16} _{-0.26} (n ₅) -1.06 ^{+0.11} _{-0.15} (n ₁₀)
NGC6306	17:07:36.98	+60:43:44.00	(18.22;17.27;21.83)	Virgo N	0.69 (3D) 0.69 (2D)	31.13 (3D) 30.24 (2D)	57	59655	3	12.50	0.17 ^{+0.16} _{-0.26} (n ₅) -0.35 ^{+0.11} _{-0.15} (n ₁₀)	-0.19 ^{+0.16} _{-0.26} (n ₅) -0.35 ^{+0.11} _{-0.15} (n ₁₀)
UGC10721	17:08:25.55	+25:31:02.60	(-0.16;15.70;31.18)	VirgoIII Ext.	1.90 (3D) 1.50 (2D)	32.19 (3D) 31.67 (2D)	42	59676	1	11.86	-0.70 ^{+0.16} _{-0.26} (n ₅) -1.51 ^{+0.11} _{-0.15} (n ₁₀)	-1.42 ^{+0.16} _{-0.26} (n ₅) -1.51 ^{+0.11} _{-0.15} (n ₁₀)
UGC10968	17:44:10.45	+57:59:16.40	(17.20;14.33;22.94)	Virgo N	2.64 (3D) 1.14 (2D)	30.73 (3D) 30.41 (2D)	44	60769	1	11.15	-0.56 ^{+0.16} _{-0.26} (n ₅) -1.43 ^{+0.16} _{-0.26} (n ₁₀)	-1.47 ^{+0.16} _{-0.26} (n ₅) -1.43 ^{+0.11} _{-0.15} (n ₁₀)

Table B.1: Environmental properties for the filament galaxies in the sample. Column description. (1) Galaxy name; (2-4) RA, Dec. and Super Galactic coordinates of the galaxy; (5) filament name; (6-7) distance of the galaxy to the filament spine and to the Virgo cluster, estimated both in 3D in 2D; (8) orientation between the major axis of the galaxy and the direction of the filament spine; (9-11) group PGC ID, richness, and mass, from Kourkchi & Tully (2017), where values equal to — denote galaxies not included in their group catalog; (12-13) 2D and 3D local densities.

Galaxy (1)	R.A. (hh:mm:ss.s) (2)	Dec. (dd:mm:ss.s) (3)	V_H (km/s) (4)	V_{cosmic} (km/s) (5)	$\log(D_{25}/0.1')$ (6)	i (degree) (7)	PA (degree) (8)	$\log(M_{\star}/M_{\odot})$ (9)	$\log(\frac{\text{SFR}}{M_{\odot}/\text{yr}})$ (10)	$\log(\frac{\text{SFR}}{\text{SFR}_{\text{MS}}})$ (11)	Morphology (12)
PGC022100	07:53:45.27	+21:02:57.90	2106	2240	0.92 ± 0.05	52.8	33	9.27 ± 0.10	-1.02 ± 0.20	-0.35	SABb (2.9)
IC2256	08:16:54.45	+24:10:35.76	2208	2615 ^a	0.90 ± 0.06	61.4	8	9.27 ± 0.10	-1.09 ± 0.20	-0.42	SABC (6.3)
NGC2577	08:22:43.45	+22:33:11.10	2062	2636 ^a	1.19 ± 0.04	76.3	105	10.30 ± 0.10	-1.20 ± 0.20	-1.23	E-S0 (-2.9)
UGC04375	08:23:11.28	+22:39:52.92	2061	2985 ^a	1.23 ± 0.04	51.7	179	10.01 ± 0.10	-0.43 ± 0.20	-0.27	SABc (5.3)
IC2361	08:25:44.49	+27:52:28.20	2062	2244	1.19 ± 0.04	81.6	78	9.42 ± 0.10	-0.69 ± 0.20	-0.13	SBab (2.0)
UGC04395	08:25:47.59	+28:07:04.80	2192	2824 ^a	1.00 ± 0.05	79.9	153	9.22 ± 0.10	-1.29 ± 0.20	-0.59	SBC (5.8)
NGC2592	08:27:08.05	+25:58:13.10	1979	2410 ^a	1.17 ± 0.04	51.3	47	10.20 ± 0.10	$-2.19^{+0.21}_{-0.44} e$	-2.15	E (-4.8)
NGC2594	08:27:17.16	+25:52:43.70	2362	2526	0.96 ± 0.21	65.3	20	9.99 ± 0.10	-2.07 ± 0.24	-1.89	S0 (-2.5)
PGC023706	08:27:18.07	+46:02:03.10	2154	2412	0.69 ± 0.13	52.0	28	$8.48 \pm 0.30 c$	$-0.95^{+0.10}_{-0.06} d$	0.25	I (10.0)
NGC2604	08:33:23.13	+29:32:19.68	2078	2271	1.17 ± 0.05	22.4	46 ^b	9.80 ± 0.10	0.03 ± 0.20	0.34	SBC (6.0)
PGC024012	08:33:42.55	+27:42:43.92	2250	2429	0.93 ± 0.06	57.5	36	9.00 ± 0.17	-0.86 ± 0.20	-0.01	Sbc (3.9)
NGC2608	08:35:17.04	+28:28:30.72	2135	1722 ^a	1.29 ± 0.03	64.3	64	10.34 ± 0.10	0.13 ± 0.20	0.07	Sb (3.4)
UGC04551	08:44:05.92	+49:47:37.90	1728	2019	1.23 ± 0.07	90.0	112	10.19 ± 0.10	-1.80 ± 0.22	-1.76	S0 (-1.9)
UGC04559	08:44:07.68	+30:07:08.76	2085	3040 ^a	1.57 ± 0.03	90.0	51	10.22 ± 0.12	-0.77 ± 0.20	-0.75	SBab (2.1)
PGC1925809	08:51:32.06	+30:58:03.72	2046	2256	0.73 ± 0.07	61.6	136	$8.68 \pm 0.30 c$	$-2.85^{+0.36}_{-2.15} d$	-1.78	S0-a (0.0)
NGC2679	08:51:32.94	+30:51:55.30	2017	2133 ^a	1.27 ± 0.07	0.0	169 ^b	10.21 ± 0.10	-1.65 ± 0.22	-1.62	S0 (-1.9)
UGC04659	08:54:40.53	+47:06:17.60	1756	2710 ^a	1.15 ± 0.04	90.0	109	9.14 ± 0.13	-1.13 ± 0.20	-0.38	Sd (7.8)
PGC025063	08:55:33.19	+31:12:41.76	2039	2252	0.75 ± 0.23	48.0	67	9.07 ± 0.10	-0.62 ± 0.20	0.18	Sa (1.1)
NGC2712	08:59:30.47	+44:54:50.00	1815	2296 ^a	1.47 ± 0.03	60.3	1	10.26 ± 0.10	0.07 ± 0.20	0.06	SBB (3.1)
PGC025273	09:00:13.32	+31:59:54.24	1892	2117	0.89 ± 0.06	77.0	165	8.81 ± 0.15	-0.96 ± 0.20	0.02	S0-a (-0.3)
UGC04722	09:00:23.54	+25:36:40.60	1794	1766 ^a	1.16 ± 0.03	90.0	31	8.42 ± 0.21	-0.95 ± 0.20	0.29	Sd (8.0)
NGC2780	09:12:44.40	+34:55:31.80	1979	3888 ^a	1.02 ± 0.05	45.9	147	9.53 ± 0.10	-0.87 ± 0.20	-0.38	Sb (2.7)
NGC2793	09:16:47.28	+34:25:47.64	1687	1972 ^a	1.05 ± 0.05	37.4	81 ^b	$9.43 \pm 0.30 c$	$-0.67^{+0.10}_{-0.13} f$	-0.11	Sm (8.7)
UGC04902	09:17:05.28	+25:25:45.00	1644	1860	1.13 ± 0.04	69.3	156	9.30 ± 0.10	-0.55 ± 0.20	0.10	S0-a (-1.0)
NGC2798	09:17:22.79	+41:59:59.00	1726	1734 ^a	1.39 ± 0.05	84.9	160	9.92 ± 0.10	0.69 ± 0.20	0.91	Sa (1.1)
NGC2799	09:17:31.03	+41:59:38.70	1673	2055 ^a	1.25 ± 0.05	90.0	122	9.25 ± 0.11	-0.65 ± 0.27	0.03	SBD (8.5)
NGC2844	09:21:48.01	+40:09:04.50	1486	3118 ^a	1.25 ± 0.06	70.4	11	9.93 ± 0.10	-0.73 ± 0.20	-0.51	Sa (0.7)
NGC2852	09:23:14.59	+40:09:49.70	1781	2192 ^a	0.97 ± 0.09	19.7	147 ^b	9.79 ± 0.10	-2.75 ± 0.42	-2.44	SABA (0.8)
NGC2853	09:23:17.33	+40:12:00.20	1765	2113 ^a	1.22 ± 0.06	63.0	25	9.34 ± 0.10	-1.27 ± 0.20	-0.65	S0-a (-0.7)
NGC2859	09:24:18.53	+34:30:48.60	1690	1810 ^a	1.50 ± 0.04	32.9	85	10.89 ± 0.11	-0.76 ± 0.21	-1.20	S0-a (-1.2)
UGC05015	09:25:48.00	+34:16:37.50	1650	1909	1.21 ± 0.06	20.5	30 ^b	9.11 ± 0.10	-1.29 ± 0.20	-0.51	SABd (7.6)
UGC05020	09:26:01.48	+34:39:12.24	1625	2394 ^a	1.31 ± 0.03	79.4	77	9.21 ± 0.10	-1.08 ± 0.20	-0.37	SABC (5.9)
NGC2893	09:30:16.96	+29:32:24.00	1699	2009 ^a	1.01 ± 0.04	39.1	83	9.37 ± 0.10	-0.03 ± 0.20	0.57	S0-a (0.4)
PGC027311	09:36:07.52	+29:06:42.90	1652	1898	0.87 ± 0.06	70.2	8	8.84 ± 0.10	-1.50 ± 0.20	-0.54	Sc (5.6)
NGC2964	09:42:54.23	+31:50:50.60	1328	1513 ^a	1.47 ± 0.03	42.9	97	10.30 ± 0.10	0.33 ± 0.20	0.30	Sbc (4.0)
NGC2968	09:43:12.01	+31:55:43.30	1566	1017 ^a	1.39 ± 0.03	53.3	54	10.36 ± 0.10	-1.28 ± 0.32	-1.35	Sa (0.6)
NGC2970	09:43:31.05	+31:58:37.20	1618	1999 ^a	0.93 ± 0.06	39.0	67	9.28 ± 0.10	-2.50 ± 0.26	-1.84	E (-4.5)

PGC028169	09:48:04.69	+32:52:57.00	1524	1832 ^a	0.83 ± 0.06	44.5	163	8.43 ± 0.12	-1.32 ± 0.20	-0.08	I (10.0)
NGC3003	09:48:35.46	+33:25:17.30	1478	1538 ^a	1.68 ± 0.02	87.0	79	9.71 ± 0.10	-0.04 ± 0.20	0.33	Sbc (4.4)
NGC3026	09:50:55.39	+28:33:03.96	1490	1819 ^a	1.35 ± 0.03	90.0	82	9.34 ± 0.10	-0.80 ± 0.20	-0.18	SBm (9.5)
NGC3021	09:50:57.15	+33:33:13.10	1541	1959 ^a	1.13 ± 0.07	55.7	110	9.88 ± 0.10	-0.23 ± 0.20	0.02	Sbc (4.0)
UGC05287	09:51:28.09	+32:56:35.00	1470	2363 ^a	0.98 ± 0.06	41.2	15	9.38 ± 0.10	-1.81 ± 0.22	-1.22	Sc (6.0)
NGC3032	09:52:08.15	+29:14:10.40	1562	1610 ^a	1.15 ± 0.04	26.4	90 ^b	9.91 ± 0.14	-0.54 ± 0.20	-0.31	S0 (-1.9)
UGC05326	09:55:24.50	+33:15:46.00	1417	1699	0.97 ± 0.05	16.9	111 ^b	8.95 ± 0.10	-1.71 ± 0.20	-0.83	IB (9.7)
NGC3067	09:58:21.08	+32:22:11.60	1476	1449 ^a	1.31 ± 0.02	81.5	104	9.93 ± 0.10	0.07 ± 0.20	0.29	SABa (2.1)
NGC3098	10:02:16.69	+24:42:39.90	1397	1678 ^a	1.37 ± 0.06	90.0	90	10.24 ± 0.10	-1.57 ± 0.21	-1.56	S0 (-1.5)
PGC029347	10:06:18.11	+28:56:40.40	1363	1774 ^a	0.82 ± 0.06	24.2	111 ^b	8.83 ± 0.10	-0.92 ± 0.20	0.05	S0 (-2.4)
NGC3118	10:07:11.54	+33:01:38.60	1342	1986 ^a	1.32 ± 0.03	90.0	39	8.90 ± 0.10	-0.85 ± 0.20	0.07	Sbc (4.2)
IC0598	10:12:48.57	+43:08:43.90	2256	2542	1.22 ± 0.06	90.0	7	10.07 ± 0.10	-1.31 ± 0.21	-1.19	S0-a (-0.1)
NGC3193	10:18:24.90	+21:53:38.30	1381	2133 ^a	1.37 ± 0.03	32.8	176 ^b	10.95 ± 0.10	-0.69 ± 0.21	-1.17	E (-4.8)
UGC05577	10:20:03.64	+38:36:56.00	2007	2297	0.97 ± 0.04	50.1	100	9.32 ± 0.11	-0.58 ± 0.20	0.05	SBc (5.0)
UGC05588	10:20:57.13	+25:21:53.40	1291	1815 ^a	0.74 ± 0.14	47.9	40	9.33 ± 0.27	-0.57 ± 0.20	0.06	Sc (6.0)
NGC3245A	10:27:01.13	+28:38:21.60	1322	1766 ^a	1.37 ± 0.04	90.0	148	9.19 ± 0.10	-1.31 ± 0.20	-0.59	SBb (3.3)
NGC3245	10:27:18.39	+28:30:26.80	1326	1583 ^a	1.56 ± 0.03	61.9	176	10.55 ± 0.10	-0.51 ± 0.20	-0.71	S0 (-2.1)
NGC3248	10:27:45.44	+22:50:49.90	1481	1766	1.23 ± 0.04	70.6	135	10.01 ± 0.10	-1.83 ± 0.21	-1.67	S0 (-2.0)
NGC3254	10:29:19.94	+29:29:30.60	1355	2541 ^a	1.37 ± 0.03	64.4	50	10.09 ± 0.10	-0.42 ± 0.20	-0.31	Sbc (4.0)
NGC3265	10:31:06.77	+28:47:48.00	1319	1619	0.98 ± 0.09	65.4	73	9.18 ± 0.10	-0.30 ± 0.20	0.43	E (-4.7)
NGC3277	10:32:55.45	+28:30:42.20	1408	1875 ^a	1.32 ± 0.03	43.6	29	10.22 ± 0.10	-0.83 ± 0.20	-0.81	Sab (1.8)
PGC031357	10:35:22.72	+37:40:18.00	1697	2015	0.88 ± 0.06	68.6	46	8.62 ± 0.10	-1.06 ± 0.20	0.05	I (10.0)
PGC031387	10:35:42.04	+26:07:33.00	1392	1698	0.76 ± 0.08	42.1	11	8.74 ± 0.30 ^c	-1.20 ^{+0.07} _{-0.06} ^d	-0.17	IB (10.0)
NGC3294	10:36:16.25	+37:19:28.90	1586	2106 ^a	1.49 ± 0.04	60.7	119	10.38 ± 0.10	0.21 ± 0.20	0.12	SABC (5.1)
UGC05870	10:45:59.38	+34:57:53.60	2032	2327	1.04 ± 0.08	25.6	135 ^b	9.76 ± 0.10	-0.83 ± 0.20	-0.50	S0 (-1.5)
NGC3381	10:48:24.82	+34:42:41.10	1629	1958	1.30 ± 0.05	26.3	76	9.65 ± 0.10	-0.23 ± 0.20	0.18	SBbc (3.6)
NGC3424	10:51:46.33	+32:54:02.70	1494	2075 ^a	1.40 ± 0.06	79.2	111	10.11 ± 0.10	0.22 ± 0.20	0.32	SBb (3.1)
NGC3430	10:52:11.40	+32:57:01.60	1586	2137 ^a	1.60 ± 0.04	58.0	32	10.20 ± 0.13	0.13 ± 0.20	0.16	Sc (5.1)
UGC05990	10:52:38.34	+34:28:59.30	1569	2348 ^a	1.11 ± 0.04	90.0	15	9.22 ± 0.10	-1.22 ± 0.20	-0.52	SBab (2.1)
NGC3442	10:53:08.11	+33:54:37.30	1733	2289 ^a	0.74 ± 0.05	52.4	18	9.22 ± 0.10	-0.32 ± 0.20	0.38	Sab (1.6)
UGC06070	10:59:46.28	+33:23:30.60	1853	2170	0.74 ± 0.14	37.6	29 ^b	9.04 ± 0.10	-0.34 ± 0.20	0.48	Scd (7.2)
NGC3504	11:03:11.21	+27:58:21.00	1525	1469 ^a	1.39 ± 0.03	26.4	150 ^b	10.29 ± 0.10	0.87 ± 0.20	0.84	Sab (2.1)
NGC3595	11:15:25.55	+47:26:49.30	2177	2503	1.18 ± 0.08	90.0	176	10.37 ± 0.14	-1.41 ± 0.42	-1.49	S0 (-1.9)
NGC3629	11:20:31.81	+26:57:48.10	1508	2506 ^a	1.25 ± 0.03	51.2	35	9.80 ± 0.10	0.01 ± 0.20	0.32	SABC (5.9)
NGC3648	11:22:31.49	+39:52:37.00	1970	2301	1.08 ± 0.04	64.5	73	10.23 ± 0.10	-3.75 ± 1.17	-3.74	S0 (-2.1)
NGC3658	11:23:58.49	+38:33:46.90	2039	2363	1.24 ± 0.07	25.4	40 ^b	10.42 ± 0.10	-1.06 ± 0.20	-1.18	S0 (-2.1)
NGC3665	11:24:43.40	+38:45:43.90	2069	1704 ^a	1.61 ± 0.04	50.3	29	10.47 ± 0.10	-0.92 ± 0.20	-1.07	S0 (-2.1)
UGC06455	11:27:21.91	+40:00:47.00	2025	2354	1.19 ± 0.04	70.1	82	9.29 ± 0.11	-1.94 ± 0.22	-1.29	SBb (3.0)

NGC3687	11:28:00.60	+29:30:39.80	2507	1944 ^a	1.15 ± 0.03	74.4	173	10.18 ± 0.10	-0.28 ± 0.20	-0.23	Sbc (3.8)
NGC3689	11:28:10.99	+25:39:40.00	2739	3082 ^a	1.17 ± 0.06	50.2	94	10.52 ± 0.10	0.29 ± 0.20	0.11	SABc (5.3)
NGC3694	11:28:54.12	+35:24:50.40	2243	2660 ^a	1.00 ± 0.10	51.0	116	9.97 ± 0.10	-0.72 ± 0.20	-0.53	E (-4.0)
PGC035472	11:30:33.37	+38:14:26.60	1924	2261	0.91 ± 0.06	90.0	177	9.10 ± 0.10	-2.05 ± 0.23	-1.27	E (-5.0)
PGC035503	11:31:07.42	+35:35:23.10	1880	2220	0.98 ± 0.05	68.8	31	8.81 ± 0.15	-1.56 ± 0.20	-0.58	Sc (5.0)
PGC035508	11:31:09.55	+36:36:02.50	1968	2299	0.64 ± 0.31	39.2	172	9.15 ± 0.10	-1.28 ± 0.20	-0.53	Sbc (4.0)
UGC06517	11:32:02.39	+36:41:52.70	2491	2781	1.20 ± 0.07	56.9	38	9.78 ± 0.10	-0.26 ± 0.20	0.06	Sbc (3.9)
UGC06526	11:32:39.50	+35:19:42.10	1840	1342 ^a	1.21 ± 0.06	83.4	87	8.89 ± 0.10	-1.14 ± 0.20	-0.22	Sc (6.3)
PGC035688	11:33:30.15	+33:30:27.80	2574	2850	0.99 ± 0.18	77.3	176	9.38 ± 0.10	-0.68 ± 0.20	-0.09	SBc (5.5)
UGC06545	11:33:44.00	+32:38:00.90	2619	2890	1.02 ± 0.08	75.2	134	9.86 ± 0.10	-0.06 ± 0.20	0.21	SBB (3.1)
UGC06610	11:38:44.09	+33:48:20.90	1851	2483 ^a	1.29 ± 0.03	80.5	13	9.34 ± 0.15	-1.03 ± 0.20	-0.41	SBc (5.9)
NGC3786	11:39:42.50	+31:54:32.90	2678	3319 ^a	1.29 ± 0.03	65.1	72	10.35 ± 0.10	0.18 ± 0.20	0.11	SABA (1.1)
NGC3788	11:39:44.65	+31:55:52.30	2699	3926 ^a	1.30 ± 0.03	86.0	179	10.41 ± 0.10	-0.03 ± 0.20	-0.14	Sab (2.3)
UGC06637	11:40:24.87	+28:22:26.30	1836	3303 ^a	0.88 ± 0.05	90.0	68	9.50 ± 0.10	-0.60 ± 0.20	-0.09	E (-4.1)
NGC3796	11:40:31.00	+60:17:56.00	1250	1633	1.16 ± 0.08	71.2	126	9.76 ± 0.10	-1.70 ± 0.20	-1.37	E-SO (-3.0)
NGC3838	11:44:13.00	+57:56:53.00	1308	1692	1.15 ± 0.08	80.2	141	9.99 ± 0.10	-1.90 ± 0.21	-1.72	S0-a (-0.3)
NGC3900	11:49:09.46	+27:01:19.30	1798	2202 ^a	1.41 ± 0.03	70.5	2	10.31 ± 0.10	-0.61 ± 0.20	-0.65	S0-a (-0.2)
NGC3898	11:49:15.00	+56:05:03.00	1176	1648 ^a	1.54 ± 0.02	56.3	107	10.67 ± 0.10	-0.53 ± 0.20	-0.82	Sab (1.7)
UGC06791	11:49:23.61	+26:44:29.70	1852	2437 ^a	1.32 ± 0.05	87.5	0	9.25 ± 0.10	-1.36 ± 0.20	-0.68	Sc (6.4)
NGC3912	11:50:04.46	+26:28:45.30	1779	1734 ^a	1.18 ± 0.04	68.1	4	9.65 ± 0.10	-0.31 ± 0.20	0.10	Sb (3.0)
NGC3953	11:53:48.00	+52:19:36.00	1052	1315 ^a	1.79 ± 0.02	62.3	14	10.57 ± 0.10	0.22 ± 0.20	0.00	Sbc (4.0)
NGC3982	11:56:28.00	+55:07:30.00	1109	1524 ^a	1.27 ± 0.04	29.3	24	9.90 ± 0.10	0.14 ± 0.20	0.38	SABB (3.2)
NGC3992	11:57:35.00	+53:22:28.00	1048	1479 ^a	1.85 ± 0.03	47.4	75	10.70 ± 0.10	-0.07 ± 0.20	-0.38	Sbc (4.0)
NGC3998	11:57:56.00	+55:27:12.00	1048	1561 ^a	1.44 ± 0.03	42.5	138	10.40 ± 0.10	-0.83 ± 0.20	-0.93	S0 (-2.2)
NGC4026	11:59:25.00	+50:57:42.00	985	1168 ^a	1.64 ± 0.03	90.0	178	10.26 ± 0.10	-2.54 ± 0.28	-2.55	S0 (-1.8)
NGC4051	12:03:09.00	+44:31:52.00	700	1033 ^a	1.77 ± 0.02	48.7	139	10.34 ± 0.10	0.43 ± 0.20	0.37	SABB (4.0)
NGC4088	12:05:34.00	+50:32:20.00	757	1074 ^a	1.74 ± 0.02	71.3	47	10.36 ± 0.10	0.51 ± 0.20	0.44	SABC (4.7)
NGC4096	12:06:01.00	+47:28:42.00	566	906 ^a	1.75 ± 0.02	80.5	20	9.79 ± 0.11	-0.52 ± 0.20	-0.21	SABc (5.3)
NGC4100	12:06:08.00	+49:34:57.00	1074	1503 ^a	1.66 ± 0.02	79.5	167	10.25 ± 0.10	0.02 ± 0.20	0.02	Sbc (4.1)
NGC4111	12:07:03.00	+43:03:56.00	792	1018 ^a	1.25 ± 0.03	90.0	151	10.34 ± 0.10	-1.16 ± 0.20	-1.22	S0-a (-1.3)
NGC4138	12:09:29.00	+43:41:07.00	888	1211 ^a	1.46 ± 0.03	61.4	150	10.07 ± 0.10	-0.78 ± 0.20	-0.66	S0-a (-0.8)
NGC4143	12:09:36.00	+42:32:03.00	946	1300 ^a	1.42 ± 0.03	68.3	144	10.29 ± 0.10	-1.29 ± 0.20	-1.32	S0 (-2.0)
NGC4144	12:09:58.00	+46:27:25.00	265	507 ^a	1.72 ± 0.03	85.5	103	9.17 ± 0.30 ^c	-3.45 ^{+1.38} _{-1.55} ^d	-2.72	SABC (6.1)
NGC4151	12:10:32.00	+39:24:20.00	995	834 ^a	1.46 ± 0.04	42.0	50	10.03 ± 0.10	0.30 ± 0.20	0.45	Sab (1.9)
NGC4152	12:10:37.50	+16:01:58.50	2169	2191 ^a	1.14 ± 0.03	50.7	136	9.98 ± 0.10	0.44 ± 0.20	0.62	SABC (4.9)
UGC07271	12:15:33.00	+43:26:02.00	547	932 ^a	1.07 ± 0.04	90.0	160	8.00 ± 0.10	-2.06 ± 0.20	-0.53	Scd (7.1)
NGC4214	12:15:39.00	+36:19:36.00	291	212 ^a	1.83 ± 0.03	43.7	137 ^b	9.06 ± 0.30 ^c	-0.73 ± 0.03 ^e	0.08	I (9.8)
NGC4244	12:17:29.00	+37:48:25.00	244	315 ^a	2.21 ± 0.03	65.4	45	9.43 ± 0.30 ^c	-0.96 ± 0.05 ^e	-0.40	Sc (6.0)
NGC4314	12:22:31.00	+29:53:45.00	963	726 ^a	1.57 ± 0.03	16.2	146 ^b	10.52 ± 0.10	-0.48 ± 0.20	-0.66	Sa (1.0)

NGC4359	12:24:11.00	+31:31:18.00	1253	1362 ^a	1.14 ± 0.04	54.5	108	9.23 ± 0.10	-1.10 ± 0.20	-0.41	SBC (5.1)
NGC4414	12:26:27.00	+31:13:24.00	716	1303 ^a	1.29 ± 0.04	56.6	162	10.65 ± 0.10	0.46 ± 0.20	0.19	Sc (5.2)
NGC4448	12:28:15.00	+28:37:13.00	661	1494 ^a	1.20 ± 0.07	52.5	117 ^b	10.26 ± 0.10	-0.72 ± 0.20	-0.73	SBab (1.8)
NGC4525	12:33:51.00	+30:16:38.00	1172	963 ^a	1.30 ± 0.04	60.6	53	9.40 ± 0.10	-1.06 ± 0.20	-0.48	Sc (5.9)
NGC4559	12:35:57.00	+27:57:35.00	807	578 ^a	2.02 ± 0.02	64.8	148	9.81 ± 0.10	-0.18 ± 0.20	0.12	Sc (6.0)
NGC4793	12:54:40.62	+28:56:19.20	2484	2094 ^a	1.26 ± 0.04	61.1	54	10.42 ± 0.10	0.77 ± 0.20	0.65	Sc (5.0)
UGC08076	12:57:49.94	+29:39:15.10	2526	2821	0.94 ± 0.04	51.0	91	9.06 ± 0.10	-0.80 ± 0.20	0.01	Sc (6.2)
NGC4961	13:05:47.57	+27:44:02.90	2535	2957 ^a	1.05 ± 0.05	38.7	106	9.61 ± 0.10	-0.25 ± 0.20	0.19	Sc (5.6)
IC0851	13:08:34.27	+21:02:59.90	2615	3303 ^a	1.05 ± 0.04	72.3	152	9.69 ± 0.10	-0.34 ± 0.20	0.04	Sc (4.9)
NGC5012	13:11:37.04	+22:54:55.80	2619	2735 ^a	1.42 ± 0.02	58.8	10	10.68 ± 0.10	0.41 ± 0.20	0.12	Sc (5.1)
NGC5016	13:12:06.68	+24:05:42.00	2612	2985 ^a	1.20 ± 0.03	44.7	57	10.25 ± 0.10	0.07 ± 0.20	0.07	SABb (4.4)
UGC08290	13:12:41.78	+22:49:47.20	2581	3012 ^a	0.92 ± 0.05	26.8	43 ^b	9.41 ± 0.10	-0.32 ± 0.20	0.25	SBm (8.8)
UGC08318	13:14:30.59	+35:23:12.60	2395	2819 ^a	0.95 ± 0.05	51.6	80	9.06 ± 0.10	-1.18 ± 0.20	-0.37	SBC (5.8)
NGC5116	13:22:55.61	+26:58:50.60	2891	3228 ^a	1.29 ± 0.03	73.7	39	10.21 ± 0.10	-0.11 ± 0.20	-0.08	SBC (4.9)
NGC5117	13:22:56.47	+28:18:59.10	2382	2864 ^a	1.19 ± 0.04	62.5	154	9.40 ± 0.10	-0.49 ± 0.20	0.09	Sc (5.8)
UGC08409	13:23:00.86	+23:18:22.90	2805	3178 ^a	0.98 ± 0.05	57.5	81	9.29 ± 0.10	-1.37 ± 0.20	-0.72	Sd (8.0)
NGC5169	13:28:10.05	+46:40:19.70	2436	3141 ^a	1.18 ± 0.04	70.4	104	9.80 ± 0.10	-0.13 ± 0.20	0.18	Sbc (4.1)
NGC5173	13:28:25.27	+46:35:29.90	2424	2850 ^a	1.04 ± 0.04	25.8	104 ^b	10.43 ± 0.10	-0.45 ± 0.20	-0.57	E (-4.7)
IC4263	13:28:33.19	+46:55:37.80	2719	3040 ^a	1.23 ± 0.04	79.4	102	9.35 ± 0.10	-0.81 ± 0.20	-0.20	SBcd (6.6)
PGC047274	13:28:33.65	+46:29:59.70	2574	2910	0.96 ± 0.05	71.0	136	9.26 ± 0.26	-1.13 ± 0.20	-0.46	Sbc (4.1)
PGC047295	13:28:49.76	+46:15:44.60	2672	3004	0.93 ± 0.06	51.3	125	9.70 ± 0.13	-0.99 ± 0.20	-0.62	Sa (1.0)
NGC5198	13:30:11.40	+46:40:14.80	2519	3054 ^a	1.31 ± 0.07	48.9	15	10.89 ± 0.10	-0.82 ± 0.20	-1.26	E (-4.8)
NGC5248	13:37:32.02	+08:53:06.60	1151	934 ^a	1.61 ± 0.03	56.4	120	10.20 ± 0.10	0.18 ± 0.20	0.21	SABb (4.0)
UGC08630	13:38:24.87	+33:07:03.70	2438	2565 ^a	1.25 ± 0.03	79.5	94	9.19 ± 0.11	-0.70 ± 0.20	0.02	Scd (6.6)
UGC08662	13:41:17.25	+33:46:21.40	2023	2254 ^a	1.16 ± 0.03	85.9	73	8.94 ± 0.10	-0.99 ± 0.20	-0.10	Sc (6.0)
UGC08693	13:44:28.40	+35:11:31.90	2438	3169 ^a	1.07 ± 0.04	63.4	170	9.75 ± 0.10	-0.68 ± 0.20	-0.34	Sbc (4.2)
NGC5289	13:45:08.71	+41:30:12.20	2526	2978 ^a	1.37 ± 0.04	85.3	100	10.17 ± 0.10	-0.69 ± 0.20	-0.64	SABA (2.0)
NGC5290	13:45:19.18	+41:42:45.30	2573	2636 ^a	1.51 ± 0.06	80.6	95	10.69 ± 0.10	-0.13 ± 0.20	-0.43	Sbc (4.0)
NGC5297	13:46:23.67	+43:52:20.40	2409	2254 ^a	1.57 ± 0.03	82.2	146	10.41 ± 0.11	0.12 ± 0.20	0.01	Sc (4.9)
NGC5300	13:48:16.04	+03:57:03.10	1171	1452 ^a	1.45 ± 0.03	50.8	147	9.65 ± 0.10	-0.59 ± 0.20	-0.18	SABC (5.3)
UGC08733	13:48:38.99	+43:24:44.20	2338	2285 ^a	1.29 ± 0.03	62.1	6	9.31 ± 0.12	-0.58 ± 0.20	0.06	Sc (6.0)
PGC049002	13:48:45.16	+41:42:35.30	2695	3019	0.83 ± 0.06	44.4	2	9.52 ± 0.30 ^c	-0.40 ^{+0.17} _{-0.12} ^d	0.10	S0 (-2.0)
NGC5311	13:48:56.08	+39:59:06.40	2698	3017	1.30 ± 0.03	37.6	102	10.69 ± 0.10	-0.41 ± 0.20	-0.71	S0-a (-0.2)
UGC08736	13:49:04.55	+39:29:51.60	2384	2718	1.13 ± 0.04	67.8	175	10.61 ± 0.26	-0.11 ± 0.63	-0.35	Sc (5.0)
NGC5313	13:49:44.34	+39:59:05.20	2538	3228 ^a	1.26 ± 0.07	57.2	42	10.41 ± 0.10	0.11 ± 0.20	0.00	SABb (3.1)
NGC5320	13:50:20.38	+41:21:58.40	2619	2685 ^a	1.26 ± 0.04	61.9	17	10.06 ± 0.10	-0.15 ± 0.20	-0.02	SABC (5.1)
IC4336	13:50:43.37	+39:42:24.40	2530	2857	1.14 ± 0.04	80.9	155	9.91 ± 0.10	-0.35 ± 0.20	-0.12	Sb (3.1)
NGC5326	13:50:50.70	+39:34:29.50	2520	1990 ^a	1.34 ± 0.03	69.4	136	10.50 ± 0.10	-0.82 ± 0.20	-0.99	Sa (0.8)

PGC049191	13:51:25.37	+40:12:47.70	2466	2837 ^a	0.81 ± 0.07	21.6	7 ^b	8.92 ± 0.10	-0.55 ± 0.20	0.35	E (-5.0)
NGC5336	13:52:09.79	+43:14:34.60	2336	2680	1.09 ± 0.04	41.8	101	9.67 ± 0.10	-0.24 ± 0.20	0.15	SABc (5.9)
NGC5337	13:52:23.03	+39:41:14.10	2165	3655 ^a	1.22 ± 0.06	66.8	22	10.58 ± 0.10	-0.34 ± 0.20	-0.56	SBab (1.7)
PGC2151881	13:52:24.87	+39:33:27.40	2703	3022	0.59 ± 0.07	23.1	135 ^b	9.22 ± 0.30 ^c	-1.06 ^{+0.15} _{-0.12} ^d	-0.36	SBa (1.0)
NGC5346	13:53:01.89	+39:34:50.80	2519	2818 ^a	1.19 ± 0.04	68.0	160	9.63 ± 0.10	-0.95 ± 0.20	-0.53	SABc (5.9)
NGC5347	13:53:17.83	+33:29:27.00	2335	1531 ^a	1.21 ± 0.03	45.3	122	10.09 ± 0.11	0.64 ± 0.20	0.75	Sab (2.0)
NGC5350	13:53:21.60	+40:21:50.00	2321	2143 ^a	1.43 ± 0.02	54.1	35	10.69 ± 0.15	0.24 ± 0.20	-0.06	Sbc (3.6)
NGC5353	13:53:26.69	+40:16:58.90	2325	2502 ^a	1.38 ± 0.03	81.9	152	10.99 ± 0.11	-0.83 ± 0.29	-1.33	S0 (-2.1)
NGC5355	13:53:45.56	+40:20:19.20	2344	2634 ^a	1.06 ± 0.04	62.3	30	10.05 ± 0.10	-1.49 ± 0.20	-1.35	S0 (-2.0)
PGC049386	13:53:59.49	+39:42:56.00	2613	2936	0.75 ± 0.08	50.5	72	9.40 ± 0.30 ^c	-2.46 ^{+0.07} _{-0.08} ^g	-1.88	S0 (-2.0)
NGC5358	13:54:00.41	+40:16:38.30	2412	2747	1.05 ± 0.04	90.0	138	9.87 ± 0.10	-2.57 ± 0.40	-2.31	S0-a (-0.4)
NGC5348	13:54:11.27	+05:13:38.80	1451	1346 ^a	1.59 ± 0.04	90.0	175	9.18 ± 0.12	-1.14 ± 0.20	-0.41	SBbc (3.8)
NGC5362	13:54:53.30	+41:18:48.70	2175	2074 ^a	1.28 ± 0.03	70.2	87	10.00 ± 0.10	-0.35 ± 0.20	-0.18	Sb (3.4)
NGC5356	13:54:58.46	+05:20:01.40	1374	1840 ^a	1.45 ± 0.03	90.0	16	9.72 ± 0.11	-1.12 ± 0.20	-0.76	Sbc (3.8)
NGC5360	13:55:38.75	+04:59:06.20	1171	1632 ^a	1.04 ± 0.05	62.3	63	9.01 ± 0.10	-1.80 ± 0.20	-0.96	S0-a (0.1)
NGC5371	13:55:39.94	+40:27:42.30	2558	2103 ^a	1.60 ± 0.02	54.0	7	10.94 ± 0.10	0.50 ± 0.20	0.03	Sbc (4.0)
NGC5363	13:56:07.21	+05:15:17.20	1139	1436 ^a	1.62 ± 0.03	53.7	133	10.69 ± 0.10	-0.84 ± 0.20	-1.14	S0-a (0.1)
NGC5364	13:56:12.00	+05:00:52.10	1241	1270 ^a	1.58 ± 0.03	67.5	45	10.22 ± 0.10	-0.14 ± 0.20	-0.12	Sbc (4.0)
NGC5375	13:56:56.00	+29:09:51.70	2386	3013 ^a	1.37 ± 0.03	44.8	179	10.38 ± 0.10	-0.36 ± 0.20	-0.45	SBab (2.5)
NGC5383	13:57:04.97	+41:50:46.50	2270	2667 ^a	1.39 ± 0.03	42.3	98	10.49 ± 0.10	0.32 ± 0.20	0.16	Sb (3.1)
NGC5403	13:59:50.75	+38:10:57.20	2746	3060	1.44 ± 0.03	78.8	143	10.62 ± 0.10	-0.01 ± 0.20	-0.26	Sbb (2.9)
PGC049824	13:59:57.09	+38:12:03.30	2730	3045	0.89 ± 0.18	86.0	50	9.74 ± 0.11	-1.18 ± 0.24	-0.83	S0 (-2.0)
PGC049852	14:00:25.00	+38:31:13.00	2609	2930	0.67 ± 0.07	42.1	157	9.24 ± 0.11	-1.38 ± 0.21	-0.69	Scd (7.0)
PGC049927	14:01:24.02	+36:48:00.30	2706	3125 ^a	0.87 ± 0.06	24.1	120 ^b	9.26 ± 0.10	-0.34 ± 0.20	0.33	S0-a (-1.5)
NGC5470	14:06:31.91	+06:01:46.90	1026	1783 ^a	1.42 ± 0.03	90.0	62	9.53 ± 0.11	-1.31 ± 0.20	-0.82	Sb (3.3)
NGC5560	14:20:04.49	+03:59:32.90	1729	1417 ^a	1.54 ± 0.04	90.0	109	10.03 ± 0.14	-0.35 ± 0.20	-0.20	Sb (3.1)
NGC5566	14:20:19.89	+03:56:01.50	1507	1371 ^a	1.73 ± 0.04	75.6	35	10.86 ± 0.10	-0.37 ± 0.20	-0.78	SBab (1.6)
NGC5574	14:20:55.97	+03:14:16.80	1589	1807 ^a	1.12 ± 0.04	65.0	61	10.00 ± 0.10	-1.45 ± 0.20	-1.28	E-S0 (-2.7)
NGC5576	14:21:03.68	+03:16:15.60	1506	1574 ^a	1.45 ± 0.03	90.0	91	10.75 ± 0.10	-1.42 ± 0.20	-1.76	E (-4.9)
NGC5577	14:21:13.11	+03:26:08.80	1489	1718 ^a	1.46 ± 0.03	83.9	61	9.89 ± 0.10	-0.60 ± 0.20	-0.36	Sbc (3.8)
UGC09215	14:23:27.12	+01:43:34.70	1397	1859 ^a	1.32 ± 0.03	63.7	163	9.33 ± 0.12	-0.28 ± 0.20	0.35	SBC (6.4)
NGC5636	14:29:39.02	+03:15:58.70	1745	2001	1.14 ± 0.04	55.5	56	9.76 ± 0.10	-1.17 ± 0.20	-0.84	S0-a (-0.3)
NGC5638	14:29:40.38	+03:13:59.90	1676	1858 ^a	1.29 ± 0.04	39.8	154	10.60 ± 0.10	-1.14 ± 0.20	-1.38	E (-4.8)
IC1022	14:30:01.84	+03:46:22.30	1722	2874 ^a	0.98 ± 0.04	75.7	163	9.37 ± 0.10	-0.84 ± 0.20	-0.24	SBB (3.4)
NGC5645	14:30:39.35	+07:16:30.30	1370	1406 ^a	1.30 ± 0.04	58.6	85	9.62 ± 0.10	-0.42 ± 0.20	0.01	SBcd (6.6)
IC1024	14:31:27.20	+03:00:32.70	1479	1626 ^a	1.04 ± 0.06	90.0	29	9.56 ± 0.10	-0.18 ± 0.20	0.29	S0 (-1.8)
NGC5661	14:31:57.39	+06:15:01.50	2354	3471 ^a	1.06 ± 0.05	60.6	22	9.34 ± 0.10	-0.35 ± 0.20	0.27	Sb (3.2)
NGC5658	14:32:28.51	+00:17:38.40	1672	1733 ^a	1.25 ± 0.03	90.0	115 ^b	9.30 ± 0.10	-1.05 ± 0.20	-0.40	S0-a (-0.9)
NGC5668	14:33:24.34	+04:27:01.60	1577	1951 ^a	1.28 ± 0.04	33.0	107	9.75 ± 0.10	0.06 ± 0.20	0.40	Sed (6.9)

NGC5692	14:38:18.11	+03:24:37.20	1561	1850 ^a	0.98 ± 0.10	53.4	36	9.22 ± 0.10	-0.62 ± 0.20	0.08	Sbc (4.0)
NGC5701	14:39:11.08	+05:21:48.50	1505	1954 ^a	1.30 ± 0.04	40.5	4	10.38 ± 0.10	-0.94 ± 0.20	-1.03	S0-a (-0.3)
NGC5725	14:40:58.32	+02:11:11.60	1627	1759 ^a	0.98 ± 0.05	61.7	31	9.09 ± 0.10	-0.78 ± 0.20	0.01	SBcd (7.1)
IC1048	14:42:58.00	+04:53:22.10	1636	2167 ^a	1.32 ± 0.03	90.0	163	9.77 ± 0.10	-0.62 ± 0.20	-0.29	Sb (3.3)
NGC5740	14:44:24.45	+01:40:47.20	1572	2123 ^a	1.43 ± 0.02	63.9	165	9.99 ± 0.10	-0.27 ± 0.20	-0.09	Sb (3.0)
NGC5746	14:44:55.92	+01:57:18.00	1724	2189 ^a	1.86 ± 0.02	90.0	172	10.91 ± 0.10	-0.14 ± 0.20	-0.59	Sb (3.0)
UGC09556	14:49:46.09	+60:23:54.70	2324	4059 ^a	0.91 ± 0.05	77.2	135	9.38 ± 0.13	-0.64 ± 0.20	-0.05	Sc (5.9)
NGC5777	14:51:17.85	+58:58:40.60	2145	3382 ^a	1.47 ± 0.03	90.0	145	10.28 ± 0.10	-0.38 ± 0.20	-0.40	Sb (3.2)
IC1066	14:53:02.80	+03:17:46.00	1577	2382 ^a	1.08 ± 0.04	59.9	69	9.58 ± 0.11	-0.82 ± 0.20	-0.36	SABb (3.2)
IC1067	14:53:05.25	+03:19:54.40	1577	1826	1.26 ± 0.06	37.1	128	9.96 ± 0.11	-0.69 ± 0.20	-0.49	Sb (3.0)
NGC5770	14:53:15.02	+03:57:35.00	1471	1539 ^a	1.04 ± 0.06	41.1	112 ^b	9.92 ± 0.10	-3.01 ± 0.36	-2.79	S0 (-1.9)
NGC5806	15:00:00.40	+01:53:28.70	1359	1841 ^a	1.48 ± 0.02	60.4	172	10.57 ± 0.10	-0.03 ± 0.20	-0.25	Sb (3.2)
NGC5813	15:01:11.23	+01:42:07.10	1956	2189 ^a	1.62 ± 0.02	90.0	143	11.15 ± 0.10	-0.56 ± 0.20	-1.17	E (-4.9)
UGC09661	15:02:03.51	+01:50:28.60	1242	1456	1.02 ± 0.04	28.5	139	9.04 ± 0.10	-1.07 ± 0.20	-0.25	SBd (8.0)
NGC5831	15:04:07.00	+01:13:11.70	1656	2011 ^a	1.35 ± 0.03	38.6	130	10.59 ± 0.10	-1.77 ± 0.22	-2.00	E (-4.8)
NGC5838	15:05:26.26	+02:05:57.60	1341	1993 ^a	1.59 ± 0.02	90.0	40	10.84 ± 0.10	-0.76 ± 0.20	-1.16	E-S0 (-2.6)
NGC5839	15:05:27.49	+01:38:05.30	1220	1753 ^a	1.16 ± 0.04	29.9	103	10.09 ± 0.10	-1.50 ± 0.20	-1.39	S0 (-2.0)
PGC2586382	15:05:35.73	+59:05:37.60	2606	2967	0.91 ± 0.06	90.0	74	9.49 ± 0.10	-0.95 ± 0.20	-0.43	Sa (1.0)
NGC5845	15:06:00.81	+01:38:01.70	1472	2133 ^a	1.00 ± 0.07	72.1	152	10.22 ± 0.10	-1.55 ± 0.20	-1.53	E (-4.9)
NGC5846	15:06:29.28	+01:36:20.20	1712	1860 ^a	1.63 ± 0.03	25.0	40 ^b	11.19 ± 0.10	-0.70 ± 0.21	-1.34	E (-4.8)
NGC5854	15:07:47.70	+02:34:07.10	1663	1628 ^a	1.48 ± 0.04	90.0	55	10.35 ± 0.13	-1.69 ± 0.24	-1.76	S0-a (-1.1)
PGC054037	15:08:05.85	+01:39:05.50	1837	2055	0.76 ± 0.12	71.5	114	9.15 ± 0.10	-1.22 ± 0.20	-0.47	IB (10.0)
NGC5864	15:09:33.55	+03:03:10.00	1885	1919 ^a	1.40 ± 0.06	90.0	67	10.39 ± 0.10	-1.76 ± 0.22	-1.86	S0 (-1.6)
NGC5869	15:09:49.44	+00:28:12.10	2085	2051 ^a	1.34 ± 0.03	61.5	114	10.39 ± 0.10	-1.27 ± 0.20	-1.37	S0 (-2.2)
NGC5894	15:11:40.98	+59:48:32.20	2466	2925 ^a	1.47 ± 0.05	90.0	14	10.57 ± 0.11	-0.02 ± 0.20	-0.24	Scd (7.3)
PGC054346	15:13:29.18	+58:30:33.70	2540	2903	0.92 ± 0.16	24.0	83 ^b	9.64 ± 0.12	-0.65 ± 0.20	-0.24	S0-a (0.0)
PGC054452	15:15:34.61	+02:14:53.80	1918	2132	0.98 ± 0.05	42.3	109	9.70 ± 0.14	-1.76 ± 0.21	-1.39	S0-a (-1.3)
UGC09837	15:23:51.67	+58:03:10.60	2657	3082 ^a	1.23 ± 0.06	23.2	28 ^b	9.59 ± 0.10	-0.14 ± 0.20	0.31	SABC (5.3)
NGC5951	15:33:43.06	+15:00:26.20	1780	1986 ^a	1.48 ± 0.03	84.6	4	9.80 ± 0.10	-0.50 ± 0.20	-0.19	SBc (5.2)
NGC5953	15:34:32.38	+15:11:37.60	1965	1710 ^a	1.17 ± 0.04	43.9	44 ^b	10.04 ± 0.10	0.31 ± 0.20	0.45	S0-a (0.1)
NGC5954	15:34:35.02	+15:12:00.30	1959	2404 ^a	1.01 ± 0.08	63.6	19	9.49 ± 0.10	-0.01 ± 0.20	0.51	SABC (5.9)
NGC5956	15:34:58.54	+11:45:01.00	1899	2155	1.17 ± 0.06	0.0	30 ^b	10.06 ± 0.10	-0.39 ± 0.20	-0.26	SBc (5.8)
NGC5957	15:35:23.21	+12:02:51.40	1827	2088	1.39 ± 0.06	17.5	92 ^b	10.27 ± 0.10	-0.24 ± 0.20	-0.25	Sb (2.9)
NGC5981	15:37:53.45	+59:23:30.30	1764	3766 ^a	1.44 ± 0.05	90.0	139	10.76 ± 0.10	-0.11 ± 0.20	-0.46	SBbc (4.2)
NGC5970	15:38:29.97	+12:11:11.80	1957	2075 ^a	1.44 ± 0.03	47.9	88	10.35 ± 0.11	0.12 ± 0.20	0.05	SBc (5.0)
NGC5982	15:38:39.83	+59:21:21.00	3017	2673 ^a	1.49 ± 0.06	90.0	110	11.13 ± 0.10	-0.83 ± 0.20	-1.43	E (-4.8)
NGC5985	15:39:37.09	+59:19:55.00	2517	2924 ^a	1.60 ± 0.03	63.3	15	11.07 ± 0.10	0.42 ± 0.20	-0.14	Sb (3.1)
NGC5989	15:41:32.80	+59:45:18.80	2878	3234	0.95 ± 0.10	22.1	27 ^b	9.94 ± 0.10	0.01 ± 0.20	0.22	Sc (5.9)

UGC09991	15:43:23.97	+14:26:08.90	1932	2944 ^a	1.09 ± 0.04	80.6	70	9.42 ± 0.10	-1.25 ± 0.20	-0.69	Sc (5.9)
NGC6012	15:54:13.94	+14:36:04.50	1854	1432 ^a	1.25 ± 0.03	47.1	164	10.25 ± 0.11	-0.15 ± 0.20	-0.15	SBab (1.7)
UGC10086	15:54:41.25	+16:37:01.90	2217	2685 ^a	0.81 ± 0.13	67.0	177	8.82 ± 0.10	-1.03 ± 0.20	-0.06	S0-a (0.3)
IC1151	15:58:32.34	+17:26:29.30	2169	2540 ^a	1.35 ± 0.02	69.6	32	9.54 ± 0.10	-0.52 ± 0.20	-0.04	SBc (5.1)
IC1210	16:14:30.15	+62:32:12.10	2929	3631 ^a	1.14 ± 0.08	84.7	169	10.01 ± 0.10	0.03 ± 0.20	0.19	Sab (2.1)
PGC057611	16:15:02.83	+61:46:55.40	2942	3299	0.52 ± 0.41	34.8	120	9.87 ± 0.13	-0.97 ± 0.20	-0.71	Sab (2.0)
UGC10297	16:15:28.82	+18:54:17.50	2305	2786 ^a	1.33 ± 0.03	90.0	1	9.49 ± 0.11	-0.82 ± 0.20	-0.30	SBc (5.2)
UGC10413	16:29:27.13	+21:20:11.70	2986	3396 ^a	1.01 ± 0.05	71.5	171	9.69 ± 0.11	-0.53 ± 0.20	-0.15	SABc (5.7)
NGC6181	16:32:20.96	+19:49:35.60	2375	2423 ^a	1.38 ± 0.02	68.3	177	10.35 ± 0.10	0.55 ± 0.20	0.48	SABC (5.1)
NGC6186	16:34:25.48	+21:32:27.20	2937	3190	1.20 ± 0.04	71.0	59	10.47 ± 0.10	0.31 ± 0.20	0.16	Sa (1.2)
NGC6267	16:58:08.66	+22:59:06.40	2980	3926 ^a	1.11 ± 0.04	41.5	33	10.15 ± 0.20	-0.13 ± 0.20	-0.06	Sc (4.8)
NGC6276	17:00:45.09	+23:02:38.40	2754	3015	0.81 ± 0.08	33.3	136 ^b	9.72 ± 0.12	-1.52 ± 0.21	-1.16	Sa (1.0)
NGC6278	17:00:50.33	+23:00:39.70	2832	2740 ^a	1.24 ± 0.04	78.8	128	10.73 ± 0.10	-1.03 ± 0.20	-1.36	S0 (-1.8)
NGC6306	17:07:36.98	+60:43:44.00	2973	3327	1.12 ± 0.05	76.0	161	9.84 ± 0.10	0.45 ± 0.20	0.73	SBab (2.0)
UGC10721	17:08:25.55	+25:31:02.60	2920	3491 ^a	1.10 ± 0.04	56.0	110	10.09 ± 0.11	0.01 ± 0.20	0.12	Sc (5.7)
UGC10968	17:44:10.45	+57:59:16.40	2855	3206	0.72 ± 0.09	68.2	149	9.30 ± 0.10	-1.91 ± 0.22	-1.26	SABB (4.0)

Table B.2: Properties of our sample of filament galaxies. Column description. (1) Galaxy ID; (2-4) RA, Dec., and heliocentric velocity; (5) assumed distance of the galaxy, estimated as V_{cosmic}/H_0 ; (6-8) D_{25} diameter, inclination, and position angle (PA) from HyperLeda, while for the sources denoted with the symbol ^b the PA has been estimated by visual inspection, see notes below; (9) stellar mass; (10) star formation rate; (11) SFR normalized to the value of the main sequence SFR_{MS}, following the MS prescription by Leroy et al. (2019); (12) morphology from HyperLeda, among parentheses we report the de Vaucouleurs classification.

Notes:

^a Recession velocities inferred from redshift independent distances

^b Position Angles estimated by inspection of optical images from AladinLite and Legacy Survey databases

^c Stellar masses from Nasa Sloan Atlas

^d SFR from Chang et al. (2015)

^e SFR from the DustPedia-CIGALE archive

^f SFR by Mayya & Romano (2002) for the ring galaxy NGC 2793

^g SFR estimated using W4 WISE emission and the Calzetti et al. (2007) relation for PGC 049386 (i.e., CGCG 219-021).

Galaxy	Distance (Mpc)	$\log(D_{25}/0.1')$	CO(J → J – 1)	$S_{\text{CO}(J \rightarrow J-1)} \Delta v$ (Jy km s ⁻¹)	f_{ap}	FWHM (km/s)	$\log\left(\frac{L'_{\text{CO}(J \rightarrow J-1)}}{\text{K km s}^{-1} \text{ pc}^2}\right)$	r_{21}	$\log\left(\frac{M_{\text{H}_2}}{M_{\odot}}\right)$
(1)	(2)	(3)	(4)	(5)	(6)	(7)	(8)	(9)	(10)
IC2256	35.33 ^a	0.90 ± 0.06	1 → 0	< 10.02	0.71	—	< 7.63	—	$7.76^{+0.10}_{-0.12}$
			2 → 1	6.16 ± 1.53	0.44	21 ± 35	$7.03^{+0.10}_{-0.12}$	—	
UGC04375	40.34 ^a	1.23 ± 0.04	1 → 0	14.79 ± 1.86	0.38	156 ± 21	$8.19^{+0.05}_{-0.09}$	0.30 ± 0.07	$8.83^{+0.05}_{-0.06}$
			2 → 1	7.49 ± 1.64	0.16	145 ± 27	$7.67^{+0.09}_{-0.11}$	—	
IC2361	30.33	1.19 ± 0.04	1 → 0	11.51 ± 1.92	0.53	116 ± 22	$7.69^{+0.07}_{-0.08}$	0.67 ± 0.13	$8.32^{+0.07}_{-0.08}$
			2 → 1	17.65 ± 1.79	0.30	120 ± 14	$7.51^{+0.09}_{-0.05}$	—	
UGC04395	38.17 ^a	1.00 ± 0.05	1 → 0	< 4.30	0.69	—	< 7.35	—	< 7.78
			2 → 1	< 5.56	0.44	—	< 7.05	—	
PGC023706	32.60	0.69 ± 0.13	1 → 0	< 2.86	0.83	—	< 6.95	—	< 7.03
			2 → 1	< 1.85	0.60	—	< 6.30	—	
NGC2604	30.69	1.17 ± 0.05	1 → 0	5.73 ± 0.90	0.36	59 ± 10	$7.56^{+0.06}_{-0.07}$	0.81 ± 0.17	$8.20^{+0.06}_{-0.07}$
			2 → 1	7.72 ± 1.13	0.15	72 ± 12	$7.47^{+0.06}_{-0.07}$	—	
PGC024012	32.82	0.93 ± 0.06	1 → 0	< 7.16	0.68	—	< 7.45	—	< 7.82
			2 → 1	< 7.41	0.40	—	< 7.09	—	
NGC2608	23.27 ^a	1.29 ± 0.03	1 → 0	46.85 ± 1.76	0.37	140 ± 6	8.22 ± 0.02	0.31 ± 0.02	8.85 ± 0.02
			2 → 1	25.44 ± 1.76	0.16	106 ± 9	7.71 ± 0.03	—	
UGC04559	41.08 ^a	1.57 ± 0.03	1 → 0	15.46 ± 2.60	0.29	239 ± 55	$8.35^{+0.07}_{-0.08}$	0.36 ± 0.08	$8.98^{+0.07}_{-0.08}$
			2 → 1	11.83 ± 1.87	0.15	88 ± 20	$7.90^{+0.06}_{-0.07}$	—	
PGC1925809	30.48	0.73 ± 0.07	1 → 0	< 4.30	0.83	—	< 7.07	—	< 7.46
			2 → 1	< 5.56	0.60	—	< 6.72	—	
UGC04659	36.62 ^a	1.15 ± 0.04	1 → 0	< 4.30	0.58	—	< 7.39	—	< 7.66
			2 → 1	< 3.71	0.36	—	< 6.93	—	
PGC025063	30.43	0.75 ± 0.23	1 → 0	21.86 ± 3.19	0.79	261 ± 42	$7.80^{+0.06}_{-0.07}$	0.63 ± 0.11	$8.43^{+0.06}_{-0.07}$
			2 → 1	37.42 ± 2.92	0.53	193 ± 15	$7.60^{+0.03}_{-0.04}$	—	
NGC2712	31.02 ^a	1.47 ± 0.03	1 → 0	48.14 ± 1.79	0.22	195 ± 7	8.71 ± 0.02	0.88 ± 0.04	9.34 ± 0.02
			2 → 1	63.01 ± 1.72	0.08	202 ± 6	8.65 ± 0.01	—	
PGC025273	28.60	0.89 ± 0.06	1 → 0	< 2.86	0.76	—	< 6.88	—	< 7.28
			2 → 1	< 3.71	0.52	—	< 6.55	—	
NGC2780	52.55 ^a	1.02 ± 0.05	1 → 0	21.87 ± 2.14	0.55	158 ± 16	8.43 ± 0.04	0.34 ± 0.05	9.06 ± 0.04
			2 → 1	15.15 ± 1.88	0.28	112 ± 18	$7.96^{+0.05}_{-0.06}$	—	
NGC2793	26.65 ^a	1.05 ± 0.05	1 → 0	6.87 ± 1.30	0.50	106 ± 27	$7.37^{+0.08}_{-0.09}$	0.22 ± 0.09	$8.01^{+0.08}_{-0.09}$
			2 → 1	2.89 ± 1.09	0.24	69 ± 30	$6.71^{+0.14}_{-0.21}$	—	
UGC04902	25.14	1.13 ± 0.04	1 → 0	10.37 ± 1.09	0.54	129 ± 15	$7.47^{+0.04}_{-0.05}$	0.97 ± 0.13	$8.11^{+0.04}_{-0.05}$
			2 → 1	21.18 ± 1.67	0.28	129 ± 12	$7.46^{+0.03}_{-0.04}$	—	
NGC2798	23.43 ^a	1.39 ± 0.05	1 → 0	223.19 ± 2.00	0.40	243 ± 2	8.88 ± 0.01	1.00 ± 0.01	9.51 ± 0.01
			2 → 1	474.19 ± 1.79	0.21	251 ± 1	8.88 ± 0.01	—	
NGC2799	27.78 ^a	1.25 ± 0.05	1 → 0	5.91 ± 1.24	0.51	105 ± 29	$7.34^{+0.08}_{-0.10}$	0.55 ± 0.13	$7.98^{+0.08}_{-0.10}$
			2 → 1	7.74 ± 0.80	0.30	48 ± 6	$7.09^{+0.04}_{-0.05}$	—	
NGC2844	42.14 ^a	1.25 ± 0.06	1 → 0	30.50 ± 2.72	0.44	265 ± 23	8.48 ± 0.04	0.73 ± 0.08	9.11 ± 0.04
			2 → 1	42.74 ± 2.35	0.21	218 ± 12	8.34 ± 0.02	—	
NGC2853	28.55 ^a	1.22 ± 0.06	1 → 0	12.33 ± 1.87	0.43	144 ± 23	$7.76^{+0.06}_{-0.07}$	0.51 ± 0.11	$8.39^{+0.06}_{-0.07}$
			2 → 1	11.65 ± 1.73	0.20	107 ± 18	$7.47^{+0.06}_{-0.07}$	—	
UGC05015	25.79	1.21 ± 0.06	1 → 0	< 4.30	0.33	—	< 7.33	—	< 7.96
			2 → 1	< 7.41	0.13	—	< 7.36	—	

UGC05020	32.36 ^a	1.31 ± 0.03	1 → 0 2 → 1	< 2.76 2.24 ± 0.87	0.43 0.22	— 57 ± 20	< 7.22 $6.81^{+0.14}_{-0.21} b$	—	$7.54^{+0.14}_{-0.21}$
NGC2893	27.14 ^a	1.01 ± 0.04	1 → 0 2 → 1	36.74 ± 1.13 63.60 ± 1.35	0.55 0.28	44 ± 2 50 ± 1	8.08 ± 0.01 8.02 ± 0.01	0.86 ± 0.03	8.72 ± 0.01
NGC2968	13.74 ^a	1.39 ± 0.03	1 → 0 2 → 1	< 4.30 < 3.71	0.25 0.09	— —	< 6.90 < 6.66	—	< 7.39
NGC2970	27.02 ^a	0.93 ± 0.06	1 → 0 2 → 1	< 5.73 < 5.56	0.62 0.34	— —	< 7.22 < 6.87	—	< 7.60
PGC028169	24.76 ^a	0.83 ± 0.06	1 → 0 2 → 1	3.83 ± 0.89 < 3.71	0.72 0.44	91 ± 21 —	$6.90^{+0.09}_{-0.12}$ < 6.50	< 0.40	$7.54^{+0.09}_{-0.12}$
NGC3003	20.78 ^a	1.68 ± 0.02	1 → 0 2 → 1	25.51 ± 1.57 26.94 ± 1.46	0.23 0.11	88 ± 6 54 ± 4	8.08 ± 0.03 7.81 ± 0.02	0.54 ± 0.04	8.71 ± 0.03
NGC3026	24.59 ^a	1.35 ± 0.03	1 → 0 2 → 1	4.65 ± 0.96 1.89 ± 0.93	0.43 0.25	72 ± 17 71 ± 36	$7.20^{+0.08}_{-0.10}$ $6.45^{+0.17}_{-0.29} b$	0.18 ± 0.10	$7.84^{+0.08}_{-0.10}$
NGC3021	26.47 ^a	1.13 ± 0.07	1 → 0 2 → 1	83.64 ± 2.50 80.15 ± 2.25	0.48 0.23	196 ± 6 164 ± 5	8.47 ± 0.01 8.18 ± 0.01	0.50 ± 0.02	9.11 ± 0.01
UGC05287	31.93 ^a	0.98 ± 0.06	1 → 0 2 → 1	< 4.30 < 3.71	0.58 0.30	— —	< 7.27 < 6.89	—	< 7.62
UGC05326	22.96	0.97 ± 0.05	1 → 0 2 → 1	< 2.86 < 3.71	0.55 0.27	— —	< 6.83 < 6.64	—	< 7.37
NGC3067	19.58 ^a	1.31 ± 0.02	1 → 0 2 → 1	100.21 ± 1.95 104.32 ± 1.79	0.44 0.23	158 ± 3 120 ± 2	8.33 ± 0.01 8.03 ± 0.01	0.49 ± 0.01	8.97 ± 0.01
PGC029347	23.97 ^a	0.82 ± 0.06	1 → 0 2 → 1	2.06 ± 0.55 2.52 ± 0.70	0.69 0.41	59 ± 15 50 ± 14	$6.62^{+0.10}_{-0.13}$ $6.33^{+0.11}_{-0.14}$	0.52 ± 0.20	$7.25^{+0.10}_{-0.13}$
NGC3118	26.84 ^a	1.32 ± 0.03	1 → 0 2 → 1	3.03 ± 0.89 3.45 ± 0.89	0.45 0.26	95 ± 30 82 ± 22	$7.07^{+0.11}_{-0.15}$ $6.77^{+0.10}_{-0.13}$	0.50 ± 0.19	$7.70^{+0.11}_{-0.15}$
UGC05577	31.04	0.97 ± 0.04	1 → 0 2 → 1	4.03 ± 0.66 5.82 ± 0.57	0.61 0.33	48 ± 11 35 ± 4	$7.19^{+0.07}_{-0.08}$ 7.01 ± 0.04	0.67 ± 0.13	$7.83^{+0.07}_{-0.08}$
UGC05588	24.53 ^a	0.74 ± 0.14	1 → 0 2 → 1	23.98 ± 1.68 34.94 ± 1.57	0.79 0.54	105 ± 8 100 ± 5	7.65 ± 0.03 7.38 ± 0.02	0.54 ± 0.04	8.28 ± 0.03
NGC3245A	23.86 ^a	1.37 ± 0.04	1 → 0 2 → 1	< 7.16 < 7.41	0.42 0.24	— —	< 7.38 < 7.04	—	< 7.77
NGC3254	34.33 ^a	1.37 ± 0.03	1 → 0 2 → 1	4.67 ± 1.51 3.63 ± 1.48	0.31 0.13	60 ± 31 73 ± 42	$7.64^{+0.12}_{-0.17}$ $7.32^{+0.15}_{-0.23} b$	0.47 ± 0.25	$8.27^{+0.12}_{-0.17}$
PGC031357	27.23	0.88 ± 0.06	1 → 0 2 → 1	< 5.73 < 7.41	0.75 0.49	— —	< 7.14 < 6.84	—	< 7.57
PGC031387	22.94	0.76 ± 0.08	1 → 0 2 → 1	3.09 ± 1.46 2.67 ± 0.84	0.77 0.50	134 ± 95 48 ± 14	$6.71^{+0.17}_{-0.28} b$ $6.23^{+0.12}_{-0.16}$	0.33 ± 0.19	$6.97^{+0.12}_{-0.16}$
UGC05870	31.44	1.04 ± 0.08	1 → 0 2 → 1	4.28 ± 0.99 4.07 ± 0.88	0.48 0.23	70 ± 16 33 ± 8	$7.33^{+0.09}_{-0.11}$ $7.03^{+0.09}_{-0.11}$	0.51 ± 0.16	$7.96^{+0.09}_{-0.11}$
NGC3381	26.46	1.30 ± 0.05	1 → 0 2 → 1	12.49 ± 0.87 18.14 ± 0.83	0.26 0.10	34 ± 2 33 ± 2	7.92 ± 0.03 7.91 ± 0.02	0.97 ± 0.08	8.56 ± 0.03
UGC05990	31.73 ^a	1.11 ± 0.04	1 → 0 2 → 1	2.48 ± 0.76 2.63 ± 1.20	0.61 0.38	84 ± 23 116 ± 38	$7.00^{+0.12}_{-0.16}$ $6.62^{+0.16}_{-0.26} b$	0.42 ± 0.23	$7.63^{+0.12}_{-0.16}$
NGC3442	30.93 ^a	0.74 ± 0.05	1 → 0 2 → 1	23.58 ± 0.98 30.04 ± 1.21	0.81 0.56	100 ± 5 79 ± 4	7.83 ± 0.02 7.50 ± 0.02	0.46 ± 0.03	8.47 ± 0.02

UGC06070	29.32	0.74 ± 0.14	1 → 0 2 → 1	3.84 ± 0.98 5.22 ± 1.19	0.78 0.51	78 ± 20 67 ± 14	$7.02_{-0.13}^{+0.10}$ $6.73_{-0.11}^{+0.09}$	0.52 ± 0.18	$7.65_{-0.13}^{+0.10}$
NGC3629	33.86 ^a	1.25 ± 0.03	1 → 0 2 → 1	< 5.73 < 5.56	0.36 0.15	— —	< 7.65 < 7.41	— —	< 8.14
UGC06455	31.81	1.19 ± 0.04	1 → 0 2 → 1	< 2.86 < 7.41	0.49 0.25	— —	< 7.16 < 7.27	— —	< 7.79
NGC3687	26.27 ^a	1.15 ± 0.03	1 → 0 2 → 1	10.86 ± 1.45 8.63 ± 1.18	0.55 0.30	132 ± 17 106 ± 14	$7.53_{-0.06}^{+0.05}$ 7.09 ± 0.06	0.36 ± 0.07	$8.16_{-0.06}^{+0.05}$
NGC3689	41.66 ^a	1.17 ± 0.06	1 → 0 2 → 1	109.55 ± 2.80 104.16 ± 2.71	0.43 0.19	254 ± 7 214 ± 6	9.04 ± 0.01 8.76 ± 0.01	0.53 ± 0.02	9.67 ± 0.01
PGC035472	30.56	0.91 ± 0.06	1 → 0 2 → 1	< 4.30 6.01 ± 2.28	0.76 0.53	— 68 ± 32	< 7.11 $6.81_{-0.21}^{+0.14}$ ^b	— —	$7.54_{-0.21}^{+0.14}$
PGC035503	29.99	0.98 ± 0.05	1 → 0 2 → 1	2.11 ± 0.54 1.85 ± 0.77	0.67 0.41	63 ± 14 21 ± 30	$6.84_{-0.13}^{+0.10}$ $6.40_{-0.23}^{+0.15}$ ^b	0.36 ± 0.18	$7.47_{-0.13}^{+0.10}$
PGC035508	31.07	0.64 ± 0.31	1 → 0 2 → 1	1.93 ± 0.52 3.45 ± 0.99	0.84 0.61	47 ± 14 40 ± 15	$6.73_{-0.14}^{+0.10}$ $6.52_{-0.15}^{+0.11}$	0.62 ± 0.24	$7.37_{-0.14}^{+0.10}$
UGC06517	37.58	1.20 ± 0.07	1 → 0 2 → 1	10.84 ± 1.75 4.50 ± 1.71	0.42 0.19	180 ± 31 96 ± 44	$7.95_{-0.08}^{+0.06}$ $7.31_{-0.21}^{+0.14}$ ^b	0.23 ± 0.09	$8.58_{-0.08}^{+0.06}$
UGC06526	18.14 ^a	1.21 ± 0.06	1 → 0 2 → 1	10.65 ± 2.13 14.68 ± 1.88	0.52 0.30	183 ± 35 118 ± 18	$7.21_{-0.10}^{+0.08}$ $6.99_{-0.06}^{+0.05}$	0.60 ± 0.14	$7.85_{-0.10}^{+0.08}$
PGC035688	38.52	0.99 ± 0.18	1 → 0 2 → 1	6.79 ± 1.40 4.45 ± 1.49	0.68 0.43	165 ± 35 128 ± 40	$7.56_{-0.10}^{+0.08}$ $6.97_{-0.18}^{+0.13}$ ^b	0.26 ± 0.10	$8.19_{-0.10}^{+0.08}$
UGC06545	39.05	1.02 ± 0.08	1 → 0 2 → 1	16.73 ± 2.15 19.66 ± 2.25	0.66 0.40	140 ± 21 136 ± 17	$7.98_{-0.06}^{+0.05}$ 7.66 ± 0.05	0.48 ± 0.08	$8.61_{-0.06}^{+0.05}$
UGC06610	33.55 ^a	1.29 ± 0.03	1 → 0 2 → 1	< 5.73 < 9.26	0.45 0.23	— —	< 7.55 < 7.43	— —	< 8.16
NGC3786	44.85 ^a	1.29 ± 0.03	1 → 0 2 → 1	57.33 ± 2.63 103.15 ± 3.77	0.38 0.17	270 ± 13 288 ± 11	8.88 ± 0.02 8.88 ± 0.02	1.02 ± 0.06	9.51 ± 0.02
NGC3788	53.05 ^a	1.30 ± 0.03	1 → 0 2 → 1	28.49 ± 2.59 29.74 ± 2.64	0.46 0.26	276 ± 29 236 ± 23	8.63 ± 0.04 8.29 ± 0.04	0.46 ± 0.06	9.26 ± 0.04
UGC06637	44.63 ^a	0.88 ± 0.05	1 → 0 2 → 1	3.34 ± 0.76 3.89 ± 0.56	0.78 0.56	114 ± 29 56 ± 11	$7.32_{-0.11}^{+0.09}$ $6.93_{-0.07}^{+0.06}$	0.41 ± 0.11	$7.95_{-0.11}^{+0.09}$
NGC3900	29.76 ^a	1.41 ± 0.03	1 → 0 2 → 1	6.17 ± 1.32 2.49 ± 0.78	0.31 0.13	124 ± 28 21 ± 22	$7.64_{-0.10}^{+0.08}$ $7.01_{-0.16}^{+0.12}$	0.24 ± 0.09	$8.27_{-0.10}^{+0.08}$
UGC06791	32.94 ^a	1.32 ± 0.05	1 → 0 2 → 1	3.47 ± 0.78 8.16 ± 1.61	0.45 0.25	80 ± 18 137 ± 37	$7.31_{-0.11}^{+0.09}$ $7.33_{-0.10}^{+0.08}$	1.04 ± 0.31	$7.95_{-0.11}^{+0.09}$
NGC3912	23.43 ^a	1.18 ± 0.04	1 → 0 2 → 1	22.44 ± 1.36 20.97 ± 1.75	0.49 0.25	96 ± 7 78 ± 7	7.79 ± 0.03 $7.46_{-0.04}^{+0.03}$	0.47 ± 0.05	8.42 ± 0.03
NGC4152	29.61 ^a	1.14 ± 0.03	1 → 0 2 → 1	42.38 ± 2.70 39.05 ± 1.93	0.46 0.21	140 ± 9 111 ± 6	8.30 ± 0.03 7.99 ± 0.02	0.50 ± 0.04	8.93 ± 0.03
NGC4793	28.29 ^a	1.26 ± 0.04	1 → 0 2 → 1	125.15 ± 2.65 128.96 ± 4.30	0.39 0.17	187 ± 5 102 ± 4	8.80 ± 0.01 8.57 ± 0.01	0.59 ± 0.02	9.44 ± 0.01
UGC08076	38.13	0.94 ± 0.04	1 → 0 2 → 1	1.28 ± 0.27 0.81 ± 0.36	0.64 0.36	25 ± 6 10 ± 79	$6.85_{-0.10}^{+0.08}$ $6.30_{-0.25}^{+0.16}$ ^b	0.28 ± 0.14	$7.48_{-0.10}^{+0.08}$
NGC4961	39.96 ^a	1.05 ± 0.05	1 → 0 2 → 1	11.58 ± 1.25 11.13 ± 1.51	0.51 0.25	120 ± 13 68 ± 10	$7.95_{-0.05}^{+0.04}$ 7.65 ± 0.06	0.50 ± 0.09	$8.58_{-0.05}^{+0.04}$

IC0851	44.63 ^a	1.05 ± 0.04	1 → 0 2 → 1	4.00 ± 1.01 4.48 ± 1.14	0.62 0.36	131 ± 43 76 ± 21	$7.50^{+0.10}_{-0.13}$ $7.18^{+0.10}_{-0.13}$	0.48 ± 0.17	$8.13^{+0.10}_{-0.13}$
NGC5012	36.96 ^a	1.42 ± 0.02	1 → 0 2 → 1	82.85 ± 2.18 100.42 ± 4.23	0.25 0.09	270 ± 7 253 ± 12	9.05 ± 0.01 8.95 ± 0.02	0.80 ± 0.04	9.68 ± 0.01
NGC5016	40.34 ^a	1.20 ± 0.03	1 → 0 2 → 1	27.84 ± 2.49 39.15 ± 2.95	0.38 0.16	158 ± 16 157 ± 14	8.46 ± 0.04 8.38 ± 0.03	0.82 ± 0.10	9.09 ± 0.04
UGC08290	40.71 ^a	0.92 ± 0.05	1 → 0 2 → 1	2.53 ± 0.65 1.14 ± 0.49	0.61 0.32	78 ± 22 21 ± 49	$7.23^{+0.10}_{-0.13}$ $6.55^{+0.16}_{-0.24}$ ^b	0.21 ± 0.11	$7.86^{+0.10}_{-0.13}$
UGC08318	38.10 ^a	0.95 ± 0.05	1 → 0 2 → 1	2.67 ± 0.66 < 7.41	0.64 0.36	59 ± 16 —	$7.17^{+0.10}_{-0.12}$ < 7.27	< 1.24	$7.81^{+0.10}_{-0.12}$
NGC5116	43.62 ^a	1.29 ± 0.03	1 → 0 2 → 1	23.10 ± 1.42 21.92 ± 1.38	0.42 0.20	166 ± 11 150 ± 10	8.41 ± 0.03 8.10 ± 0.03	0.49 ± 0.04	9.04 ± 0.03
NGC5117	38.70 ^a	1.19 ± 0.04	1 → 0 2 → 1	2.91 ± 0.55 4.22 ± 1.30	0.46 0.22	106 ± 20 127 ± 35	$7.37^{+0.08}_{-0.09}$ $7.25^{+0.12}_{-0.16}$	0.77 ± 0.28	$8.00^{+0.08}_{-0.09}$
UGC08409	42.95 ^a	0.98 ± 0.05	1 → 0 2 → 1	< 1.43 4.70 ± 0.88	0.63 0.35	— 169 ± 36	< 7.01 $7.18^{+0.07}_{-0.09}$	—	$7.91^{+0.07}_{-0.09}$
NGC5169	42.44 ^a	1.18 ± 0.04	1 → 0 2 → 1	6.00 ± 0.79 11.27 ± 1.38	0.50 0.26	116 ± 14 118 ± 14	$7.72^{+0.05}_{-0.06}$ $7.69^{+0.05}_{-0.06}$	0.92 ± 0.17	$8.36^{+0.05}_{-0.06}$
IC4263	41.08 ^a	1.23 ± 0.04	1 → 0 2 → 1	< 1.43 1.94 ± 0.79	0.49 0.27	— 131 ± 60	< 7.08 $6.87^{+0.15}_{-0.23}$ ^b	—	$7.60^{+0.15}_{-0.23}$
PGC047274	39.33	0.96 ± 0.05	1 → 0 2 → 1	2.73 ± 0.58 3.35 ± 0.73	0.69 0.43	141 ± 33 86 ± 23	$7.17^{+0.08}_{-0.10}$ $6.87^{+0.09}_{-0.11}$	0.50 ± 0.15	$7.81^{+0.08}_{-0.10}$
PGC047295	40.59	0.93 ± 0.06	1 → 0 2 → 1	7.02 ± 1.16 10.51 ± 1.40	0.66 0.38	148 ± 28 88 ± 12	$7.63^{+0.07}_{-0.08}$ $7.45^{+0.08}_{-0.06}$	0.65 ± 0.14	$8.27^{+0.07}_{-0.08}$
UGC08630	34.66 ^a	1.25 ± 0.03	1 → 0 2 → 1	8.53 ± 1.89 9.49 ± 3.21	0.48 0.26	372 ± 80 318 ± 12	$7.72^{+0.09}_{-0.11}$ $7.43^{+0.13}_{-0.18}$ ^b	0.52 ± 0.21	$8.35^{+0.09}_{-0.11}$
UGC08662	30.46 ^a	1.16 ± 0.03	1 → 0 2 → 1	< 8.59 < 3.71	0.57 0.35	— —	< 7.53 < 6.78	—	< 7.51
UGC08693	42.82 ^a	1.07 ± 0.04	1 → 0 2 → 1	7.11 ± 0.84 7.40 ± 1.55	0.57 0.30	114 ± 17 119 ± 31	7.75 ± 0.05 $7.44^{+0.08}_{-0.10}$	0.49 ± 0.12	8.38 ± 0.05
NGC5289	40.24 ^a	1.37 ± 0.04	1 → 0 2 → 1	6.42 ± 1.27 8.77 ± 2.18	0.41 0.22	158 ± 46 271 ± 76	$7.79^{+0.08}_{-0.10}$ $7.59^{+0.10}_{-0.12}$	0.63 ± 0.20	$8.43^{+0.08}_{-0.10}$
NGC5290	35.62 ^a	1.51 ± 0.06	1 → 0 2 → 1	99.00 ± 2.25 126.23 ± 3.09	0.29 0.13	248 ± 6 242 ± 7	9.03 ± 0.01 8.87 ± 0.01	0.70 ± 0.02	9.66 ± 0.01
NGC5297	30.46 ^a	1.57 ± 0.03	1 → 0 2 → 1	27.59 ± 1.75 28.79 ± 2.86	0.26 0.12	145 ± 10 169 ± 19	8.38 ± 0.03 $8.15^{+0.04}_{-0.05}$	0.58 ± 0.07	9.02 ± 0.03
UGC08733	30.88 ^a	1.29 ± 0.03	1 → 0 2 → 1	3.56 ± 0.68 3.03 ± 1.03	0.37 0.16	84 ± 18 87 ± 26	$7.36^{+0.08}_{-0.09}$ $7.05^{+0.13}_{-0.18}$ ^b	0.49 ± 0.19	$7.99^{+0.08}_{-0.09}$
PGC049002	40.79	0.83 ± 0.06	1 → 0 2 → 1	18.26 ± 1.69 34.43 ± 2.39	0.72 0.44	163 ± 18 147 ± 12	8.01 ± 0.04 7.90 ± 0.03	0.77 ± 0.09	8.65 ± 0.04
NGC5311	40.78	1.30 ± 0.03	1 → 0 2 → 1	40.76 ± 3.12 49.82 ± 3.74	0.28 0.11	452 ± 34 283 ± 25	8.78 ± 0.03 8.68 ± 0.03	0.80 ± 0.09	9.41 ± 0.03
UGC08736	36.73	1.13 ± 0.04	1 → 0 2 → 1	8.66 ± 1.66 8.62 ± 1.72	0.53 0.28	79 ± 20 64 ± 15	$7.73^{+0.08}_{-0.09}$ $7.41^{+0.08}_{-0.10}$	0.48 ± 0.13	$8.36^{+0.08}_{-0.09}$
NGC5313	43.62 ^a	1.26 ± 0.07	1 → 0 2 → 1	79.00 ± 3.21 91.14 ± 3.19	0.37 0.16	283 ± 12 266 ± 10	8.99 ± 0.02 $8.82^{+0.01}_{-0.02}$	0.67 ± 0.04	9.63 ± 0.02

NGC5320	36.28 ^a	1.26 ± 0.04	1 → 0 2 → 1	21.11 ± 1.83 19.73 ± 2.67	0.39 0.17	198 ± 20 181 ± 28	8.24 ± 0.04 7.97 ± 0.06	0.53 ± 0.08	8.88 ± 0.04
IC4336	38.61	1.14 ± 0.04	1 → 0 2 → 1	25.80 ± 1.95 42.73 ± 2.30	0.58 0.34	174 ± 14 131 ± 8	8.21 ± 0.03 8.06 ± 0.02	0.70 ± 0.07	8.84 ± 0.03
NGC5326	26.90 ^a	1.34 ± 0.03	1 → 0 2 → 1	4.84 ± 1.58 8.86 ± 2.16	0.36 0.16	318 ± 12 198 ± 66	$7.38^{+0.12}_{-0.17}$ $7.40^{+0.09}_{-0.12}$	1.04 ± 0.42	$8.01^{+0.12}_{-0.17}$
PGC049191	38.34 ^a	0.81 ± 0.07	1 → 0 2 → 1	3.02 ± 0.55 5.75 ± 0.81	0.70 0.41	39 ± 9 23 ± 4	$7.19^{+0.07}_{-0.09}$ $7.10^{+0.06}_{-0.07}$	0.80 ± 0.18	$7.83^{+0.07}_{-0.09}$
NGC5336	36.22	1.09 ± 0.04	1 → 0 2 → 1	5.62 ± 1.01 4.15 ± 1.49	0.48 0.22	158 ± 29 48 ± 22	$7.58^{+0.07}_{-0.09}$ $7.17^{+0.13}_{-0.19} b$	0.39 ± 0.16	$8.21^{+0.07}_{-0.09}$
NGC5337	49.40 ^a	1.22 ± 0.06	1 → 0 2 → 1	17.98 ± 2.60 9.82 ± 3.59	0.45 0.21	328 ± 56 321 ± 34	$8.38^{+0.06}_{-0.07}$ $7.84^{+0.14}_{-0.20} b$	0.29 ± 0.11	$9.01^{+0.06}_{-0.07}$
PGC2151881	40.83	0.59 ± 0.07	1 → 0 2 → 1	2.37 ± 0.69 2.87 ± 0.94	0.85 0.62	89 ± 29 58 ± 23	$7.06^{+0.11}_{-0.15}$ $6.67^{+0.12}_{-0.17}$	0.41 ± 0.18	$7.69^{+0.11}_{-0.15}$
NGC5346	38.09 ^a	1.19 ± 0.04	1 → 0 2 → 1	2.73 ± 0.74 < 3.71	0.48 0.23	126 ± 47 —	$7.31^{+0.10}_{-0.14}$ < 7.15	< 0.69	$7.94^{+0.10}_{-0.14}$
NGC5347	20.69 ^a	1.21 ± 0.03	1 → 0 2 → 1	36.37 ± 1.58 55.74 ± 2.09	0.37 0.16	96 ± 5 82 ± 4	8.01 ± 0.02 7.96 ± 0.02	0.91 ± 0.05	8.64 ± 0.02
NGC5350	28.95 ^a	1.43 ± 0.02	1 → 0 2 → 1	48.05 ± 1.95 71.26 ± 3.11	0.23 0.08	258 ± 12 220 ± 11	8.64 ± 0.02 8.64 ± 0.02	1.01 ± 0.06	9.27 ± 0.02
PGC049386	39.68	0.75 ± 0.08	1 → 0 2 → 1	3.29 ± 1.10 5.04 ± 1.01	0.79 0.54	75 ± 40 84 ± 18	$7.20^{+0.13}_{-0.18} b$ $6.95^{+0.08}_{-0.10}$	0.56 ± 0.22	$7.69^{+0.08}_{-0.10}$
NGC5358	37.12	1.05 ± 0.04	1 → 0 2 → 1	< 3.37 < 3.30	0.66 0.43	—	< 7.24 < 6.81	—	< 7.54
NGC5348	18.18 ^a	1.59 ± 0.04	1 → 0 2 → 1	8.35 ± 1.93 3.91 ± 1.11	0.28 0.15	124 ± 32 81 ± 22	$7.39^{+0.09}_{-0.11}$ $6.73^{+0.11}_{-0.14}$	0.22 ± 0.08	$8.02^{+0.09}_{-0.11}$
NGC5362	28.03 ^a	1.28 ± 0.03	1 → 0 2 → 1	10.98 ± 1.82 12.52 ± 1.84	0.41 0.19	134 ± 25 147 ± 24	$7.71^{+0.07}_{-0.08}$ $7.49^{+0.06}_{-0.07}$	0.61 ± 0.14	$8.34^{+0.07}_{-0.08}$
NGC5360	22.05 ^a	1.04 ± 0.05	1 → 0 2 → 1	4.30 ± 0.75 3.57 ± 0.56	0.59 0.32	59 ± 15 39 ± 7	$6.94^{+0.07}_{-0.08}$ $6.52^{+0.06}_{-0.07}$	0.38 ± 0.09	$7.57^{+0.07}_{-0.08}$
NGC5371	28.43 ^a	1.60 ± 0.02	1 → 0 2 → 1	52.90 ± 3.18 67.46 ± 4.26	0.13 0.04	361 ± 23 326 ± 23	8.90 ± 0.03 8.88 ± 0.03	0.97 ± 0.08	9.53 ± 0.03
NGC5375	40.71 ^a	1.37 ± 0.03	1 → 0 2 → 1	7.48 ± 1.09 19.32 ± 2.14	0.24 0.09	117 ± 18 203 ± 27	$8.10^{+0.06}_{-0.07}$ 8.34 ± 0.05	1.74 ± 0.32	$8.73^{+0.06}_{-0.07}$
NGC5383	36.03 ^a	1.39 ± 0.03	1 → 0 2 → 1	153.53 ± 2.63 114.84 ± 4.19	0.22 0.08	210 ± 4 150 ± 8	9.34 ± 0.01 9.06 ± 0.02	0.52 ± 0.02	9.98 ± 0.01
NGC5403	41.35	1.44 ± 0.03	1 → 0 2 → 1	70.50 ± 3.03 84.83 ± 3.18	0.33 0.15	323 ± 15 251 ± 11	8.95 ± 0.02 8.77 ± 0.02	0.65 ± 0.04	9.59 ± 0.02
PGC049824	41.14	0.89 ± 0.18	1 → 0 2 → 1	1.04 ± 0.34 2.54 ± 0.79	0.77 0.55	37 ± 12 59 ± 25	$6.75^{+0.12}_{-0.17}$ $6.68^{+0.12}_{-0.16}$	0.87 ± 0.39	$7.38^{+0.12}_{-0.17}$
PGC049852	39.59	0.67 ± 0.07	1 → 0 2 → 1	2.32 ± 0.74 3.18 ± 1.26	0.83 0.59	98 ± 31 61 ± 22	$7.03^{+0.12}_{-0.17}$ $6.71^{+0.15}_{-0.22} b$	0.48 ± 0.25	$7.66^{+0.12}_{-0.17}$
PGC049927	42.23 ^a	0.87 ± 0.06	1 → 0 2 → 1	3.03 ± 0.66 3.98 ± 1.05	0.65 0.36	45 ± 11 51 ± 17	$7.31^{+0.09}_{-0.11}$ $7.08^{+0.10}_{-0.13}$	0.59 ± 0.20	$7.94^{+0.09}_{-0.11}$
NGC5470	24.09 ^a	1.42 ± 0.03	1 → 0 2 → 1	15.41 ± 1.87 9.99 ± 1.68	0.38 0.21	90 ± 12 77 ± 16	$7.76^{+0.05}_{-0.06}$ $7.22^{+0.05}_{-0.08}$	0.29 ± 0.06	$8.39^{+0.05}_{-0.06}$

NGC5566	18.53 ^a	1.73 ± 0.04	$1 \rightarrow 0$ $2 \rightarrow 1$	71.58 ± 2.58 64.28 ± 2.26	0.14 0.05	322 ± 14 192 ± 8	8.63 ± 0.02 8.43 ± 0.02	0.63 ± 0.03	9.26 ± 0.02
UGC09215	25.12 ^a	1.32 ± 0.03	$1 \rightarrow 0$ $2 \rightarrow 1$	3.08 ± 0.93 2.04 ± 0.62	0.34 0.15	53 ± 13 21 ± 35	$7.14^{+0.11}_{-0.16}$ $6.73^{+0.11}_{-0.16}$	0.39 ± 0.17	$7.77^{+0.11}_{-0.16}$
NGC5636	27.04	1.14 ± 0.04	$1 \rightarrow 0$ $2 \rightarrow 1$	4.32 ± 0.64 6.50 ± 1.50	0.48 0.23	38 ± 7 44 ± 12	$7.21^{+0.06}_{-0.07}$ $7.11^{+0.09}_{-0.11}$	0.79 ± 0.22	$7.84^{+0.06}_{-0.07}$
IC1022	38.83 ^a	0.98 ± 0.04	$1 \rightarrow 0$ $2 \rightarrow 1$	1.25 ± 0.39 4.20 ± 1.22	0.69 0.43	21 ± 88 72 ± 24	$6.83^{+0.12}_{-0.11}$ $6.95^{+0.11}_{-0.15}$	1.33 ± 0.56	$7.46^{+0.12}_{-0.16}$
NGC5661	46.91 ^a	1.06 ± 0.05	$1 \rightarrow 0$ $2 \rightarrow 1$	14.90 ± 1.49 25.64 ± 1.50	0.57 0.30	187 ± 17 141 ± 9	$8.15^{+0.04}_{-0.05}$ $8.06^{+0.02}_{-0.03}$	0.81 ± 0.09	$8.78^{+0.04}_{-0.05}$
NGC5658	23.42 ^a	1.25 ± 0.03	$1 \rightarrow 0$ $2 \rightarrow 1$	2.04 ± 0.80 13.53 ± 1.93	0.50 0.30	35 ± 23 174 ± 37	$6.74^{+0.14}_{-0.22}$ $7.18^{+0.06}_{-0.07}$	2.80 ± 1.17	$7.91^{+0.06}_{-0.07}$
NGC5668	26.36 ^a	1.28 ± 0.04	$1 \rightarrow 0$ $2 \rightarrow 1$	6.21 ± 1.15 4.53 ± 1.08	0.29 0.11	32 ± 10 43 ± 12	$7.57^{+0.07}_{-0.09}$ $7.24^{+0.09}_{-0.12}$	0.47 ± 0.14	$8.20^{+0.07}_{-0.09}$
NGC5692	24.99 ^a	0.98 ± 0.10	$1 \rightarrow 0$ $2 \rightarrow 1$	12.33 ± 1.54 24.08 ± 1.82	0.62 0.34	93 ± 17 108 ± 10	$7.49^{+0.05}_{-0.06}$ 7.43 ± 0.03	0.89 ± 0.13	$8.12^{+0.05}_{-0.06}$
NGC5701	26.40 ^a	1.30 ± 0.04	$1 \rightarrow 0$ $2 \rightarrow 1$	< 5.73 < 3.71	0.29 0.11	— —	< 7.53 < 7.16	— —	< 7.89
NGC5725	23.77 ^a	0.98 ± 0.05	$1 \rightarrow 0$ $2 \rightarrow 1$	6.49 ± 1.09 5.16 ± 0.94	0.64 0.37	129 ± 29 72 ± 14	$7.14^{+0.07}_{-0.08}$ $6.68^{+0.07}_{-0.09}$	0.35 ± 0.09	$7.78^{+0.07}_{-0.08}$
IC1048	29.29 ^a	1.32 ± 0.03	$1 \rightarrow 0$ $2 \rightarrow 1$	36.33 ± 2.18 44.96 ± 2.11	0.45 0.26	165 ± 11 156 ± 8	8.23 ± 0.03 7.96 ± 0.02	0.54 ± 0.04	8.86 ± 0.03
NGC5740	28.69 ^a	1.43 ± 0.02	$1 \rightarrow 0$ $2 \rightarrow 1$	75.98 ± 2.40 118.04 ± 2.49	0.26 0.10	260 ± 8 284 ± 6	8.77 ± 0.01 8.77 ± 0.01	1.00 ± 0.04	9.40 ± 0.01
NGC5746	29.58 ^a	1.86 ± 0.02	$1 \rightarrow 0$ $2 \rightarrow 1$	22.20 ± 2.59 47.38 ± 5.21	0.16 0.08	111 ± 16 448 ± 60	8.48 ± 0.05 8.50 ± 0.05	1.04 ± 0.17	9.11 ± 0.05
UGC09556	54.85 ^a	0.91 ± 0.05	$1 \rightarrow 0$ $2 \rightarrow 1$	1.41 ± 0.54 < 7.41	0.75 0.50	55 ± 18 —	$7.14^{+0.14}_{-0.21}$ < 7.43	< 1.94	$7.78^{+0.14}_{-0.21}$
NGC5777	45.71 ^a	1.47 ± 0.03	$1 \rightarrow 0$ $2 \rightarrow 1$	43.13 ± 2.89 46.17 ± 4.02	0.35 0.19	321 ± 26 206 ± 20	8.80 ± 0.03 8.49 ± 0.04	0.49 ± 0.05	9.44 ± 0.03
IC1066	32.19 ^a	1.08 ± 0.04	$1 \rightarrow 0$ $2 \rightarrow 1$	14.70 ± 1.66 9.70 ± 1.43	0.54 0.28	118 ± 16 111 ± 19	7.84 ± 0.05 $7.34^{+0.06}_{-0.07}$	0.32 ± 0.06	8.47 ± 0.05
IC1067	24.67	1.26 ± 0.06	$1 \rightarrow 0$ $2 \rightarrow 1$	4.98 ± 1.18 3.23 ± 1.05	0.31 0.12	108 ± 22 74 ± 22	$7.38^{+0.09}_{-0.12}$ $6.99^{+0.12}_{-0.17}$	0.41 ± 0.16	$8.01^{+0.09}_{-0.12}$
NGC5806	24.89 ^a	1.48 ± 0.02	$1 \rightarrow 0$ $2 \rightarrow 1$	75.02 ± 2.89 93.33 ± 3.06	0.21 0.08	247 ± 11 250 ± 9	8.73 ± 0.02 8.65 ± 0.01	0.85 ± 0.04	9.36 ± 0.02
UGC09661	19.68	1.02 ± 0.04	$1 \rightarrow 0$ $2 \rightarrow 1$	10.23 ± 1.13 < 9.26	0.51 0.25	94 ± 12 —	7.28 ± 0.05 < 6.95	< 0.47	7.91 ± 0.05
PGC2586382	40.10	0.91 ± 0.06	$1 \rightarrow 0$ $2 \rightarrow 1$	5.54 ± 1.86 10.73 ± 1.72	0.76 0.54	159 ± 58 131 ± 27	$7.46^{+0.13}_{-0.18}$ $7.29^{+0.06}_{-0.08}$	0.69 ± 0.26	$8.02^{+0.06}_{-0.08}$
PGC054037	27.78	0.76 ± 0.12	$1 \rightarrow 0$ $2 \rightarrow 1$	6.88 ± 1.43 6.09 ± 1.08	0.83 0.61	70 ± 16 53 ± 10	$7.19^{+0.08}_{-0.10}$ $6.67^{+0.07}_{-0.08}$	0.30 ± 0.08	$7.83^{+0.08}_{-0.10}$
NGC5894	39.53 ^a	1.47 ± 0.05	$1 \rightarrow 0$ $2 \rightarrow 1$	34.95 ± 2.07 16.79 ± 3.33	0.34 0.19	175 ± 12 84 ± 19	$8.59^{+0.02}_{-0.03}$ $7.93^{+0.08}_{-0.10}$	0.22 ± 0.05	$9.22^{+0.02}_{-0.03}$
PGC054346	39.22	0.92 ± 0.16	$1 \rightarrow 0$ $2 \rightarrow 1$	11.33 ± 2.39 10.70 ± 1.54	0.60 0.32	206 ± 52 113 ± 15	$7.85^{+0.08}_{-0.10}$ $7.50^{+0.06}_{-0.07}$	0.44 ± 0.11	$8.48^{+0.08}_{-0.10}$

UGC09837	41.66 ^a	1.23 ± 0.06	1 → 0 2 → 1	2.53 ± 0.61 1.77 ± 0.74	0.31 0.12	73 ± 21 30 ± 16	7.53 ^{+0.09} _{-0.12} 7.18 ^{+0.15} _{-0.24} ^b	0.44 ± 0.21	8.17 ^{+0.09} _{-0.12}
NGC5951	26.84 ^a	1.48 ± 0.03	1 → 0 2 → 1	15.04 ± 1.76 8.26 ± 1.53	0.33 0.16	97 ± 13 60 ± 13	7.91 ± 0.05 7.34 ^{+0.07} _{-0.09}	0.27 ± 0.06	8.54 ± 0.05
NGC5953	23.10 ^a	1.17 ± 0.04	1 → 0 2 → 1	193.24 ± 2.46 355.60 ± 2.34	0.41 0.18	186 ± 2 188 ± 1	8.79 ± 0.01 8.81 ± 0.01	1.05 ± 0.02	9.42 ± 0.01
NGC5954	32.48 ^a	1.01 ± 0.08	1 → 0 2 → 1	96.77 ± 2.51 167.63 ± 1.86	0.63 0.35	147 ± 4 135 ± 2	8.60 ± 0.01 8.49 ± 0.01	0.77 ± 0.02	9.23 ± 0.01
NGC5956	29.12	1.17 ± 0.06	1 → 0 2 → 1	19.44 ± 1.87 27.28 ± 1.72	0.34 0.14	94 ± 10 103 ± 7	8.07 ± 0.04 8.00 ± 0.03	0.86 ± 0.10	8.70 ± 0.04
NGC5957	28.21	1.39 ± 0.06	1 → 0 2 → 1	17.69 ± 1.74 27.14 ± 1.57	0.19 0.07	62 ± 7 55 ± 4	8.25 ± 0.04 8.29 ^{+0.02} _{-0.03}	1.10 ± 0.13	8.89 ± 0.04
NGC5981	50.90 ^a	1.44 ± 0.05	1 → 0 2 → 1	29.66 ± 2.21 27.34 ± 4.02	0.37 0.20	205 ± 17 234 ± 32	8.71 ± 0.03 8.33 ^{+0.06} _{-0.07}	0.42 ± 0.07	9.34 ± 0.03
NGC5970	28.04 ^a	1.44 ± 0.03	1 → 0 2 → 1	37.54 ± 2.47 22.36 ± 2.50	0.20 0.07	153 ± 12 122 ± 16	8.55 ± 0.03 8.17 ± 0.05	0.42 ± 0.05	9.18 ± 0.03
NGC5985	39.51 ^a	1.60 ± 0.03	1 → 0 2 → 1	15.10 ± 2.77 6.70 ± 2.53	0.16 0.05	226 ± 61 83 ± 43	8.57 ^{+0.07} _{-0.09} 8.08 ^{+0.14} _{-0.21} ^b	0.32 ± 0.13	9.20 ^{+0.07} _{-0.09}
NGC5989	43.70	0.95 ± 0.10	1 → 0 2 → 1	23.98 ± 1.95 23.44 ± 2.00	0.57 0.30	104 ± 9 84 ± 8	8.29 ^{+0.03} _{-0.04} 7.97 ± 0.04	0.47 ± 0.06	8.92 ^{+0.03} _{-0.04}
UGC09991	39.78 ^a	1.09 ± 0.04	1 → 0 2 → 1	< 10.02 < 11.12	0.61 0.37	— —	< 7.80 < 7.46	— —	< 8.19
NGC6012	19.35 ^a	1.25 ± 0.03	1 → 0 2 → 1	28.77 ± 1.29 25.37 ± 1.40	0.35 0.14	138 ± 6 123 ± 7	7.88 ± 0.02 7.61 ± 0.02	0.53 ± 0.04	8.51 ± 0.02
UGC10086	36.28 ^a	0.81 ± 0.13	1 → 0 2 → 1	10.49 ± 1.87 12.51 ± 1.41	0.79 0.55	171 ± 36 126 ± 15	7.63 ^{+0.07} _{-0.09} 7.26 ± 0.05	0.43 ± 0.09	8.26 ^{+0.07} _{-0.09}
IC1151	34.32 ^a	1.35 ± 0.02	1 → 0 2 → 1	14.47 ± 2.28 17.39 ± 2.11	0.35 0.15	128 ± 23 124 ± 17	8.08 ^{+0.06} _{-0.07} 7.91 ^{+0.05} _{-0.06}	0.69 ± 0.14	8.71 ^{+0.06} _{-0.07}
IC1210	49.06 ^a	1.14 ± 0.08	1 → 0 2 → 1	22.35 ± 3.02 23.72 ± 2.11	0.58 0.35	196 ± 35 147 ± 12	8.35 ± 0.06 7.99 ± 0.04	0.44 ± 0.07	8.99 ± 0.06
PGC057611	44.58	0.52 ± 0.41	1 → 0 2 → 1	11.70 ± 1.90 11.08 ± 1.72	0.90 0.71	80 ± 14 80 ± 14	7.80 ^{+0.07} _{-0.08} 7.28 ^{+0.06} _{-0.07}	0.30 ± 0.07	8.44 ^{+0.07} _{-0.08}
UGC10297	37.64 ^a	1.33 ± 0.03	1 → 0 2 → 1	2.29 ± 1.41 4.65 ± 1.18	0.44 0.25	104 ± 62 79 ± 27	7.26 ^{+0.21} _{-0.41} ^b 7.20 ^{+0.10} _{-0.13}	0.89 ± 0.59	7.93 ^{+0.10} _{-0.13}
UGC10413	45.89 ^a	1.01 ± 0.05	1 → 0 2 → 1	3.62 ± 1.71 3.84 ± 1.02	0.65 0.39	77 ± 50 76 ± 21	7.46 ^{+0.17} _{-0.28} ^b 7.10 ^{+0.10} _{-0.13}	0.44 ± 0.24	7.83 ^{+0.10} _{-0.13}
NGC6181	32.75 ^a	1.38 ± 0.02	1 → 0 2 → 1	137.81 ± 3.55 150.55 ± 2.84	0.32 0.13	261 ± 7 275 ± 5	9.05 ± 0.01 8.87 ± 0.01	0.65 ± 0.02	9.69 ± 0.01
NGC6186	43.10	1.20 ± 0.04	1 → 0 2 → 1	94.24 ± 2.65 195.23 ± 2.62	0.49 0.25	214 ± 6 224 ± 3	8.94 ± 0.01 8.95 ± 0.01	1.02 ± 0.03	9.58 ± 0.01
NGC6267	53.05 ^a	1.11 ± 0.04	1 → 0 2 → 1	17.63 ± 2.19 14.53 ± 1.82	0.45 0.21	134 ± 16 103 ± 16	8.43 ^{+0.05} _{-0.06} 8.08 ^{+0.05} _{-0.06}	0.45 ± 0.08	9.06 ^{+0.05} _{-0.06}
NGC6276	40.74	0.81 ± 0.08	1 → 0 2 → 1	3.44 ± 0.96 2.18 ± 1.00	0.72 0.44	90 ± 26 40 ± 13	7.29 ^{+0.11} _{-0.14} 6.70 ^{+0.16} _{-0.27} ^b	0.26 ± 0.14	7.92 ^{+0.11} _{-0.14}
NGC6278	37.03 ^a	1.24 ± 0.04	1 → 0 2 → 1	< 7.16 < 14.82	0.49 0.26	— —	< 7.69 < 7.68	— —	< 8.33

NGC6306	44.96	1.12 ± 0.05	$1 \rightarrow 0$ $2 \rightarrow 1$	36.00 ± 1.68 61.70 ± 1.85	0.58 0.33	182 ± 8 200 ± 6	8.49 ± 0.02 8.37 ± 0.01	0.75 ± 0.04	9.12 ± 0.02
UGC10721	47.18 ^a	1.10 ± 0.04	$1 \rightarrow 0$ $2 \rightarrow 1$	25.30 ± 2.50 36.62 ± 4.08	0.51 0.25	199 ± 19 157 ± 20	$8.43_{-0.05}^{+0.04}$ 8.30 ± 0.05	0.73 ± 0.11	$9.06_{-0.05}^{+0.04}$
UGC10968	43.32	0.72 ± 0.09	$1 \rightarrow 0$ $2 \rightarrow 1$	3.14 ± 1.27 10.84 ± 3.80	0.85 0.63	44 ± 22 98 ± 44	$7.23_{-0.19}^{+0.15} b$ $7.29_{-0.13}^{+0.22} b$	1.16 ± 0.62	$8.02_{-0.19}^{+0.13}$
<hr/>									
PGC038859	36.01	0.81 ± 0.12	$1 \rightarrow 0$ $2 \rightarrow 1$	1.80 ± 0.78 3.79 ± 1.46	0.74 0.47	78 ± 46 80 ± 34	$6.89_{-0.25}^{+0.16} b$ $6.81_{-0.21}^{+0.14} b$	0.84 ± 0.48	$7.54_{-0.21}^{+0.14}$
UGC07143	38.36	1.00 ± 0.04	$1 \rightarrow 0$ $2 \rightarrow 1$	3.44 ± 1.26 5.95 ± 1.04	0.64 0.37	102 ± 29 70 ± 13	$7.29_{-0.20}^{+0.14} b$ $7.16_{-0.08}^{+0.07}$	0.75 ± 0.30	$7.89_{-0.08}^{+0.07}$
UGC07039	39.28 ^a	0.89 ± 0.06	$1 \rightarrow 0$ $2 \rightarrow 1$	< 4.30 < 11.12	0.71 0.44	— —	< 7.36 < 7.38	—	< 7.99
PGC214137	41.00	0.40 ± 0.42	$1 \rightarrow 0$ $2 \rightarrow 1$	7.59 ± 1.34 5.94 ± 1.51	0.95 0.84	179 ± 32 153 ± 46	$7.52_{-0.08}^{+0.07}$ $6.86_{-0.13}^{+0.10}$	0.22 ± 0.07	$8.15_{-0.08}^{+0.07}$
NGC5240	44.67 ^a	1.26 ± 0.03	$1 \rightarrow 0$ $2 \rightarrow 1$	10.15 ± 1.43 < 7.41	0.33 0.14	143 ± 22 —	$8.17_{-0.07}^{+0.06}$ < 7.82	< 0.45	$8.81_{-0.07}^{+0.06}$
NGC5089	48.57 ^a	0.98 ± 0.05	$1 \rightarrow 0$ $2 \rightarrow 1$	9.36 ± 2.04 6.96 ± 1.49	0.60 0.33	162 ± 34 106 ± 23	$7.95_{-0.11}^{+0.09}$ $7.49_{-0.10}^{+0.08}$	0.35 ± 0.11	$8.58_{-0.11}^{+0.09}$
IC0777	55.76 ^a	0.92 ± 0.06	$1 \rightarrow 0$ $2 \rightarrow 1$	15.25 ± 1.96 24.30 ± 1.38	0.71 0.44	138 ± 24 98 ± 6	$8.21_{-0.06}^{+0.05}$ $8.02_{-0.03}^{+0.02}$	0.64 ± 0.09	$8.85_{-0.06}^{+0.05}$

Table B.3: CO results of our IRAM-30m campaign. Column description. (1-3) galaxy ID, distance, and D_{25} diameter, for the sources denoted with the symbol ^a we report redshift independent distances; (4) CO($J \rightarrow J-1$) transition; (5) observed velocity integrated flux, not aperture corrected; (6) filling factor; (7) FWHM of the CO($J \rightarrow J-1$) line; (8) velocity integrated CO($J \rightarrow J-1$) luminosity, tentative detections with $\text{SNR} < 3$ are denoted with the symbol ^b; (9) excitation ratio; (10) total H₂ gas mass. The reported upper limits are at 3σ . Absent values are denoted with the symbol —. The last seven sources were observed as part of our IRAM-30m campaign, but subsequently excluded from our sample of filament galaxies. See text for further details.

Galaxy	Distance (Mpc)	$\log(D_{25}/0.1')$	CO(J → J – 1)	f_{ap}	$\log\left(\frac{L'_{\text{CO}(J \rightarrow J-1)}}{\text{K km s}^{-1} \text{pc}^2}\right)$	r_{J1}	$\log\left(\frac{M_{\text{H}_2}}{M_{\odot}}\right)$	Telescope	Reference
(1)	(2)	(3)	(4)	(5)	(6)	(7)	(8)	(9)	(10)
PGC022100	30.27	0.92 ± 0.05	$1 \rightarrow 0$	0.66	< 7.07	1.0	< 7.71	IRAM 30m	Lisenfeld et al. (2011)
NGC2577	35.62 ^a	1.19 ± 0.04	$1 \rightarrow 0$ $2 \rightarrow 1$	0.52 0.28	< 7.42 < 7.20	1.0 —	< 7.93	IRAM 30m IRAM 30m	Young et al. (2011) Young et al. (2011)
NGC2592	32.57 ^a	1.17 ± 0.04	$1 \rightarrow 0$ $2 \rightarrow 1$	0.43 0.20	< 7.44 < 7.24	1.0 —	< 7.97	IRAM 30m IRAM 30m	Young et al. (2011) Young et al. (2011)
NGC2594	34.13	0.96 ± 0.21	$1 \rightarrow 0$ $2 \rightarrow 1$	0.67 0.40	< 7.28 < 6.83	1.0 —	< 7.56	IRAM 30m IRAM 30m	Young et al. (2011) Young et al. (2011)
UGC04551	27.29	1.23 ± 0.07	$1 \rightarrow 0$ $2 \rightarrow 1$	0.52 0.31	< 7.19 < 7.05	1.0 —	< 7.78	IRAM 30m IRAM 30m	Young et al. (2011) Young et al. (2011)
NGC2679	28.83 ^a	1.27 ± 0.07	$1 \rightarrow 0$ $2 \rightarrow 1$	0.27 0.10	< 7.62 < 7.41	1.0 —	< 8.14	IRAM 30m IRAM 30m	Combes et al. (2007) Combes et al. (2007)
UGC04722	23.86 ^a	1.16 ± 0.03	$1 \rightarrow 0$	0.79	$7.62^{+0.08}_{-0.10}$	1.0	$8.25^{+0.08}_{-0.10}$	FCRAO	Lisenfeld et al. (2011)
NGC2852	29.63 ^a	0.97 ± 0.09	$1 \rightarrow 0$ $2 \rightarrow 1$	0.54 0.27	< 7.28 < 7.03	1.0 —	< 7.76	IRAM 30m IRAM 30m	Young et al. (2011) Young et al. (2011)
NGC2859	24.45 ^a	1.50 ± 0.04	$1 \rightarrow 0$ $2 \rightarrow 1$	0.14 0.05	< 7.67 < 7.62	1.0 —	< 8.31	IRAM 30m IRAM 30m	Young et al. (2011) Young et al. (2011)
PGC027311	25.65	0.87 ± 0.06	$1 \rightarrow 0$	0.74	< 6.81	1.0	< 7.44	IRAM 30m	Lisenfeld et al. (2011)
NGC2964	20.45 ^a	1.47 ± 0.03	$1 \rightarrow 0$ $2 \rightarrow 1$	0.44 0.72	$8.54^{+0.07}_{-0.08}$ 7.63 ± 0.02	1.0 0.12 ± 0.02	$9.17^{+0.07}_{-0.08}$	FCRAO IRAM 30m	Young et al. (1995) Braine et al. (1993)
NGC3032	21.76 ^a	1.15 ± 0.04	$1 \rightarrow 0$ $2 \rightarrow 1$	0.38 0.16	8.15 ± 0.01 7.85 ± 0.01	1.0 0.50 ± 0.02	8.78 ± 0.01	IRAM 30m IRAM 30m	Combes et al. (2007) Combes et al. (2007)
NGC3098	22.68 ^a	1.37 ± 0.06	$1 \rightarrow 0$ $2 \rightarrow 1$	0.42 0.24	< 7.14 < 6.83	1.0 —	< 7.56	IRAM 30m IRAM 30m	Young et al. (2011) Young et al. (2011)
IC0598	34.35	1.22 ± 0.06	$1 \rightarrow 0$ $2 \rightarrow 1$	0.53 0.32	< 7.57 < 7.25	1.0 —	< 7.98	IRAM 30m IRAM 30m	Young et al. (2011) Young et al. (2011)
NGC3193	28.82 ^a	1.37 ± 0.03	$1 \rightarrow 0$ $2 \rightarrow 1$	0.22 0.08	< 7.75 < 7.48	1.0 —	< 8.21	IRAM 30m IRAM 30m	Young et al. (2011) Young et al. (2011)
NGC3245	21.39 ^a	1.56 ± 0.03	$1 \rightarrow 0$ $2 \rightarrow 1$	0.17 0.06	$7.38^{+0.12}_{-0.16}$ < 7.25	1.0 < 0.74	$8.01^{+0.12}_{-0.16}$	IRAM 30m IRAM 30m	Young et al. (2011) Young et al. (2011)
NGC3248	23.87	1.23 ± 0.04	$1 \rightarrow 0$ $2 \rightarrow 1$	0.46 0.22	< 7.17 < 7.05	1.0 —	< 7.78	IRAM 30m IRAM 30m	Young et al. (2011) Young et al. (2011)
NGC3265	21.88	0.98 ± 0.09	$3 \rightarrow 2$	—	< 7.42	—	< 8.36	JCMT	Wilson et al. (2012)
NGC3277	25.33 ^a	1.32 ± 0.03	$1 \rightarrow 0$	0.22	$8.37^{+0.12}_{-0.18}$	1.0	$9.01^{+0.12}_{-0.18}$	Kitt-Peak 12m	Boselli et al. (2014a)
NGC3294	28.46 ^a	1.49 ± 0.04	$1 \rightarrow 0$	0.11	$8.78^{+0.12}_{-0.18}$	1.0	$9.42^{+0.12}_{-0.18}$	SEST	Boselli et al. (2014a)
NGC3424	28.04 ^a	1.40 ± 0.06	$1 \rightarrow 0$ $2 \rightarrow 1$	0.21 0.17	< 7.68 < 7.80	1.0 —	< 8.32	IRAM 30m IRAM 30m	Boselli et al. (2014a) Braine et al. (1993)
NGC3430	28.88 ^a	1.60 ± 0.04	$1 \rightarrow 0$ $2 \rightarrow 1$	0.08 0.05	< 8.51 < 8.79	1.0 —	< 9.14	IRAM 30m IRAM 30m	Boselli et al. (2014a) Braine et al. (1993)
NGC3504	19.85 ^a	1.39 ± 0.03	$1 \rightarrow 0$	—	$8.79^{+0.05}_{-0.06}$	1.0	$9.42^{+0.05}_{-0.06}$	FCRAO, SEST	Boselli et al. (2014a)
NGC3595	33.83	1.18 ± 0.08	$1 \rightarrow 0$ $2 \rightarrow 1$	0.56 0.34	< 7.37 < 6.86	1.0 —	< 7.59	IRAM 30m IRAM 30m	Young et al. (2011) Young et al. (2011)
NGC3648	31.09	1.08 ± 0.04	$1 \rightarrow 0$ $2 \rightarrow 1$	0.57 0.30	< 7.30 < 7.04	1.0 —	< 7.77	IRAM 30m IRAM 30m	Young et al. (2011) Young et al. (2011)
NGC3658	31.93	1.24 ± 0.07	$1 \rightarrow 0$ $2 \rightarrow 1$	0.31 0.12	< 7.61 < 7.44	1.0 —	< 8.17	IRAM 30m IRAM 30m	Young et al. (2011) Young et al. (2011)
NGC3665	23.03 ^a	1.61 ± 0.04	$1 \rightarrow 0$	—	8.09 ± 0.01	1.0	8.72 ± 0.01	CARMA	Alatalo et al. (2013)

NGC3694	35.95 ^a	1.00 ± 0.10	$1 \rightarrow 0$ $2 \rightarrow 1$	0.59 0.31	< 7.46 < 7.22	1.0 —	< 7.95	IRAM 30m IRAM 30m	Young et al. (2011) Young et al. (2011)
NGC3796	22.07	1.16 ± 0.08	$1 \rightarrow 0$ $2 \rightarrow 1$	0.52 0.27	< 7.07 < 6.65	1.0 —	< 7.38	IRAM 30m IRAM 30m	Young et al. (2011) Young et al. (2011)
NGC3838	22.86	1.15 ± 0.08	$1 \rightarrow 0$ $2 \rightarrow 1$	0.56 0.32	< 7.06 < 6.60	1.0 —	< 7.33	IRAM 30m IRAM 30m	Young et al. (2011) Young et al. (2011)
NGC3898	22.27 ^a	1.54 ± 0.02	$1 \rightarrow 0$	0.11	< 7.74	1.0	< 8.37	Kitt-Peak 12m	Boselli et al. (2014a)
NGC3953	17.77 ^a	1.79 ± 0.02	$1 \rightarrow 0$	—	$9.14^{+0.10}_{-0.13}$	1.0	$9.77^{+0.10}_{-0.13}$	FCRAO	Young et al. (1995)
NGC3982	20.59 ^a	1.27 ± 0.04	$1 \rightarrow 0$	0.34	$8.63^{+0.12}_{-0.18}$	1.0	$9.26^{+0.12}_{-0.18}$	Kitt-Peak 12m	Boselli et al. (2014a)
NGC3992	19.99 ^a	1.85 ± 0.03	$1 \rightarrow 0$	0.21	8.35 ± 0.04	1.0	8.99 ± 0.04	Kitt-Peak 12m	Vila-Vilaro et al. (2015)
NGC3998	21.10 ^a	1.44 ± 0.03	$1 \rightarrow 0$ $2 \rightarrow 1$	0.19 0.07	< 7.45 < 7.21	1.0 —	< 7.94	IRAM 30m IRAM 30m	Young et al. (2011) Young et al. (2011)
NGC4026	15.79 ^a	1.64 ± 0.03	$1 \rightarrow 0$ $2 \rightarrow 1$	0.25 0.13	< 7.06 < 6.56	1.0 —	< 7.29	IRAM 30m IRAM 30m	Young et al. (2011) Young et al. (2011)
NGC4051	13.95 ^a	1.77 ± 0.02	$1 \rightarrow 0$	—	$8.55^{+0.08}_{-0.09}$	1.0	$9.18^{+0.08}_{-0.09}$	FCRAO	Young et al. (1995)
NGC4088	14.51 ^a	1.74 ± 0.02	$1 \rightarrow 0$	—	$8.76^{+0.07}_{-0.08}$	1.0	$9.40^{+0.07}_{-0.08}$	FCRAO	Young et al. (1995)
NGC4096	12.24 ^a	1.75 ± 0.02	$1 \rightarrow 0$	—	$8.22^{+0.08}_{-0.10}$	1.0	$8.85^{+0.08}_{-0.10}$	FCRAO	Young et al. (1995)
NGC4100	20.31 ^a	1.66 ± 0.02	$1 \rightarrow 0$	0.14	$8.99^{+0.12}_{-0.18}$	1.0	$9.62^{+0.12}_{-0.18}$	Kitt-Peak 12m	Boselli et al. (2014a)
NGC4111	13.75 ^a	1.25 ± 0.03	$1 \rightarrow 0$ $2 \rightarrow 1$	0.50 0.30	$6.77^{+0.09}_{-0.11}$ 6.87 ± 0.04	1.0 1.25 ± 0.30	$7.41^{+0.09}_{-0.11}$	IRAM 30m IRAM 30m	Welch & Sage (2003) Welch & Sage (2003)
NGC4138	16.37 ^a	1.46 ± 0.03	$1 \rightarrow 0$	0.51	$7.82^{+0.11}_{-0.15}$	1.0	$8.45^{+0.11}_{-0.15}$	FCRAO	Young et al. (1995)
NGC4143	17.57 ^a	1.42 ± 0.03	$1 \rightarrow 0$ $2 \rightarrow 1$	0.29 0.12	< 7.15 < 7.35	1.0 —	< 7.79	IRAM 30m IRAM 30m	Welch & Sage (2003) Welch & Sage (2003)
NGC4144	6.85 ^a	1.72 ± 0.03	$1 \rightarrow 0$	—	$6.81^{+0.09}_{-0.12}$	1.0	$7.44^{+0.09}_{-0.12}$	Kitt-Peak 12m	Sage (1993)
NGC4151	11.27 ^a	1.46 ± 0.04	$1 \rightarrow 0$ $2 \rightarrow 1$	— 0.56	$8.08^{+0.09}_{-0.11}$ < 6.27	1.0 —	$8.72^{+0.09}_{-0.11}$	FCRAO IRAM 30m	Young et al. (1995) Braine et al. (1993)
UGC07271	12.59 ^a	1.07 ± 0.04	$1 \rightarrow 0$	—	< 6.81	1.0	< 7.44	Kitt-Peak 12m	Sage (1993)
NGC4214	2.87 ^a	1.83 ± 0.03	$1 \rightarrow 0$	0.16	$5.78^{+0.08}_{-0.10}$	1.0	$6.41^{+0.08}_{-0.10}$	FCRAO	Young et al. (1995)
NGC4244	4.26 ^a	2.21 ± 0.03	$1 \rightarrow 0$	—	$6.94^{+0.05}_{-0.06}$	1.0	$7.57^{+0.05}_{-0.06}$	Kitt-Peak 12m	Sage (1993)
NGC4314	9.81 ^a	1.57 ± 0.03	$1 \rightarrow 0$ $2 \rightarrow 1$	0.26 0.26	8.04 ± 0.01 7.24 ± 0.01	1.0 0.159 ± 0.003	8.67 ± 0.01	IRAM 30m IRAM 30m	Braine et al. (1993) Braine et al. (1993)
NGC4359	18.41 ^a	1.14 ± 0.04	$1 \rightarrow 0$	—	< 7.18	1.0	< 7.82	Kitt-Peak 12m	Sage (1993)
NGC4414	17.61 ^a	1.29 ± 0.04	$1 \rightarrow 0$ $2 \rightarrow 1$	— 0.86	$9.32^{+0.07}_{-0.09}$ 7.70 ± 0.02	1.0 —	$9.95^{+0.07}_{-0.09}$	FCRAO IRAM 30m	Young et al. (1995) Braine et al. (1993)
NGC4448	20.19 ^a	1.20 ± 0.07	$1 \rightarrow 0$	—	8.07 ± 0.05	1.0	8.70 ± 0.05	Kitt-Peak 12m	Sage (1993)
NGC4525	13.01 ^a	1.30 ± 0.04	$1 \rightarrow 0$	0.37	$7.40^{+0.12}_{-0.18}$	1.0	$8.03^{+0.12}_{-0.18}$	Kitt-Peak 12m	Boselli et al. (2014a)
NGC4559	7.81 ^a	2.02 ± 0.02	$1 \rightarrow 0$ $2 \rightarrow 1$ $3 \rightarrow 2$	— 0.51 —	$8.11^{+0.05}_{-0.06}$ $6.27^{+0.02}_{-0.03}$ $7.13^{+0.08}_{-0.10}$	1.0 — —	$8.75^{+0.05}_{-0.06}$	Kitt-Peak 12m IRAM 30m JCMT	Sage (1993) Braine et al. (1993) Wilson et al. (2012)
NGC5173	38.52 ^a	1.04 ± 0.04	$1 \rightarrow 0$ $2 \rightarrow 1$	— 0.23	7.66 ± 0.01 7.79 ± 0.03	1.0 1.36 ± 0.10	8.29 ± 0.01	CARMA IRAM 30m	Alatalo et al. (2013) Young et al. (2011)
NGC5198	41.27 ^a	1.31 ± 0.07	$1 \rightarrow 0$ $2 \rightarrow 1$	0.30 0.12	< 7.70 < 7.36	1.0 —	< 8.09	IRAM 30m IRAM 30m	Combes et al. (2007) Combes et al. (2007)
NGC5248	12.62 ^a	1.61 ± 0.03	$1 \rightarrow 0$	—	$8.98^{+0.05}_{-0.06}$	1.0	$9.61^{+0.05}_{-0.06}$	FCRAO	Boselli et al. (2014a)
NGC5300	19.62 ^a	1.45 ± 0.03	$1 \rightarrow 0$	0.15	$7.98^{+0.12}_{-0.18}$ ^b	1.0	$8.62^{+0.12}_{-0.18}$	Kitt-Peak 12m	Boselli et al. (2014a)

NGC5353	33.81 ^a	1.38 ± 0.03	$1 \rightarrow 0$ $2 \rightarrow 1$	0.39 0.20	$7.99^{+0.05}_{-0.06}$ $8.13^{+0.02}_{-0.03}$	1.0 1.38 ± 0.20	$8.62^{+0.05}_{-0.06}$	IRAM 30m IRAM 30m	O'Sullivan et al. (2018) O'Sullivan et al. (2018)
NGC5355	35.59 ^a	1.06 ± 0.04	$1 \rightarrow 0$ $2 \rightarrow 1$	0.57 0.31	< 7.44 < 7.35	1.0 —	< 8.08	IRAM 30m IRAM 30m	Young et al. (2011) Young et al. (2011)
NGC5356	24.87 ^a	1.45 ± 0.03	$1 \rightarrow 0$	0.41	$8.31^{+0.12}_{-0.18}$ ^b	1.0	$8.95^{+0.12}_{-0.18}$	Kitt-Peak 12m	Boselli et al. (2014a)
NGC5363	19.41 ^a	1.62 ± 0.03	$1 \rightarrow 0$	0.05	$9.00^{+0.12}_{-0.18}$	1.0	$9.63^{+0.12}_{-0.18}$	Kitt-Peak 12m	Boselli et al. (2014a)
NGC5364	17.17 ^a	1.58 ± 0.03	$1 \rightarrow 0$ $2 \rightarrow 1$	0.78 0.78	$7.36^{+0.08}_{-0.10}$ $6.76^{+0.06}_{-0.08}$	1.0 0.25 ± 0.06	$7.99^{+0.08}_{-0.10}$	IRAM 30m IRAM 30m	Braine et al. (1993) Braine et al. (1993)
NGC5560	19.15 ^a	1.54 ± 0.04	$1 \rightarrow 0$	0.43	$8.15^{+0.12}_{-0.18}$	1.0	$8.78^{+0.12}_{-0.18}$	Kitt-Peak 12m	Boselli et al. (2014a)
NGC5574	24.42 ^a	1.12 ± 0.04	$1 \rightarrow 0$ $2 \rightarrow 1$	0.53 0.27	< 7.13 < 6.76	1.0 —	< 7.49	IRAM 30m IRAM 30m	Young et al. (2011) Young et al. (2011)
NGC5576	21.27 ^a	1.45 ± 0.03	$1 \rightarrow 0$ $2 \rightarrow 1$	0.36 0.20	< 7.21 < 6.76	1.0 —	< 7.49	IRAM 30m IRAM 30m	Young et al. (2011) Young et al. (2011)
NGC5577	23.21 ^a	1.46 ± 0.03	$1 \rightarrow 0$	0.39	$7.91^{+0.12}_{-0.18}$	1.0	$8.54^{+0.12}_{-0.18}$	Kitt-Peak 12m	Boselli et al. (2014a)
NGC5638	25.10 ^a	1.29 ± 0.04	$1 \rightarrow 0$ $2 \rightarrow 1$	0.03 0.11	< 7.32 < 7.10	1.0 —	< 7.83	IRAM 30m IRAM 30m	Boselli et al. (2014a) Young et al. (2011)
NGC5645	19.00 ^a	1.30 ± 0.04	$1 \rightarrow 0$	0.29	< 7.65	1.0	< 8.29	Kitt-Peak 12m	Boselli et al. (2014a)
IC1024	21.98 ^a	1.04 ± 0.06	$1 \rightarrow 0$ $2 \rightarrow 1$	— 0.43	8.05 ± 0.01 7.73 ± 0.01	1.0 0.48 ± 0.01	8.68 ± 0.01	CARMA IRAM 30m	Alatalo et al. (2013) Young et al. (2011)
NGC5770	20.80 ^a	1.04 ± 0.06	$1 \rightarrow 0$ $2 \rightarrow 1$	0.52 0.25	< 7.02 < 6.68	1.0 —	< 7.41	IRAM 30m IRAM 30m	Young et al. (2011) Young et al. (2011)
NGC5813	29.58 ^a	1.62 ± 0.02	$1 \rightarrow 0$ $2 \rightarrow 1$	0.26 0.14	< 6.95 < 6.80	1.0 —	< 7.53	IRAM 30m IRAM 30m	O'Sullivan et al. (2018) O'Sullivan et al. (2018)
NGC5831	27.18 ^a	1.35 ± 0.03	$1 \rightarrow 0$ $2 \rightarrow 1$	0.24 0.09	< 7.74 < 7.58	1.0 —	< 8.31	IRAM 30m IRAM 30m	Combes et al. (2007) Combes et al. (2007)
NGC5838	26.94 ^a	1.59 ± 0.02	$1 \rightarrow 0$ $2 \rightarrow 1$	0.28 0.15	< 7.55 < 7.36	1.0 —	< 8.09	IRAM 30m IRAM 30m	Combes et al. (2007) Combes et al. (2007)
NGC5839	23.69 ^a	1.16 ± 0.04	$1 \rightarrow 0$ $2 \rightarrow 1$	0.38 0.16	< 7.16 < 6.84	1.0 —	< 7.57	IRAM 30m IRAM 30m	Young et al. (2011) Young et al. (2011)
NGC5845	28.82 ^a	1.00 ± 0.07	$1 \rightarrow 0$ $2 \rightarrow 1$	0.66 0.40	< 7.04 < 6.52	1.0 —	< 7.25	IRAM 30m IRAM 30m	Combes et al. (2007) Combes et al. (2007)
NGC5846	25.13 ^a	1.63 ± 0.03	$1 \rightarrow 0$ $2 \rightarrow 1$	0.09 0.03	$7.73^{+0.12}_{-0.18}$ $7.53^{+0.11}_{-0.15}$	1.0 0.64 ± 0.28	$8.36^{+0.12}_{-0.18}$	IRAM 30m IRAM 30m	O'Sullivan et al. (2018) O'Sullivan et al. (2018)
NGC5854	22.00 ^a	1.48 ± 0.04	$1 \rightarrow 0$ $2 \rightarrow 1$	0.34 0.19	< 7.21 < 6.73	1.0 —	< 7.46	IRAM 30m IRAM 30m	Young et al. (2011) Young et al. (2011)
NGC5864	25.93 ^a	1.40 ± 0.06	$1 \rightarrow 0$ $2 \rightarrow 1$	0.40 0.22	< 7.34 < 7.00	1.0 —	< 7.73	IRAM 30m IRAM 30m	Young et al. (2011) Young et al. (2011)
NGC5869	27.72 ^a	1.34 ± 0.03	$1 \rightarrow 0$ $2 \rightarrow 1$	0.32 0.13	< 7.52 < 7.23	1.0 —	< 7.96	IRAM 30m IRAM 30m	Young et al. (2011) Young et al. (2011)
PGC054452	28.82	0.98 ± 0.05	$1 \rightarrow 0$ $2 \rightarrow 1$	0.58 0.31	< 7.24 < 6.96	1.0 —	< 7.69	IRAM 30m IRAM 30m	Young et al. (2011) Young et al. (2011)
NGC5982	36.12 ^a	1.49 ± 0.06	$1 \rightarrow 0$ $2 \rightarrow 1$	0.34 0.18	< 7.03 < 7.00	1.0 —	< 7.67	IRAM 30m IRAM 30m	O'Sullivan et al. (2015) O'Sullivan et al. (2015)

Table B.4: CO results from the literature. Column description. (1-3) galaxy ID, distance, and D_{25} diameter, for the sources denoted with the symbol ^a we report redshift independent distances; (4) CO($J \rightarrow J-1$) transition; (5) filling factor, which is not reported in the cases where the CO observations correspond to multiple pointings or maps; (6) velocity integrated CO($J \rightarrow J-1$) luminosity, tentative detections with $\text{SNR} < 3$ are denoted with the symbol ^b; (7) excitation ratio; (8) total H₂ gas mass; (9) telescope; (10) reference. Absent values are denoted with the symbol —. Upper limits are at 3σ .

Galaxy (1)	Distance (Mpc) (2)	$S_{\text{HI}} \Delta v$ (Jy km s ⁻¹) (3)	FWHM (4)	$\log \left(\frac{M_{\text{HI}}}{M_{\odot}} \right)$ (5)	Reference (6)
PGC022100	30.27	1.80 ± 0.13	143 ± 11	8.59 ± 0.03	This work
IC2256	35.33^a	4.27 ± 0.53	—	$9.10^{+0.05}_{-0.06}$	Springob et al. (2005)
NGC2577	35.62^a	< 0.35	—	< 8.02	Huchtmeier & Richter (1989)
UGC04375	40.34^a	16.45 ± 2.29	—	$9.80^{+0.06}_{-0.07}$	Springob et al. (2005)
IC2361	30.33	1.09 ± 0.35	—	$8.37^{+0.12}_{-0.17}$	de Vaucouleurs et al. (1991)
UGC04395	38.17^a	6.23 ± 1.20	—	$9.33^{+0.08}_{-0.09}$	Springob et al. (2005)
NGC2592	32.57^a	0.62 ± 0.11	105 ± 19	$8.19^{+0.07}_{-0.08}$	This work
NGC2594	34.13	2.67 ± 0.45	235 ± 48	$8.87^{+0.07}_{-0.08}$	This work
PGC023706	32.60	1.44 ± 0.15	114 ± 13	$8.56^{+0.04}_{-0.05}$	This work
NGC2604	30.69	17.09 ± 3.46	—	$9.58^{+0.08}_{-0.10}$	de Vaucouleurs et al. (1991)
PGC024012	32.82	1.59 ± 0.13	163 ± 12	$8.61^{+0.03}_{-0.04}$	This work
NGC2608	23.27^a	6.24 ± 0.83	—	$8.90^{+0.05}_{-0.06}$	Springob et al. (2005)
UGC04551	27.29	< 0.39	—	< 7.84	This work
UGC04559	41.08^a	19.24 ± 2.82	—	$9.88^{+0.06}_{-0.07}$	Springob et al. (2005)
PGC1925809	30.48	< 0.39	—	< 7.94	This work
NGC2679	28.83^a	0.29 ± 0.09	93 ± 22	$7.75^{+0.12}_{-0.16}$	This work
UGC04659	36.62^a	7.29 ± 0.86	—	9.36 ± 0.05	Springob et al. (2005)
PGC025063	30.43	0.43 ± 0.08	104 ± 21	$7.97^{+0.07}_{-0.09}$	This work
NGC2712	31.02^a	24.28 ± 1.23	—	9.74 ± 0.02	Springob et al. (2005)
PGC025273	28.60	0.50 ± 0.08	91 ± 15	$7.98^{+0.06}_{-0.07}$	This work
UGC04722	23.86^a	13.58 ± 2.75	—	$9.26^{+0.08}_{-0.10}$	de Vaucouleurs et al. (1991)
NGC2780	52.55^a	1.50 ± 0.48	—	$8.99^{+0.12}_{-0.17}$	de Vaucouleurs et al. (1991)
NGC2793	26.65^a	8.26 ± 0.85	—	$9.14^{+0.04}_{-0.05}$	Springob et al. (2005)
UGC04902	25.14	0.73 ± 0.08	95 ± 10	8.03 ± 0.05	This work
NGC2798	23.43^a	9.93 ± 0.96	—	9.11 ± 0.04	de Vaucouleurs et al. (1991)
NGC2799	27.78^a	11.09 ± 3.53	—	$9.31^{+0.12}_{-0.17}$	de Vaucouleurs et al. (1991)
NGC2844	42.14^a	9.49 ± 0.99	—	$9.60^{+0.04}_{-0.05}$	Springob et al. (2005)
NGC2852	29.63^a	4.05 ± 0.16	214 ± 9	8.92 ± 0.02	This work
NGC2853	28.55^a	3.85 ± 0.13	204 ± 7	8.87 ± 0.01	This work
NGC2859	24.45^a	3.55 ± 0.75	—	$8.70^{+0.08}_{-0.10}$	Springob et al. (2005)
UGC05015	25.79	5.70 ± 1.16	—	$8.95^{+0.08}_{-0.10}$	de Vaucouleurs et al. (1991)
UGC05020	32.36^a	7.55 ± 1.04	—	9.27 ± 0.06	Springob et al. (2005)
NGC2893	27.14^a	4.88 ± 0.47	—	8.93 ± 0.04	de Vaucouleurs et al. (1991)

PGC027311	25.65	0.62 ± 0.08	106 ± 13	$7.98^{+0.05}_{-0.06}$	This work
NGC2964	20.45 ^a	25.75 ± 1.10	—	9.41 ± 0.02	Springob et al. (2005)
NGC2968	13.74 ^a	3.63 ± 1.16	—	$8.21^{+0.12}_{-0.17}$	de Vaucouleurs et al. (1991)
NGC2970	27.02 ^a	0.36 ± 0.07	53 ± 13	$7.79^{+0.07}_{-0.09}$	This work
PGC028169	24.76 ^a	2.79 ± 0.89	—	$8.61^{+0.12}_{-0.17}$	de Vaucouleurs et al. (1991)
NGC3003	20.78 ^a	113.63 ± 6.57	—	$10.06^{+0.02}_{-0.03}$	Springob et al. (2005)
NGC3026	24.59 ^a	11.20 ± 1.10	—	9.20 ± 0.04	de Vaucouleurs et al. (1991)
NGC3021	26.47 ^a	12.97 ± 1.37	—	$9.33^{+0.04}_{-0.05}$	Springob et al. (2005)
UGC05287	31.93 ^a	4.98 ± 0.55	—	9.08 ± 0.05	Springob et al. (2005)
NGC3032	21.76 ^a	0.64 ± 0.06	—	7.85 ± 0.04	Lucero & Young (2013)
UGC05326	22.96	4.30 ± 0.10	—	8.73 ± 0.01	O’Neil (2004)
NGC3067	19.58 ^a	6.80 ± 0.66	—	8.79 ± 0.04	de Vaucouleurs et al. (1991)
NGC3098	22.68 ^a	5.37 ± 1.70	—	$8.81^{+0.12}_{-0.17}$	de Vaucouleurs et al. (1991)
PGC029347	23.97 ^a	1.02 ± 0.21	—	$8.14^{+0.08}_{-0.10}$	de Vaucouleurs et al. (1991)
NGC3118	26.84 ^a	35.91 ± 5.12	—	$9.79^{+0.06}_{-0.07}$	Springob et al. (2005)
IC0598	34.35	< 0.39	—	< 8.04	This work
NGC3193	28.82 ^a	0.73 ± 0.11	192 ± 30	$8.16^{+0.06}_{-0.07}$	This work
UGC05577	31.04	4.17 ± 0.45	—	$8.98^{+0.04}_{-0.05}$	Springob et al. (2005)
UGC05588	24.53 ^a	3.55 ± 1.13	—	$8.70^{+0.12}_{-0.17}$	de Vaucouleurs et al. (1991)
NGC3245A	23.86 ^a	12.52 ± 1.21	—	9.23 ± 0.04	Springob et al. (2005)
NGC3245	21.39 ^a	< 0.70	—	< 7.88	Huchtmeier & Richter (1989)
NGC3248	23.87	< 0.39	—	< 7.72	This work
NGC3254	34.33 ^a	59.77 ± 3.66	—	10.22 ± 0.03	Springob et al. (2005)
NGC3265	21.88	1.89 ± 0.60	—	$8.33^{+0.12}_{-0.17}$	de Vaucouleurs et al. (1991)
NGC3277	25.33 ^a	4.70 ± 0.63	—	$8.85^{+0.05}_{-0.06}$	Springob et al. (2005)
PGC031357	27.23	2.03 ± 0.10	78 ± 4	8.55 ± 0.02	This work
PGC031387	22.94	1.10 ± 0.08	83 ± 7	8.14 ± 0.03	This work
NGC3294	28.46 ^a	19.36 ± 2.00	—	$9.57^{+0.04}_{-0.05}$	Springob et al. (2005)
UGC05870	31.44	3.41 ± 0.25	195 ± 13	8.90 ± 0.03	This work
NGC3381	26.46	16.39 ± 2.08	—	$9.43^{+0.05}_{-0.06}$	Springob et al. (2005)
NGC3424	28.04 ^a	13.96 ± 4.44	—	$9.41^{+0.12}_{-0.17}$	de Vaucouleurs et al. (1991)
NGC3430	28.88 ^a	98.47 ± 3.87	—	10.29 ± 0.02	Springob et al. (2005)
UGC05990	31.73 ^a	3.89 ± 1.23	—	$8.97^{+0.12}_{-0.17}$	de Vaucouleurs et al. (1991)
NGC3442	30.93 ^a	2.98 ± 0.30	—	$8.83^{+0.04}_{-0.05}$	Springob et al. (2005)

UGC06070	29.32	6.38 ± 2.03	—	$9.11^{+0.12}_{-0.17}$	de Vaucouleurs et al. (1991)
NGC3504	19.85 ^a	5.03 ± 0.48	—	8.67 ± 0.04	de Vaucouleurs et al. (1991)
NGC3595	33.83	< 0.39	—	< 8.03	This work
NGC3629	33.86 ^a	28.88 ± 3.38	—	9.89 ± 0.05	Springob et al. (2005)
NGC3648	31.09	< 0.39	—	< 7.95	This work
NGC3658	31.93	0.51 ± 0.13	139 ± 31	$8.09^{+0.10}_{-0.13}$	This work
NGC3665	23.03 ^a	< 0.39	—	< 7.69	This work
UGC06455	31.81	1.08 ± 0.17	198 ± 34	$8.41^{+0.06}_{-0.07}$	This work
NGC3687	26.27 ^a	10.01 ± 0.97	—	9.21 ± 0.04	de Vaucouleurs et al. (1991)
NGC3689	41.66 ^a	5.39 ± 0.60	—	9.34 ± 0.05	Springob et al. (2005)
NGC3694	35.95 ^a	0.24 ± 0.07	44 ± 16	$7.86^{+0.11}_{-0.16}$	This work
PGC035472	30.56	1.06 ± 0.21	150 ± 38	$8.37^{+0.08}_{-0.10}$	This work
PGC035503	29.99	1.99 ± 0.11	115 ± 7	$8.63^{+0.02}_{-0.03}$	This work
PGC035508	31.07	0.88 ± 0.27	105 ± 32	$8.30^{+0.12}_{-0.16}$	This work
UGC06517	37.58	2.67 ± 0.22	210 ± 18	$8.95^{+0.03}_{-0.04}$	This work
UGC06526	18.14 ^a	3.38 ± 1.08	—	$8.42^{+0.12}_{-0.17}$	de Vaucouleurs et al. (1991)
PGC035688	38.52	0.99 ± 0.12	150 ± 20	$8.54^{+0.05}_{-0.06}$	This work
UGC06545	39.05	0.89 ± 0.10	225 ± 26	8.51 ± 0.05	This work
UGC06610	33.55 ^a	15.74 ± 2.14	—	9.62 ± 0.06	Springob et al. (2005)
NGC3786	44.85 ^a	12.47 ± 1.50	—	$9.77^{+0.05}_{-0.06}$	Springob et al. (2005)
NGC3788	53.05 ^a	15.92 ± 1.84	—	10.02 ± 0.05	Springob et al. (2005)
UGC06637	44.63 ^a	1.73 ± 0.55	—	$8.91^{+0.12}_{-0.17}$	de Vaucouleurs et al. (1991)
NGC3796	22.07	< 0.10	—	< 7.06	Serra et al. (2012)
NGC3838	22.86	1.84 ± 0.03	—	8.36 ± 0.01	Serra et al. (2012)
NGC3900	29.76 ^a	18.30 ± 1.09	—	9.58 ± 0.03	Springob et al. (2005)
NGC3898	22.27 ^a	37.82 ± 3.63	—	9.65 ± 0.04	de Vaucouleurs et al. (1991)
UGC06791	32.94 ^a	6.37 ± 1.16	—	$9.21^{+0.07}_{-0.09}$	Springob et al. (2005)
NGC3912	23.43 ^a	6.99 ± 0.68	—	8.96 ± 0.04	de Vaucouleurs et al. (1991)
NGC3953	17.77 ^a	51.65 ± 2.46	—	9.59 ± 0.02	Springob et al. (2005)
NGC3982	20.59 ^a	20.37 ± 4.12	—	$9.31^{+0.08}_{-0.10}$	de Vaucouleurs et al. (1991)
NGC3992	19.99 ^a	73.31 ± 1.10	—	9.84 ± 0.01	de Vaucouleurs et al. (1991)
NGC3998	21.10 ^a	< 8.62	—	< 8.96	de Vaucouleurs et al. (1991)
NGC4026	15.79 ^a	< 1.70	—	< 8.00	Huchtmeier & Richter (1989)
NGC4051	13.95 ^a	46.27 ± 4.46	—	9.33 ± 0.04	de Vaucouleurs et al. (1991)
NGC4088	14.51 ^a	131.27 ± 14.39	—	9.81 ± 0.05	Springob et al. (2005)

NGC4096	12.24 ^a	77.04 ± 5.41	—	9.43 ± 0.03	Springob et al. (2005)
NGC4100	20.31 ^a	49.80 ± 2.86	—	$9.69^{+0.02}_{-0.03}$	Springob et al. (2005)
NGC4111	13.75 ^a	11.97 ± 1.34	—	8.73 ± 0.05	Springob et al. (2005)
NGC4138	16.37 ^a	19.96 ± 1.97	—	$9.10^{+0.04}_{-0.05}$	Springob et al. (2005)
NGC4143	17.57 ^a	< 10.30	—	< 8.88	Huchtmeier & Richter (1989)
NGC4144	6.85 ^a	56.17 ± 3.82	—	8.79 ± 0.03	Springob et al. (2005)
NGC4151	11.27 ^a	47.10 ± 4.70	—	$9.15^{+0.04}_{-0.05}$	Huchtmeier & Richter (1989)
NGC4152	29.61 ^a	31.76 ± 3.89	—	$9.82^{+0.05}_{-0.06}$	Springob et al. (2005)
UGC07271	12.59 ^a	8.18 ± 2.60	—	$8.49^{+0.12}_{-0.17}$	de Vaucouleurs et al. (1991)
NGC4214	2.87 ^a	200.23 ± 0.39	—	8.59 ± 0.01	Stewart et al. (2014)
NGC4244	4.26 ^a	528.24 ± 70.42	—	$9.36^{+0.05}_{-0.06}$	Springob et al. (2005)
NGC4314	9.81 ^a	0.40 ± 0.09	—	$6.96^{+0.09}_{-0.11}$	Springob et al. (2005)
NGC4359	18.41 ^a	22.82 ± 7.25	—	$9.26^{+0.12}_{-0.17}$	de Vaucouleurs et al. (1991)
NGC4414	17.61 ^a	73.70 ± 2.87	—	9.73 ± 0.02	Springob et al. (2005)
NGC4448	20.19 ^a	3.37 ± 0.57	—	$8.51^{+0.07}_{-0.08}$	Springob et al. (2005)
NGC4525	13.01 ^a	10.72 ± 1.53	—	$8.63^{+0.06}_{-0.07}$	Springob et al. (2005)
NGC4559	7.81 ^a	380.30 ± 31.14	—	$9.74^{+0.03}_{-0.04}$	Springob et al. (2005)
NGC4793	28.29 ^a	33.85 ± 3.34	—	$9.81^{+0.04}_{-0.05}$	Springob et al. (2005)
UGC08076	38.13	2.97 ± 0.35	—	9.01 ± 0.05	Springob et al. (2005)
NGC4961	39.96 ^a	16.78 ± 1.77	—	$9.80^{+0.04}_{-0.05}$	Springob et al. (2005)
IC0851	44.63 ^a	9.11 ± 0.99	—	$9.63^{+0.04}_{-0.05}$	Springob et al. (2005)
NGC5012	36.96 ^a	18.09 ± 1.91	—	$9.77^{+0.04}_{-0.05}$	Springob et al. (2005)
NGC5016	40.34 ^a	11.07 ± 1.24	—	9.63 ± 0.05	Springob et al. (2005)
UGC08290	40.71 ^a	6.11 ± 0.97	—	$9.38^{+0.06}_{-0.08}$	Springob et al. (2005)
UGC08318	38.10 ^a	16.79 ± 2.03	—	$9.76^{+0.05}_{-0.06}$	Springob et al. (2005)
NGC5116	43.62 ^a	11.66 ± 1.48	—	$9.72^{+0.05}_{-0.06}$	Springob et al. (2005)
NGC5117	38.70 ^a	14.88 ± 1.79	—	$9.72^{+0.05}_{-0.06}$	Springob et al. (2005)
UGC08409	42.95 ^a	11.37 ± 1.62	—	$9.69^{+0.06}_{-0.07}$	Springob et al. (2005)
NGC5169	42.44 ^a	15.89 ± 1.53	—	9.83 ± 0.04	de Vaucouleurs et al. (1991)
NGC5173	38.52 ^a	6.08 ± 1.23	—	$9.33^{+0.08}_{-0.10}$	de Vaucouleurs et al. (1991)
IC4263	41.08 ^a	6.83 ± 0.81	—	9.43 ± 0.05	Springob et al. (2005)
PGC047274	39.33	2.88 ± 0.12	162 ± 8	9.02 ± 0.02	This work
PGC047295	40.59	0.31 ± 0.09	46 ± 13	$8.08^{+0.11}_{-0.15}$	This work
NGC5198	41.27 ^a	0.76 ± 0.15	132 ± 38	$8.49^{+0.08}_{-0.10}$	This work
NGC5248	12.62 ^a	22.50 ± 0.20	—	8.93 ± 0.01	Popping & Braun (2011)

UGC08630	34.66 ^a	16.53 ± 1.90	—	9.67 ± 0.05	Springob et al. (2005)
UGC08662	30.46 ^a	3.75 ± 0.51	—	8.91 ± 0.06	Springob et al. (2005)
UGC08693	42.82 ^a	8.32 ± 2.66	—	$9.56^{+0.12}_{-0.17}$	de Vaucouleurs et al. (1991)
NGC5289	40.24 ^a	6.19 ± 0.95	—	$9.37^{+0.06}_{-0.07}$	Tang et al. (2008)
NGC5290	35.62 ^a	19.33 ± 1.31	—	9.76 ± 0.03	Springob et al. (2005)
NGC5297	30.46 ^a	54.51 ± 5.26	—	10.08 ± 0.04	de Vaucouleurs et al. (1991)
NGC5300	19.62 ^a	15.60 ± 0.40	—	9.15 ± 0.01	Popping & Braun (2011)
UGC08733	30.88 ^a	21.02 ± 0.92	—	9.67 ± 0.02	Springob et al. (2005)
PGC049002	40.79	1.29 ± 0.17	144 ± 24	$8.71^{+0.05}_{-0.06}$	This work
NGC5311	40.78	5.10 ± 0.89	—	$9.30^{+0.07}_{-0.08}$	Huchtmeier & Richter (1989)
UGC08736	36.73	2.92 ± 0.14	261 ± 13	8.97 ± 0.02	This work
NGC5313	43.62 ^a	8.81 ± 0.85	—	9.60 ± 0.04	de Vaucouleurs et al. (1991)
NGC5320	36.28 ^a	26.20 ± 2.64	—	$9.91^{+0.04}_{-0.05}$	Springob et al. (2005)
IC4336	38.61	0.34 ± 0.10	75 ± 34	$8.08^{+0.11}_{-0.15}$	This work
NGC5326	26.90 ^a	< 2.35	—	< 8.60	Theureau et al. (1998)
PGC049191	38.34 ^a	< 0.39	—	< 8.13	This work
NGC5336	36.22	10.31 ± 1.07	—	$9.50^{+0.04}_{-0.05}$	Springob et al. (2005)
NGC5337	49.40 ^a	< 4.13	—	< 9.38	Theureau et al. (1998)
PGC2151881	40.83	< 0.39	—	< 8.19	This work
NGC5346	38.09 ^a	4.96 ± 0.63	—	$9.23^{+0.05}_{-0.06}$	Springob et al. (2005)
NGC5347	20.69 ^a	12.27 ± 1.18	—	9.09 ± 0.04	de Vaucouleurs et al. (1991)
NGC5350	28.95 ^a	27.04 ± 1.44	—	9.73 ± 0.02	Tang et al. (2008)
NGC5353	33.81 ^a	17.60 ± 2.10	—	$9.68^{+0.05}_{-0.06}$	Huchtmeier & Richter (1989)
NGC5355	35.59 ^a	17.50 ± 1.20	—	9.72 ± 0.03	Huchtmeier & Richter (1989)
PGC049386	39.68	< 0.39	—	< 8.16	This work
NGC5358	37.12	5.30 ± 0.88	—	$9.24^{+0.07}_{-0.08}$	Huchtmeier & Richter (1989)
NGC5348	18.18 ^a	8.40 ± 0.30	—	8.82 ± 0.02	Popping & Braun (2011)
NGC5362	28.03 ^a	10.91 ± 1.24	—	9.31 ± 0.05	Springob et al. (2005)
NGC5356	24.87 ^a	4.84 ± 0.98	—	$8.85^{+0.08}_{-0.10}$	de Vaucouleurs et al. (1991)
NGC5360	22.05 ^a	0.84 ± 0.27	—	$7.98^{+0.12}_{-0.17}$	de Vaucouleurs et al. (1991)
NGC5371	28.43 ^a	33.24 ± 1.24	—	9.80 ± 0.02	Springob et al. (2005)
NGC5363	19.41 ^a	1.74 ± 0.35	—	$8.19^{+0.08}_{-0.10}$	de Vaucouleurs et al. (1991)
NGC5364	17.17 ^a	40.70 ± 0.40	—	9.45 ± 0.01	Popping & Braun (2011)
NGC5375	40.71 ^a	11.83 ± 0.76	—	9.67 ± 0.03	Tang et al. (2008)
NGC5383	36.03 ^a	21.76 ± 2.10	—	9.82 ± 0.04	de Vaucouleurs et al. (1991)

NGC5403	41.35	22.61 ± 2.15	—	9.96 ± 0.04	Theureau et al. (1998)
PGC049824	41.14	< 0.15	—	< 7.78	Vogt et al. (2004)
PGC049852	39.59	1.76 ± 0.10	90 ± 6	8.81 ± 0.02	This work
PGC049927	42.23 ^a	< 0.39	—	< 8.22	This work
NGC5470	24.09 ^a	4.50 ± 0.30	—	8.79 ± 0.03	Popping & Braun (2011)
NGC5560	19.15 ^a	11.20 ± 0.30	—	8.99 ± 0.01	Popping & Braun (2011)
NGC5566	18.53 ^a	19.27 ± 1.86	—	9.19 ± 0.04	de Vaucouleurs et al. (1991)
NGC5574	24.42 ^a	0.70 ± 0.11	—	$7.99_{-0.07}^{+0.06}$	Springob et al. (2005)
NGC5576	21.27 ^a	0.41 ± 0.13	—	$7.64_{-0.17}^{+0.12}$	de Vaucouleurs et al. (1991)
NGC5577	23.21 ^a	6.30 ± 0.50	—	$8.90_{-0.04}^{+0.03}$	Popping & Braun (2011)
UGC09215	25.12 ^a	18.60 ± 1.00	—	9.44 ± 0.02	Popping & Braun (2011)
NGC5636	27.04	1.27 ± 0.15	—	8.34 ± 0.05	Springob et al. (2005)
NGC5638	25.10 ^a	0.88 ± 0.18	—	$8.12_{-0.10}^{+0.08}$	de Vaucouleurs et al. (1991)
IC1022	38.83 ^a	5.38 ± 0.59	—	9.28 ± 0.05	Springob et al. (2005)
NGC5645	19.00 ^a	14.90 ± 0.20	—	9.10 ± 0.01	Popping & Braun (2011)
IC1024	21.98 ^a	9.90 ± 0.20	—	9.05 ± 0.01	Popping & Braun (2011)
NGC5661	46.91 ^a	17.89 ± 3.61	—	$9.97_{-0.10}^{+0.08}$	de Vaucouleurs et al. (1991)
NGC5658	23.42 ^a	4.37 ± 1.39	—	$8.75_{-0.17}^{+0.12}$	de Vaucouleurs et al. (1991)
NGC5668	26.36 ^a	42.70 ± 0.30	—	9.85 ± 0.01	Popping & Braun (2011)
NGC5692	24.99 ^a	3.76 ± 0.47	—	$8.74_{-0.06}^{+0.05}$	Huchtmeier & Richter (1989)
NGC5701	26.40 ^a	54.10 ± 0.40	—	9.95 ± 0.01	Popping & Braun (2011)
NGC5725	23.77 ^a	3.99 ± 0.81	—	$8.73_{-0.10}^{+0.08}$	de Vaucouleurs et al. (1991)
IC1048	29.29 ^a	13.90 ± 0.50	—	9.45 ± 0.02	Popping & Braun (2011)
NGC5740	28.69 ^a	35.80 ± 1.30	—	9.84 ± 0.02	Popping & Braun (2011)
NGC5746	29.58 ^a	30.70 ± 1.90	—	9.80 ± 0.03	Popping & Braun (2011)
UGC09556	54.85 ^a	11.63 ± 1.39	—	$9.92_{-0.06}^{+0.05}$	Springob et al. (2005)
NGC5777	45.71 ^a	34.62 ± 2.90	—	$10.23_{-0.04}^{+0.03}$	Springob et al. (2005)
IC1066	32.19 ^a	7.67 ± 1.55	—	$9.27_{-0.10}^{+0.08}$	de Vaucouleurs et al. (1991)
IC1067	24.67	15.81 ± 1.91	—	$9.36_{-0.06}^{+0.05}$	Springob et al. (2005)
NGC5770	20.80 ^a	< 0.63	—	< 7.81	Grossi et al. (2009)
NGC5806	24.89 ^a	13.52 ± 0.91	—	9.30 ± 0.03	Springob et al. (2005)
NGC5813	29.58 ^a	0.29 ± 0.09	73 ± 22	$7.78_{-0.17}^{+0.12}$	This work
UGC09661	19.68	1.44 ± 0.22	—	$8.12_{-0.07}^{+0.06}$	Schneider et al. (1990)
NGC5831	27.18 ^a	< 0.39	—	< 7.84	This work
NGC5838	26.94 ^a	< 0.77	—	< 8.12	Huchtmeier & Richter (1989)

NGC5839	23.69 ^a	0.69 ± 0.16	205 ± 51	$7.96^{+0.09}_{-0.11}$	This work
PGC2586382	40.10	0.54 ± 0.15	110 ± 31	$8.31^{+0.10}_{-0.14}$	This work
NGC5845	28.82 ^a	< 0.39	—	< 7.89	This work
NGC5846	25.13 ^a	2.58 ± 0.52	—	$8.58^{+0.08}_{-0.10}$	de Vaucouleurs et al. (1991)
NGC5854	22.00 ^a	0.33 ± 0.05	—	$7.58^{+0.06}_{-0.07}$	Springob et al. (2005)
PGC054037	27.78	< 0.39	—	< 7.85	This work
NGC5864	25.93 ^a	1.33 ± 0.42	—	$8.33^{+0.12}_{-0.17}$	de Vaucouleurs et al. (1991)
NGC5869	27.72 ^a	< 0.39	—	< 7.85	This work
NGC5894	39.53 ^a	13.84 ± 1.26	—	9.71 ± 0.04	Schneider et al. (1992)
PGC054346	39.22	0.48 ± 0.11	48 ± 14	$8.24^{+0.09}_{-0.12}$	This work
PGC054452	28.82	0.20 ± 0.09 ^b	66 ± 45	$7.59^{+0.16}_{-0.25}$	This work
UGC09837	41.66 ^a	9.74 ± 0.94	—	9.60 ± 0.04	de Vaucouleurs et al. (1991)
NGC5951	26.84 ^a	21.62 ± 1.72	—	$9.57^{+0.03}_{-0.04}$	Springob et al. (2005)
NGC5953	23.10 ^a	7.27 ± 1.47	—	$8.96^{+0.08}_{-0.10}$	de Vaucouleurs et al. (1991)
NGC5954	32.48 ^a	5.26 ± 0.51	—	9.12 ± 0.04	de Vaucouleurs et al. (1991)
NGC5956	29.12	7.28 ± 0.79	—	$9.16^{+0.04}_{-0.05}$	Springob et al. (2005)
NGC5957	28.21	23.87 ± 2.30	—	9.65 ± 0.04	de Vaucouleurs et al. (1991)
NGC5981	50.90 ^a	14.53 ± 1.25	—	9.95 ± 0.04	Springob et al. (2005)
NGC5970	28.04 ^a	27.75 ± 3.95	—	$9.71^{+0.06}_{-0.07}$	Springob et al. (2005)
NGC5982	36.12 ^a	< 0.39	—	< 8.08	This work
NGC5985	39.51 ^a	18.34 ± 0.35	550 ± 11	9.83 ± 0.01	This work
NGC5989	43.70	3.49 ± 0.48	—	9.20 ± 0.06	Springob et al. (2005)
UGC09991	39.78 ^a	7.81 ± 1.01	—	$9.46^{+0.05}_{-0.06}$	Springob et al. (2005)
NGC6012	19.35 ^a	22.39 ± 2.15	—	9.30 ± 0.04	de Vaucouleurs et al. (1991)
UGC10086	36.28 ^a	3.26 ± 0.18	272 ± 17	9.01 ± 0.02	This work
IC1151	34.32 ^a	17.46 ± 2.31	—	$9.69^{+0.05}_{-0.06}$	Springob et al. (2005)
IC1210	49.06 ^a	23.90 ± 2.70	—	10.13 ± 0.05	Huchtmeier & Richter (1989)
PGC057611	44.58	< 0.39	—	< 8.27	This work
UGC10297	37.64 ^a	8.92 ± 1.89	—	$9.47^{+0.08}_{-0.10}$	Springob et al. (2005)
UGC10413	45.89 ^a	19.36 ± 2.57	—	$9.98^{+0.05}_{-0.06}$	Springob et al. (2005)
NGC6181	32.75 ^a	32.16 ± 4.12	—	$9.91^{+0.05}_{-0.06}$	Springob et al. (2005)
NGC6186	43.10	2.27 ± 0.26	—	9.00 ± 0.05	Springob et al. (2005)
NGC6267	53.05 ^a	6.25 ± 0.64	—	$9.62^{+0.04}_{-0.05}$	Springob et al. (2005)
NGC6276	40.74	1.79 ± 0.11	126 ± 9	8.85 ± 0.03	This work

NGC6278	37.03 ^a	1.68 ± 0.16	—	8.73 ± 0.04	de Vaucouleurs et al. (1991)
NGC6306	44.96	1.20 ± 0.20	—	$8.76^{+0.07}_{-0.08}$	Huchtmeier & Richter (1989)
UGC10721	47.18 ^a	6.35 ± 0.64	—	$9.52^{+0.04}_{-0.05}$	Springob et al. (2005)
UGC10968	43.32	3.60 ± 0.65	—	$9.20^{+0.07}_{-0.09}$	Huchtmeier & Richter (1989)
PGC2333993	34.62	0.41 ± 0.29 ^b	67 ± 63	$8.07^{+0.23}_{-0.54}$	This work
UGC06326	32.68	2.76 ± 0.13	115 ± 6	8.84 ± 0.02	This work
PGC034951	29.71	< 0.39	—	< 7.91	This work
PGC2121110	34.17	0.19 ± 0.06	26 ± 325	$7.72^{+0.12}_{-0.18}$	This work
PGC2139858	30.85	< 0.39	—	< 7.95	This work
PGC035474	30.57	< 0.39	—	< 7.94	This work
PGC2578846	39.51	1.81 ± 0.26	124 ± 17	$8.82^{+0.06}_{-0.07}$	This work
UGC08656	43.02	2.04 ± 0.16	190 ± 18	8.95 ± 0.03	This work
NGC5841	19.91	< 0.39	—	< 7.57	This work
NGC5850	16.82 ^a	5.31 ± 0.13	186 ± 4	8.55 ± 0.01	This work
NGC6149	36.41	0.77 ± 0.14	207 ± 37	$8.38^{+0.07}_{-0.09}$	This work

Table B.5: HI results from our campaign and the literature. Column description. (1-2) galaxy ID and distance, for the sources denoted with the symbol ^a we report redshift independent distances; (3) velocity integrated HI flux, sources denoted with the symbol ^b correspond to tentative HI detections with $\text{SNR} < 3$ from our campaign at Nançay; (4) FWHM of the HI line, which is reported only for detections from our campaign; (5) HI mass; (6) reference. Upper limits are at 3σ . Absent values are denoted with the symbol —. The last 11 sources were observed as part of our campaign at Nançay, but subsequently excluded from our sample of filament galaxies. See text for further details.

Galaxy (1)	Distance (Mpc) (2)	r_{21} (3)	$\log\left(\frac{M_{\text{H}_2}}{M_{\odot}}\right)$ (4)	$\log\left(\frac{M_{\text{H}_2}}{M_{\star}}\right)$ (5)	$\log\left(\frac{M_{\text{H}_2}}{M_{\star}}\right)_{\text{MS}}$ (6)	$\log\left(\frac{\tau_{\text{dep}}}{\text{yr}}\right)$ (7)	$\log\left(\frac{\tau_{\text{dep,MS}}}{\text{yr}}\right)$ (8)	$\log\left(\frac{M_{\text{HI}}}{M_{\odot}}\right)$ (9)	$\log\left(\frac{M_{\text{HI}}}{M_{\star}}\right)$ (10)	$\log\left(\frac{M_{\text{HI}}}{M_{\star}}\right)_{\text{MS}}$ (11)	Ref. CO (12)	Ref. HI (13)
PGC022100	30.27	—	< 7.71	< -1.56	-0.99 ± 0.53	< 8.73	8.95 ± 0.08	8.59 ± 0.03	-0.68 ^{+0.09} _{-0.12}	-0.37 ± 0.25	2	1
IC2256	35.33 ^a	—	7.76 ^{+0.10} _{-0.12}	-1.51 ^{+0.13} _{-0.18}	-0.99 ± 0.53	8.85 ^{+0.18} _{-0.32}	8.95 ± 0.08	9.10 ^{+0.05} _{-0.06}	-0.17 ^{+0.10} _{-0.13}	-0.37 ± 0.25	1	2
NGC2577	35.62 ^a	—	< 7.93	< -2.37	-1.26 ± 0.53	< 9.13	9.13 ± 0.05	< 8.02	< -2.28	-0.67 ± 0.25	2	2
UGC04375	40.34 ^a	0.30 ± 0.07	8.83 ^{+0.05} _{-0.06}	-1.18 ^{+0.10} _{-0.13}	-1.17 ± 0.53	9.26 ^{+0.17} _{-0.28}	9.09 ± 0.06	9.80 ^{+0.06} _{-0.07}	-0.21 ^{+0.10} _{-0.14}	-0.58 ± 0.25	1	2
IC2361	30.33	0.67 ± 0.13	8.32 ^{+0.07} _{-0.08}	-1.10 ^{+0.11} _{-0.15}	-1.02 ± 0.53	9.01 ^{+0.17} _{-0.29}	8.98 ± 0.07	8.37 ^{+0.12} _{-0.17}	-1.05 ^{+0.14} _{-0.22}	-0.42 ± 0.25	1	2
UGC04395	38.17 ^a	—	< 7.78	< -1.44	-0.98 ± 0.53	< 9.07	8.94 ± 0.08	9.33 ^{+0.08} _{-0.09}	0.11 ^{+0.11} _{-0.16}	-0.36 ± 0.25	1	2
NGC2592	32.57 ^a	—	< 7.97	< -2.23	-1.23 ± 0.53	< 10.15	9.12 ± 0.05	8.19 ^{+0.07} _{-0.08}	-2.01 ^{+0.11} _{-0.15}	-0.64 ± 0.25	2	1
NGC2594	34.13	—	< 7.56	< -2.43	-1.16 ± 0.53	< 9.63	9.09 ± 0.06	8.87 ^{+0.07} _{-0.08}	-1.12 ^{+0.11} _{-0.15}	-0.58 ± 0.25	2	1
PGC023706	32.60	—	< 7.03	< -1.45	-0.90 ± 0.53	< 7.98	8.69 ± 0.11	8.56 ^{+0.04} _{-0.05}	0.07 ^{+0.23} _{-0.52}	-0.15 ± 0.24	1	1
NGC2604	30.69	0.81 ± 0.17	8.20 ^{+0.06} _{-0.07}	-1.60 ^{+0.11} _{-0.14}	-1.11 ± 0.53	8.17 ^{+0.17} _{-0.29}	9.06 ± 0.06	9.58 ^{+0.08} _{-0.10}	-0.22 ^{+0.12} _{-0.16}	-0.52 ± 0.25	1	2
PGC024012	32.82	—	< 7.82	< -1.18	-0.94 ± 0.53	< 8.68	8.87 ± 0.09	8.61 ^{+0.03} _{-0.04}	-0.39 ^{+0.15} _{-0.22}	-0.30 ± 0.25	1	1
NGC2608	23.27 ^a	0.31 ± 0.02	8.85 ± 0.02	-1.49 ^{+0.09} _{-0.12}	-1.27 ± 0.53	8.72 ^{+0.16} _{-0.27}	9.13 ± 0.05	8.90 ^{+0.05} _{-0.06}	-1.44 ^{+0.10} _{-0.13}	-0.68 ± 0.25	1	2
UGC04551	27.29	—	< 7.78	< -2.41	-1.22 ± 0.53	< 9.58	9.12 ± 0.05	< 7.84	< -2.35	-0.64 ± 0.25	2	1
UGC04559	41.08 ^a	0.36 ± 0.08	8.98 ^{+0.07} _{-0.08}	-1.24 ^{+0.12} _{-0.17}	-1.23 ± 0.53	9.75 ^{+0.17} _{-0.29}	9.12 ± 0.05	9.88 ^{+0.06} _{-0.07}	-0.34 ^{+0.12} _{-0.16}	-0.64 ± 0.25	1	2
PGC1925809	30.48	—	< 7.46	< -1.22	-0.91 ± 0.53	< 10.31	8.77 ± 0.10	< 7.94	< -0.74	-0.20 ± 0.25	1	1
NGC2679	28.83 ^a	—	< 8.14	< -2.07	-1.23 ± 0.53	< 9.79	9.12 ± 0.05	7.75 ^{+0.12} _{-0.16}	-2.46 ^{+0.14} _{-0.21}	-0.64 ± 0.25	2	1
UGC04659	36.62 ^a	—	< 7.66	< -1.48	-0.96 ± 0.53	< 8.79	8.91 ± 0.08	9.36 ± 0.05	0.22 ^{+0.12} _{-0.17}	-0.34 ± 0.25	1	2
PGC025063	30.43	0.63 ± 0.11	8.43 ^{+0.06} _{-0.07}	-0.64 ^{+0.10} _{-0.14}	-0.95 ± 0.53	9.05 ^{+0.17} _{-0.29}	8.89 ± 0.09	7.97 ^{+0.07} _{-0.09}	-1.10 ^{+0.11} _{-0.15}	-0.32 ± 0.25	1	1
NGC2712	31.02 ^a	0.88 ± 0.04	9.34 ± 0.02	-0.92 ^{+0.09} _{-0.12}	-1.25 ± 0.53	9.27 ^{+0.16} _{-0.27}	9.13 ± 0.05	9.74 ± 0.02	-0.52 ^{+0.09} _{-0.12}	-0.66 ± 0.25	1	2
PGC025273	28.60	—	< 7.28	< -1.53	-0.92 ± 0.53	< 8.24	8.81 ± 0.10	7.98 ^{+0.06} _{-0.07}	-0.83 ^{+0.14} _{-0.21}	-0.24 ± 0.25	1	1
UGC04722	23.86 ^a	—	8.25 ^{+0.08} _{-0.10}	-0.17 ^{+0.18} _{-0.33}	-0.90 ± 0.53	9.20 ^{+0.18} _{-0.31}	8.67 ± 0.12	9.26 ^{+0.08} _{-0.10}	0.84 ^{+0.18} _{-0.32}	-0.13 ± 0.24	2	2
NGC2780	52.55 ^a	0.34 ± 0.05	9.06 ± 0.04	-0.47 ^{+0.10} _{-0.13}	-1.04 ± 0.53	9.93 ^{+0.17} _{-0.28}	9.01 ± 0.07	8.99 ^{+0.12} _{-0.17}	-0.54 ^{+0.14} _{-0.22}	-0.45 ± 0.25	1	2
NGC2793	26.65 ^a	0.22 ± 0.09	8.01 ^{+0.08} _{-0.09}	-1.42 ^{+0.23} _{-0.55}	-1.02 ± 0.53	8.67 ^{+0.13} _{-0.15}	8.99 ± 0.07	9.14 ^{+0.04} _{-0.05}	-0.29 ^{+0.23} _{-0.52}	-0.42 ± 0.25	1	2
UGC04902	25.14	0.97 ± 0.13	8.11 ^{+0.04} _{-0.05}	-1.19 ^{+0.10} _{-0.13}	-0.99 ± 0.53	8.66 ^{+0.17} _{-0.28}	8.96 ± 0.08	8.03 ± 0.05	-1.27 ^{+0.10} _{-0.13}	-0.38 ± 0.25	1	1
NGC2798	23.43 ^a	1.00 ± 0.01	9.51 ± 0.01	-0.41 ^{+0.09} _{-0.11}	-1.14 ± 0.53	8.82 ^{+0.16} _{-0.27}	9.08 ± 0.06	9.11 ± 0.04	-0.81 ^{+0.10} _{-0.12}	-0.56 ± 0.25	1	2
NGC2799	27.78 ^a	0.55 ± 0.13	7.98 ^{+0.08} _{-0.10}	-1.27 ^{+0.12} _{-0.17}	-0.98 ± 0.53	8.63 ^{+0.22} _{-0.46}	8.94 ± 0.08	9.31 ^{+0.12} _{-0.17}	0.06 ^{+0.15} _{-0.23}	-0.37 ± 0.25	1	2
NGC2844	42.14 ^a	0.73 ± 0.08	9.11 ± 0.04	-0.82 ^{+0.10} _{-0.12}	-1.14 ± 0.53	9.84 ^{+0.17} _{-0.27}	9.08 ± 0.06	9.60 ^{+0.04} _{-0.05}	-0.33 ^{+0.10} _{-0.13}	-0.56 ± 0.25	1	2
NGC2852	29.63 ^a	—	< 7.76	< -2.03	-1.11 ± 0.53	< 10.51	9.06 ± 0.06	8.92 ± 0.02	-0.87 ^{+0.09} _{-0.12}	-0.52 ± 0.25	2	1
NGC2853	28.55 ^a	0.51 ± 0.11	8.39 ^{+0.06} _{-0.07}	-0.95 ^{+0.11} _{-0.14}	-1.00 ± 0.53	9.66 ^{+0.17} _{-0.29}	8.97 ± 0.08	8.87 ± 0.01	-0.47 ^{+0.09} _{-0.12}	-0.39 ± 0.25	1	1
NGC2859	24.45 ^a	—	< 8.31	< -2.58	-1.48 ± 0.53	< 9.07	9.17 ± 0.05	8.70 ^{+0.08} _{-0.10}	-2.19 ^{+0.12} _{-0.17}	-0.83 ± 0.26	2	2
UGC05015	25.79	—	< 7.96	< -1.15	-0.96 ± 0.53	< 9.25	8.91 ± 0.09	8.95 ^{+0.08} _{-0.10}	-0.16 ^{+0.12} _{-0.16}	-0.33 ± 0.25	1	2
UGC05020	32.36 ^a	—	7.54 ^{+0.14} _{-0.21}	-1.67 ^{+0.16} _{-0.26}	-0.98 ± 0.53	8.62 ^{+0.21} _{-0.40}	8.93 ± 0.08	9.27 ± 0.06	0.06 ^{+0.10} _{-0.14}	-0.36 ± 0.25	1	2
NGC2893	27.14 ^a	0.86 ± 0.03	8.72 ± 0.01	-0.65 ^{+0.09} _{-0.11}	-1.01 ± 0.53	8.75 ^{+0.16} _{-0.27}	8.97 ± 0.08	8.93 ± 0.04	-0.44 ^{+0.10} _{-0.12}	-0.40 ± 0.25	1	2
PGC027311	25.65	—	< 7.44	< -1.40	-0.92 ± 0.53	< 8.94	8.82 ± 0.10	7.98 ^{+0.05} _{-0.06}	-0.86 ^{+0.10} _{-0.13}	-0.25 ± 0.25	2	1
NGC2964	20.45 ^a	0.12 ± 0.02	9.17 ^{+0.07} _{-0.08}	-1.13 ^{+0.11} _{-0.15}	-1.26 ± 0.53	8.84 ^{+0.17} _{-0.30}	9.13 ± 0.05	9.41 ± 0.02	-0.89 ^{+0.09} _{-0.12}	-0.67 ± 0.25	2	2

NGC2968	13.74 ^a	—	< 7.39	< -2.97	-1.28 ± 0.53	< 8.67	9.14 ± 0.05	8.21 ^{+0.12} _{-0.17}	-2.15 ^{+0.14} _{-0.22}	-0.68 ± 0.25	1	2
NGC2970	27.02 ^a	—	< 7.60	< -1.68	-0.99 ± 0.53	< 10.10	8.95 ± 0.08	7.79 ^{+0.07} _{-0.09}	-1.49 ^{+0.11} _{-0.15}	-0.38 ± 0.25	1	1
PGC028169	24.76 ^a	< 0.40	7.54 ^{+0.09} _{-0.12}	-0.89 ^{+0.13} _{-0.19}	-0.90 ± 0.53	8.86 ^{+0.18} _{-0.32}	8.67 ± 0.11	8.61 ^{+0.12} _{-0.17}	0.18 ^{+0.15} _{-0.24}	-0.13 ± 0.24	1	2
NGC3003	20.78 ^a	0.54 ± 0.04	8.71 ± 0.03	-1.00 ^{+0.09} _{-0.12}	-1.08 ± 0.53	8.75 ^{+0.17} _{-0.27}	9.04 ± 0.06	10.06 ^{+0.02} _{-0.03}	0.35 ^{+0.09} _{-0.12}	-0.50 ± 0.25	1	2
NGC3026	24.59 ^a	0.18 ± 0.10	7.84 ^{+0.08} _{-0.10}	-1.50 ^{+0.12} _{-0.16}	-1.00 ± 0.53	8.64 ^{+0.18} _{-0.31}	8.97 ± 0.08	9.20 ± 0.04	-0.14 ^{+0.10} _{-0.13}	-0.39 ± 0.25	1	2
NGC3021	26.47 ^a	0.50 ± 0.02	9.11 ± 0.01	-0.77 ^{+0.09} _{-0.11}	-1.13 ± 0.53	9.34 ^{+0.16} _{-0.27}	9.07 ± 0.06	9.33 ^{+0.04} _{-0.05}	-0.55 ^{+0.10} _{-0.13}	-0.55 ± 0.25	1	2
UGC05287	31.93 ^a	—	< 7.62	< -1.76	-1.01 ± 0.53	< 9.43	8.98 ± 0.08	9.08 ± 0.05	-0.30 ^{+0.10} _{-0.13}	-0.40 ± 0.25	1	2
NGC3032	21.76 ^a	0.50 ± 0.02	8.78 ± 0.01	-1.13 ^{+0.12} _{-0.17}	-1.14 ± 0.53	9.32 ^{+0.16} _{-0.27}	9.08 ± 0.06	7.85 ± 0.04	-2.06 ^{+0.13} _{-0.18}	-0.56 ± 0.25	2	2
UGC05326	22.96	—	< 7.37	< -1.58	-0.94 ± 0.53	< 9.08	8.86 ± 0.09	8.73 ± 0.01	-0.22 ^{+0.09} _{-0.11}	-0.28 ± 0.25	1	2
NGC3067	19.58 ^a	0.49 ± 0.01	8.97 ± 0.01	-0.96 ^{+0.09} _{-0.11}	-1.14 ± 0.53	8.90 ^{+0.16} _{-0.27}	9.08 ± 0.06	8.79 ± 0.04	-1.14 ^{+0.10} _{-0.12}	-0.56 ± 0.25	1	2
NGC3098	22.68 ^a	—	< 7.56	< -2.68	-1.24 ± 0.53	< 9.13	9.12 ± 0.05	8.81 ^{+0.12} _{-0.17}	-1.43 ^{+0.14} _{-0.22}	-0.65 ± 0.25	2	2
PGC029347	23.97 ^a	0.52 ± 0.20	7.25 ^{+0.10} _{-0.13}	-1.58 ^{+0.13} _{-0.19}	-0.92 ± 0.53	8.17 ^{+0.19} _{-0.33}	8.82 ± 0.10	8.14 ^{+0.08} _{-0.10}	-0.69 ^{+0.12} _{-0.16}	-0.25 ± 0.25	1	2
NGC3118	26.84 ^a	0.50 ± 0.19	7.70 ^{+0.11} _{-0.15}	-1.20 ^{+0.14} _{-0.20}	-0.93 ± 0.53	8.55 ^{+0.19} _{-0.34}	8.84 ± 0.09	9.79 ^{+0.06} _{-0.07}	0.89 ^{+0.10} _{-0.14}	-0.27 ± 0.25	1	2
IC0598	34.35	—	< 7.98	< -2.09	-1.18 ± 0.53	< 9.29	9.10 ± 0.05	< 8.04	< -2.03	-0.60 ± 0.25	2	1
NGC3193	28.82 ^a	—	< 8.21	< -2.74	-1.51 ± 0.53	< 8.90	9.17 ± 0.05	8.16 ^{+0.06} _{-0.07}	-2.79 ^{+0.11} _{-0.14}	-0.85 ± 0.26	2	1
UGC05577	31.04	0.67 ± 0.13	7.83 ^{+0.07} _{-0.08}	-1.49 ^{+0.11} _{-0.16}	-1.00 ± 0.53	8.41 ^{+0.17} _{-0.29}	8.96 ± 0.08	8.98 ^{+0.04} _{-0.05}	-0.34 ^{+0.11} _{-0.14}	-0.39 ± 0.25	1	2
UGC05588	24.53 ^a	0.54 ± 0.04	8.28 ± 0.03	-1.05 ^{+0.21} _{-0.43}	-1.00 ± 0.53	8.85 ^{+0.17} _{-0.27}	8.96 ± 0.08	8.70 ^{+0.12} _{-0.17}	-0.63 ^{+0.23} _{-0.52}	-0.39 ± 0.25	1	2
NGC3245A	23.86 ^a	—	< 7.77	< -1.42	-0.97 ± 0.53	< 9.08	8.93 ± 0.08	9.23 ± 0.04	0.04 ^{+0.10} _{-0.12}	-0.35 ± 0.25	1	2
NGC3245	21.39 ^a	—	8.01 ^{+0.12} _{-0.16}	-2.54 ^{+0.14} _{-0.21}	-1.35 ± 0.53	8.52 ^{+0.19} _{-0.35}	9.15 ± 0.05	< 7.88	< -2.67	-0.74 ± 0.26	2	2
NGC3248	23.87	—	< 7.78	< -2.23	-1.17 ± 0.53	< 9.61	9.09 ± 0.06	< 7.72	< -2.29	-0.58 ± 0.25	2	1
NGC3254	34.33 ^a	0.47 ± 0.25	8.27 ^{+0.12} _{-0.17}	-1.82 ^{+0.15} _{-0.22}	-1.19 ± 0.53	8.69 ^{+0.19} _{-0.36}	9.11 ± 0.05	10.22 ± 0.03	0.13 ^{+0.09} _{-0.12}	-0.61 ± 0.25	1	2
NGC3265	21.88	—	< 8.36	< -0.82	-0.97 ± 0.53	< 8.66	8.92 ± 0.08	8.33 ^{+0.12} _{-0.17}	-0.85 ^{+0.14} _{-0.22}	-0.35 ± 0.25	2	2
NGC3277	25.33 ^a	—	9.01 ^{+0.12} _{-0.18}	-1.21 ^{+0.15} _{-0.23}	-1.23 ± 0.53	9.84 ^{+0.20} _{-0.37}	9.12 ± 0.05	8.85 ^{+0.05} _{-0.06}	-1.37 ^{+0.10} _{-0.13}	-0.64 ± 0.25	2	2
PGC031357	27.23	—	< 7.57	< -1.05	-0.90 ± 0.53	< 8.63	8.75 ± 0.11	8.55 ± 0.02	-0.07 ^{+0.09} _{-0.12}	-0.19 ± 0.25	1	1
PGC031387	22.94	0.33 ± 0.19	6.97 ^{+0.12} _{-0.16}	-1.78 ^{+0.25} _{-0.62}	-0.91 ± 0.53	8.16 ^{+0.13} _{-0.19}	8.79 ± 0.10	8.14 ± 0.03	-0.61 ^{+0.23} _{-0.52}	-0.22 ± 0.25	1	1
NGC3294	28.46 ^a	—	9.42 ^{+0.12} _{-0.18}	-0.96 ^{+0.15} _{-0.23}	-1.29 ± 0.53	9.21 ^{+0.20} _{-0.37}	9.14 ± 0.05	9.57 ^{+0.04} _{-0.05}	-0.81 ^{+0.10} _{-0.13}	-0.69 ± 0.25	2	2
UGC05870	31.44	0.51 ± 0.16	7.96 ^{+0.09} _{-0.11}	-1.80 ^{+0.12} _{-0.17}	-1.10 ± 0.53	8.79 ^{+0.18} _{-0.31}	9.05 ± 0.06	8.90 ± 0.03	-0.86 ^{+0.09} _{-0.12}	-0.51 ± 0.25	1	1
NGC3381	26.46	0.97 ± 0.08	8.56 ± 0.03	-1.09 ^{+0.09} _{-0.12}	-1.07 ± 0.53	8.79 ^{+0.17} _{-0.27}	9.03 ± 0.07	9.43 ^{+0.05} _{-0.06}	-0.22 ^{+0.10} _{-0.13}	-0.48 ± 0.25	1	2
NGC3424	28.04 ^a	—	< 8.32	< -1.79	-1.20 ± 0.53	< 8.10	9.11 ± 0.05	9.41 ^{+0.12} _{-0.17}	-0.70 ^{+0.14} _{-0.22}	-0.61 ± 0.25	2	2
NGC3430	28.88 ^a	—	< 9.14	< -1.06	-1.23 ± 0.53	< 9.01	9.12 ± 0.05	10.29 ± 0.02	0.09 ^{+0.11} _{-0.16}	-0.64 ± 0.25	2	2
UGC05990	31.73 ^a	0.42 ± 0.23	7.63 ^{+0.12} _{-0.16}	-1.59 ^{+0.14} _{-0.21}	-0.98 ± 0.53	8.85 ^{+0.19} _{-0.35}	8.94 ± 0.08	8.97 ^{+0.12} _{-0.17}	-0.25 ^{+0.14} _{-0.22}	-0.36 ± 0.25	1	2
NGC3442	30.93 ^a	0.46 ± 0.03	8.47 ± 0.02	-0.75 ^{+0.09} _{-0.12}	-0.98 ± 0.53	8.79 ^{+0.17} _{-0.27}	8.94 ± 0.08	8.83 ^{+0.04} _{-0.05}	-0.39 ^{+0.10} _{-0.13}	-0.36 ± 0.25	1	2
UGC06070	29.32	0.52 ± 0.18	7.65 ^{+0.10} _{-0.13}	-1.39 ^{+0.13} _{-0.18}	-0.95 ± 0.53	7.99 ^{+0.18} _{-0.32}	8.89 ± 0.09	9.11 ^{+0.12} _{-0.17}	0.07 ^{+0.14} _{-0.22}	-0.31 ± 0.25	1	2
NGC3504	19.85 ^a	—	9.42 ^{+0.05} _{-0.06}	-0.87 ^{+0.10} _{-0.13}	-1.26 ± 0.53	8.55 ^{+0.17} _{-0.28}	9.13 ± 0.05	8.67 ± 0.04	-1.62 ^{+0.10} _{-0.12}	-0.66 ± 0.25	2	2
NGC3595	33.83	—	< 7.59	< -2.78	-1.28 ± 0.53	< 9.00	9.14 ± 0.05	< 8.03	< -2.34	-0.69 ± 0.25	2	1
NGC3629	33.86 ^a	—	< 8.14	< -1.66	-1.11 ± 0.53	< 8.13	9.06 ± 0.06	9.89 ± 0.05	0.09 ^{+0.10} _{-0.13}	-0.52 ± 0.25	1	2
NGC3648	31.09	—	< 7.77	< -2.46	-1.24 ± 0.53	< 11.52	9.12 ± 0.05	< 7.95	< -2.28	-0.65 ± 0.25	2	1

NGC3658	31.93	—	< 8.17	< -2.25	-1.30 ± 0.53	< 9.23	9.14 ± 0.05	8.09 ^{+0.10} _{-0.13}	-2.33 ^{+0.13} _{-0.19}	-0.70 ± 0.25	2	1
NGC3665	23.03 ^a	—	8.72 ± 0.01	-1.75 ^{+0.09} _{-0.11}	-1.32 ± 0.53	9.64 ^{+0.16} _{-0.27}	9.15 ± 0.05	< 7.69	< -2.78	-0.72 ± 0.26	2	1
UGC06455	31.81	—	< 7.79	< -1.50	-0.99 ± 0.53	< 9.73	8.95 ± 0.08	8.41 ^{+0.06} _{-0.07}	-0.88 ^{+0.11} _{-0.15}	-0.38 ± 0.25	1	1
NGC3687	26.27 ^a	0.36 ± 0.07	8.16 ^{+0.05} _{-0.06}	-2.02 ^{+0.10} _{-0.13}	-1.22 ± 0.53	8.44 ^{+0.17} _{-0.28}	9.12 ± 0.05	9.21 ± 0.04	-0.97 ^{+0.10} _{-0.12}	-0.63 ± 0.25	1	2
NGC3689	41.66 ^a	0.53 ± 0.02	9.67 ± 0.01	-0.85 ^{+0.09} _{-0.11}	-1.34 ± 0.53	9.38 ^{+0.16} _{-0.27}	9.15 ± 0.05	9.34 ± 0.05	-1.18 ^{+0.10} _{-0.13}	-0.73 ± 0.26	1	2
NGC3694	35.95 ^a	—	< 7.95	< -2.02	-1.16 ± 0.53	< 8.67	9.09 ± 0.06	7.86 ^{+0.11} _{-0.16}	-2.11 ^{+0.14} _{-0.21}	-0.57 ± 0.25	2	1
PGC035472	30.56	—	7.54 ^{+0.14} _{-0.21}	-1.56 ^{+0.16} _{-0.26}	-0.96 ± 0.53	9.59 ^{+0.22} _{-0.46}	8.90 ± 0.09	8.37 ^{+0.08} _{-0.10}	-0.73 ^{+0.12} _{-0.16}	-0.32 ± 0.25	1	1
PGC035503	29.99	0.36 ± 0.18	7.47 ^{+0.10} _{-0.13}	-1.34 ^{+0.15} _{-0.24}	-0.92 ± 0.53	9.03 ^{+0.18} _{-0.32}	8.81 ± 0.10	8.63 ^{+0.02} _{-0.03}	-0.18 ^{+0.13} _{-0.19}	-0.24 ± 0.25	1	1
PGC035508	31.07	0.62 ± 0.24	7.37 ^{+0.10} _{-0.14}	-1.78 ^{+0.13} _{-0.19}	-0.97 ± 0.53	8.65 ^{+0.19} _{-0.33}	8.92 ± 0.08	8.30 ^{+0.12} _{-0.16}	-0.85 ^{+0.14} _{-0.21}	-0.34 ± 0.25	1	1
UGC06517	37.58	0.23 ± 0.09	8.58 ^{+0.06} _{-0.08}	-1.20 ^{+0.11} _{-0.14}	-1.10 ± 0.53	8.84 ^{+0.17} _{-0.29}	9.06 ± 0.06	8.95 ^{+0.03} _{-0.04}	-0.83 ^{+0.09} _{-0.12}	-0.52 ± 0.25	1	1
UGC06526	18.14 ^a	0.60 ± 0.14	7.85 ^{+0.08} _{-0.10}	-1.04 ^{+0.12} _{-0.16}	-0.93 ± 0.53	8.99 ^{+0.18} _{-0.30}	8.84 ± 0.09	8.42 ^{+0.12} _{-0.17}	-0.47 ^{+0.14} _{-0.22}	-0.27 ± 0.25	1	2
PGC035688	38.52	0.26 ± 0.10	8.19 ^{+0.08} _{-0.10}	-1.19 ^{+0.12} _{-0.16}	-1.01 ± 0.53	8.87 ^{+0.18} _{-0.31}	8.98 ± 0.08	8.54 ^{+0.05} _{-0.06}	-0.84 ^{+0.10} _{-0.13}	-0.40 ± 0.25	1	1
UGC06545	39.05	0.48 ± 0.08	8.61 ^{+0.05} _{-0.06}	-1.25 ^{+0.10} _{-0.13}	-1.12 ± 0.53	8.67 ^{+0.17} _{-0.28}	9.07 ± 0.06	8.51 ± 0.05	-1.35 ^{+0.10} _{-0.13}	-0.54 ± 0.25	1	1
UGC06610	33.55 ^a	—	< 8.16	< -1.18	-1.00 ± 0.53	< 9.19	8.97 ± 0.08	9.62 ± 0.06	0.28 ^{+0.14} _{-0.20}	-0.39 ± 0.25	1	2
NGC3786	44.85 ^a	1.02 ± 0.06	9.51 ± 0.02	-0.84 ^{+0.09} _{-0.12}	-1.28 ± 0.53	9.33 ^{+0.17} _{-0.27}	9.14 ± 0.05	9.77 ^{+0.05} _{-0.06}	-0.58 ^{+0.10} _{-0.13}	-0.68 ± 0.25	1	2
NGC3788	53.05 ^a	0.46 ± 0.06	9.26 ± 0.04	-1.15 ^{+0.10} _{-0.12}	-1.30 ± 0.53	9.29 ^{+0.17} _{-0.28}	9.14 ± 0.05	10.02 ± 0.05	-0.39 ^{+0.10} _{-0.13}	-0.70 ± 0.25	1	2
UGC06637	44.63 ^a	0.41 ± 0.11	7.95 ^{+0.09} _{-0.11}	-1.55 ^{+0.12} _{-0.17}	-1.03 ± 0.53	8.55 ^{+0.18} _{-0.31}	9.00 ± 0.07	8.91 ^{+0.12} _{-0.17}	-0.59 ^{+0.14} _{-0.22}	-0.44 ± 0.25	1	2
NGC3796	22.07	—	< 7.38	< -2.38	-1.10 ± 0.53	< 9.08	9.05 ± 0.06	< 7.06	< -2.70	-0.51 ± 0.25	2	2
NGC3838	22.86	—	< 7.33	< -2.66	-1.16 ± 0.53	< 9.23	9.09 ± 0.06	8.36 ± 0.01	-1.63 ^{+0.09} _{-0.11}	-0.58 ± 0.25	2	2
NGC3900	29.76 ^a	0.24 ± 0.09	8.27 ^{+0.08} _{-0.10}	-2.04 ^{+0.12} _{-0.16}	-1.26 ± 0.53	8.88 ^{+0.18} _{-0.31}	9.13 ± 0.05	9.58 ± 0.03	-0.73 ^{+0.09} _{-0.12}	-0.67 ± 0.25	1	2
NGC3898	22.27 ^a	—	< 8.37	< -2.30	-1.39 ± 0.53	< 8.90	9.16 ± 0.05	9.65 ± 0.04	-1.02 ^{+0.10} _{-0.12}	-0.77 ± 0.26	2	2
UGC06791	32.94 ^a	1.04 ± 0.31	7.95 ^{+0.09} _{-0.11}	-1.30 ^{+0.12} _{-0.17}	-0.98 ± 0.53	9.31 ^{+0.18} _{-0.31}	8.94 ± 0.08	9.21 ^{+0.07} _{-0.09}	-0.04 ^{+0.11} _{-0.15}	-0.37 ± 0.25	1	2
NGC3912	23.43 ^a	0.47 ± 0.05	8.42 ± 0.03	-1.23 ^{+0.09} _{-0.12}	-1.07 ± 0.53	8.73 ^{+0.17} _{-0.27}	9.03 ± 0.07	8.96 ± 0.04	-0.69 ^{+0.10} _{-0.12}	-0.48 ± 0.25	1	2
NGC3953	17.77 ^a	—	9.77 ^{+0.10} _{-0.13}	-0.80 ^{+0.13} _{-0.18}	-1.35 ± 0.53	9.55 ^{+0.18} _{-0.32}	9.15 ± 0.05	9.59 ± 0.02	-0.98 ^{+0.09} _{-0.12}	-0.74 ± 0.26	2	2
NGC3982	20.59 ^a	—	9.26 ^{+0.12} _{-0.18}	-0.64 ^{+0.15} _{-0.23}	-1.14 ± 0.53	9.12 ^{+0.20} _{-0.37}	9.08 ± 0.06	9.31 ^{+0.08} _{-0.10}	-0.59 ^{+0.12} _{-0.16}	-0.55 ± 0.25	2	2
NGC3992	19.99 ^a	—	8.99 ± 0.04	-1.71 ^{+0.10} _{-0.12}	-1.40 ± 0.53	9.06 ^{+0.17} _{-0.28}	9.16 ± 0.05	9.84 ± 0.01	-0.86 ^{+0.09} _{-0.11}	-0.78 ± 0.26	2	2
NGC3998	21.10 ^a	—	< 7.94	< -2.46	-1.29 ± 0.53	< 8.77	9.14 ± 0.05	< 8.96	< -1.44	-0.70 ± 0.25	2	2
NGC4026	15.79 ^a	—	< 7.29	< -2.97	-1.25 ± 0.53	< 9.83	9.13 ± 0.05	< 8.00	< -2.26	-0.66 ± 0.25	2	2
NGC4051	13.95 ^a	—	9.18 ^{+0.08} _{-0.09}	-1.16 ^{+0.11} _{-0.15}	-1.27 ± 0.53	8.75 ^{+0.18} _{-0.30}	9.13 ± 0.05	9.33 ± 0.04	-1.01 ^{+0.10} _{-0.12}	-0.68 ± 0.25	2	2
NGC4088	14.51 ^a	—	9.40 ^{+0.07} _{-0.08}	-0.96 ^{+0.11} _{-0.15}	-1.28 ± 0.53	8.89 ^{+0.17} _{-0.30}	9.14 ± 0.05	9.81 ± 0.05	-0.55 ^{+0.10} _{-0.13}	-0.68 ± 0.25	2	2
NGC4096	12.24 ^a	—	8.85 ^{+0.08} _{-0.10}	-0.94 ^{+0.12} _{-0.17}	-1.11 ± 0.53	9.37 ^{+0.18} _{-0.30}	9.06 ± 0.06	9.43 ± 0.03	-0.36 ^{+0.10} _{-0.13}	-0.52 ± 0.25	2	2
NGC4100	20.31 ^a	—	9.62 ^{+0.12} _{-0.18}	-0.63 ^{+0.15} _{-0.23}	-1.24 ± 0.53	9.60 ^{+0.20} _{-0.37}	9.12 ± 0.05	9.69 ^{+0.02} _{-0.03}	-0.56 ^{+0.09} _{-0.12}	-0.65 ± 0.25	2	2
NGC4111	13.75 ^a	1.25 ± 0.30	7.41 ^{+0.09} _{-0.11}	-2.93 ^{+0.12} _{-0.17}	-1.27 ± 0.53	8.57 ^{+0.18} _{-0.31}	9.13 ± 0.05	8.73 ± 0.05	-1.61 ^{+0.10} _{-0.13}	-0.68 ± 0.25	2	2
NGC4138	16.37 ^a	—	8.45 ^{+0.11} _{-0.15}	-1.62 ^{+0.14} _{-0.21}	-1.18 ± 0.53	9.23 ^{+0.19} _{-0.35}	9.10 ± 0.05	9.10 ^{+0.04} _{-0.05}	-0.97 ^{+0.10} _{-0.13}	-0.60 ± 0.25	2	2
NGC4143	17.57 ^a	—	< 7.79	< -2.50	-1.26 ± 0.53	< 9.08	9.13 ± 0.05	< 8.88	< -1.41	-0.66 ± 0.25	2	2
NGC4144	6.85 ^a	—	7.44 ^{+0.09} _{-0.12}	-1.73 ^{+0.24} _{-0.57}	-0.97 ± 0.53	10.89 ^{+0.66} _{-0.74}	8.92 ± 0.08	8.79 ± 0.03	-0.38 ^{+0.23} _{-0.51}	-0.35 ± 0.25	2	2
NGC4151	11.27 ^a	—	8.72 ^{+0.09} _{-0.11}	-1.31 ^{+0.12} _{-0.17}	-1.17 ± 0.53	8.42 ^{+0.18} _{-0.31}	9.10 ± 0.06	9.15 ^{+0.04} _{-0.05}	-0.88 ^{+0.10} _{-0.13}	-0.59 ± 0.25	2	2

NGC4152	29.61 ^a	0.50 ± 0.04	8.93 ± 0.03	-1.05 ^{+0.09} _{-0.12}	-1.16 ± 0.53	8.49 ^{+0.17} _{-0.27}	9.09 ± 0.06	9.82 ^{+0.05} _{-0.06}	-0.16 ^{+0.10} _{-0.13}	-0.58 ± 0.25	1	2
UGC07271	12.59 ^a	—	< 7.44	< -0.56	-0.92 ± 0.54	< 9.50	8.46 ± 0.13	8.49 ^{+0.12} _{-0.17}	0.49 ^{+0.14} _{-0.22}	-0.01 ± 0.24	2	2
NGC4214	2.87 ^a	—	6.41 ^{+0.08} _{-0.10}	-2.65 ^{+0.24} _{-0.55}	-0.95 ± 0.53	7.14 ^{+0.08} _{-0.10}	8.89 ± 0.09	8.59 ± 0.01	-0.47 ^{+0.23} _{-0.51}	-0.31 ± 0.25	2	2
NGC4244	4.26 ^a	—	7.57 ^{+0.05} _{-0.06}	-1.86 ^{+0.23} _{-0.53}	-1.02 ± 0.53	8.53 ^{+0.07} _{-0.08}	8.99 ± 0.07	9.36 ^{+0.05} _{-0.06}	-0.08 ^{+0.23} _{-0.53}	-0.42 ± 0.25	2	2
NGC4314	9.81 ^a	0.159 ± 0.003	8.67 ± 0.01	-1.85 ^{+0.09} _{-0.11}	-1.34 ± 0.53	9.15 ^{+0.16} _{-0.27}	9.15 ± 0.05	6.96 ^{+0.09} _{-0.11}	-3.56 ^{+0.12} _{-0.17}	-0.73 ± 0.26	2	2
NGC4359	18.41 ^a	—	< 7.82	< -1.41	-0.98 ± 0.53	< 8.92	8.94 ± 0.08	9.26 ^{+0.12} _{-0.17}	0.03 ^{+0.14} _{-0.22}	-0.36 ± 0.25	2	2
NGC4414	17.61 ^a	—	9.95 ^{+0.07} _{-0.09}	-0.70 ^{+0.11} _{-0.15}	-1.38 ± 0.53	9.49 ^{+0.17} _{-0.30}	9.16 ± 0.05	9.73 ± 0.02	-0.92 ^{+0.09} _{-0.12}	-0.77 ± 0.26	2	2
NGC4448	20.19 ^a	—	8.70 ± 0.05	-1.56 ^{+0.10} _{-0.13}	-1.25 ± 0.53	9.42 ^{+0.17} _{-0.28}	9.13 ± 0.05	8.51 ^{+0.07} _{-0.08}	-1.75 ^{+0.11} _{-0.15}	-0.66 ± 0.25	2	2
NGC4525	13.01 ^a	—	8.03 ^{+0.12} _{-0.18}	-1.37 ^{+0.15} _{-0.23}	-1.01 ± 0.53	9.09 ^{+0.20} _{-0.37}	8.98 ± 0.07	8.63 ^{+0.06} _{-0.07}	-0.77 ^{+0.10} _{-0.14}	-0.41 ± 0.25	2	2
NGC4559	7.81 ^a	—	8.75 ^{+0.05} _{-0.06}	-1.06 ^{+0.10} _{-0.13}	-1.11 ± 0.53	8.93 ^{+0.17} _{-0.28}	9.06 ± 0.06	9.74 ^{+0.03} _{-0.04}	-0.07 ^{+0.09} _{-0.12}	-0.53 ± 0.25	2	2
NGC4793	28.29 ^a	0.59 ± 0.02	9.44 ± 0.01	-0.98 ^{+0.09} _{-0.11}	-1.30 ± 0.53	8.67 ^{+0.16} _{-0.27}	9.14 ± 0.05	9.81 ^{+0.04} _{-0.05}	-0.61 ^{+0.10} _{-0.13}	-0.70 ± 0.25	1	2
UGC08076	38.13	0.28 ± 0.14	7.48 ^{+0.08} _{-0.10}	-1.58 ^{+0.12} _{-0.16}	-0.95 ± 0.53	8.28 ^{+0.18} _{-0.31}	8.89 ± 0.09	9.01 ± 0.05	-0.05 ^{+0.10} _{-0.13}	-0.31 ± 0.25	1	2
NGC4961	39.96 ^a	0.50 ± 0.09	8.58 ^{+0.04} _{-0.05}	-1.03 ^{+0.10} _{-0.13}	-1.06 ± 0.53	8.83 ^{+0.17} _{-0.28}	9.03 ± 0.07	9.80 ^{+0.04} _{-0.05}	0.19 ^{+0.10} _{-0.13}	-0.47 ± 0.25	1	2
IC0851	44.63 ^a	0.48 ± 0.17	8.13 ^{+0.10} _{-0.13}	-1.56 ^{+0.13} _{-0.18}	-1.08 ± 0.53	8.47 ^{+0.18} _{-0.32}	9.04 ± 0.06	9.63 ^{+0.04} _{-0.05}	-0.06 ^{+0.10} _{-0.13}	-0.49 ± 0.25	1	2
NGC5012	36.96 ^a	0.80 ± 0.04	9.68 ± 0.01	-1.00 ^{+0.09} _{-0.11}	-1.40 ± 0.53	9.27 ^{+0.16} _{-0.27}	9.16 ± 0.05	9.77 ^{+0.04} _{-0.05}	-0.91 ^{+0.10} _{-0.13}	-0.77 ± 0.26	1	2
NGC5016	40.34 ^a	0.82 ± 0.10	9.09 ± 0.04	-1.16 ^{+0.10} _{-0.12}	-1.24 ± 0.53	9.02 ^{+0.17} _{-0.28}	9.12 ± 0.05	9.63 ± 0.05	-0.62 ^{+0.10} _{-0.13}	-0.65 ± 0.25	1	2
UGC08290	40.71 ^a	0.21 ± 0.11	7.86 ^{+0.10} _{-0.13}	-1.55 ^{+0.13} _{-0.18}	-1.02 ± 0.53	8.18 ^{+0.18} _{-0.33}	8.98 ± 0.07	9.38 ^{+0.06} _{-0.08}	-0.03 ^{+0.11} _{-0.14}	-0.41 ± 0.25	1	2
UGC08318	38.10 ^a	< 1.24	7.81 ^{+0.10} _{-0.12}	-1.25 ^{+0.13} _{-0.18}	-0.95 ± 0.53	8.99 ^{+0.18} _{-0.32}	8.89 ± 0.09	9.76 ^{+0.05} _{-0.06}	0.70 ^{+0.10} _{-0.13}	-0.31 ± 0.25	1	2
NGC5116	43.62 ^a	0.49 ± 0.04	9.04 ± 0.03	-1.17 ^{+0.09} _{-0.12}	-1.23 ± 0.53	9.15 ^{+0.17} _{-0.27}	9.12 ± 0.05	9.72 ^{+0.05} _{-0.06}	-0.49 ^{+0.10} _{-0.13}	-0.64 ± 0.25	1	2
NGC5117	38.70 ^a	0.77 ± 0.28	8.00 ^{+0.08} _{-0.09}	-1.40 ^{+0.11} _{-0.15}	-1.01 ± 0.53	8.49 ^{+0.18} _{-0.30}	8.98 ± 0.07	9.72 ^{+0.05} _{-0.06}	0.32 ^{+0.10} _{-0.13}	-0.41 ± 0.25	1	2
UGC08409	42.95 ^a	—	7.91 ^{+0.07} _{-0.09}	-1.38 ^{+0.11} _{-0.15}	-0.99 ± 0.53	9.28 ^{+0.18} _{-0.30}	8.95 ± 0.08	9.69 ^{+0.06} _{-0.07}	0.40 ^{+0.10} _{-0.14}	-0.38 ± 0.25	1	2
NGC5169	42.44 ^a	0.92 ± 0.17	8.36 ^{+0.05} _{-0.06}	-1.44 ^{+0.10} _{-0.13}	-1.11 ± 0.53	8.49 ^{+0.17} _{-0.28}	9.06 ± 0.06	9.83 ± 0.04	0.03 ^{+0.10} _{-0.12}	-0.52 ± 0.25	1	2
NGC5173	38.52 ^a	1.36 ± 0.10	8.29 ± 0.01	-2.14 ^{+0.09} _{-0.11}	-1.30 ± 0.53	8.74 ^{+0.16} _{-0.27}	9.14 ± 0.05	9.33 ^{+0.08} _{-0.10}	-1.10 ^{+0.12} _{-0.16}	-0.70 ± 0.25	2	2
IC4263	41.08 ^a	—	7.60 ^{+0.15} _{-0.23}	-1.75 ^{+0.17} _{-0.27}	-1.00 ± 0.53	8.41 ^{+0.21} _{-0.41}	8.97 ± 0.08	9.43 ± 0.05	0.08 ^{+0.10} _{-0.13}	-0.40 ± 0.25	1	2
PGC047274	39.33	0.50 ± 0.15	7.81 ^{+0.08} _{-0.10}	-1.45 ^{+0.21} _{-0.44}	-0.99 ± 0.53	8.94 ^{+0.18} _{-0.31}	8.95 ± 0.08	9.02 ± 0.02	-0.24 ^{+0.20} _{-0.40}	-0.37 ± 0.25	1	1
PGC047295	40.59	0.65 ± 0.14	8.27 ^{+0.07} _{-0.08}	-1.43 ^{+0.13} _{-0.18}	-1.08 ± 0.53	9.26 ^{+0.17} _{-0.29}	9.04 ± 0.06	8.08 ^{+0.11} _{-0.15}	-1.62 ^{+0.15} _{-0.23}	-0.50 ± 0.25	1	1
NGC5198	41.27 ^a	—	< 8.09	< -2.80	-1.48 ± 0.53	< 8.91	9.17 ± 0.05	8.49 ^{+0.08} _{-0.10}	-2.40 ^{+0.12} _{-0.16}	-0.83 ± 0.26	2	1
NGC5248	12.62 ^a	—	9.61 ^{+0.05} _{-0.06}	-0.59 ^{+0.10} _{-0.13}	-1.23 ± 0.53	9.43 ^{+0.17} _{-0.28}	9.12 ± 0.05	8.93 ± 0.01	-1.27 ^{+0.09} _{-0.11}	-0.64 ± 0.25	2	2
UGC08630	34.66 ^a	0.52 ± 0.21	8.35 ^{+0.09} _{-0.11}	-0.84 ^{+0.13} _{-0.18}	-0.97 ± 0.53	9.05 ^{+0.18} _{-0.31}	8.93 ± 0.08	9.67 ± 0.05	0.48 ^{+0.11} _{-0.14}	-0.35 ± 0.25	1	2
UGC08662	30.46 ^a	—	< 7.51	< -1.43	-0.94 ± 0.53	< 8.50	8.86 ± 0.09	8.91 ± 0.06	-0.03 ^{+0.10} _{-0.14}	-0.28 ± 0.25	1	2
UGC08693	42.82 ^a	0.49 ± 0.12	8.38 ± 0.05	-1.37 ^{+0.10} _{-0.13}	-1.09 ± 0.53	9.06 ^{+0.17} _{-0.28}	9.05 ± 0.06	9.56 ^{+0.12} _{-0.17}	-0.19 ^{+0.14} _{-0.22}	-0.51 ± 0.25	1	2
NGC5289	40.24 ^a	0.63 ± 0.20	8.43 ^{+0.08} _{-0.10}	-1.74 ^{+0.12} _{-0.16}	-1.22 ± 0.53	9.12 ^{+0.18} _{-0.30}	9.12 ± 0.05	9.37 ^{+0.06} _{-0.07}	-0.80 ^{+0.11} _{-0.14}	-0.63 ± 0.25	1	2
NGC5290	35.62 ^a	0.70 ± 0.02	9.66 ± 0.01	-1.03 ^{+0.09} _{-0.11}	-1.40 ± 0.53	9.79 ^{+0.16} _{-0.27}	9.16 ± 0.05	9.76 ± 0.03	-0.93 ^{+0.09} _{-0.12}	-0.78 ± 0.26	1	2
NGC5297	30.46 ^a	0.58 ± 0.07	9.02 ± 0.03	-1.39 ^{+0.10} _{-0.13}	-1.30 ± 0.53	8.90 ^{+0.17} _{-0.27}	9.14 ± 0.05	10.08 ± 0.04	-0.33 ^{+0.10} _{-0.14}	-0.70 ± 0.25	1	2
NGC5300	19.62 ^a	—	8.62 ^{+0.12} _{-0.18}	-1.03 ^{+0.15} _{-0.23}	-1.07 ± 0.53	9.21 ^{+0.20} _{-0.37}	9.03 ± 0.07	9.15 ± 0.01	-0.50 ^{+0.09} _{-0.11}	-0.48 ± 0.25	2	2
UGC08733	30.88 ^a	0.49 ± 0.19	7.99 ^{+0.08} _{-0.09}	-1.32 ^{+0.13} _{-0.18}	-1.00 ± 0.53	8.57 ^{+0.18} _{-0.30}	8.96 ± 0.08	9.67 ± 0.02	0.36 ^{+0.11} _{-0.14}	-0.38 ± 0.25	1	2

PGC049002	40.79	0.77 ± 0.09	8.65 ± 0.04	-0.87 ^{+0.23} _{-0.52}	-1.04 ± 0.53	9.05 ^{+0.11} _{-0.22}	9.01 ± 0.07	8.71 ^{+0.05} _{-0.06}	-0.81 ^{+0.23} _{-0.53}	-0.44 ± 0.25	1	1
NGC5311	40.78	0.80 ± 0.09	9.41 ± 0.03	-1.28 ^{+0.09} _{-0.12}	-1.40 ± 0.53	9.82 ^{+0.17} _{-0.27}	9.16 ± 0.05	9.30 ^{+0.07} _{-0.08}	-1.39 ^{+0.11} _{-0.15}	-0.78 ± 0.26	1	2
UGC08736	36.73	0.48 ± 0.13	8.36 ^{+0.08} _{-0.09}	-2.25 ^{+0.21} _{-0.43}	-1.37 ± 0.53	8.47 ^{+0.39} _{-0.48}	9.16 ± 0.05	8.97 ± 0.02	-1.64 ^{+0.20} _{-0.40}	-0.76 ± 0.26	1	1
NGC5313	43.62 ^a	0.67 ± 0.04	9.63 ± 0.02	-0.78 ^{+0.09} _{-0.12}	-1.30 ± 0.53	9.52 ^{+0.17} _{-0.27}	9.14 ± 0.05	9.60 ± 0.04	-0.81 ^{+0.10} _{-0.12}	-0.70 ± 0.25	1	2
NGC5320	36.28 ^a	0.53 ± 0.08	8.88 ± 0.04	-1.18 ^{+0.10} _{-0.12}	-1.18 ± 0.53	9.03 ^{+0.17} _{-0.27}	9.10 ± 0.05	9.91 ^{+0.04} _{-0.05}	-0.15 ^{+0.10} _{-0.13}	-0.60 ± 0.25	1	2
IC4336	38.61	0.70 ± 0.07	8.84 ± 0.03	-1.07 ^{+0.09} _{-0.12}	-1.14 ± 0.53	9.19 ^{+0.17} _{-0.27}	9.08 ± 0.06	8.08 ^{+0.11} _{-0.15}	-1.83 ^{+0.14} _{-0.20}	-0.56 ± 0.25	1	1
NGC5326	26.90 ^a	1.04 ± 0.42	8.01 ^{+0.12} _{-0.17}	-2.49 ^{+0.15} _{-0.22}	-1.33 ± 0.53	8.83 ^{+0.19} _{-0.36}	9.15 ± 0.05	< 8.60	< -1.90	-0.72 ± 0.26	1	2
PGC049191	38.34 ^a	0.80 ± 0.18	7.83 ^{+0.07} _{-0.09}	-1.09 ^{+0.11} _{-0.15}	-0.93 ± 0.53	8.38 ^{+0.17} _{-0.30}	8.85 ± 0.09	< 8.13	< -0.79	-0.27 ± 0.25	1	1
NGC5336	36.22	0.39 ± 0.16	8.21 ^{+0.07} _{-0.09}	-1.46 ^{+0.11} _{-0.15}	-1.07 ± 0.53	8.45 ^{+0.17} _{-0.30}	9.04 ± 0.06	9.50 ^{+0.04} _{-0.05}	-0.17 ^{+0.10} _{-0.13}	-0.49 ± 0.25	1	2
NGC5337	49.40 ^a	0.29 ± 0.11	9.01 ^{+0.06} _{-0.07}	-1.57 ^{+0.10} _{-0.14}	-1.36 ± 0.53	9.35 ^{+0.17} _{-0.29}	9.15 ± 0.05	< 9.38	< -1.20	-0.75 ± 0.26	1	2
PGC2151881	40.83	0.41 ± 0.18	7.69 ^{+0.11} _{-0.15}	-1.53 ^{+0.24} _{-0.60}	-0.98 ± 0.53	8.75 ^{+0.15} _{-0.27}	8.94 ± 0.08	< 8.19	< -1.03	-0.36 ± 0.25	1	1
NGC5346	38.09 ^a	< 0.69	7.94 ^{+0.10} _{-0.14}	-1.69 ^{+0.13} _{-0.19}	-1.06 ± 0.53	8.89 ^{+0.19} _{-0.33}	9.03 ± 0.07	9.23 ^{+0.05} _{-0.06}	-0.40 ^{+0.10} _{-0.13}	-0.48 ± 0.25	1	2
NGC5347	20.69 ^a	0.91 ± 0.05	8.64 ± 0.02	-1.45 ^{+0.10} _{-0.13}	-1.19 ± 0.53	8.00 ^{+0.17} _{-0.27}	9.11 ± 0.05	9.09 ± 0.04	-1.00 ^{+0.10} _{-0.14}	-0.61 ± 0.25	1	2
NGC5350	28.95 ^a	1.01 ± 0.06	9.27 ± 0.02	-1.42 ^{+0.13} _{-0.19}	-1.40 ± 0.53	9.03 ^{+0.17} _{-0.27}	9.16 ± 0.05	9.73 ± 0.02	-0.96 ^{+0.13} _{-0.19}	-0.78 ± 0.26	1	2
NGC5353	33.81 ^a	1.38 ± 0.20	8.62 ^{+0.05} _{-0.06}	-2.37 ^{+0.11} _{-0.15}	-1.52 ± 0.53	9.45 ^{+0.23} _{-0.50}	9.17 ± 0.06	9.68 ^{+0.05} _{-0.06}	-1.31 ^{+0.11} _{-0.14}	-0.86 ± 0.26	2	2
NGC5355	35.59 ^a	—	< 8.08	< -1.97	-1.18 ± 0.53	< 9.57	9.10 ± 0.05	9.72 ± 0.03	-0.33 ^{+0.09} _{-0.12}	-0.60 ± 0.25	2	2
PGC049386	39.68	0.56 ± 0.22	7.69 ^{+0.08} _{-0.10}	-1.72 ^{+0.24} _{-0.55}	-1.01 ± 0.53	10.14 ^{+0.11} _{-0.13}	8.98 ± 0.07	< 8.16	< -1.24	-0.41 ± 0.25	1	1
NGC5358	37.12	—	< 7.54	< -2.33	-1.13 ± 0.53	< 10.11	9.07 ± 0.06	9.24 ^{+0.07} _{-0.08}	-0.63 ^{+0.11} _{-0.15}	-0.54 ± 0.25	1	2
NGC5348	18.18 ^a	0.22 ± 0.08	8.02 ^{+0.09} _{-0.11}	-1.16 ^{+0.13} _{-0.19}	-0.97 ± 0.53	9.16 ^{+0.18} _{-0.31}	8.92 ± 0.08	8.82 ± 0.02	-0.36 ^{+0.11} _{-0.14}	-0.35 ± 0.25	1	2
NGC5362	28.03 ^a	0.61 ± 0.14	8.34 ^{+0.07} _{-0.08}	-1.66 ^{+0.11} _{-0.14}	-1.16 ± 0.53	8.69 ^{+0.17} _{-0.29}	9.09 ± 0.06	9.31 ± 0.05	-0.69 ^{+0.10} _{-0.13}	-0.58 ± 0.25	1	2
NGC5356	24.87 ^a	—	8.95 ^{+0.12} _{-0.18}	-0.77 ^{+0.15} _{-0.24}	-1.09 ± 0.53	10.07 ^{+0.20} _{-0.37}	9.05 ± 0.06	8.85 ^{+0.08} _{-0.10}	-0.87 ^{+0.12} _{-0.17}	-0.50 ± 0.25	2	2
NGC5360	22.05 ^a	0.38 ± 0.09	7.57 ^{+0.07} _{-0.08}	-1.44 ^{+0.11} _{-0.15}	-0.94 ± 0.53	9.37 ^{+0.17} _{-0.29}	8.88 ± 0.09	7.98 ^{+0.12} _{-0.17}	-1.03 ^{+0.14} _{-0.22}	-0.30 ± 0.25	1	2
NGC5371	28.43 ^a	0.97 ± 0.08	9.53 ± 0.03	-1.41 ^{+0.09} _{-0.12}	-1.50 ± 0.53	9.03 ^{+0.17} _{-0.27}	9.17 ± 0.05	9.80 ± 0.02	-1.14 ^{+0.09} _{-0.12}	-0.85 ± 0.26	1	2
NGC5363	19.41 ^a	—	9.63 ^{+0.12} _{-0.18}	-1.06 ^{+0.15} _{-0.23}	-1.40 ± 0.53	10.47 ^{+0.20} _{-0.37}	9.16 ± 0.05	8.19 ^{+0.08} _{-0.10}	-2.50 ^{+0.12} _{-0.16}	-0.78 ± 0.26	2	2
NGC5364	17.17 ^a	0.25 ± 0.06	7.99 ^{+0.08} _{-0.10}	-2.23 ^{+0.12} _{-0.16}	-1.23 ± 0.53	8.13 ^{+0.18} _{-0.30}	9.12 ± 0.05	9.45 ± 0.01	-0.77 ^{+0.09} _{-0.11}	-0.64 ± 0.25	2	2
NGC5375	40.71 ^a	1.74 ± 0.32	8.73 ^{+0.06} _{-0.07}	-1.65 ^{+0.10} _{-0.14}	-1.29 ± 0.53	9.09 ^{+0.17} _{-0.29}	9.14 ± 0.05	9.67 ± 0.03	-0.71 ^{+0.09} _{-0.12}	-0.69 ± 0.25	1	2
NGC5383	36.03 ^a	0.52 ± 0.02	9.98 ± 0.01	-0.51 ^{+0.09} _{-0.11}	-1.33 ± 0.53	9.66 ^{+0.16} _{-0.27}	9.15 ± 0.05	9.82 ± 0.04	-0.67 ^{+0.10} _{-0.12}	-0.72 ± 0.26	1	2
NGC5403	41.35	0.65 ± 0.04	9.59 ± 0.02	-1.03 ^{+0.09} _{-0.12}	-1.37 ± 0.53	9.60 ^{+0.17} _{-0.27}	9.16 ± 0.05	9.96 ± 0.04	-0.66 ^{+0.10} _{-0.12}	-0.76 ± 0.26	1	2
PGC049824	41.14	0.87 ± 0.39	7.38 ^{+0.12} _{-0.17}	-2.36 ^{+0.15} _{-0.23}	-1.09 ± 0.53	8.56 ^{+0.22} _{-0.45}	9.05 ± 0.06	< 7.78	< -1.96	-0.51 ± 0.25	1	2
PGC049852	39.59	0.48 ± 0.25	7.66 ^{+0.12} _{-0.17}	-1.58 ^{+0.15} _{-0.23}	-0.98 ± 0.53	9.04 ^{+0.20} _{-0.38}	8.94 ± 0.08	8.81 ± 0.02	-0.43 ^{+0.10} _{-0.13}	-0.36 ± 0.25	1	1
PGC049927	42.23 ^a	0.59 ± 0.20	7.94 ^{+0.09} _{-0.11}	-1.32 ^{+0.12} _{-0.17}	-0.99 ± 0.53	8.28 ^{+0.18} _{-0.31}	8.95 ± 0.08	< 8.22	< -1.04	-0.37 ± 0.25	1	1
NGC5470	24.09 ^a	0.29 ± 0.06	8.39 ^{+0.05} _{-0.06}	-1.14 ^{+0.11} _{-0.14}	-1.04 ± 0.53	9.70 ^{+0.17} _{-0.28}	9.01 ± 0.07	8.79 ± 0.03	-0.74 ^{+0.10} _{-0.13}	-0.45 ± 0.25	1	2
NGC5560	19.15 ^a	—	8.78 ^{+0.12} _{-0.18}	-1.25 ^{+0.17} _{-0.27}	-1.17 ± 0.53	9.13 ^{+0.20} _{-0.37}	9.10 ± 0.06	8.99 ± 0.01	-1.04 ^{+0.12} _{-0.17}	-0.59 ± 0.25	2	2
NGC5566	18.53 ^a	0.63 ± 0.03	9.26 ± 0.02	-1.60 ^{+0.09} _{-0.12}	-1.47 ± 0.53	9.63 ^{+0.16} _{-0.27}	9.17 ± 0.05	9.19 ± 0.04	-1.67 ^{+0.10} _{-0.12}	-0.83 ± 0.26	1	2
NGC5574	24.42 ^a	—	< 7.49	< -2.51	-1.16 ± 0.53	< 8.94	9.09 ± 0.06	7.99 ^{+0.06} _{-0.07}	-2.01 ^{+0.11} _{-0.14}	-0.58 ± 0.25	2	2
NGC5576	21.27 ^a	—	< 7.49	< -3.26	-1.42 ± 0.53	< 8.91	9.16 ± 0.05	7.64 ^{+0.12} _{-0.17}	-3.11 ^{+0.14} _{-0.22}	-0.79 ± 0.26	2	2
NGC5577	23.21 ^a	—	8.54 ^{+0.12} _{-0.18}	-1.35 ^{+0.15} _{-0.23}	-1.13 ± 0.53	9.14 ^{+0.20} _{-0.37}	9.08 ± 0.06	8.90 ^{+0.03} _{-0.04}	-0.99 ^{+0.09} _{-0.12}	-0.55 ± 0.25	2	2

UGC09215	25.12 ^a	0.39 ± 0.17	7.77 ^{+0.11} _{-0.16}	-1.56 ^{+0.15} _{-0.23}	-1.00 ± 0.53	8.05 ^{+0.19} _{-0.35}	8.96 ± 0.08	9.44 ± 0.02	0.11 ^{+0.11} _{-0.14}	-0.39 ± 0.25	1	2
NGC5636	27.04	0.79 ± 0.22	7.84 ^{+0.06} _{-0.07}	-1.92 ^{+0.11} _{-0.14}	-1.10 ± 0.53	9.01 ^{+0.17} _{-0.29}	9.05 ± 0.06	8.34 ± 0.05	-1.42 ^{+0.10} _{-0.13}	-0.51 ± 0.25	1	2
NGC5638	25.10 ^a	—	< 7.83	< -2.77	-1.37 ± 0.53	< 8.97	9.16 ± 0.05	8.12 ^{+0.08} _{-0.10}	-2.48 ^{+0.12} _{-0.16}	-0.75 ± 0.26	2	2
IC1022	38.83 ^a	1.33 ± 0.56	7.46 ^{+0.12} _{-0.16}	-1.91 ^{+0.14} _{-0.21}	-1.01 ± 0.53	8.30 ^{+0.19} _{-0.35}	8.97 ± 0.08	9.28 ± 0.05	-0.09 ^{+0.10} _{-0.13}	-0.40 ± 0.25	1	2
NGC5645	19.00 ^a	—	< 8.29	< -1.33	-1.06 ± 0.53	< 8.71	9.03 ± 0.07	9.10 ± 0.01	-0.52 ^{+0.09} _{-0.11}	-0.47 ± 0.25	2	2
IC1024	21.98 ^a	0.48 ± 0.01	8.68 ± 0.01	-0.88 ^{+0.09} _{-0.11}	-1.05 ± 0.53	8.86 ^{+0.16} _{-0.27}	9.02 ± 0.07	9.05 ± 0.01	-0.51 ^{+0.09} _{-0.11}	-0.46 ± 0.25	2	2
NGC5661	46.91 ^a	0.81 ± 0.09	8.78 ^{+0.04} _{-0.05}	-0.56 ^{+0.10} _{-0.13}	-1.00 ± 0.53	9.13 ^{+0.17} _{-0.28}	8.97 ± 0.08	9.97 ^{+0.08} _{-0.10}	0.63 ^{+0.12} _{-0.16}	-0.39 ± 0.25	1	2
NGC5658	23.42 ^a	2.80 ± 1.17	7.91 ^{+0.06} _{-0.07}	-1.39 ^{+0.10} _{-0.14}	-0.99 ± 0.53	8.96 ^{+0.17} _{-0.29}	8.96 ± 0.08	8.75 ^{+0.12} _{-0.17}	-0.55 ^{+0.14} _{-0.22}	-0.38 ± 0.25	1	2
NGC5668	26.36 ^a	0.47 ± 0.14	8.20 ^{+0.07} _{-0.09}	-1.55 ^{+0.11} _{-0.15}	-1.09 ± 0.53	8.14 ^{+0.18} _{-0.30}	9.05 ± 0.06	9.85 ± 0.01	0.10 ^{+0.09} _{-0.11}	-0.51 ± 0.25	1	2
NGC5692	24.99 ^a	0.89 ± 0.13	8.12 ^{+0.05} _{-0.06}	-1.10 ^{+0.10} _{-0.13}	-0.98 ± 0.53	8.74 ^{+0.17} _{-0.28}	8.94 ± 0.08	8.74 ^{+0.05} _{-0.06}	-0.48 ^{+0.10} _{-0.13}	-0.36 ± 0.25	1	2
NGC5701	26.40 ^a	—	< 7.89	< -2.49	-1.29 ± 0.53	< 8.83	9.14 ± 0.05	9.95 ± 0.01	-0.43 ^{+0.09} _{-0.11}	-0.69 ± 0.25	1	2
NGC5725	23.77 ^a	0.35 ± 0.09	7.78 ^{+0.07} _{-0.08}	-1.31 ^{+0.11} _{-0.15}	-0.96 ± 0.53	8.56 ^{+0.17} _{-0.29}	8.90 ± 0.09	8.73 ^{+0.08} _{-0.10}	-0.36 ^{+0.12} _{-0.16}	-0.32 ± 0.25	1	2
IC1048	29.29 ^a	0.54 ± 0.04	8.86 ± 0.03	-0.91 ^{+0.09} _{-0.12}	-1.10 ± 0.53	9.48 ^{+0.17} _{-0.27}	9.06 ± 0.06	9.45 ± 0.02	-0.32 ^{+0.09} _{-0.12}	-0.52 ± 0.25	1	2
NGC5740	28.69 ^a	1.00 ± 0.04	9.40 ± 0.01	-0.59 ^{+0.09} _{-0.11}	-1.16 ± 0.53	9.67 ^{+0.16} _{-0.27}	9.09 ± 0.06	9.84 ± 0.02	-0.15 ^{+0.09} _{-0.12}	-0.58 ± 0.25	1	2
NGC5746	29.58 ^a	1.04 ± 0.17	9.11 ± 0.05	-1.80 ^{+0.10} _{-0.13}	-1.49 ± 0.53	9.25 ^{+0.17} _{-0.28}	9.17 ± 0.05	9.80 ± 0.03	-1.11 ^{+0.09} _{-0.12}	-0.84 ± 0.26	1	2
UGC09556	54.85 ^a	< 1.94	7.78 ^{+0.14} _{-0.21}	-1.60 ^{+0.17} _{-0.29}	-1.01 ± 0.53	8.42 ^{+0.20} _{-0.39}	8.98 ± 0.08	9.92 ^{+0.05} _{-0.06}	0.54 ^{+0.12} _{-0.17}	-0.40 ± 0.25	1	2
NGC5777	45.71 ^a	0.49 ± 0.05	9.44 ± 0.03	-0.84 ^{+0.09} _{-0.12}	-1.25 ± 0.53	9.82 ^{+0.17} _{-0.27}	9.13 ± 0.05	10.23 ^{+0.03} _{-0.04}	-0.05 ^{+0.10} _{-0.12}	-0.66 ± 0.25	1	2
IC1066	32.19 ^a	0.32 ± 0.06	8.47 ± 0.05	-1.11 ^{+0.11} _{-0.14}	-1.05 ± 0.53	9.29 ^{+0.17} _{-0.28}	9.02 ± 0.07	9.27 ^{+0.08} _{-0.10}	-0.31 ^{+0.12} _{-0.17}	-0.46 ± 0.25	1	2
IC1067	24.67	0.41 ± 0.16	8.01 ^{+0.09} _{-0.12}	-1.95 ^{+0.13} _{-0.18}	-1.15 ± 0.53	8.70 ^{+0.18} _{-0.32}	9.09 ± 0.06	9.36 ^{+0.05} _{-0.06}	-0.60 ^{+0.11} _{-0.14}	-0.57 ± 0.25	1	2
NGC5770	20.80 ^a	—	< 7.41	< -2.51	-1.14 ± 0.53	< 10.42	9.08 ± 0.06	< 7.81	< -2.11	-0.56 ± 0.25	2	2
NGC5806	24.89 ^a	0.85 ± 0.04	9.36 ± 0.02	-1.21 ^{+0.09} _{-0.12}	-1.35 ± 0.53	9.39 ^{+0.16} _{-0.27}	9.15 ± 0.05	9.30 ± 0.03	-1.27 ^{+0.09} _{-0.12}	-0.74 ± 0.26	1	2
NGC5813	29.58 ^a	—	< 7.53	< -3.62	-1.59 ± 0.53	< 8.09	9.17 ± 0.06	7.78 ^{+0.12} _{-0.17}	-3.37 ^{+0.15} _{-0.22}	-0.91 ± 0.26	2	1
UGC09661	19.68	< 0.47	7.91 ± 0.05	-1.13 ^{+0.10} _{-0.13}	-0.95 ± 0.53	8.98 ^{+0.17} _{-0.28}	8.89 ± 0.09	8.12 ^{+0.06} _{-0.07}	-0.92 ^{+0.11} _{-0.14}	-0.31 ± 0.25	1	2
NGC5831	27.18 ^a	—	< 8.31	< -2.28	-1.36 ± 0.53	< 10.08	9.15 ± 0.05	< 7.84	< -2.75	-0.75 ± 0.26	2	1
NGC5838	26.94 ^a	—	< 8.09	< -2.75	-1.46 ± 0.53	< 8.85	9.17 ± 0.05	< 8.12	< -2.72	-0.82 ± 0.26	2	2
NGC5839	23.69 ^a	—	< 7.57	< -2.52	-1.19 ± 0.53	< 9.07	9.11 ± 0.05	7.96 ^{+0.09} _{-0.11}	-2.13 ^{+0.12} _{-0.17}	-0.61 ± 0.25	2	1
PGC2586382	40.10	0.69 ± 0.26	8.02 ^{+0.06} _{-0.08}	-1.47 ^{+0.11} _{-0.14}	-1.03 ± 0.53	8.97 ^{+0.17} _{-0.29}	9.00 ± 0.07	8.31 ^{+0.10} _{-0.14}	-1.18 ^{+0.13} _{-0.19}	-0.44 ± 0.25	1	1
NGC5845	28.82 ^a	—	< 7.25	< -2.97	-1.23 ± 0.53	< 8.80	9.12 ± 0.05	< 7.89	< -2.33	-0.64 ± 0.25	2	1
NGC5846	25.13 ^a	0.64 ± 0.28	8.36 ^{+0.12} _{-0.18}	-2.83 ^{+0.15} _{-0.23}	-1.61 ± 0.53	9.06 ^{+0.20} _{-0.38}	9.17 ± 0.06	8.58 ^{+0.08} _{-0.10}	-2.61 ^{+0.12} _{-0.16}	-0.92 ± 0.26	2	2
NGC5854	22.00 ^a	—	< 7.46	< -2.89	-1.28 ± 0.53	< 9.15	9.14 ± 0.05	7.58 ^{+0.06} _{-0.07}	-2.77 ^{+0.13} _{-0.18}	-0.68 ± 0.25	2	2
PGC054037	27.78	0.30 ± 0.08	7.83 ^{+0.08} _{-0.10}	-1.32 ^{+0.12} _{-0.16}	-0.97 ± 0.53	9.05 ^{+0.18} _{-0.31}	8.92 ± 0.08	< 7.85	< -1.30	-0.34 ± 0.25	1	1
NGC5864	25.93 ^a	—	< 7.73	< -2.66	-1.29 ± 0.53	< 9.49	9.14 ± 0.05	8.33 ^{+0.12} _{-0.17}	-2.06 ^{+0.14} _{-0.22}	-0.69 ± 0.25	2	2
NGC5869	27.72 ^a	—	< 7.96	< -2.43	-1.29 ± 0.53	< 9.23	9.14 ± 0.05	< 7.85	< -2.54	-0.69 ± 0.25	2	1
NGC5894	39.53 ^a	0.22 ± 0.05	9.22 ^{+0.02} _{-0.03}	-1.35 ^{+0.10} _{-0.13}	-1.35 ± 0.53	9.24 ^{+0.17} _{-0.27}	9.15 ± 0.05	9.71 ± 0.04	-0.86 ^{+0.10} _{-0.14}	-0.74 ± 0.26	1	2
PGC054346	39.22	0.44 ± 0.11	8.48 ^{+0.08} _{-0.10}	-1.16 ^{+0.13} _{-0.19}	-1.07 ± 0.53	9.13 ^{+0.18} _{-0.31}	9.03 ± 0.07	8.24 ^{+0.09} _{-0.12}	-1.40 ^{+0.13} _{-0.20}	-0.48 ± 0.25	1	1
PGC054452	28.82	—	< 7.69	< -2.01	-1.08 ± 0.53	< 9.45	9.04 ± 0.06	7.59 ^{+0.16} _{-0.25}	-2.11 ^{+0.19} _{-0.34}	-0.50 ± 0.25	2	1
UGC09837	41.66 ^a	0.44 ± 0.21	8.17 ^{+0.09} _{-0.12}	-1.42 ^{+0.12} _{-0.18}	-1.06 ± 0.53	8.31 ^{+0.18} _{-0.32}	9.02 ± 0.07	9.60 ± 0.04	0.01 ^{+0.10} _{-0.12}	-0.46 ± 0.25	1	2

NGC5951	26.84 ^a	0.27 ± 0.06	8.54 ± 0.05	$-1.26_{-0.13}^{+0.10}$	-1.11 ± 0.53	$9.04_{-0.28}^{+0.17}$	9.06 ± 0.06	$9.57_{-0.04}^{+0.03}$	$-0.23_{-0.12}^{+0.09}$	-0.52 ± 0.25	1	2
NGC5953	23.10 ^a	1.05 ± 0.02	9.42 ± 0.01	$-0.62_{-0.11}^{+0.09}$	-1.18 ± 0.53	$9.11_{-0.27}^{+0.16}$	9.10 ± 0.06	$8.96_{-0.10}^{+0.08}$	$-1.08_{-0.16}^{+0.12}$	-0.59 ± 0.25	1	2
NGC5954	32.48 ^a	0.77 ± 0.02	9.23 ± 0.01	$-0.26_{-0.11}^{+0.09}$	-1.03 ± 0.53	$9.24_{-0.27}^{+0.16}$	9.00 ± 0.07	9.12 ± 0.04	$-0.37_{-0.12}^{+0.10}$	-0.44 ± 0.25	1	2
NGC5956	29.12	0.86 ± 0.10	8.70 ± 0.04	$-1.36_{-0.12}^{+0.10}$	-1.18 ± 0.53	$9.09_{-0.28}^{+0.17}$	9.10 ± 0.05	$9.16_{-0.05}^{+0.04}$	$-0.90_{-0.13}^{+0.10}$	-0.60 ± 0.25	1	2
NGC5957	28.21	1.10 ± 0.13	8.89 ± 0.04	$-1.38_{-0.13}^{+0.10}$	-1.25 ± 0.53	$9.13_{-0.28}^{+0.17}$	9.13 ± 0.05	9.65 ± 0.04	$-0.62_{-0.12}^{+0.10}$	-0.66 ± 0.25	1	2
NGC5981	50.90 ^a	0.42 ± 0.07	9.34 ± 0.03	$-1.42_{-0.12}^{+0.09}$	-1.43 ± 0.53	$9.45_{-0.27}^{+0.17}$	9.16 ± 0.05	9.95 ± 0.04	$-0.81_{-0.12}^{+0.10}$	-0.80 ± 0.26	1	2
NGC5970	28.04 ^a	0.42 ± 0.05	9.18 ± 0.03	$-1.17_{-0.13}^{+0.10}$	-1.28 ± 0.53	$9.06_{-0.27}^{+0.17}$	9.14 ± 0.05	$9.71_{-0.07}^{+0.06}$	$-0.64_{-0.15}^{+0.11}$	-0.68 ± 0.25	1	2
NGC5982	36.12 ^a	—	< 7.67	< -3.46	-1.59 ± 0.53	< 8.50	9.17 ± 0.06	< 8.08	< -3.05	-0.90 ± 0.26	2	1
NGC5985	39.51 ^a	0.32 ± 0.13	$9.20_{-0.09}^{+0.07}$	$-1.87_{-0.15}^{+0.11}$	-1.56 ± 0.53	$8.78_{-0.30}^{+0.17}$	9.17 ± 0.06	9.83 ± 0.01	$-1.24_{-0.11}^{+0.09}$	-0.89 ± 0.26	1	1
NGC5989	43.70	0.47 ± 0.06	$8.92_{-0.04}^{+0.03}$	$-1.02_{-0.12}^{+0.09}$	-1.15 ± 0.53	$8.91_{-0.27}^{+0.17}$	9.08 ± 0.06	9.20 ± 0.06	$-0.74_{-0.14}^{+0.10}$	-0.56 ± 0.25	1	2
UGC09991	39.78 ^a	—	< 8.19	< -1.23	-1.02 ± 0.53	< 9.44	8.98 ± 0.07	$9.46_{-0.06}^{+0.05}$	$0.04_{-0.13}^{+0.10}$	-0.42 ± 0.25	1	2
NGC6012	19.35 ^a	0.53 ± 0.04	8.51 ± 0.02	$-1.74_{-0.13}^{+0.10}$	-1.24 ± 0.53	$8.66_{-0.27}^{+0.17}$	9.12 ± 0.05	9.30 ± 0.04	$-0.95_{-0.14}^{+0.10}$	-0.65 ± 0.25	1	2
UGC10086	36.28 ^a	0.43 ± 0.09	$8.26_{-0.09}^{+0.07}$	$-0.56_{-0.15}^{+0.11}$	-0.92 ± 0.53	$9.29_{-0.30}^{+0.17}$	8.82 ± 0.10	9.01 ± 0.02	$0.19_{-0.12}^{+0.09}$	-0.25 ± 0.25	1	1
IC1151	34.32 ^a	0.69 ± 0.14	$8.71_{-0.07}^{+0.06}$	$-0.83_{-0.14}^{+0.11}$	-1.04 ± 0.53	$9.23_{-0.29}^{+0.17}$	9.01 ± 0.07	$9.69_{-0.06}^{+0.05}$	$0.15_{-0.13}^{+0.10}$	-0.45 ± 0.25	1	2
IC1210	49.06 ^a	0.44 ± 0.07	8.99 ± 0.06	$-1.02_{-0.13}^{+0.10}$	-1.17 ± 0.53	$8.96_{-0.28}^{+0.17}$	9.09 ± 0.06	10.13 ± 0.05	$0.12_{-0.13}^{+0.10}$	-0.58 ± 0.25	1	2
PGC057611	44.58	0.30 ± 0.07	$8.44_{-0.08}^{+0.07}$	$-1.43_{-0.18}^{+0.13}$	-1.13 ± 0.53	$9.41_{-0.29}^{+0.17}$	9.07 ± 0.06	< 8.27	< -1.60	-0.54 ± 0.25	1	1
UGC10297	37.64 ^a	0.89 ± 0.59	$7.93_{-0.13}^{+0.10}$	$-1.56_{-0.19}^{+0.13}$	-1.03 ± 0.53	$8.75_{-0.32}^{+0.18}$	9.00 ± 0.07	$9.47_{-0.10}^{+0.08}$	$-0.02_{-0.17}^{+0.12}$	-0.44 ± 0.25	1	2
UGC10413	45.89 ^a	0.44 ± 0.24	$7.83_{-0.13}^{+0.10}$	$-1.86_{-0.20}^{+0.14}$	-1.08 ± 0.53	$8.36_{-0.33}^{+0.19}$	9.04 ± 0.06	$9.98_{-0.06}^{+0.05}$	$0.29_{-0.15}^{+0.11}$	-0.49 ± 0.25	1	2
NGC6181	32.75 ^a	0.65 ± 0.02	9.69 ± 0.01	$-0.66_{-0.11}^{+0.09}$	-1.28 ± 0.53	$9.14_{-0.27}^{+0.16}$	9.14 ± 0.05	$9.91_{-0.06}^{+0.05}$	$-0.44_{-0.13}^{+0.10}$	-0.68 ± 0.25	1	2
NGC6186	43.10	1.02 ± 0.03	9.58 ± 0.01	$-0.89_{-0.11}^{+0.09}$	-1.32 ± 0.53	$9.27_{-0.27}^{+0.16}$	9.15 ± 0.05	9.00 ± 0.05	$-1.47_{-0.13}^{+0.10}$	-0.72 ± 0.26	1	2
NGC6267	53.05 ^a	0.45 ± 0.08	$9.06_{-0.06}^{+0.05}$	$-1.09_{-0.28}^{+0.17}$	-1.21 ± 0.53	$9.19_{-0.28}^{+0.17}$	9.11 ± 0.05	$9.62_{-0.05}^{+0.04}$	$-0.53_{-0.28}^{+0.17}$	-0.62 ± 0.25	1	2
NGC6276	40.74	0.26 ± 0.14	$7.92_{-0.14}^{+0.11}$	$-1.80_{-0.22}^{+0.14}$	-1.09 ± 0.53	$9.44_{-0.36}^{+0.19}$	9.05 ± 0.06	8.85 ± 0.03	$-0.87_{-0.14}^{+0.11}$	-0.50 ± 0.25	1	1
NGC6278	37.03 ^a	—	< 8.33	< -2.40	-1.42 ± 0.53	< 9.36	9.16 ± 0.05	8.73 ± 0.04	$-2.00_{-0.12}^{+0.10}$	-0.79 ± 0.26	1	2
NGC6306	44.96	0.75 ± 0.04	9.12 ± 0.02	$-0.72_{-0.12}^{+0.09}$	-1.12 ± 0.53	$8.67_{-0.27}^{+0.17}$	9.07 ± 0.06	$8.76_{-0.08}^{+0.07}$	$-1.08_{-0.15}^{+0.11}$	-0.54 ± 0.25	1	2
UGC10721	47.18 ^a	0.73 ± 0.11	$9.06_{-0.05}^{+0.04}$	$-1.03_{-0.14}^{+0.10}$	-1.19 ± 0.53	$9.05_{-0.28}^{+0.17}$	9.11 ± 0.05	$9.52_{-0.05}^{+0.04}$	$-0.57_{-0.14}^{+0.10}$	-0.61 ± 0.25	1	2
UGC10968	43.32	1.16 ± 0.62	$8.02_{-0.19}^{+0.13}$	$-1.28_{-0.24}^{+0.15}$	-0.99 ± 0.53	$9.93_{-0.42}^{+0.21}$	8.96 ± 0.08	$9.20_{-0.09}^{+0.07}$	$-0.10_{-0.15}^{+0.11}$	-0.38 ± 0.25	1	2

Table B.6: Summary of molecular and atomic gas properties for our sample of filament galaxies. Column description. (1-2) galaxy ID and distance, for the sources denoted with the symbol ^a we report redshift independent distances; (3) excitation ratio; (4) H₂ mass; (5) M_{H_2}/M_{\star} ratio; (6) M_{H_2}/M_{\star} at the main sequence (MS); (7) depletion time; (8) depletion time at the MS; (8) H I mass; (9) M_{HI}/M_{\star} ratio; (10) M_{HI}/M_{\star} at the MS; (11-12) references for CO and HI denoted as follows: this work (1) and literature (2). Quantities at the MS are estimated as in Appendix D.

Appendix C: CO and HI spectra

In this section we show CO and HI spectra from our IRAM-30m and Nançay campaigns.

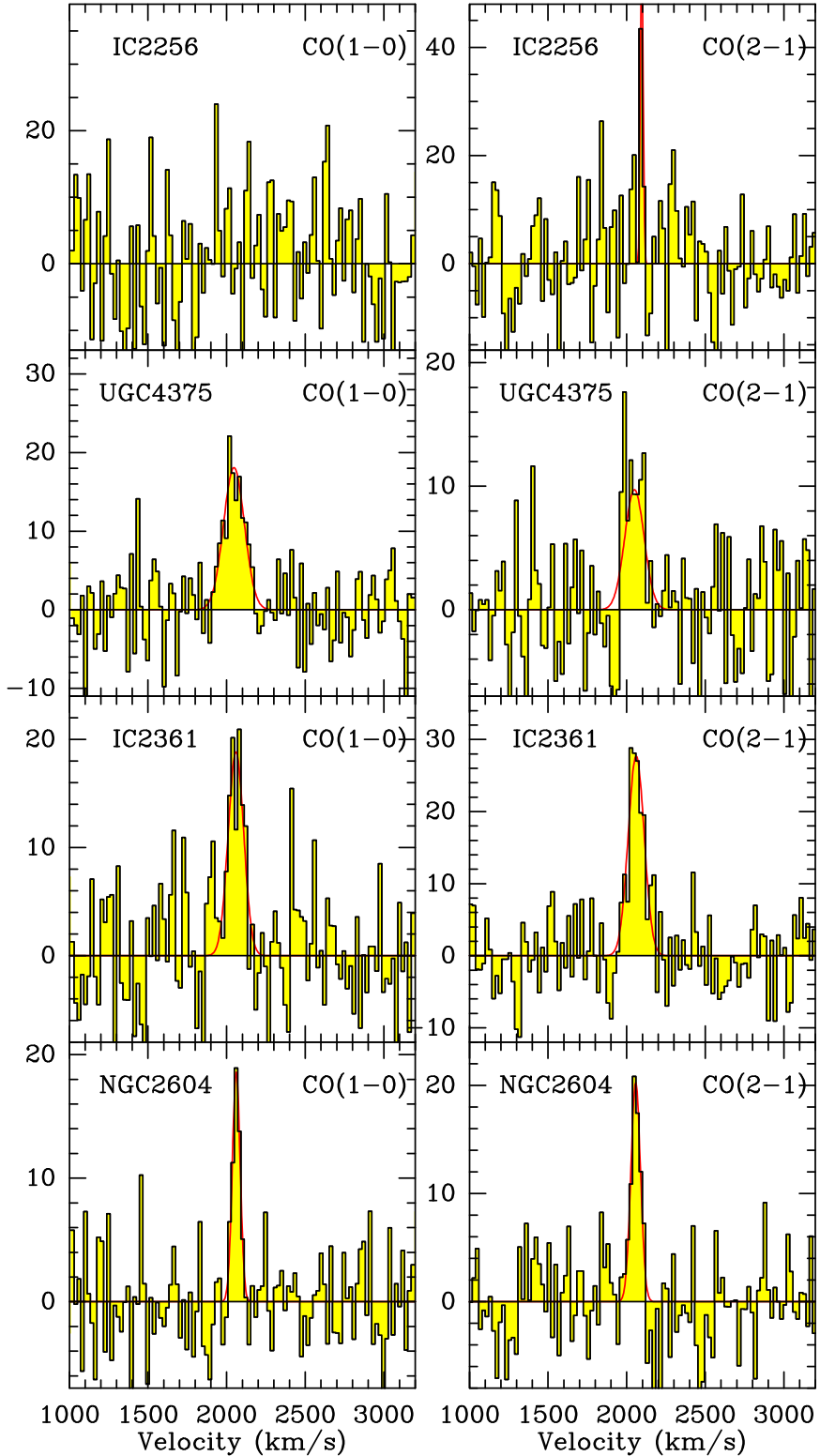


Fig. C.1: Baseline subtracted CO($1 \rightarrow 0$) (left) and CO($2 \rightarrow 1$) (right) spectra from our IRAM-30m campaign for the sources with secure or tentative detections in CO. For each spectrum, the x-axis shows the relative velocity, while in the y-axis T_{mb} is shown in units of mK. Solid red curves show the Gaussian fits to the CO($1 \rightarrow 0$) and CO($2 \rightarrow 1$) lines.

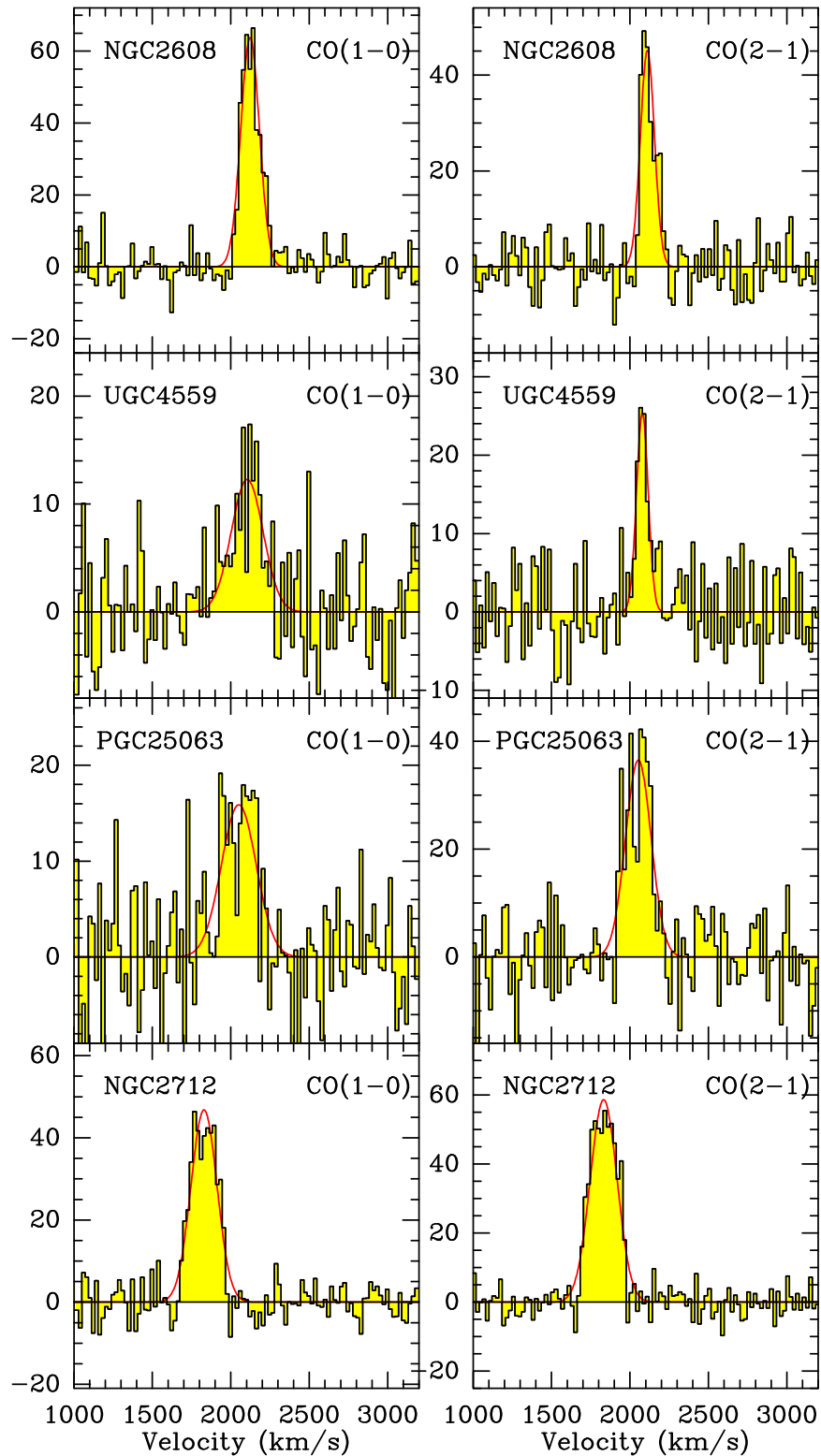


Fig. C.1: Continued.

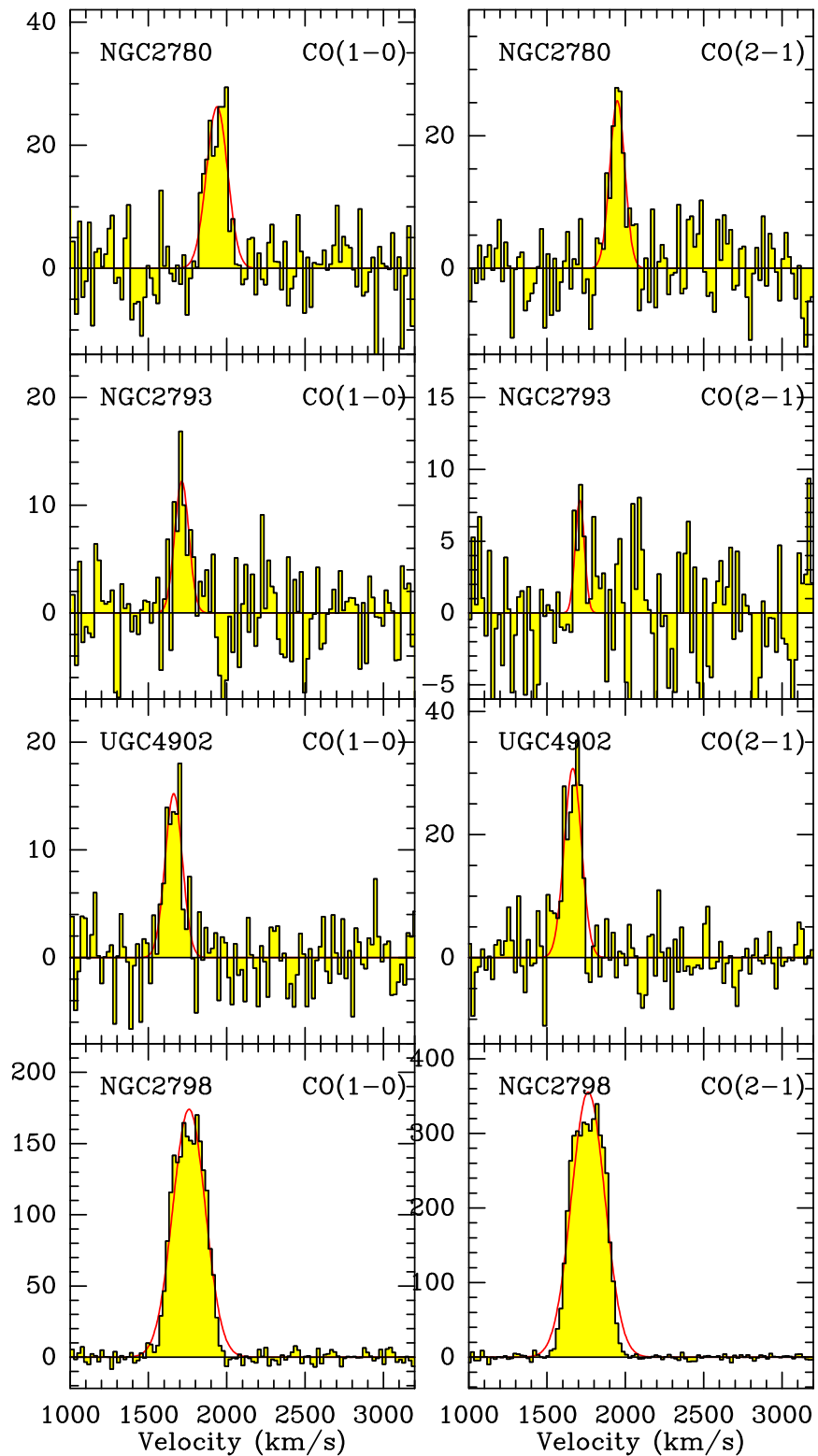


Fig. C.1: Continued.

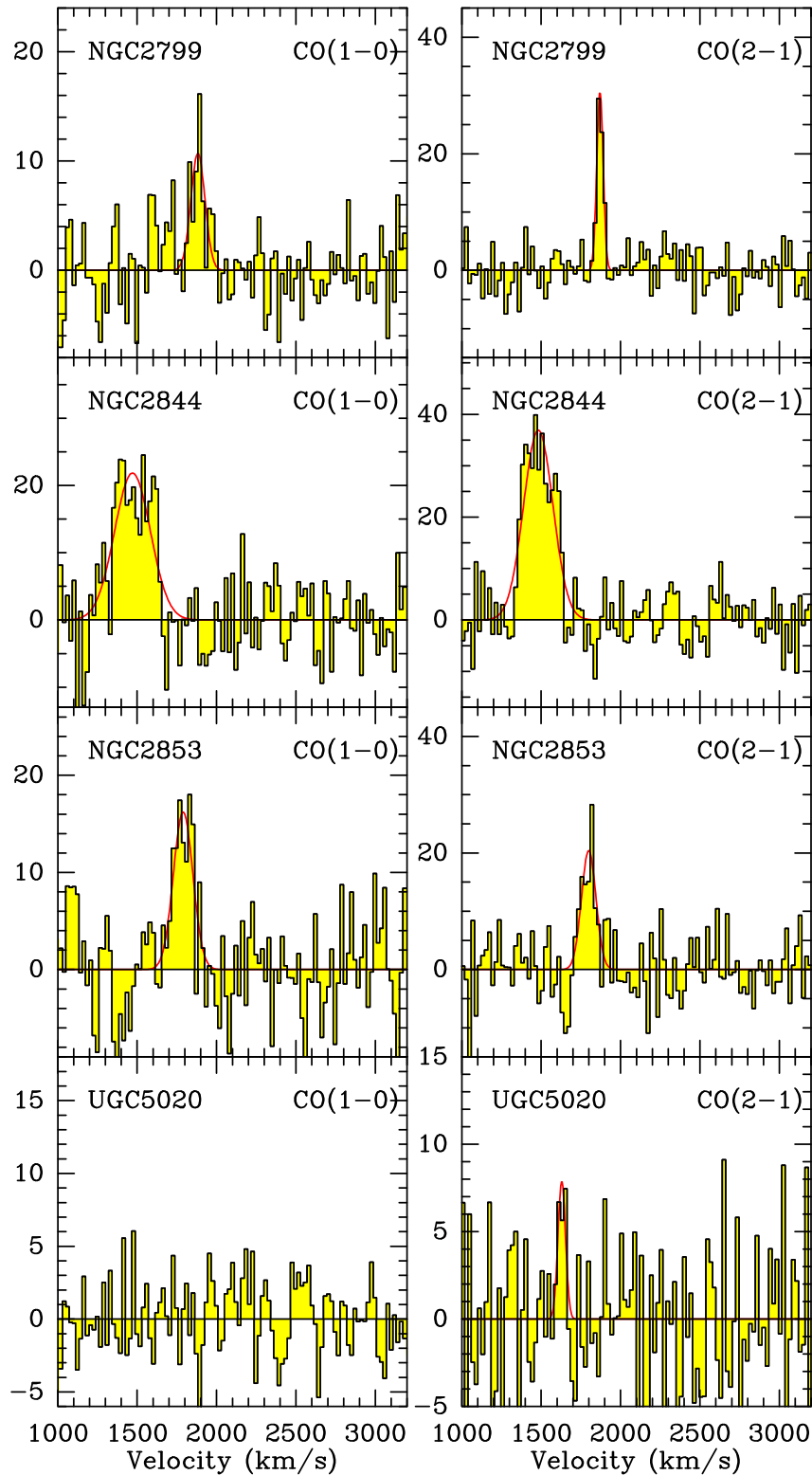


Fig. C.1: Continued.

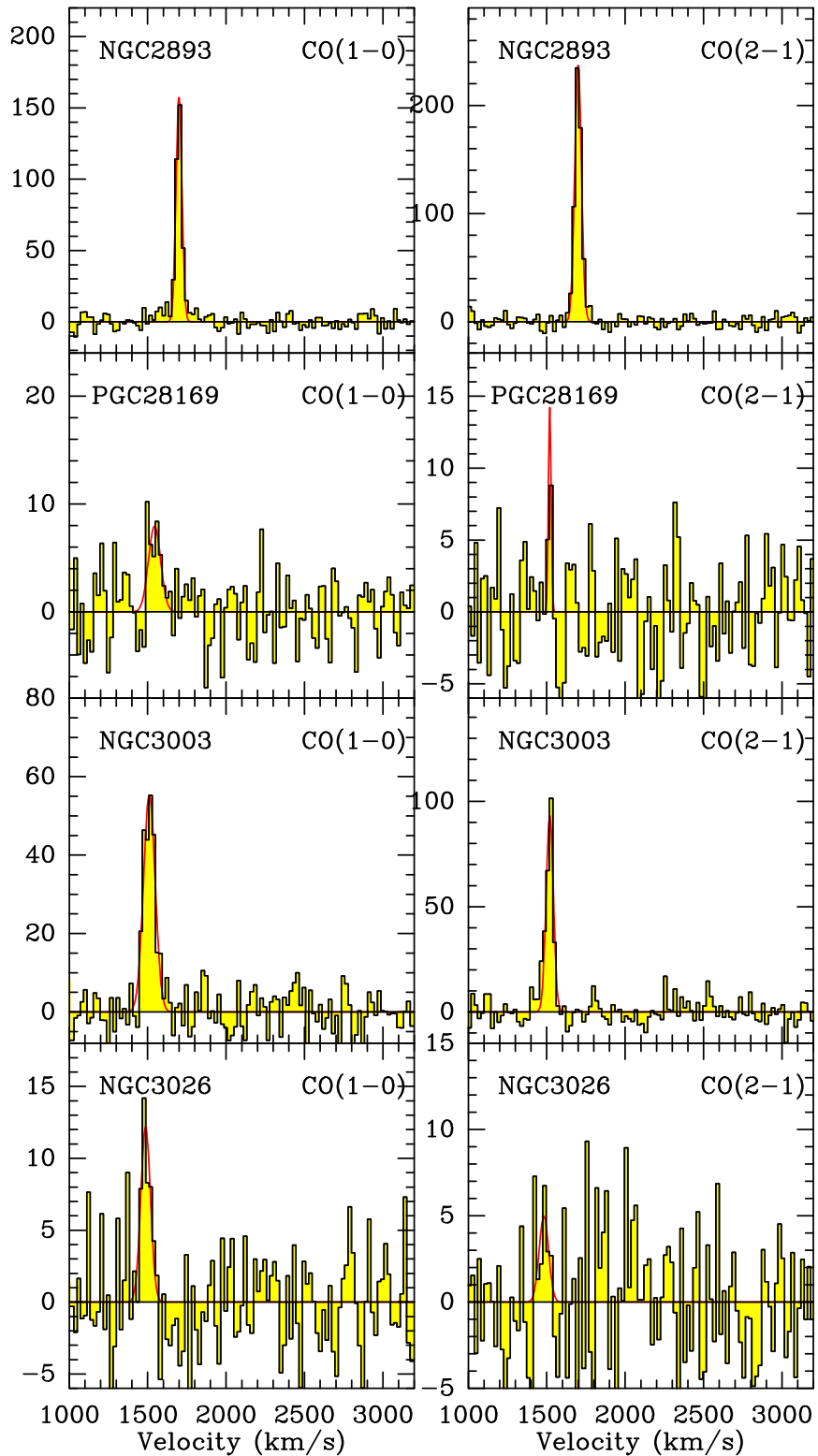


Fig. C.1: Continued.

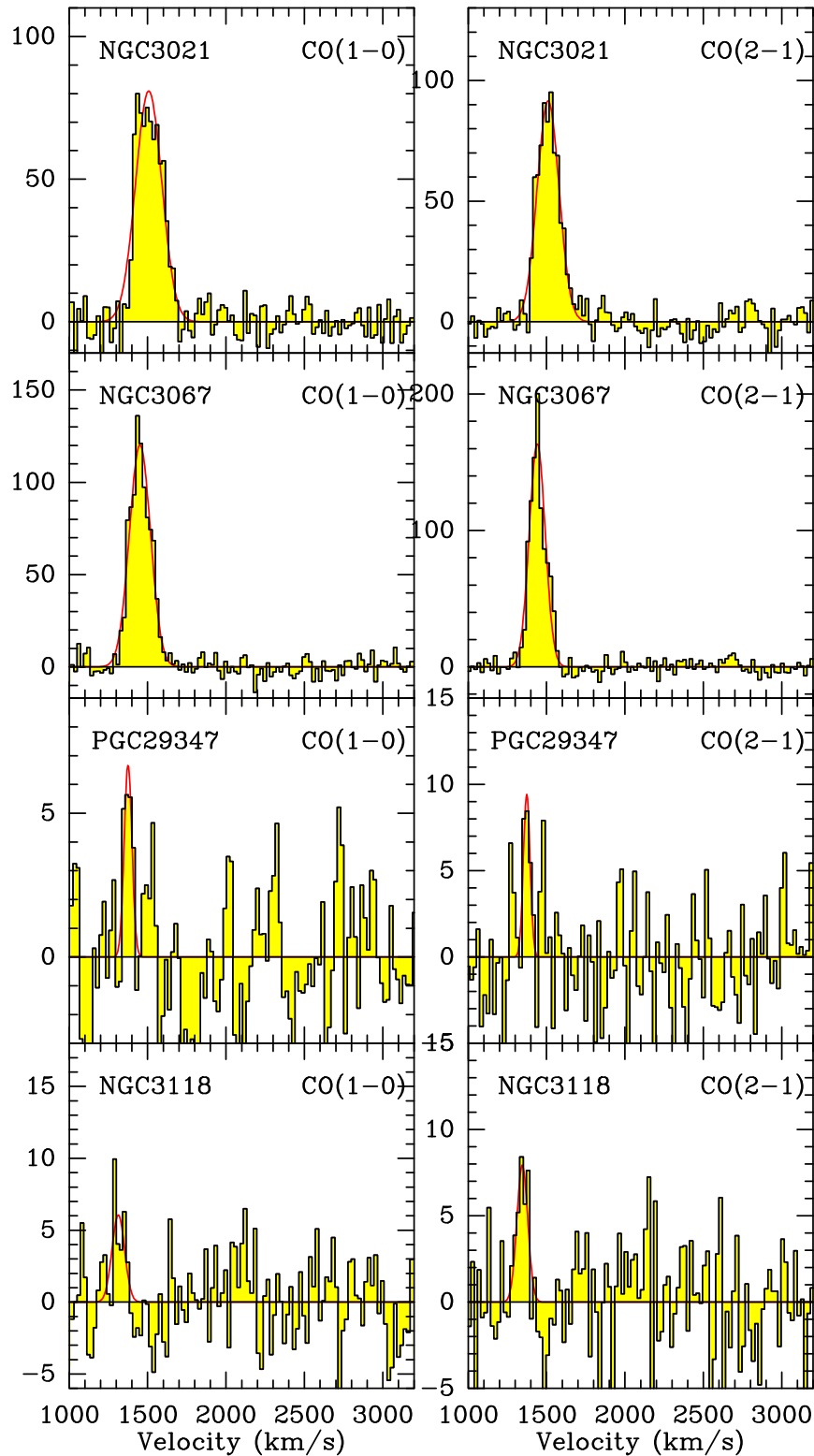


Fig. C.1: Continued.

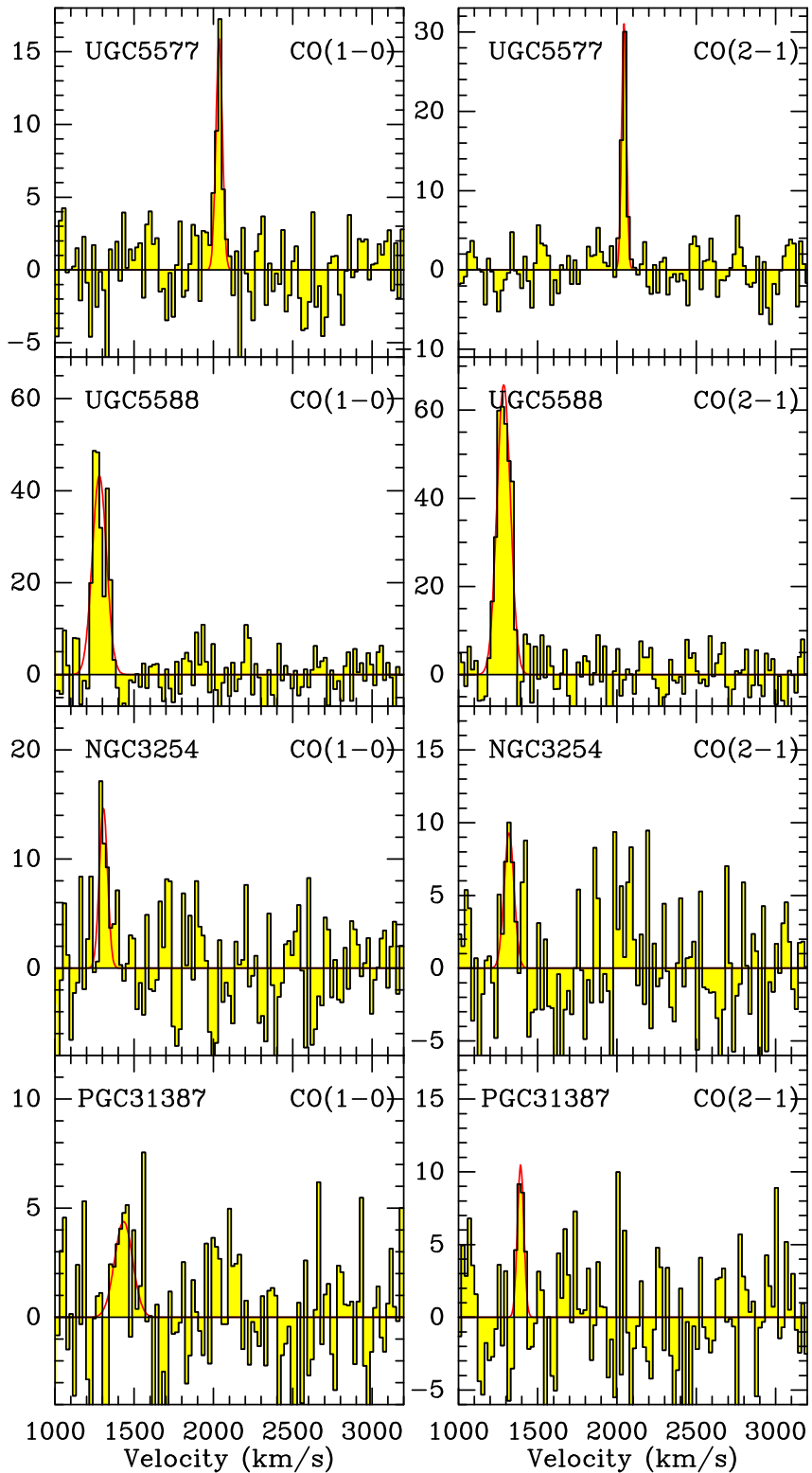


Fig. C.1: Continued.

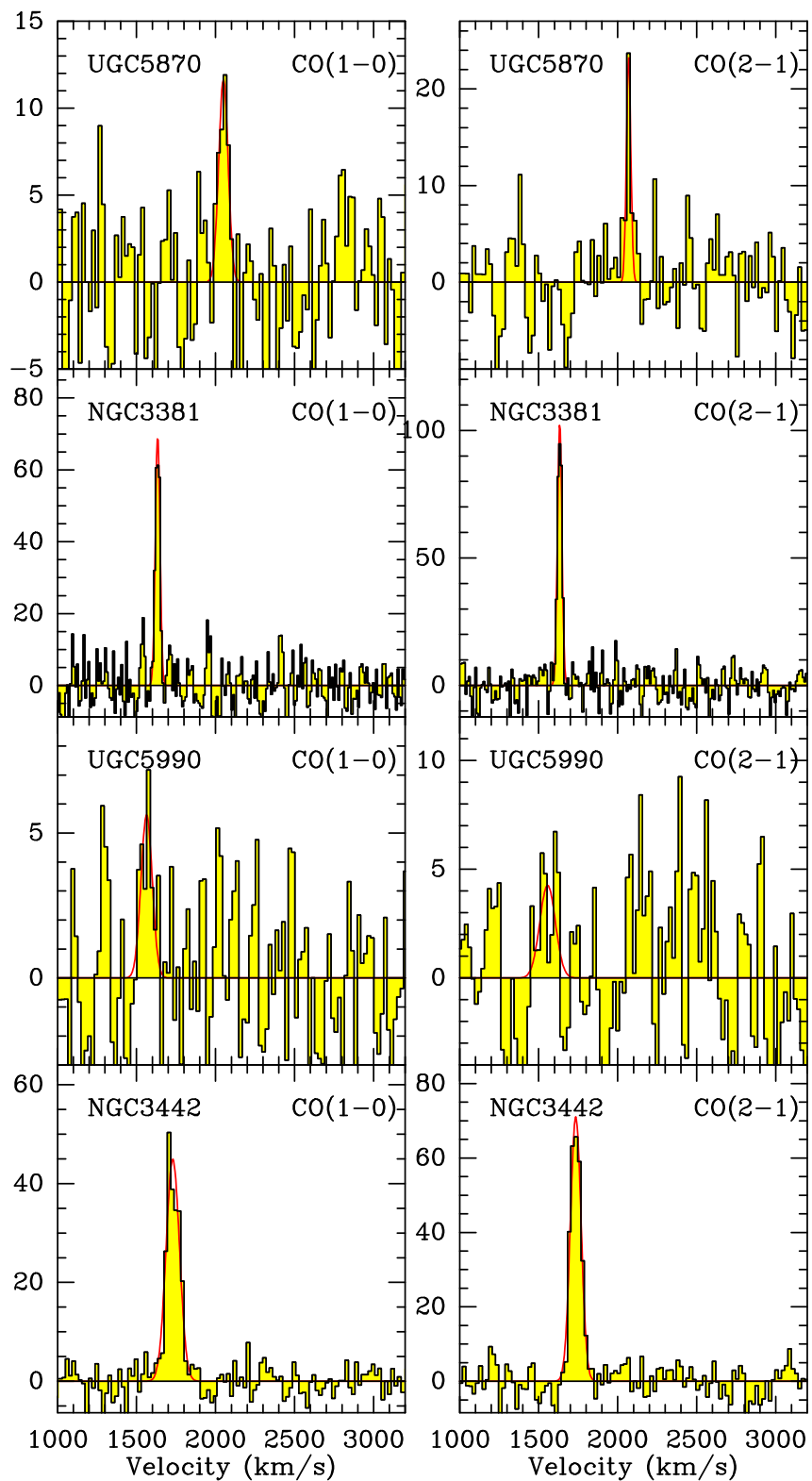


Fig. C.1: Continued.

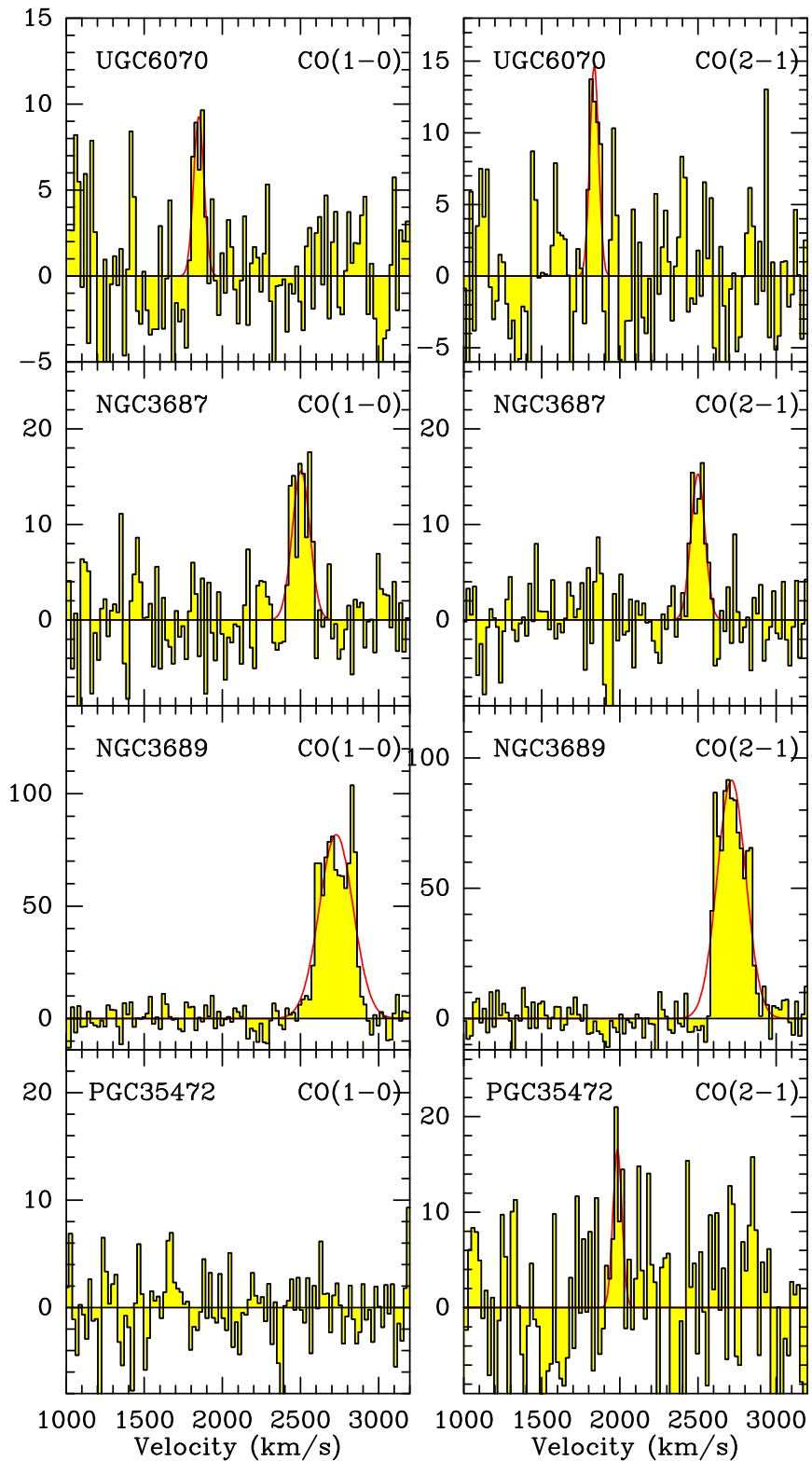


Fig. C.1: Continued.

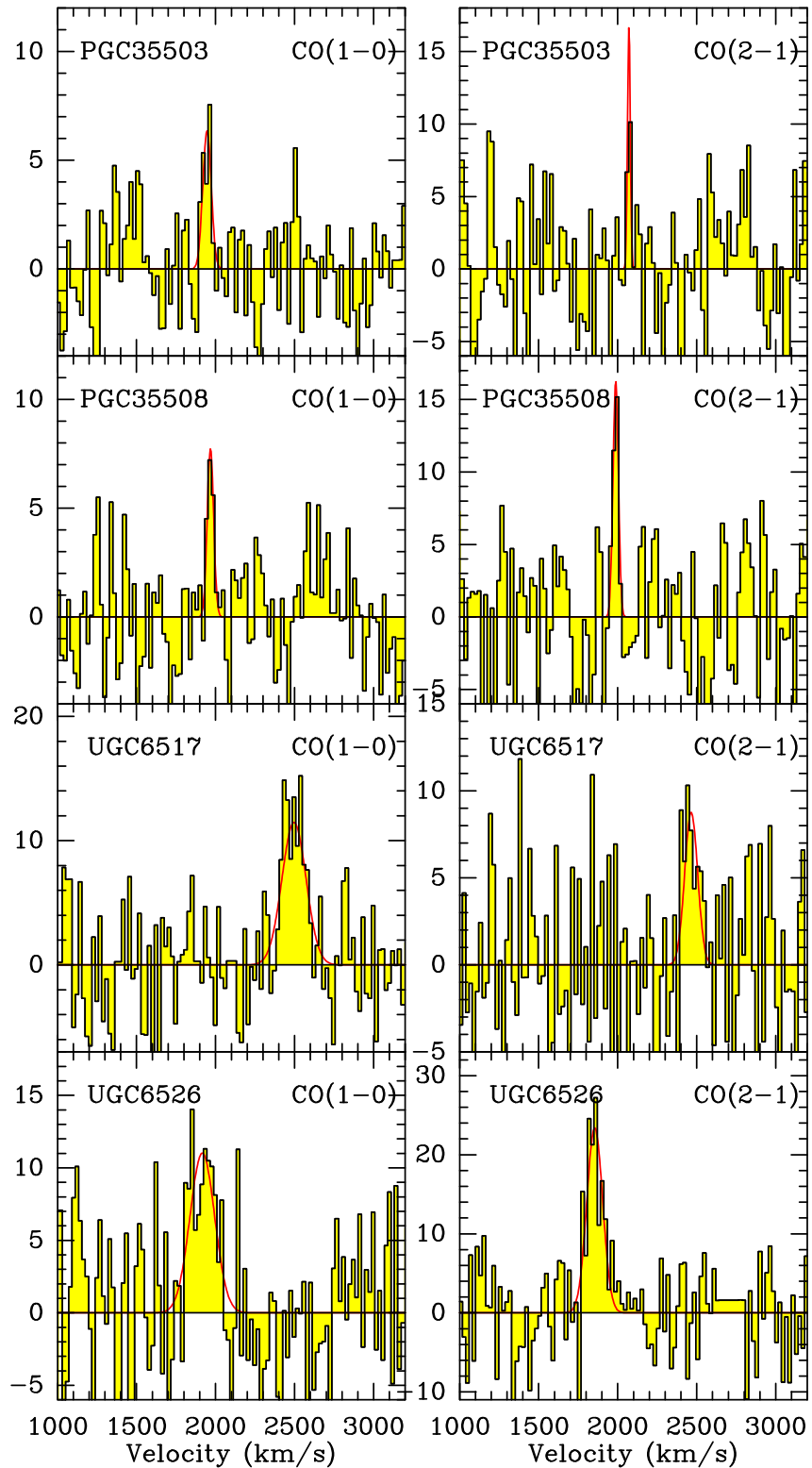


Fig. C.1: Continued.

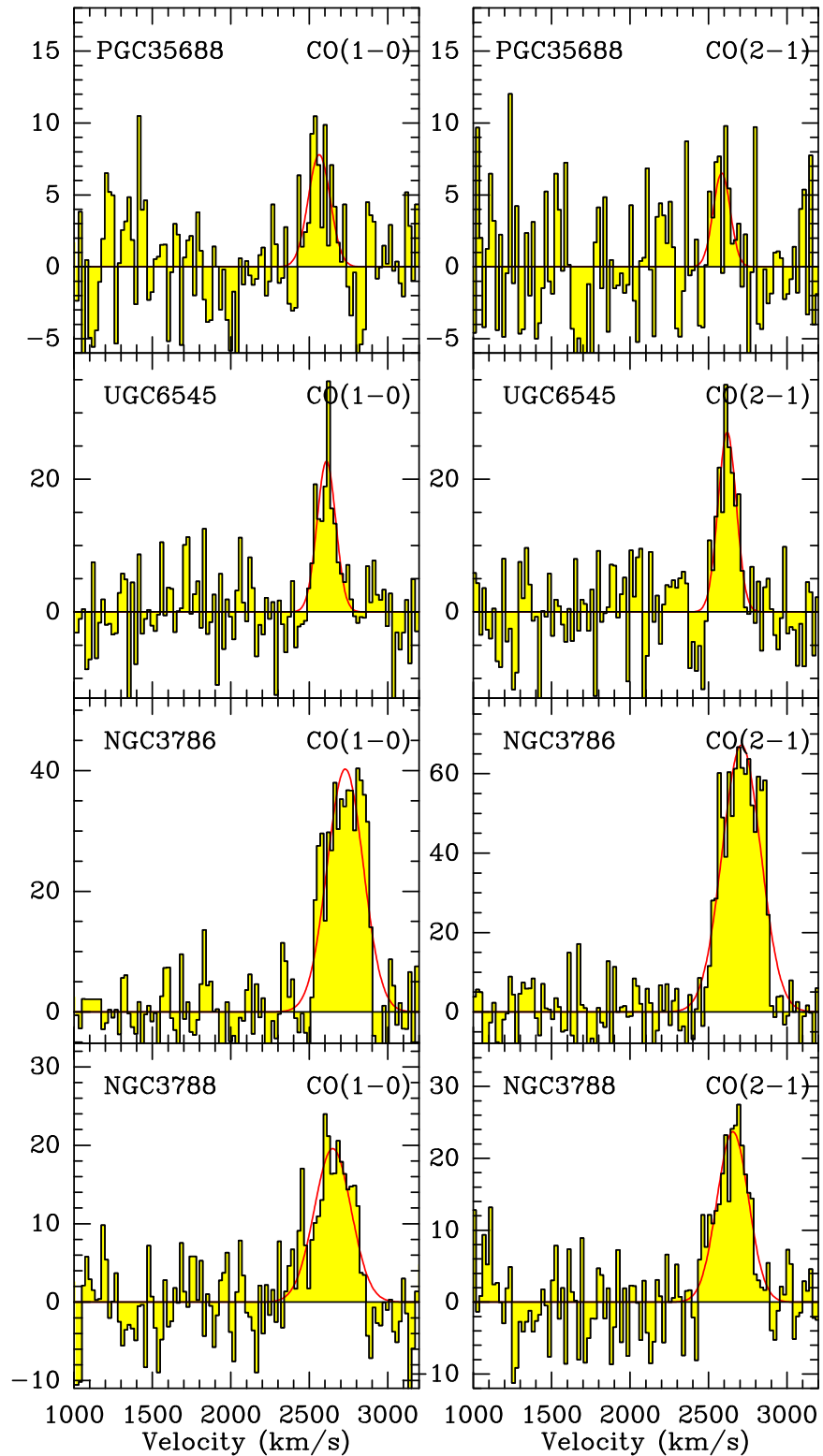


Fig. C.1: Continued.

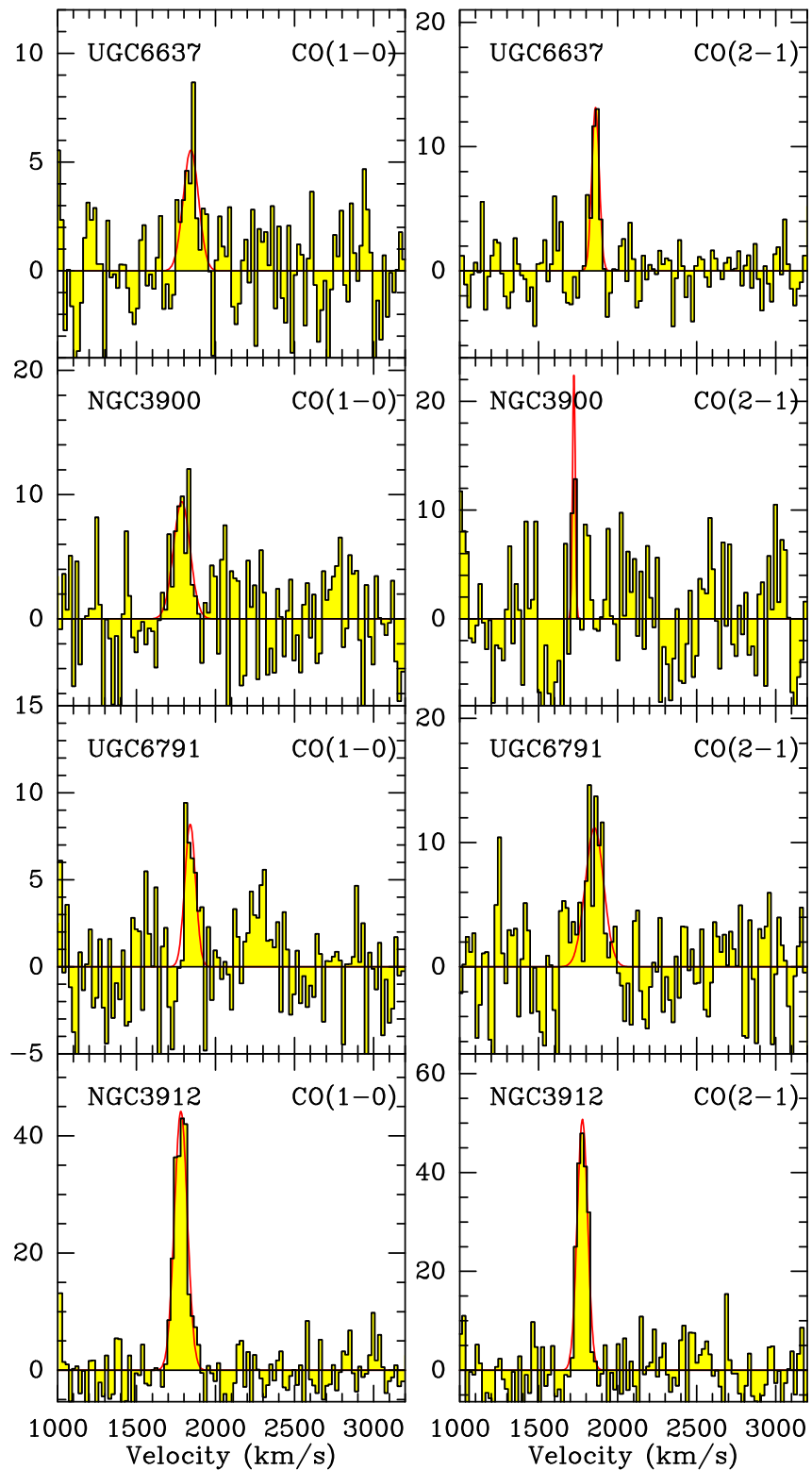


Fig. C.1: Continued.

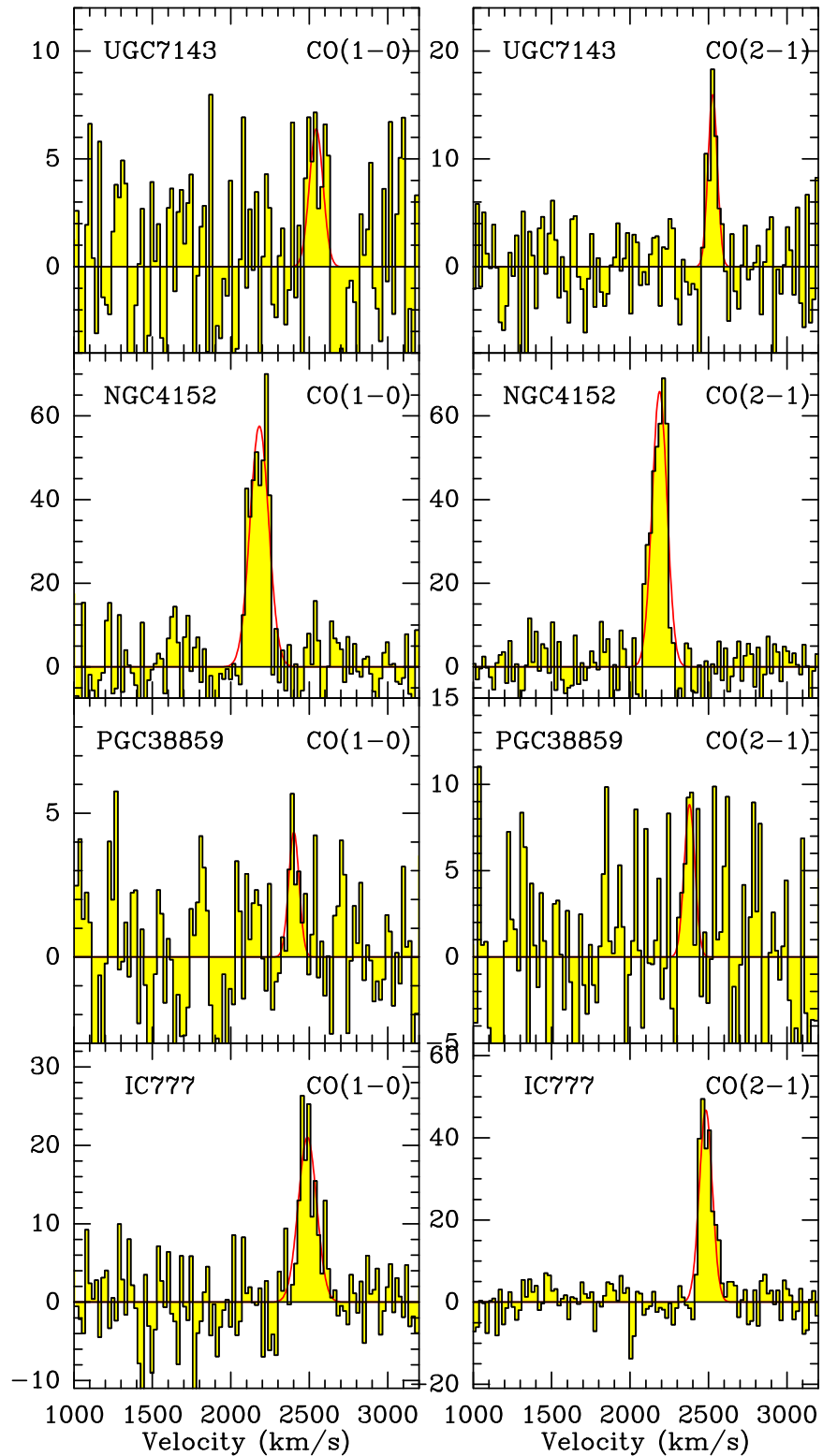


Fig. C.1: Continued.

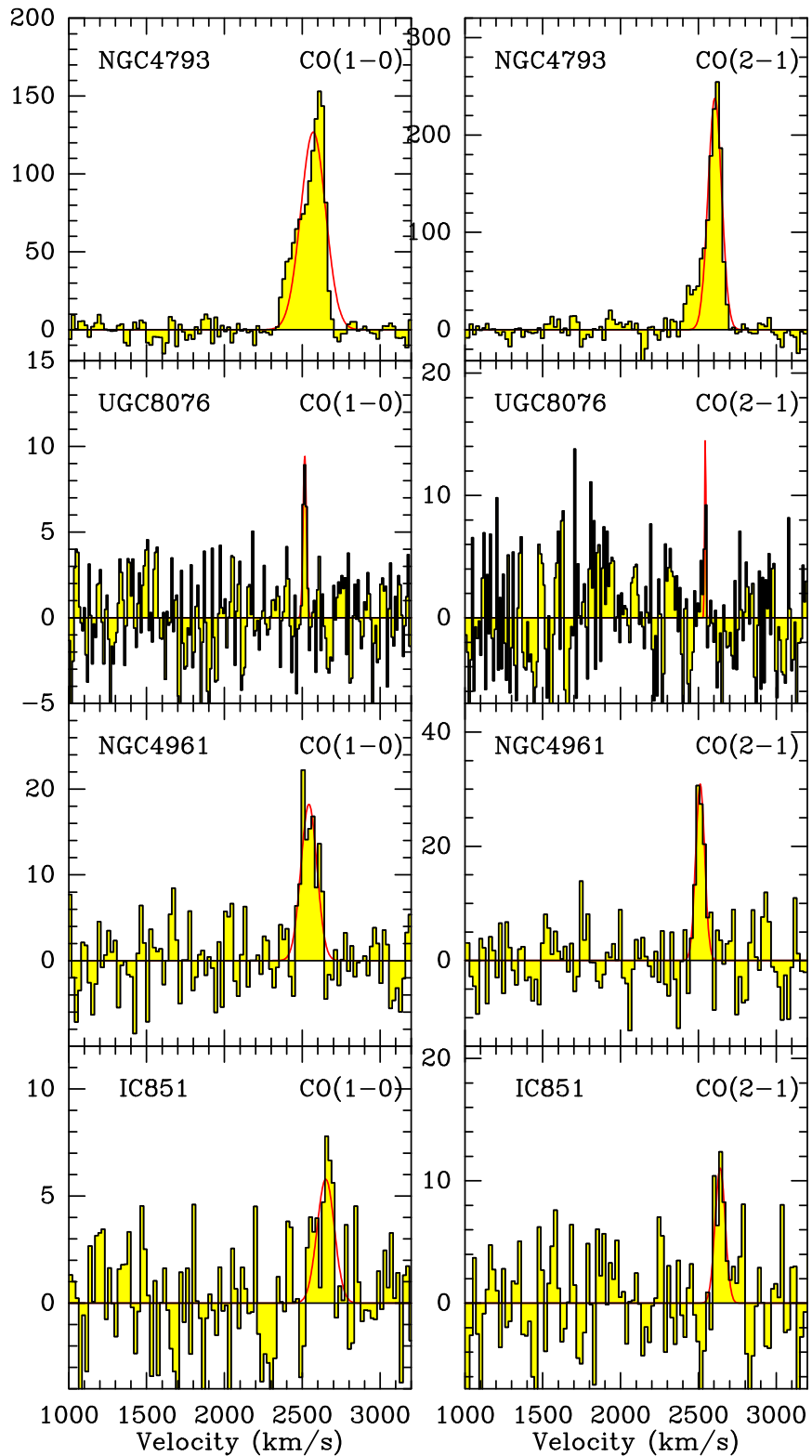


Fig. C.1: Continued.

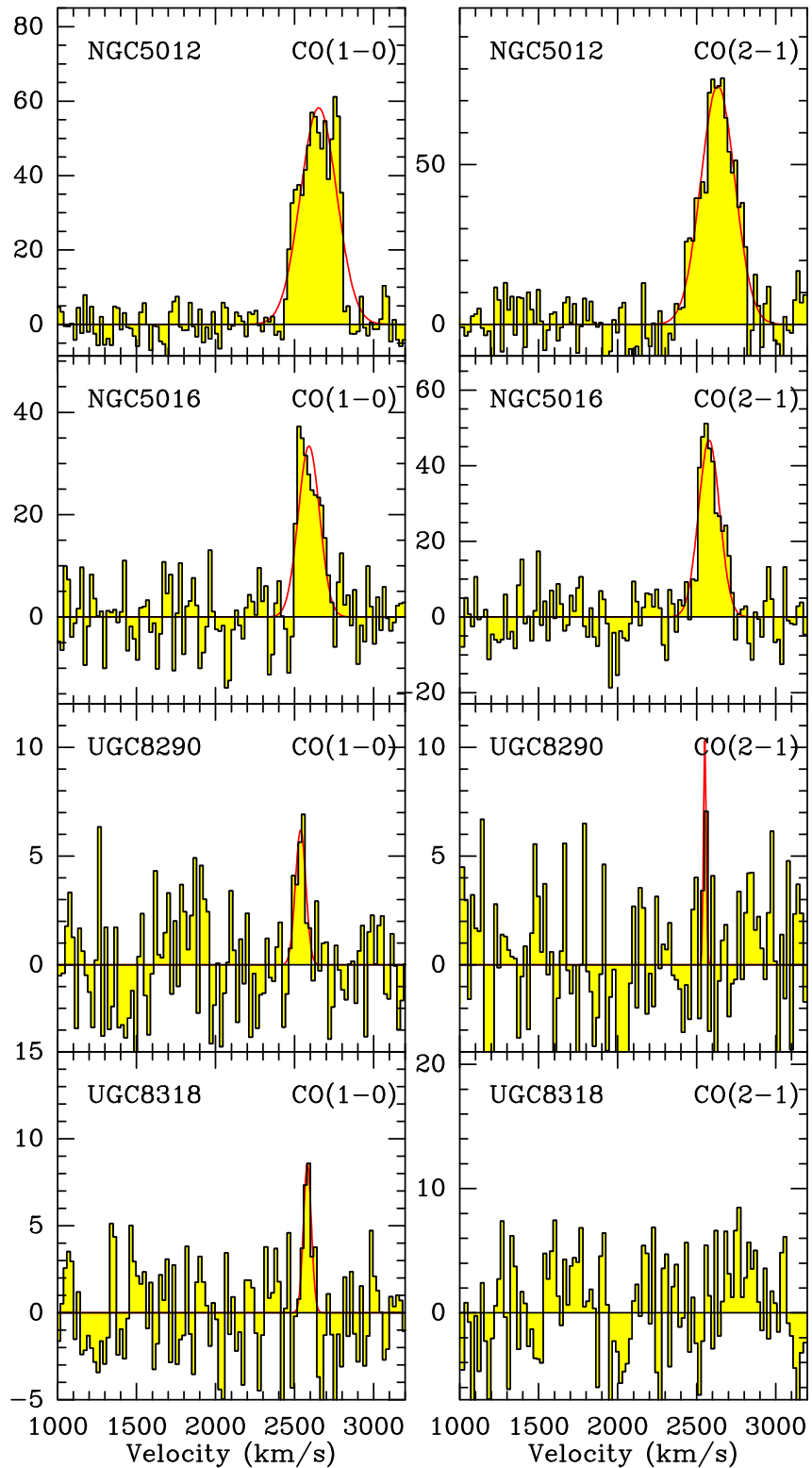


Fig. C.1: Continued.

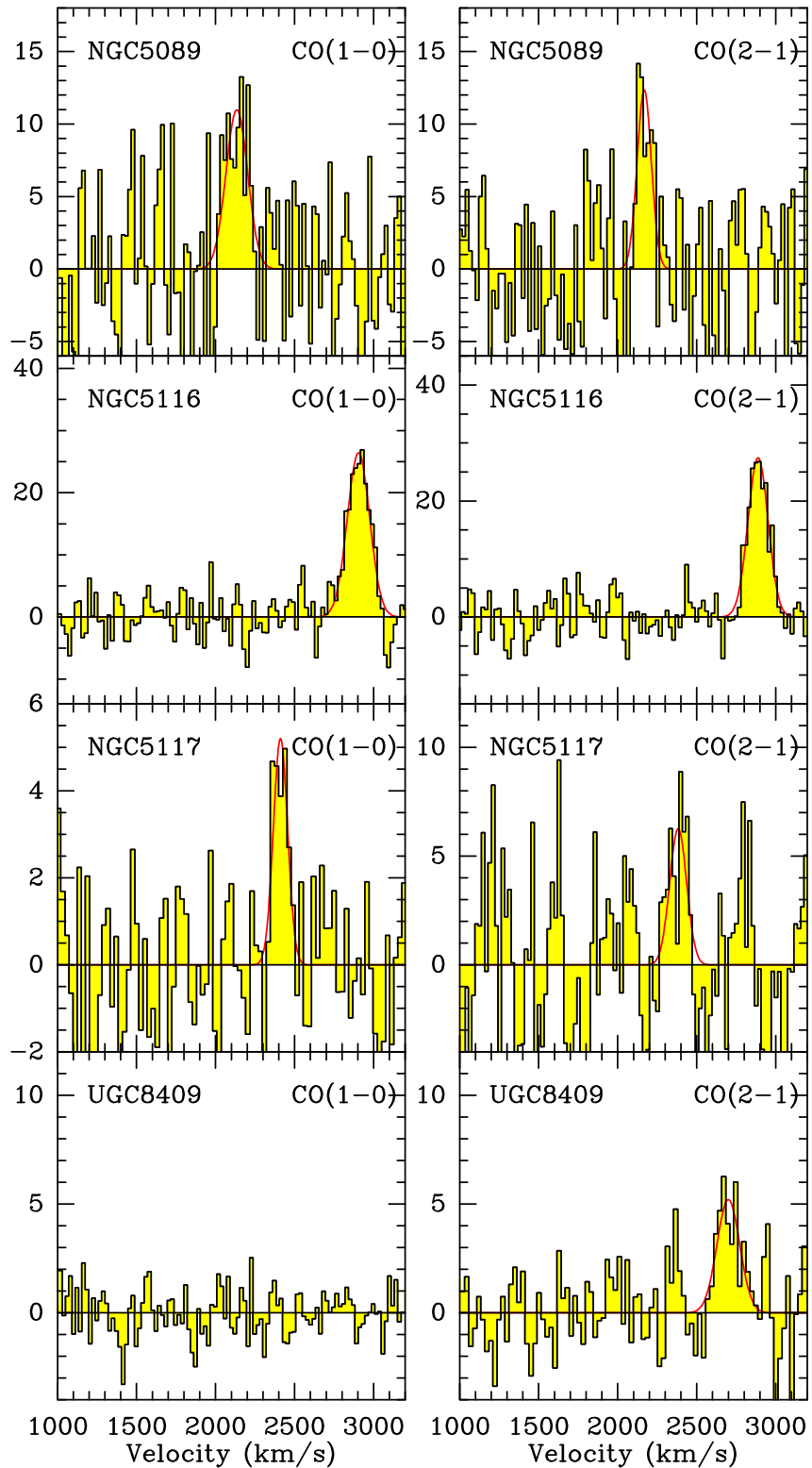


Fig. C.1: Continued.

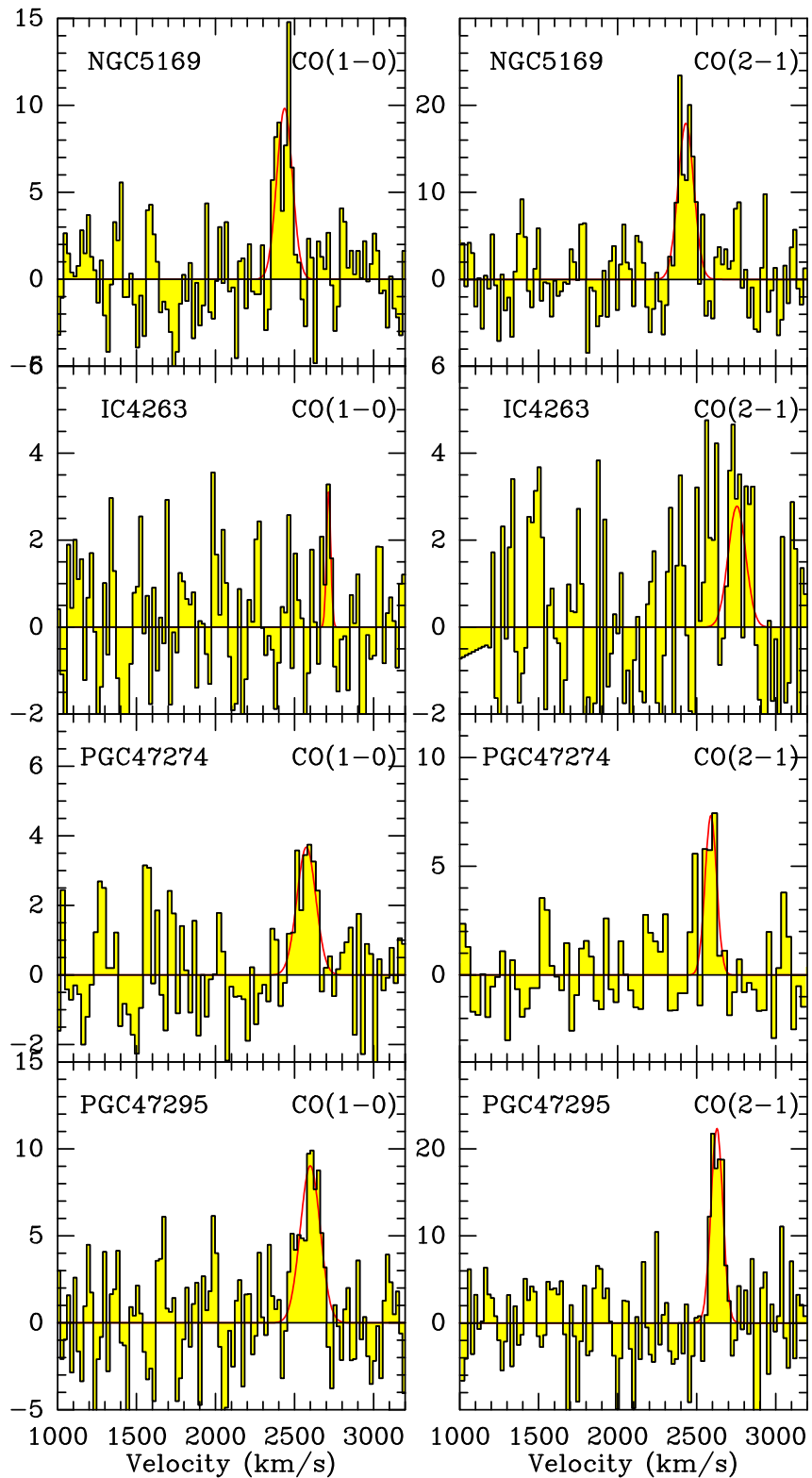


Fig. C.1: Continued.

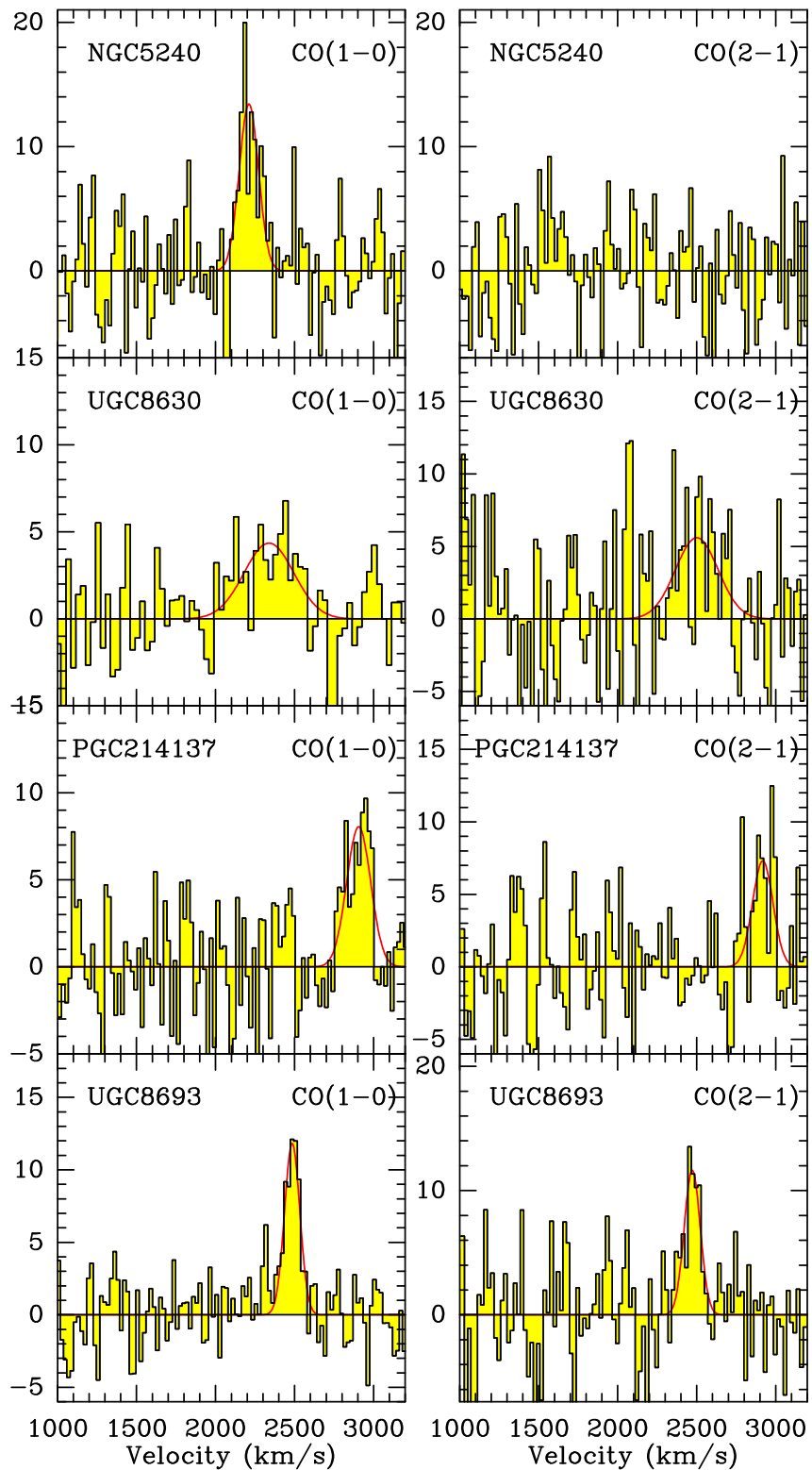


Fig. C.1: Continued.

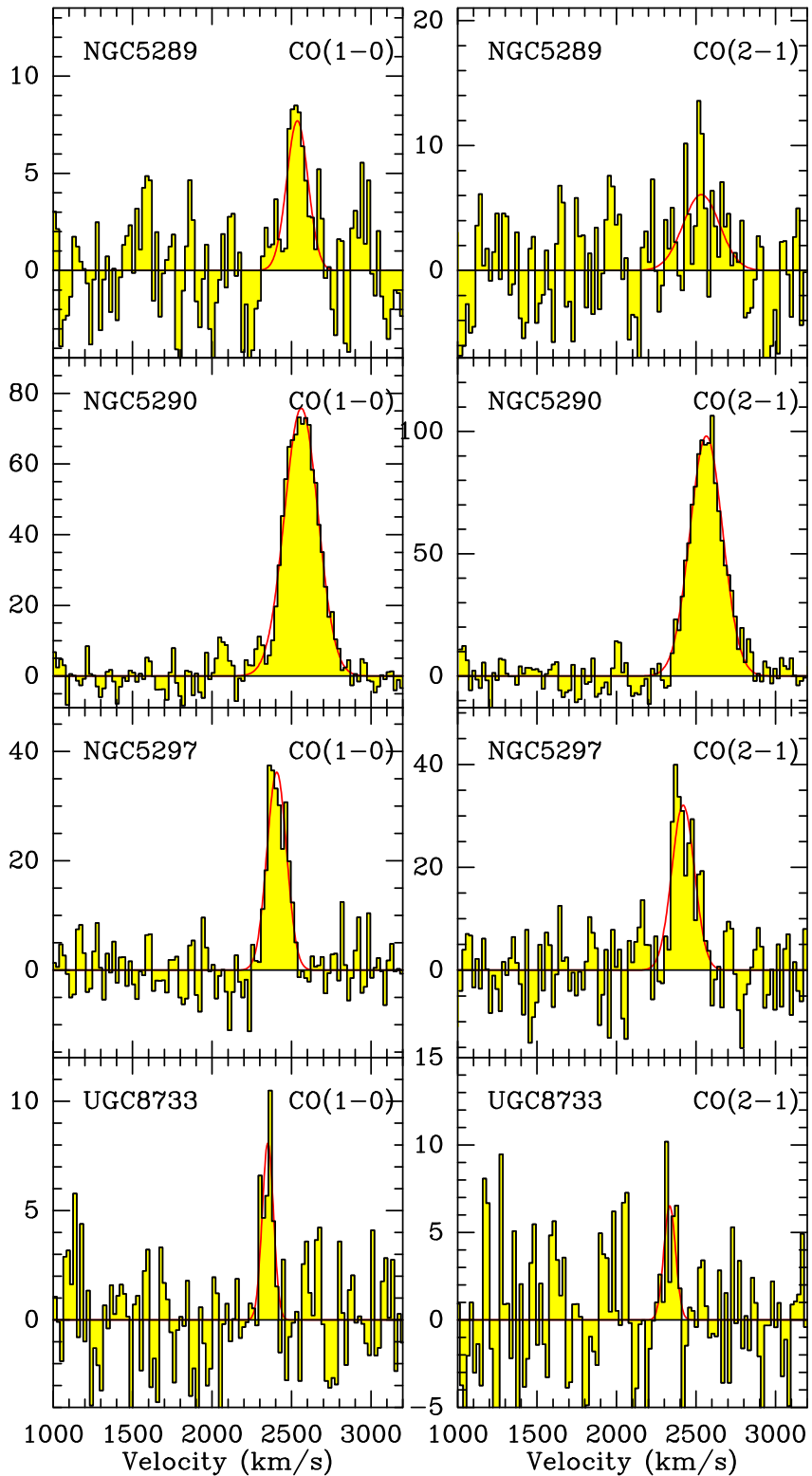


Fig. C.1: Continued.

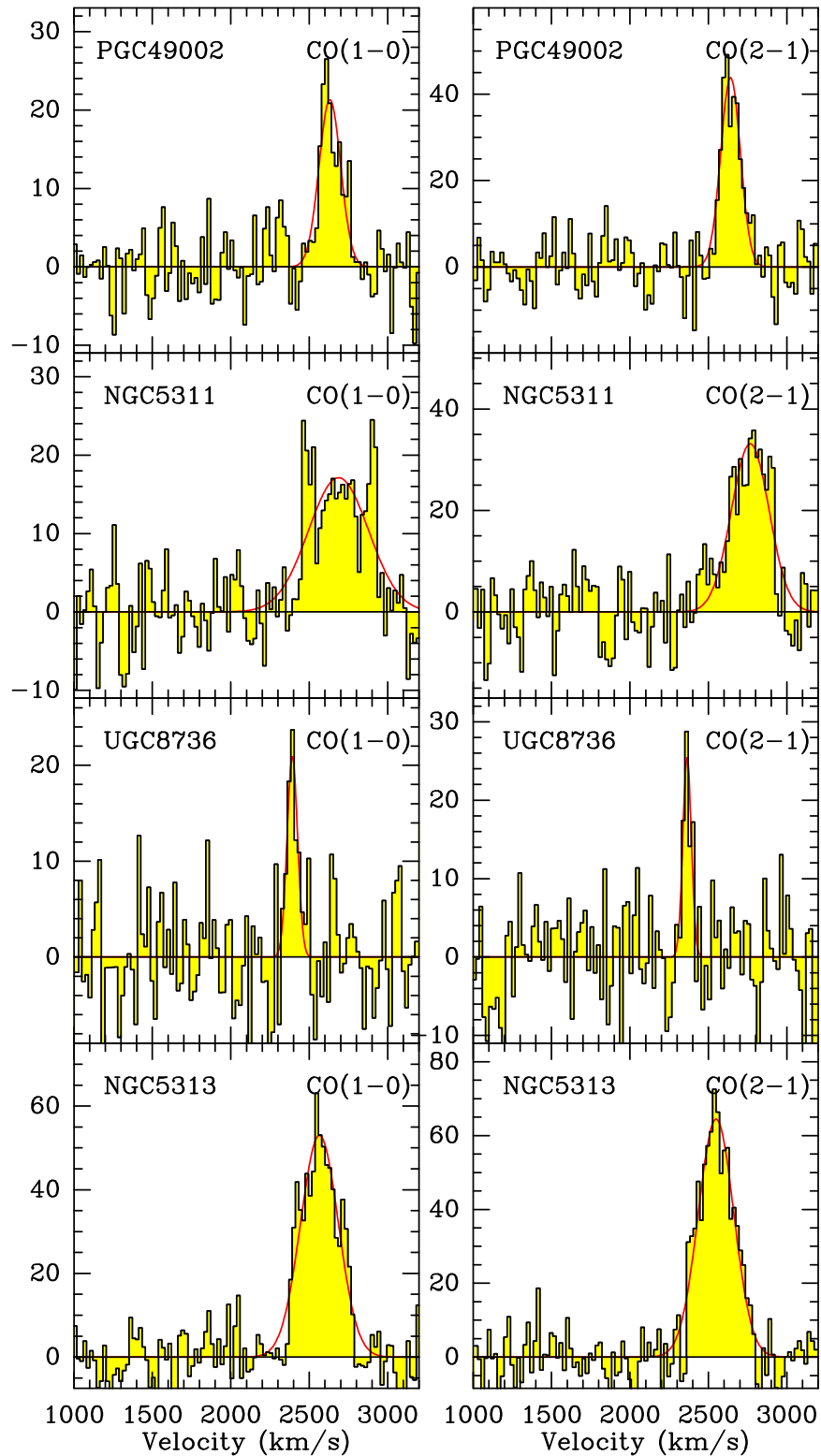


Fig. C.1: Continued.

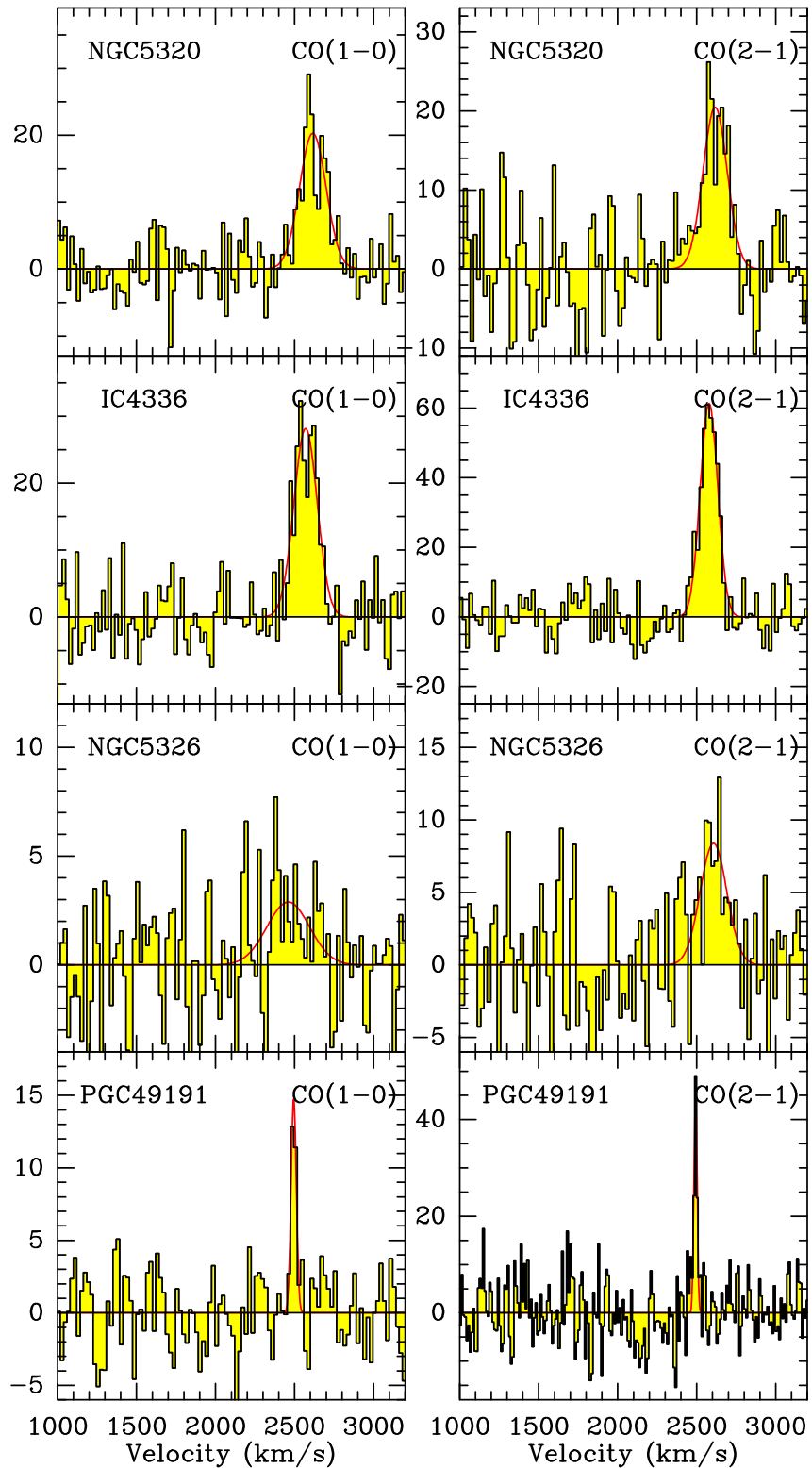


Fig. C.1: Continued.

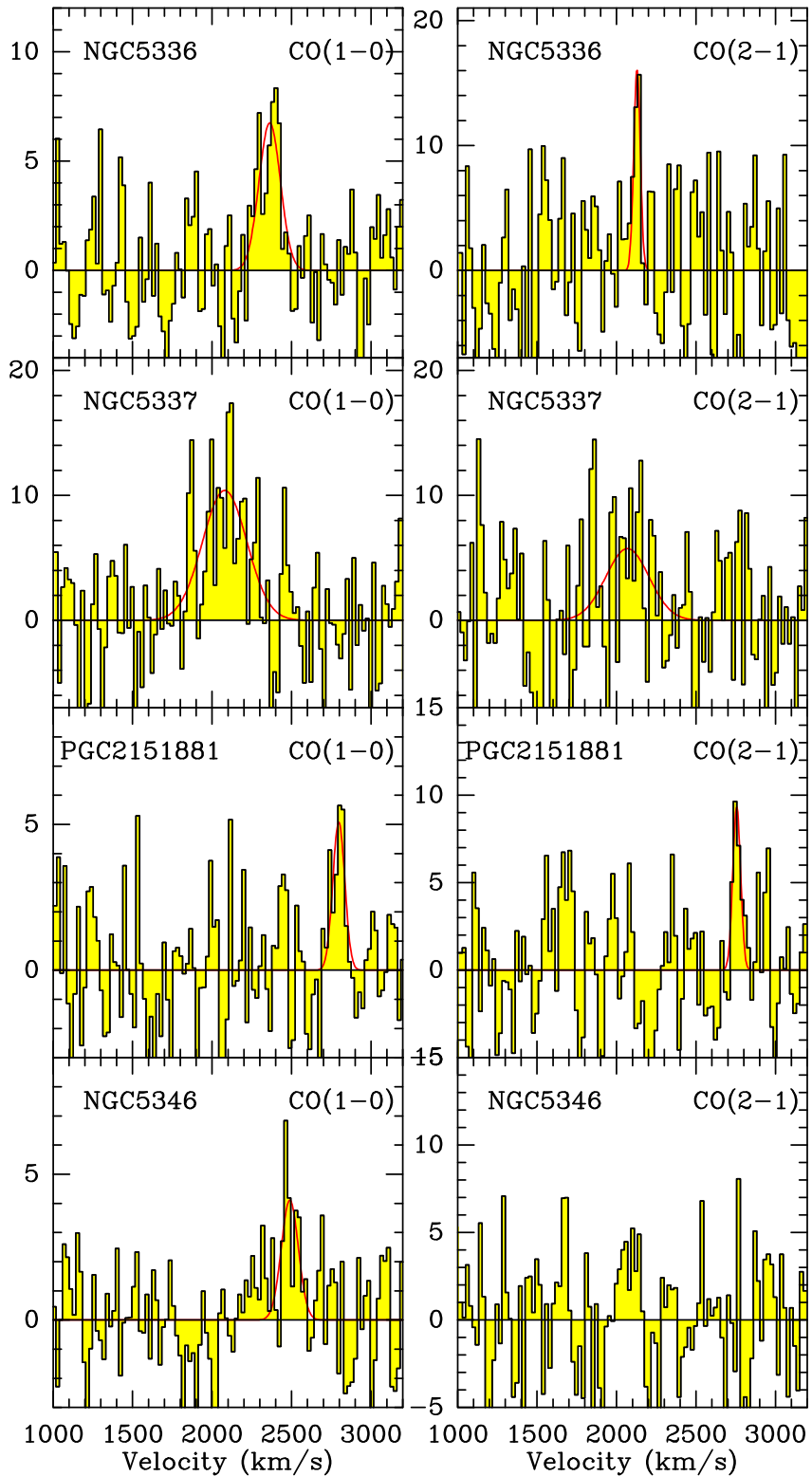


Fig. C.1: Continued.

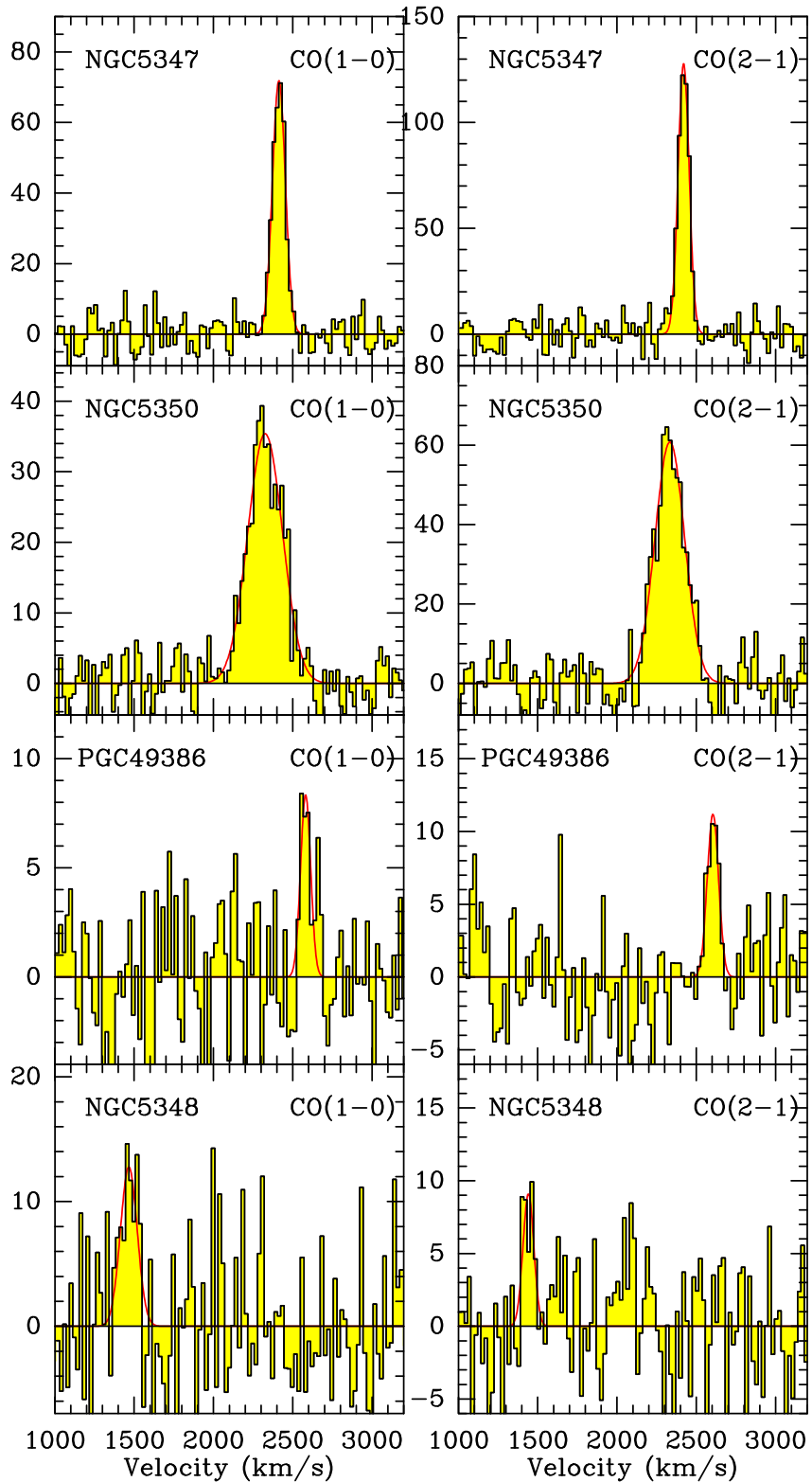


Fig. C.1: Continued.

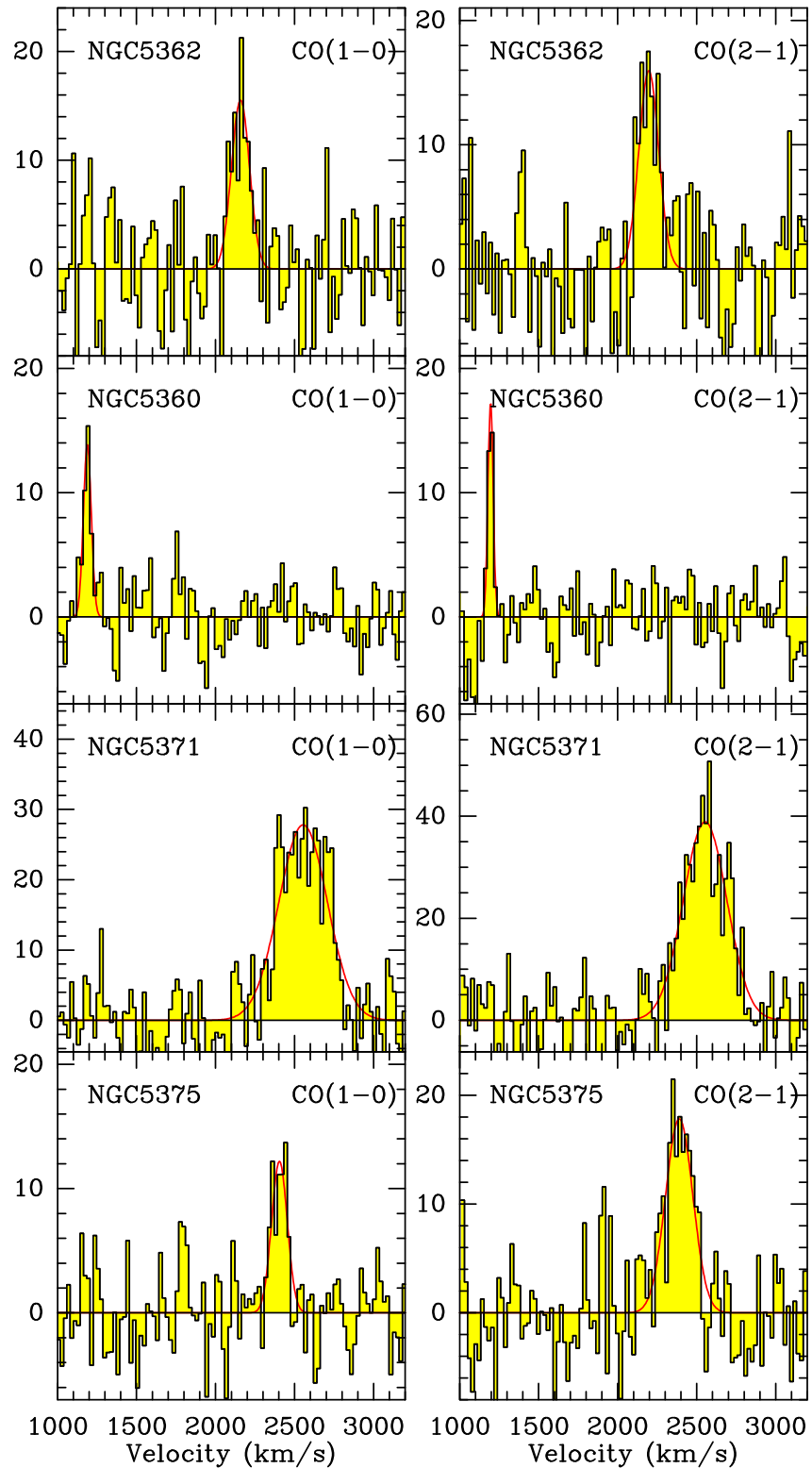


Fig. C.1: Continued.

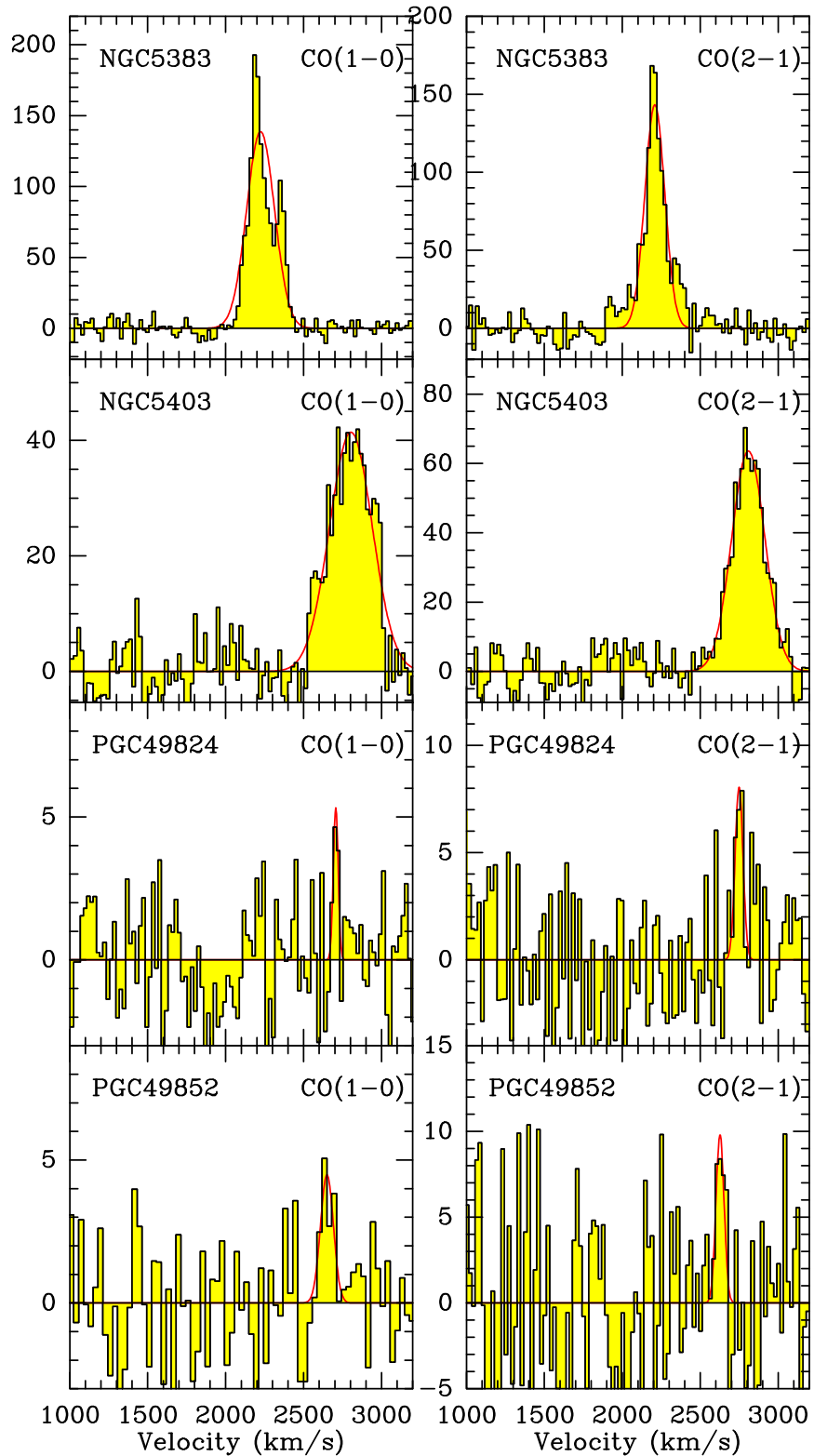


Fig. C.1: Continued.

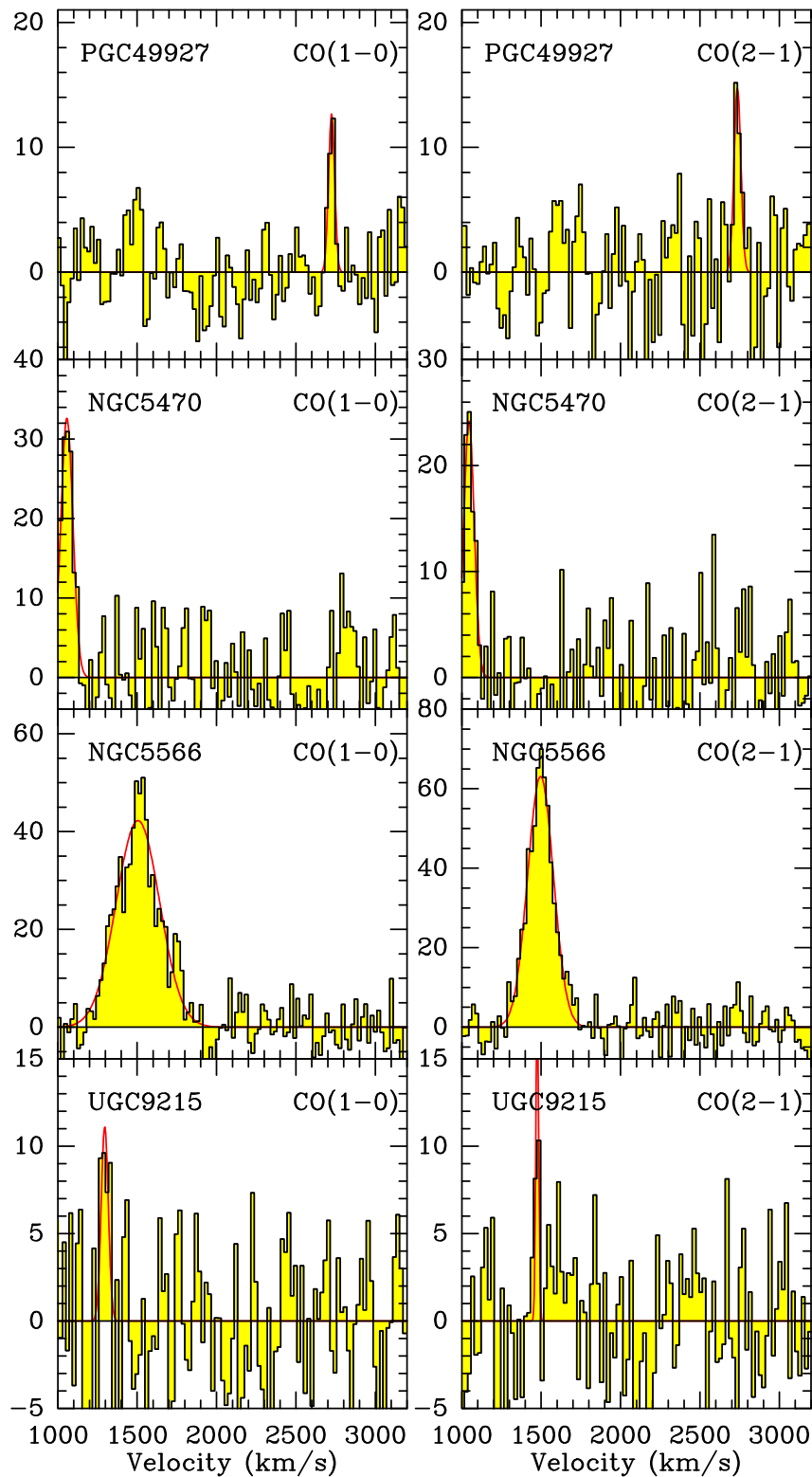


Fig. C.1: Continued.

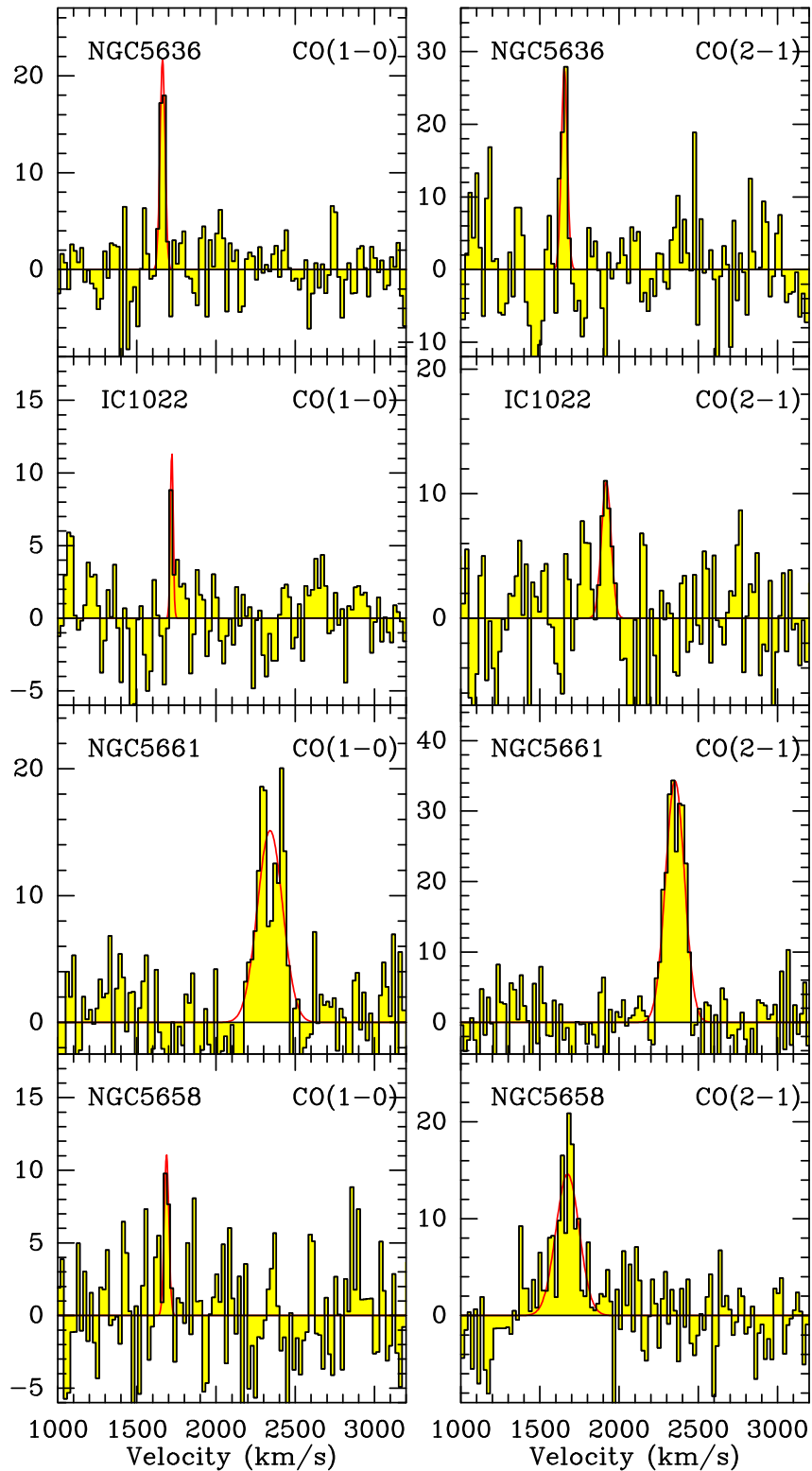


Fig. C.1: Continued.

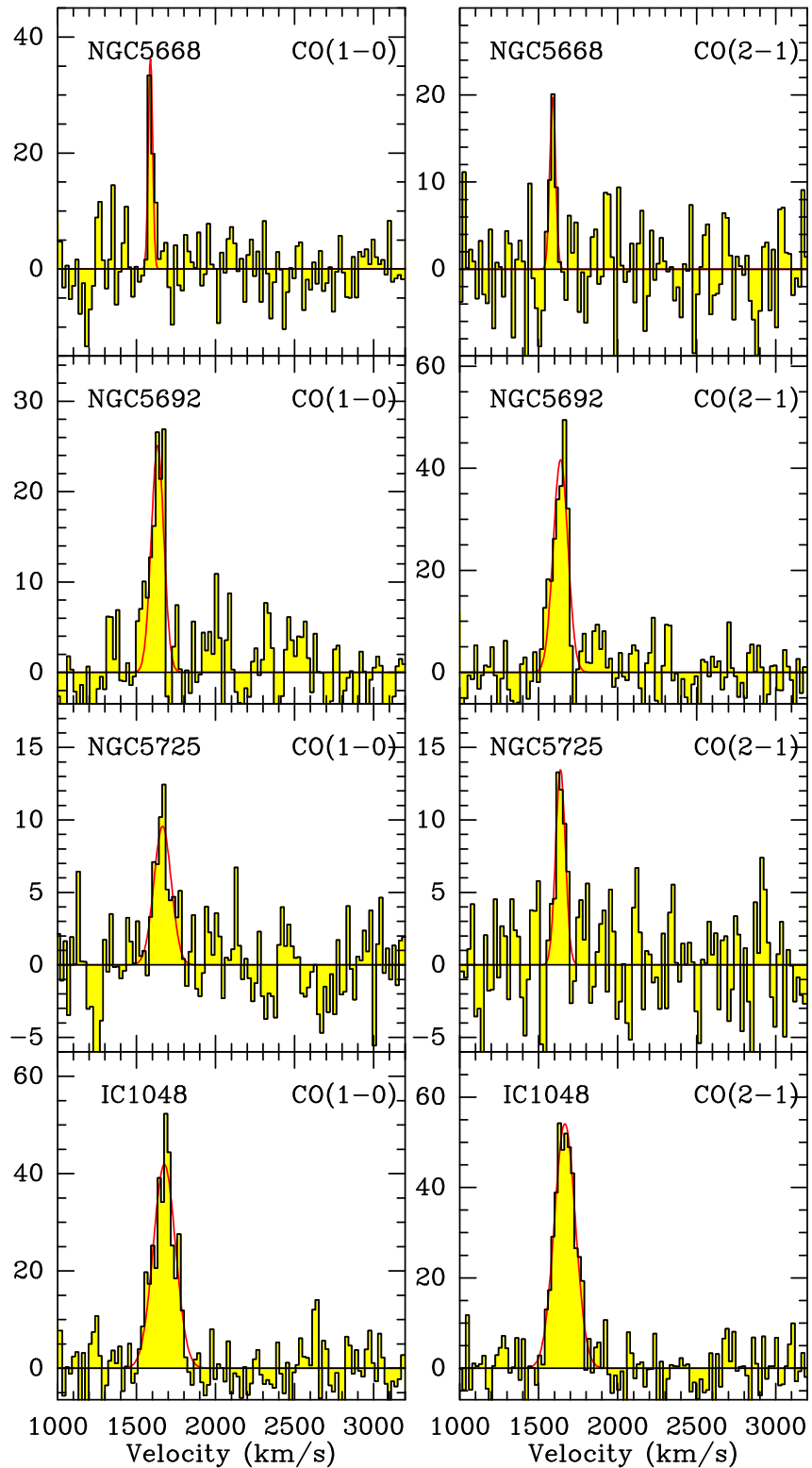


Fig. C.1: Continued.

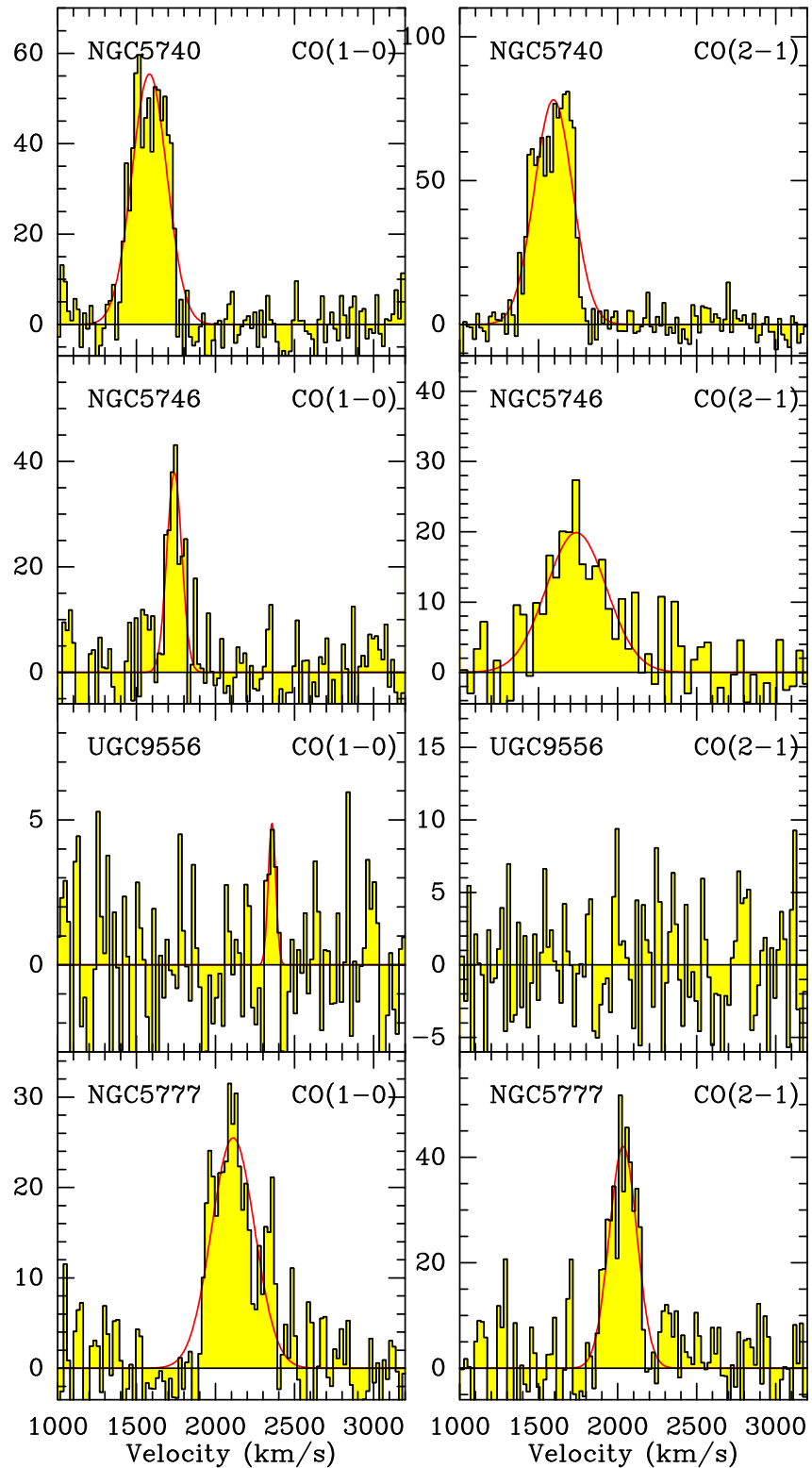


Fig. C.1: Continued.

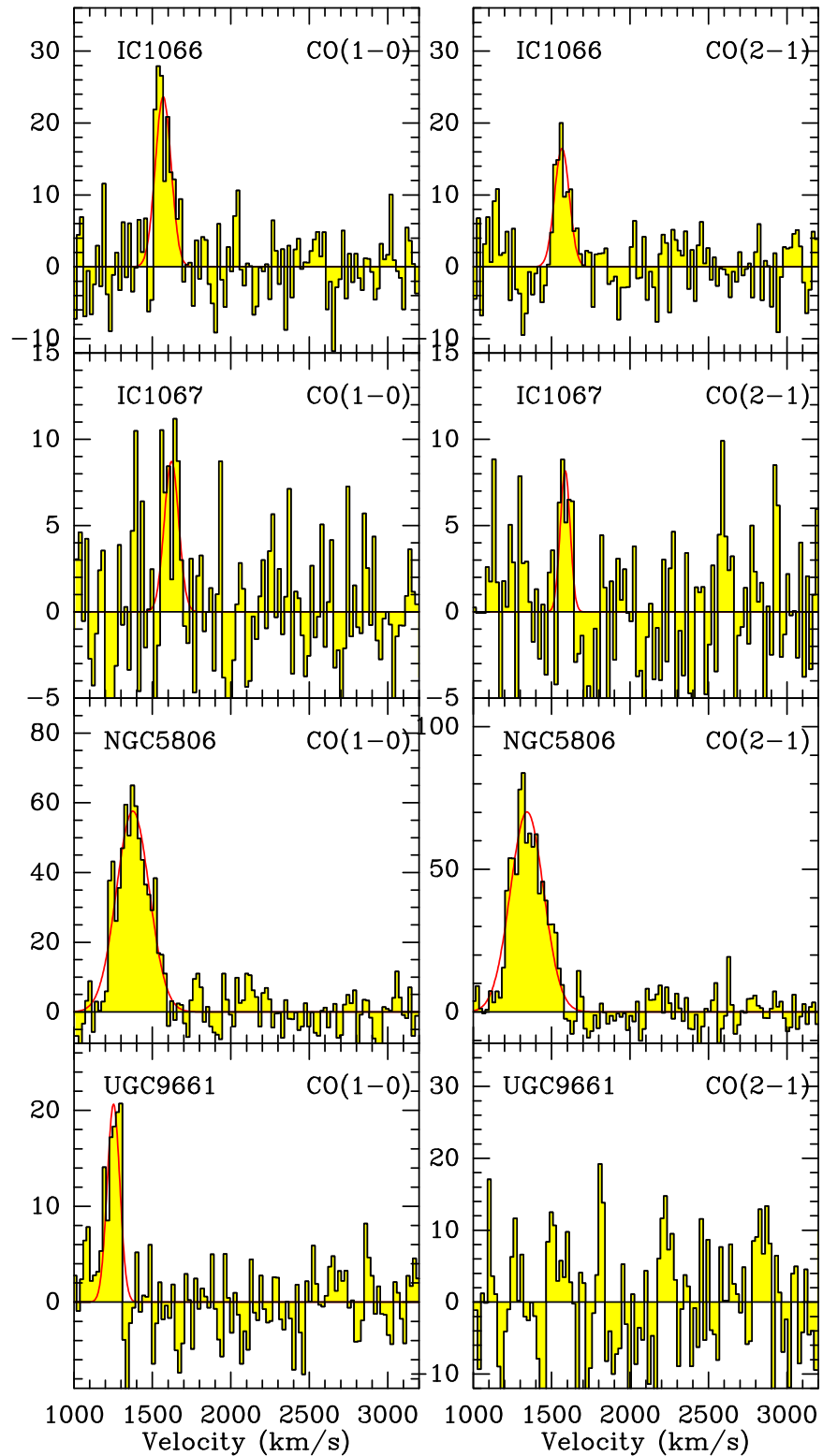


Fig. C.1: Continued.

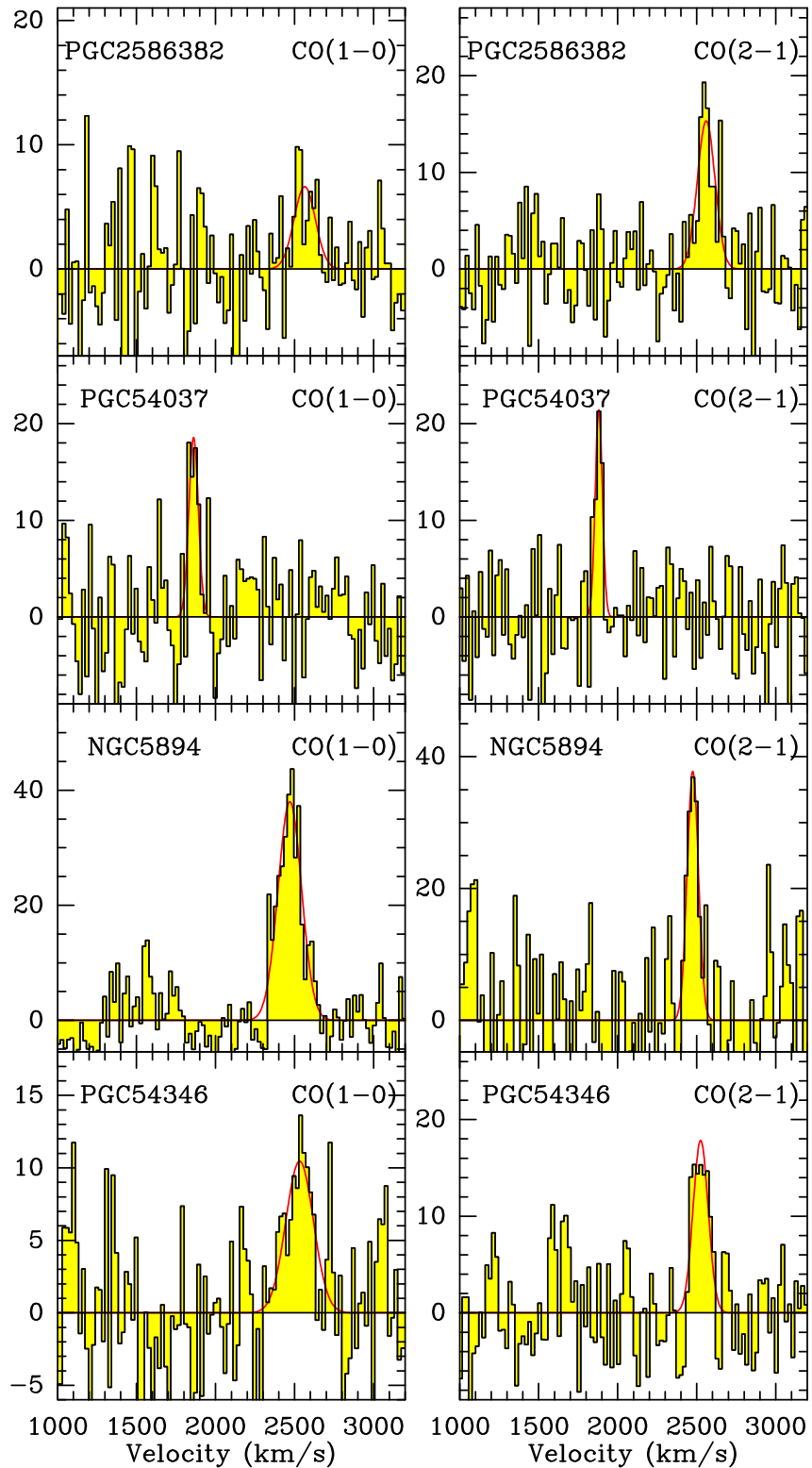


Fig. C.1: Continued.

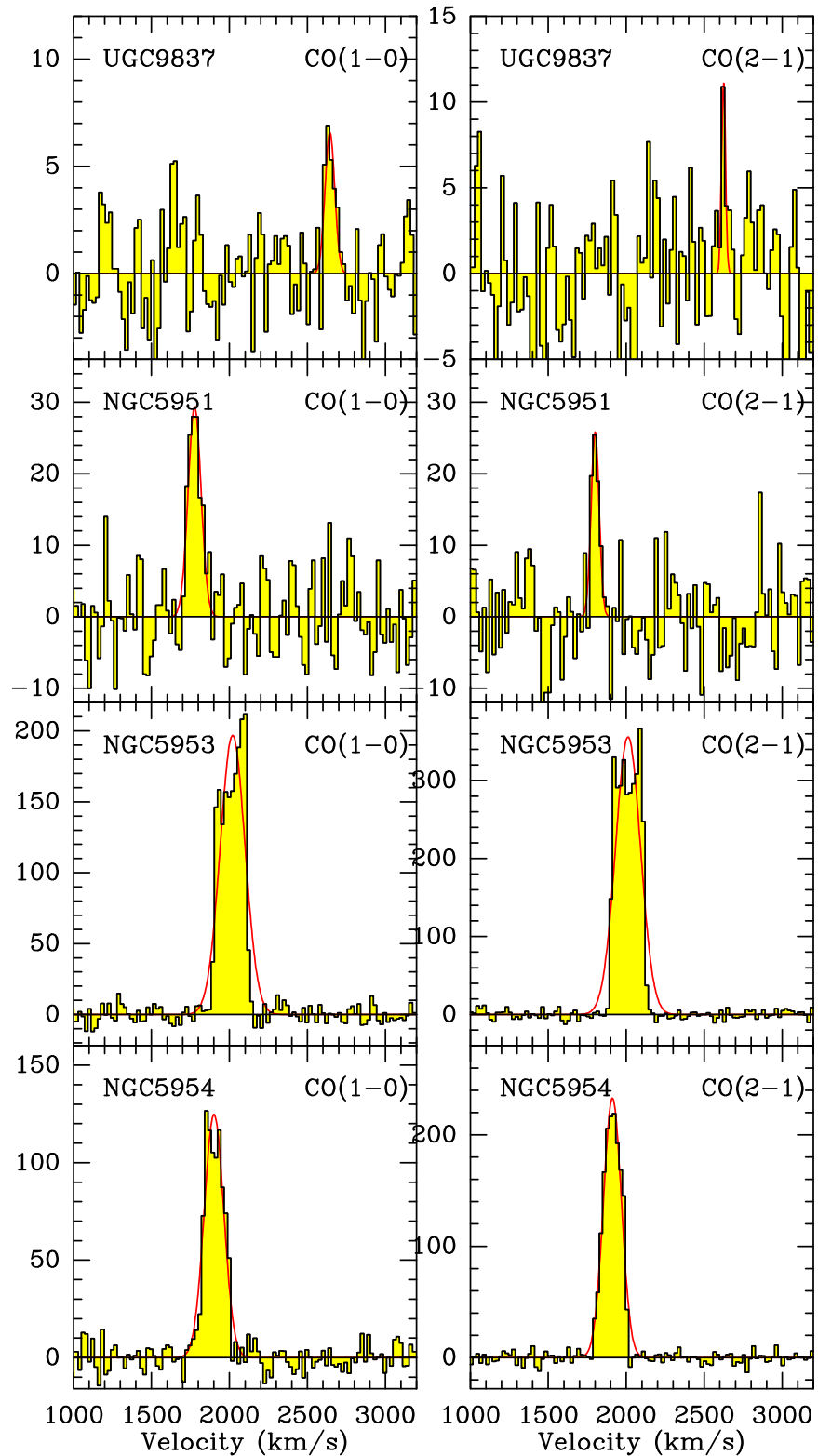


Fig. C.1: Continued.

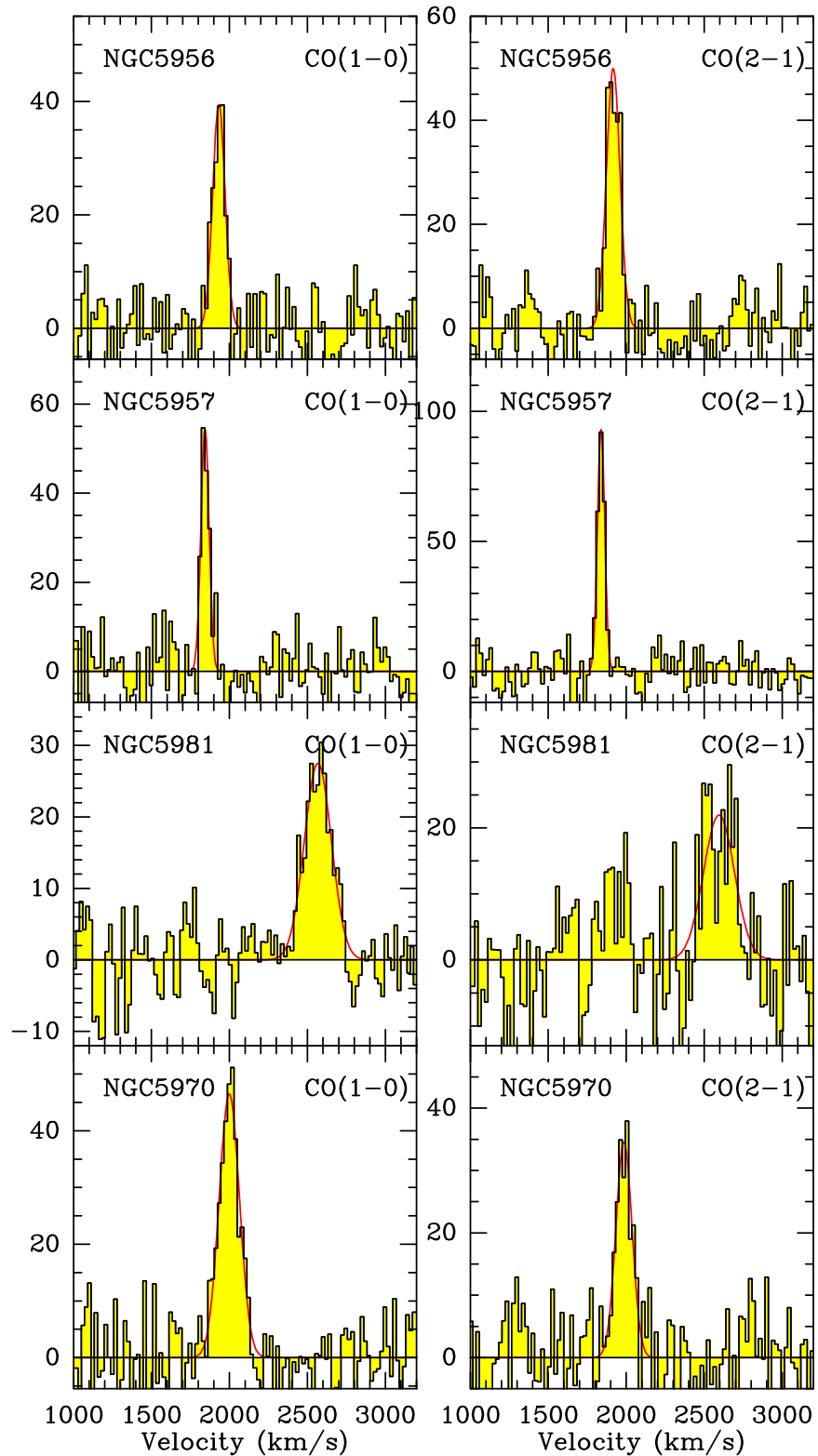


Fig. C.1: Continued.

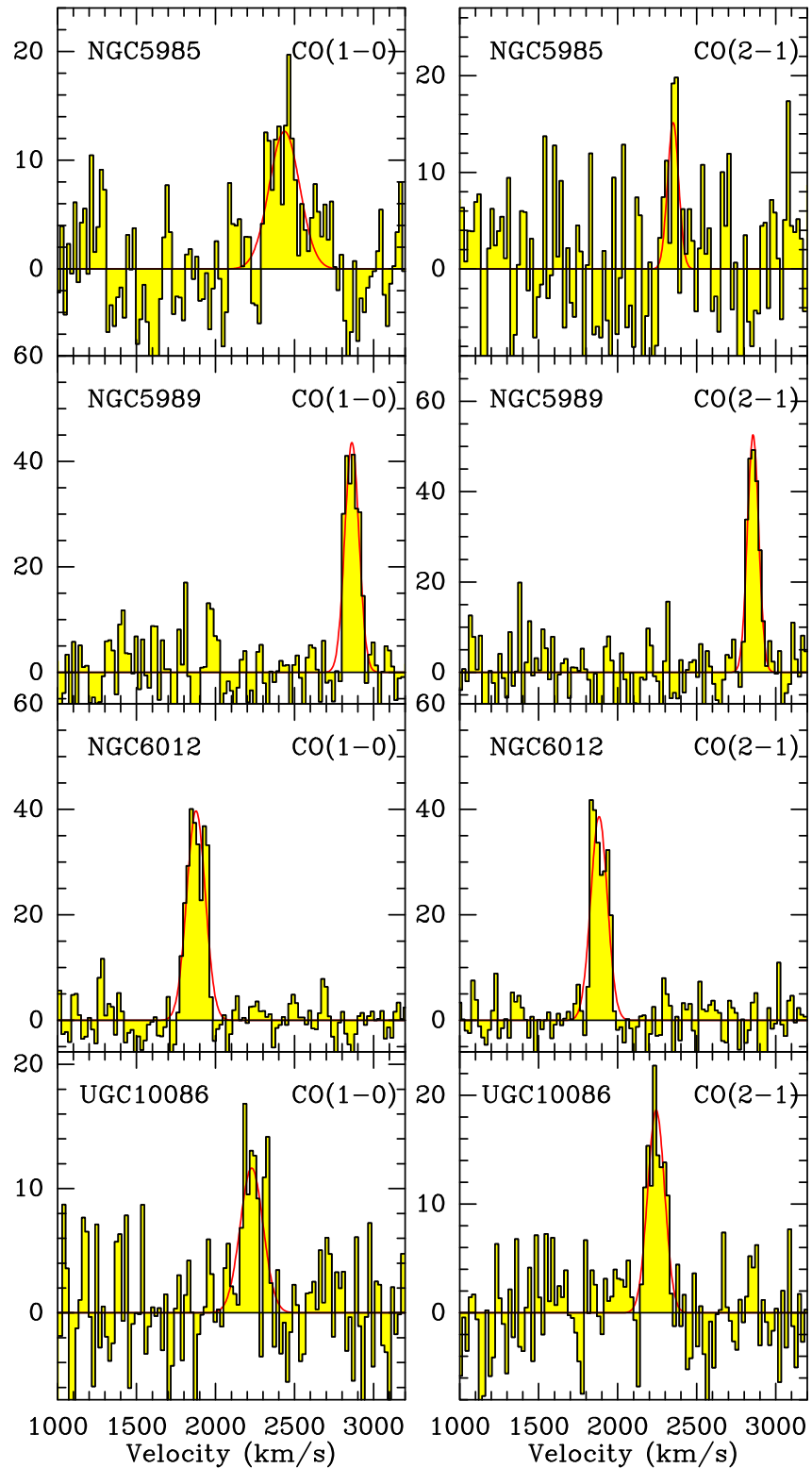


Fig. C.1: Continued.

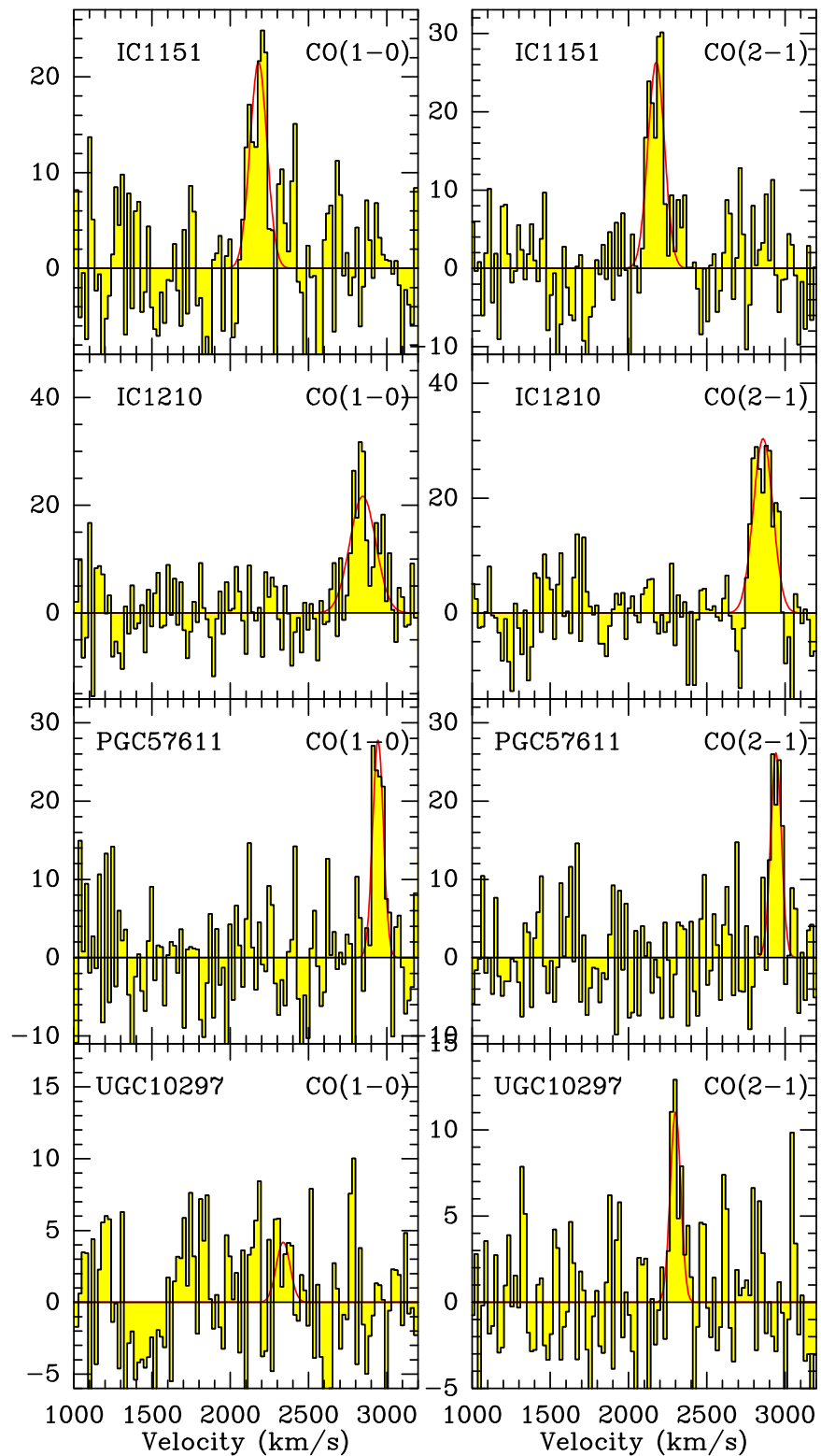


Fig. C.1: Continued.

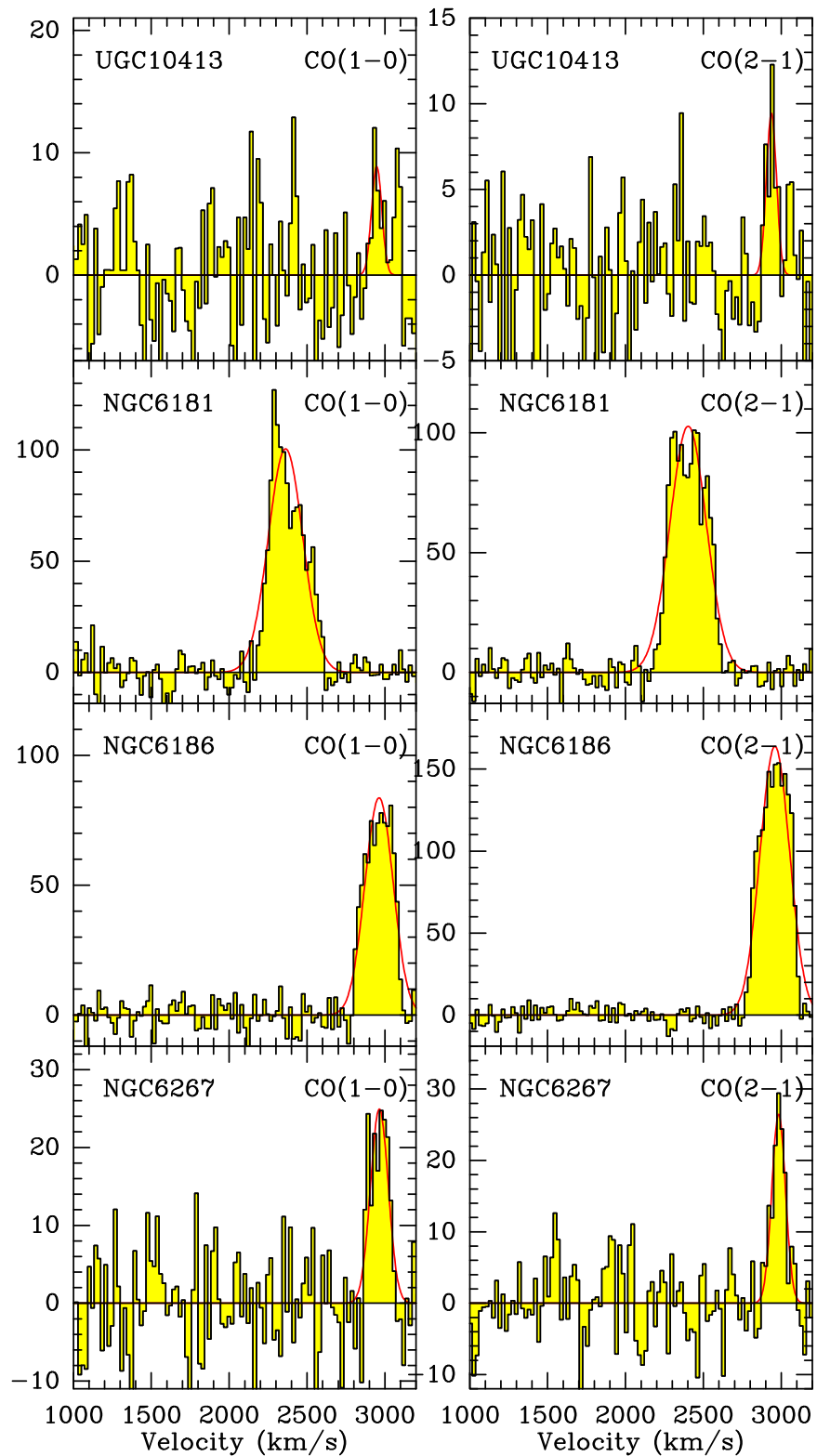


Fig. C.1: Continued.

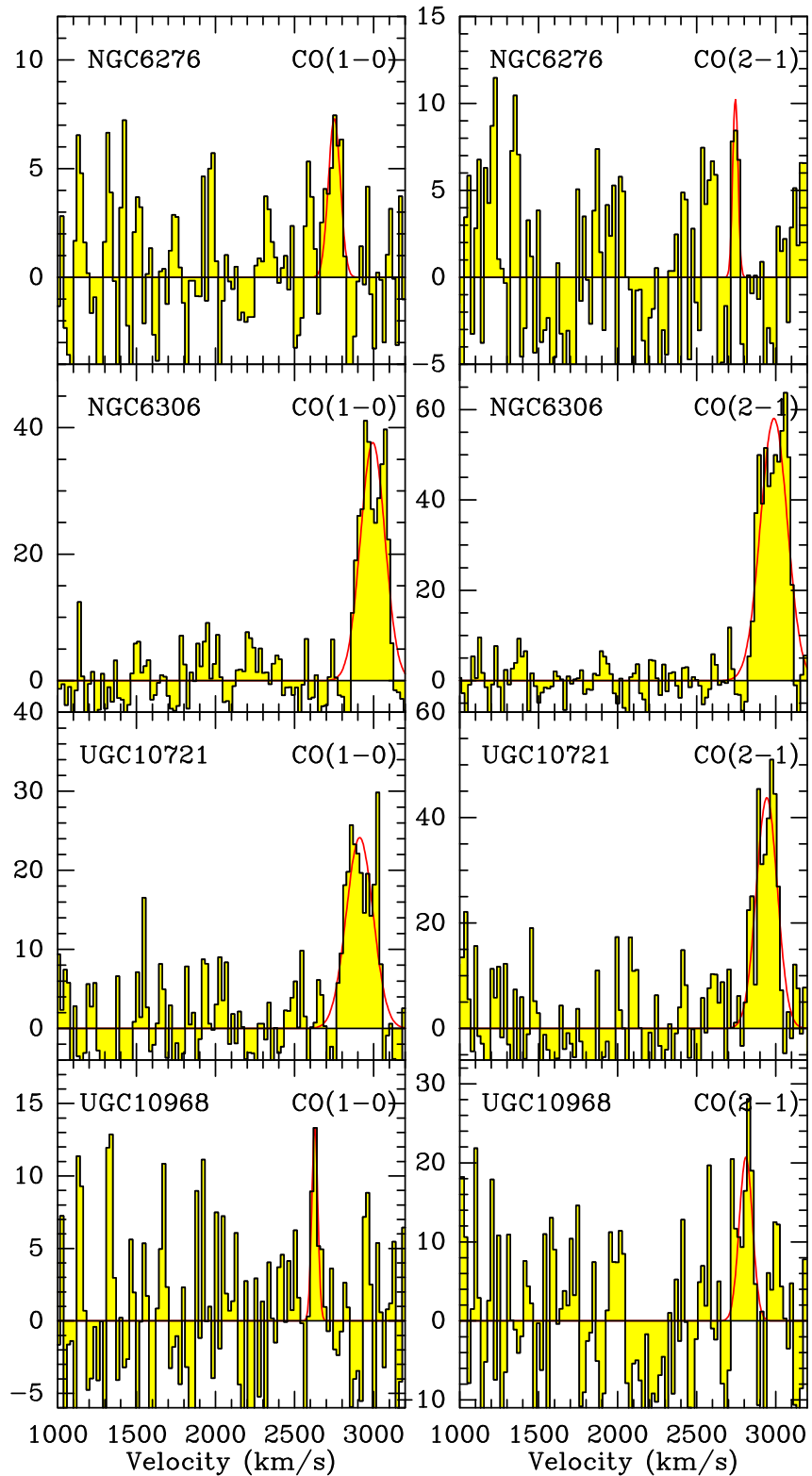


Fig. C.1: Continued.

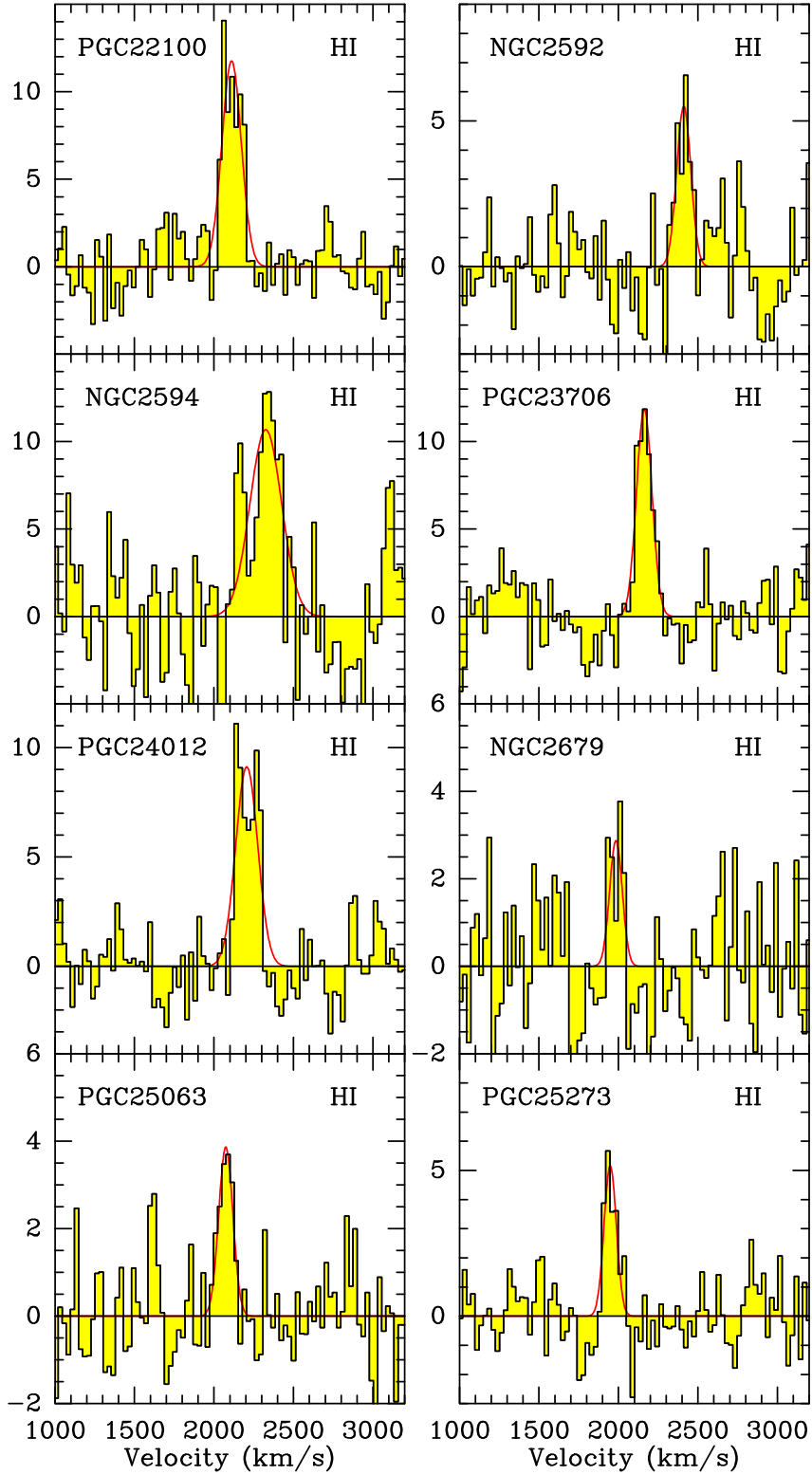


Fig. C.2: Baseline subtracted HI spectra from our Nançay campaign for the sources with HI detections. For each spectrum, the x-axis shows the relative velocity, while in the y-axis T_{mb} is shown in units of mK. Solid red curves show the Gaussian fits to the HI emission.

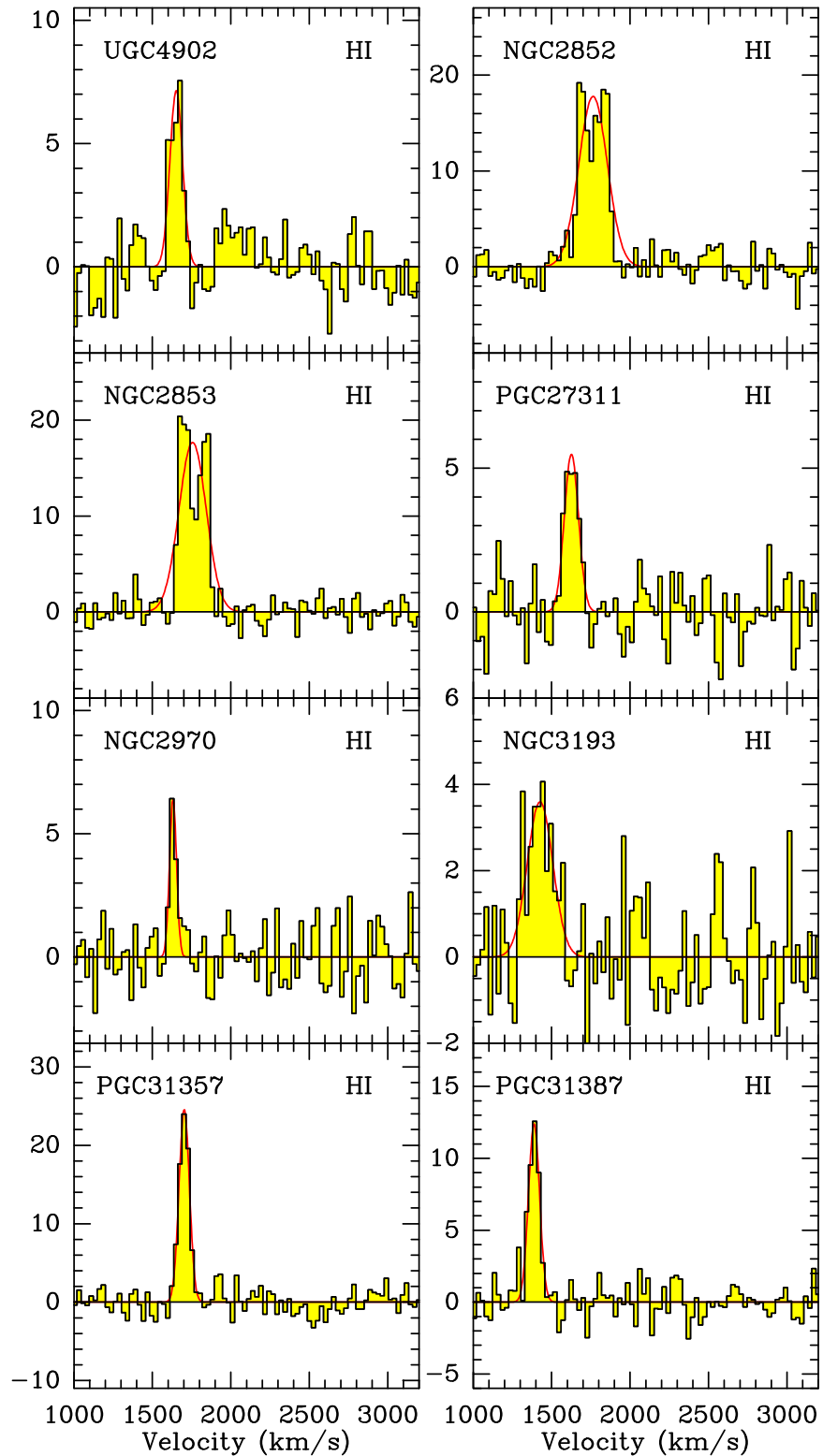


Fig. C.2: Continued.

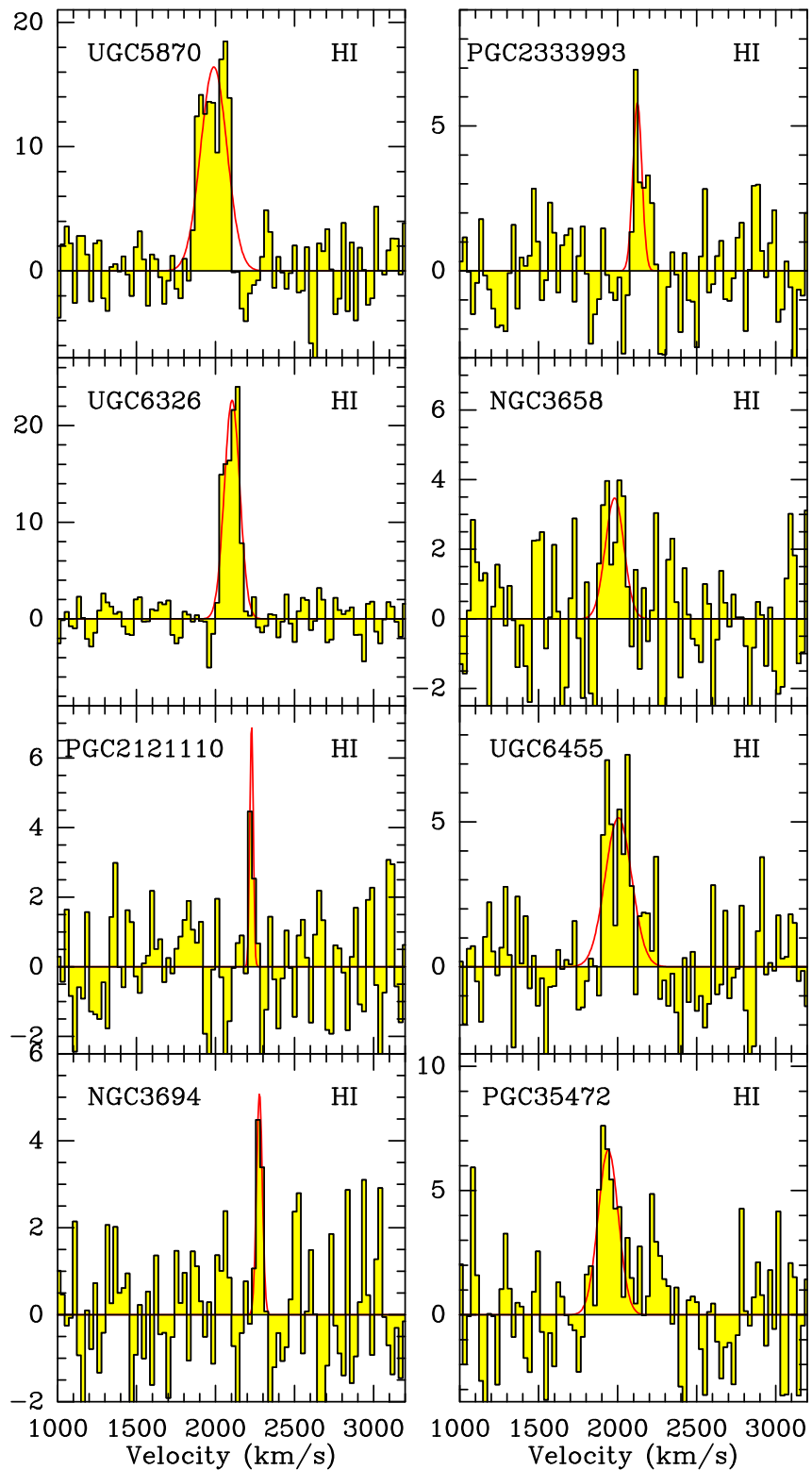


Fig. C.2: Continued.

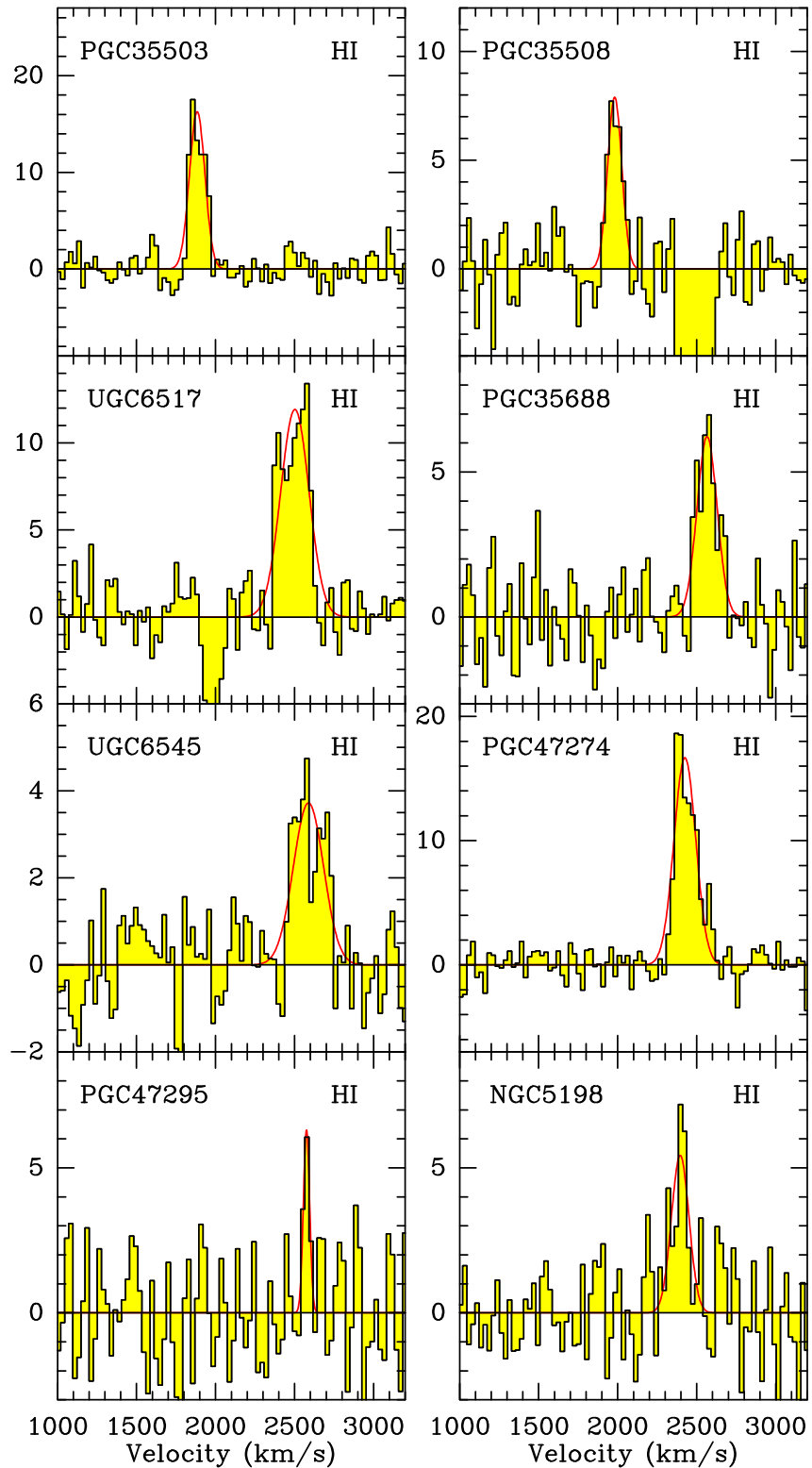


Fig. C.2: Continued.

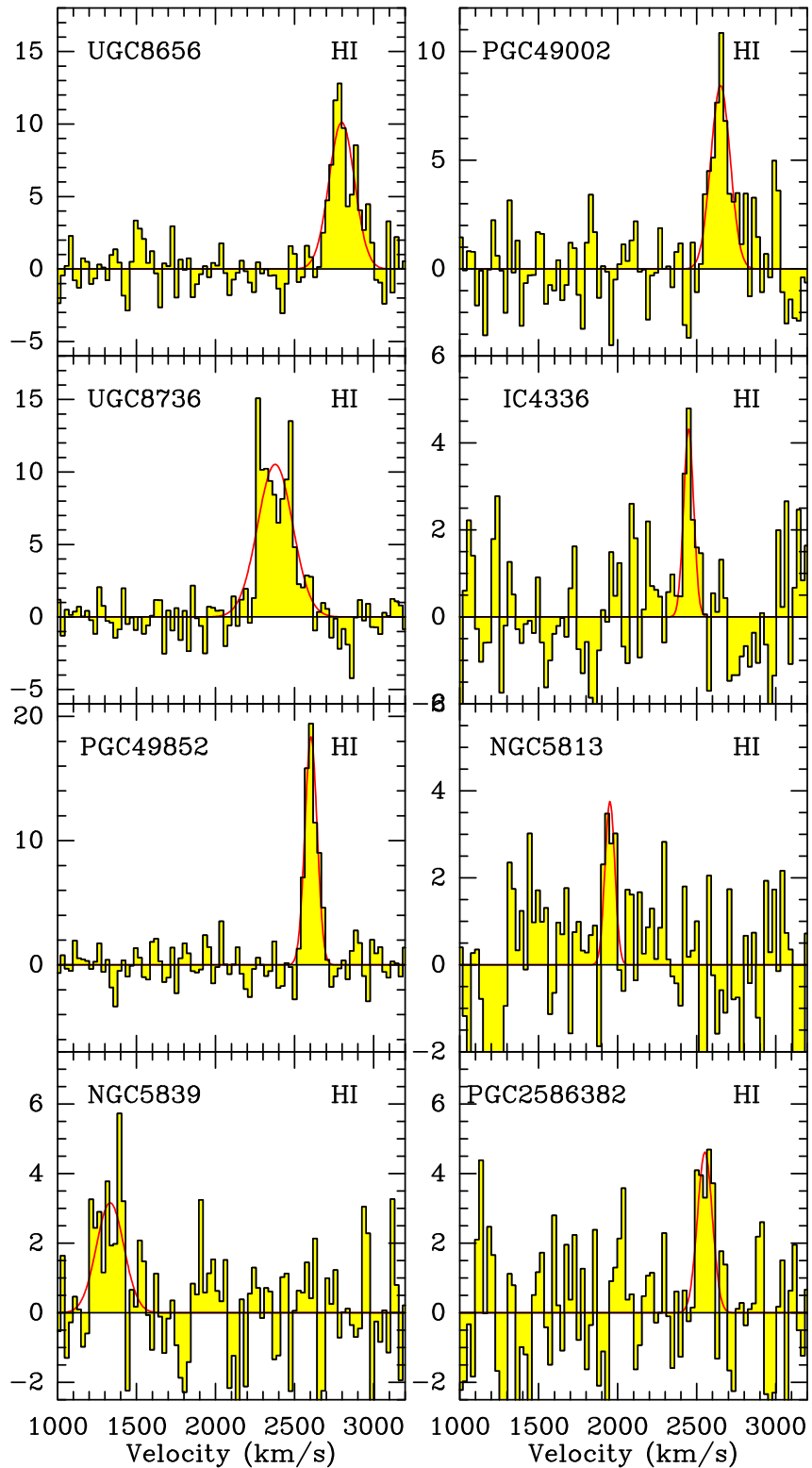


Fig. C.2: Continued.

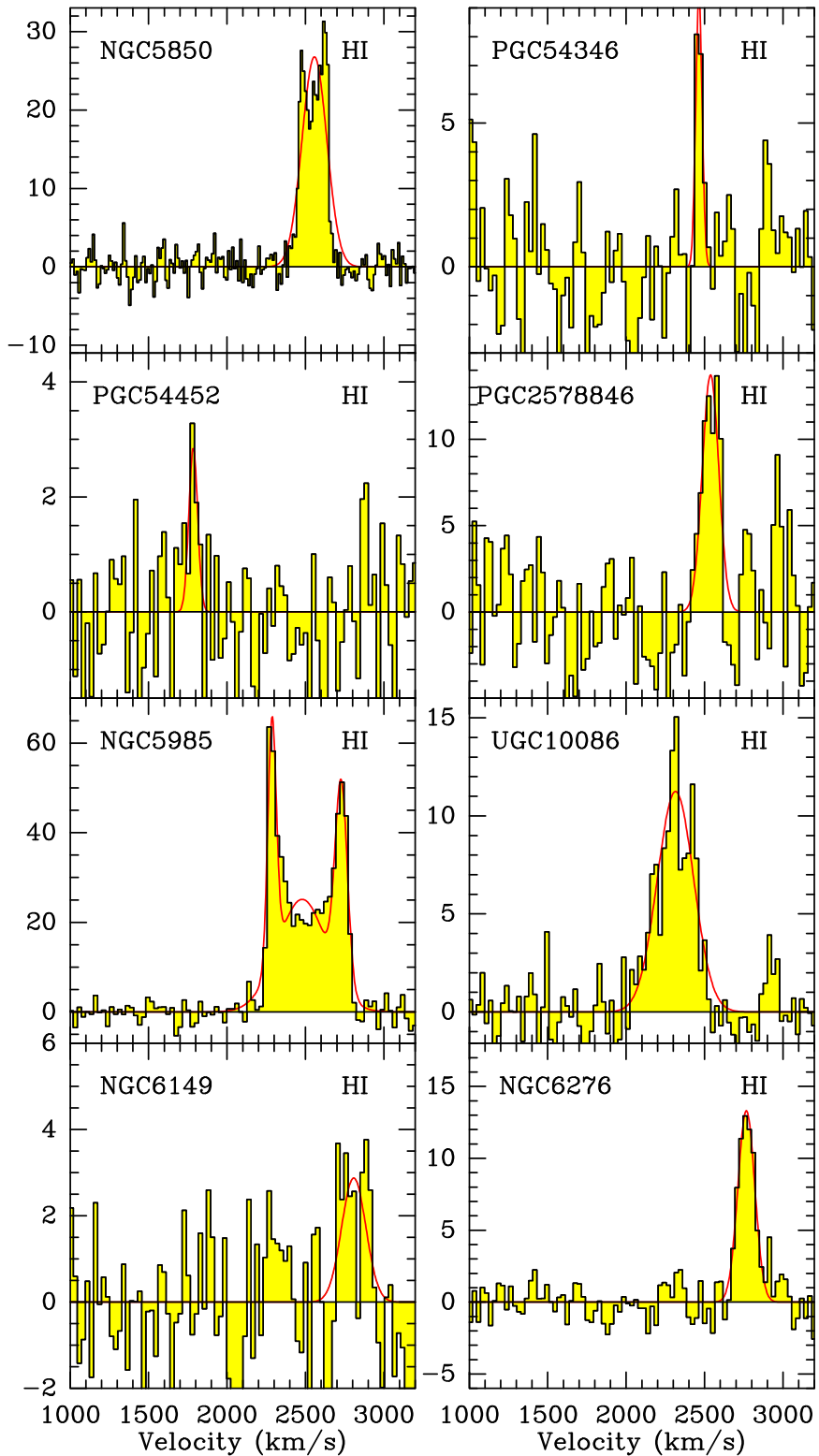


Fig. C.2: Continued.

Appendix D: Star formation, stellar mass, and gas content diagnostic

In this Section we report diagnostic plots between gas content, stellar mass, and star formation. The aim of the analysis is to show the consistency of all essential galaxy properties used in this work (i.e., M_\star , SFR, M_{HI} , and M_{H_2}).

Appendix D.1: Line widths, gas masses, and stellar masses

Fig. D.1 shows the FWHM distribution of the sources observed and detected in CO(1→0), CO(2→1), or HI with our campaigns. The associated median values are $\text{FWHM} = 129^{+103}_{-62} \text{ km s}^{-1}$ for CO(1→0), $107^{+97}_{-55} \text{ km s}^{-1}$ for CO(2→1), and $125^{+81}_{-51} \text{ km s}^{-1}$ for HI. The reported values are fairly consistent between each other and safely below the value of 300 km s^{-1} that we adopted to estimate conservative upper limits, as discussed in Sect. 3.3.

In Fig. D.2 we report HI and H₂ gas masses as a function of the stellar mass for our sample of Virgo filament galaxies as well as the AMIGA field isolated galaxies and Virgo cluster galaxies for a comparison. In the M_{HI} vs. M_\star plots we overlay the relation by De Looze et al. (2020) for local field galaxies, evaluated at the MS using the SFR vs. M_\star prescription by Leroy et al. (2019). In the M_{H_2} vs. M_\star plots we overlay instead the local M_{H_2} vs. M_\star relation by Tacconi et al. (2018) for MS galaxies, calibrated using the Galactic conversion factor $\alpha_{\text{CO}} = 4.3 M_\odot (\text{K km s}^{-1} \text{ pc}^2)^{-1}$ used in this work. Note in fact that Tacconi et al. (2018) adopted a metallicity-dependent conversion.

Within the range of stellar masses $\log(M_\star/M_\odot) \sim 9 - 11$ considered, LTGs overall follow the field scaling relations for both HI and H₂, although with a large associated dispersion.⁸ On the other hand, the H₂ and HI content of ETGs is significantly lower than what is expected for MS galaxies at a given stellar mass.⁹ These results imply that LTGs in the three different environments (field, filaments, cluster) overall follow the local MS relations for field galaxies. However, this does not apply to ETGs. Indeed, as further discussed in the text (Sect. 7.1) while the majority of LTGs are within the MS, ETGs are preferentially below the MS and in the quenching phase.

For the three different environments (field, filaments, cluster) there are thus strong similarities in what concerns the distribution and split of ETGs and LTGs, separately, when comparing the gas mass vs. M_\star and the SFR vs. M_\star plots. This motivated us to investigate further how the gas content traces the star formation specifically in filament galaxies, as described below.

Appendix D.2: SFR vs. gas masses

Figures D.3 and D.4 display the SFR against the HI and H₂ gas masses, respectively, for filament galaxies as well as for AMIGA and Virgo cluster galaxies as comparison. Similarly to our previous plots, we overlay here the scaling relations for MS field galaxies by De Looze et al. (2020) and Tacconi et al. (2018), respectively.

Filament galaxies overall follow the field MS scaling relations between the SFR and gas mass. The agreement with the scaling relations is found for both HI and H₂, even if the latter traces better the ongoing star formation. This is true for the field (Bigiel et

⁸ For LTGs the median logarithmic difference between M_{HI} and the MS prediction is $(0.18^{+0.31}_{-0.53}) \text{ dex}$ (AMIGA), $(-0.01^{+0.46}_{-0.51}) \text{ dex}$ (filaments), and $(-0.48^{+0.75}_{-0.74}) \text{ dex}$ (Virgo cluster). For M_{H_2} the median offsets are: $(-0.14^{+0.38}_{-0.30}) \text{ dex}$ (AMIGA), $(-0.18^{+0.52}_{-0.37}) \text{ dex}$ (filaments), and $(0.20^{+0.35}_{-0.77}) \text{ dex}$ (Virgo cluster).

⁹ For ETGs the median logarithmic difference between M_{HI} and the MS prediction is $(-1.11^{+0.55}_{-0.24}) \text{ dex}$ (AMIGA), $(-1.37^{+1.00}_{-0.47}) \text{ dex}$ (filaments), and $(-2.61^{+0.67}_{-0.33}) \text{ dex}$ (Virgo cluster). For M_{H_2} the median offsets are: $(-0.55^{+0.36}_{-0.41}) \text{ dex}$ (AMIGA), $(-1.06^{+0.63}_{-0.34}) \text{ dex}$ (filaments), and $(-1.78^{+1.32}_{-0.16}) \text{ dex}$ (Virgo cluster).

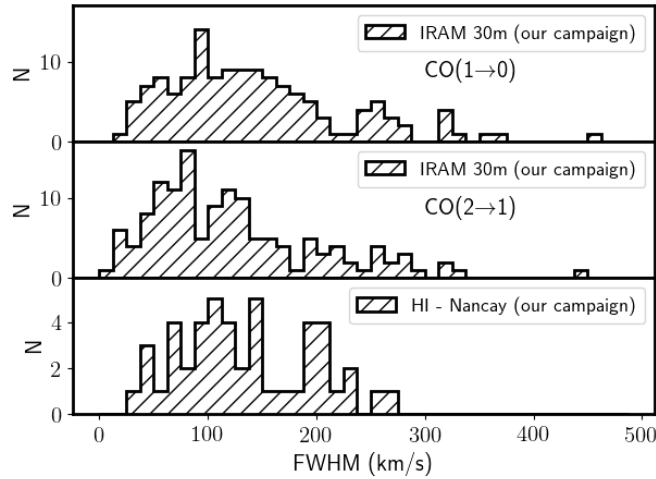


Fig. D.1: FWHM distributions for CO(1→0), CO(2→1), and HI from our IRAM-30m and Nançay campaigns.

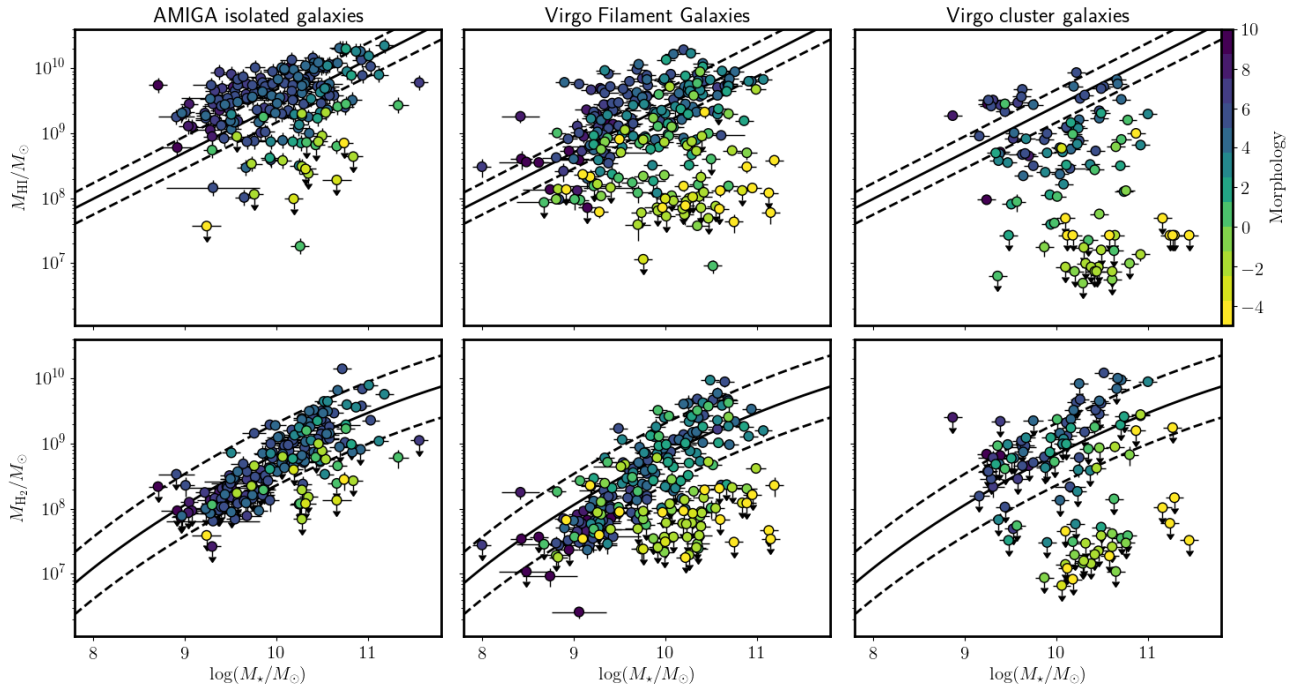


Fig. D.2: HI mass (top row) and H₂ mass (bottom row) plotted against M_{\star} , for the Virgo filament sources in our sample (center), AMIGA isolated galaxies (left), and Virgo cluster galaxies (right). Sources are color-coded according to their morphological classification. Solid lines correspond to local prescriptions at the MS, while dashed lines denote the uncertainties. For HI (top row) we have used the prescription by De Looze et al. (2020), while for H₂ that by Tacconi et al. (2018), calibrated using a Galactic conversion factor $\alpha_{\text{CO}} = 4.3 M_{\odot} (\text{K km s}^{-1} \text{ pc}^2)^{-1}$.

al. 2008; Schruba et al. 2011; Leroy et al. 2013), and we show with this work that this is also valid for filament galaxies. The rms of the SFR around the scaling relation is found to be ~ 0.53 dex when considering the SFR vs. M_{H_2} scatter plot. It is thus lower than that of ~ 0.67 dex around the SFR vs. M_{HI} relation.

Furthermore, for all three considered environments, while in the gas mass vs. M_{\star} and in the SFR vs. M_{\star} plots LTGs and ETGs are fairly split, in the SFR vs. gas mass (HI, H₂) plane they both nicely follow the MS relations for field galaxies, with only some exceptions discussed below. This suggests a self-consistency of the adopted α_{CO} conversion factor, as well as an overall universality in the way H₂ gas is consumed to form new stars. This is translated into a limited scatter for the star formation efficiency or for its inverse, the depletion time scale, as further discussed in Sect. 7.2.3. The above mentioned exceptions are those galaxies in filaments, as well as in AMIGA and in the cluster, with only upper limits to the gas content, at the low gas mass end $\lesssim 10^8 M_{\odot}$. As seen in Figs. D.3 and D.4, this region of low gas masses (HI, H₂) is mostly populated by ETGs, in filaments and also in the cluster, while for the AMIGA sample it is overall underpopulated, since isolated ETGs are rare.

Interestingly, a fraction of these ETGs with low $M_{\text{H}_2} \lesssim 10^8 M_{\odot}$ have also low SFR, both in filaments and in the cluster, while others have instead high SFR with respect to the MS, in particular in Virgo cluster. The former low SFR sources correspond to ETGs in the phase of quenching, where the H₂ gas reservoir has been consumed, or in the process of exhaustion. The latter are instead a population of more star forming ETGs, with low H₂ gas content and thus relatively low depletion time (upper limits) of $\tau_{\text{dep}} \lesssim 10^{8-9}$ yr. They correspond to ETGs still forming stars, but in a rapid phase of quenching, similarly to their higher- z star forming analogs found in cluster cores (Castignani et al. 2020). They are experiencing a rapid phase of quenching and will possibly turn, in less than 1 Gyr, into *red and dead* galaxies, that are commonly seen in cluster cores. On the other hand, the observed population of filament and Virgo cluster galaxies with low $M_{\text{HI}} \lesssim 10^8 M_{\odot}$ can be explained as galaxies having already experienced the removal of the HI envelope, likely via ram-pressure stripping in dense environments. Both in filaments and in Virgo, this population with low M_{HI} is mostly comprised by ETGs, for which the HI content is impacted more than for LTGs. We refer to the text for further discussion.

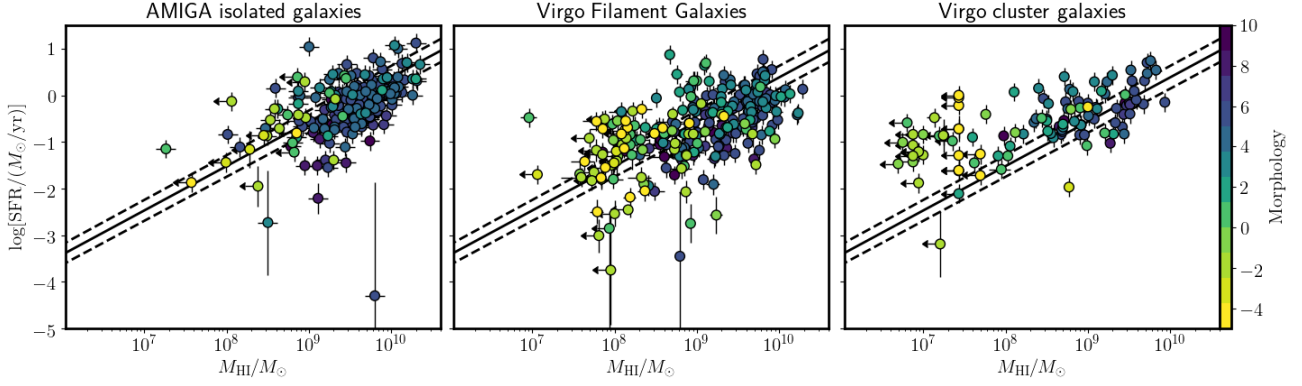


Fig. D.3: SFR vs. HI mass scatter plot for the Virgo filament sources in our sample (center), AMIGA isolated galaxies (left), and Virgo cluster galaxies (right). Sources are color-coded according to their morphological classification. Solid and dashed lines correspond to the local prescription and model uncertainties by De Looze et al. (2020) for MS galaxies.

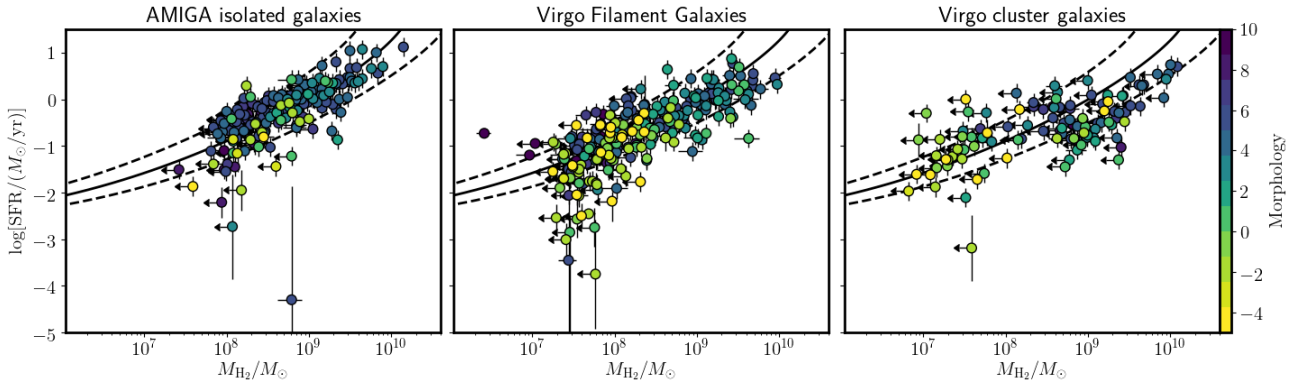


Fig. D.4: SFR vs. H_2 mass scatter plot for the Virgo filament sources in our sample (center), AMIGA isolated galaxies (left), and Virgo cluster galaxies (right). Sources are color-coded according to their morphological classification. Solid and dashed lines correspond to the local prescription and model uncertainties by Tacconi et al. (2018) for MS galaxies, calibrated to a Galactic $\alpha_{\text{CO}} = 4.3 M_{\odot} (\text{K km s}^{-1} \text{pc}^2)^{-1}$.